Low-Complexity Techniques for Ultra-Wideband Communication Systems

Martin Weisenhorn

Technische Universität München
Fachgebiet Methoden der Signalverarbeitung

Low-Complexity Techniques for Ultra-Wideband Communication Systems

Martin Weisenhorn

Vollständiger Abdruck der von der Fakultät für Elektrotechnik und Informationstechnik der Technischen Universität München zur Erlangung des akademischen Grades eines

Doktor-Ingenieurs

genehmigten Dissertation.

Vorsitzender: Univ.-Prof. Dr.techn. Peter Russer
Prüfer der Dissertation:

1. Univ.-Prof. Dr.-Ing. Wolfgang Utschick
2. Ao.Univ.-Prof. Dr.techn. Franz Hlawatsch,
   Technische Universität Wien/Österreich

Die Dissertation wurde am 12.06.2006 bei der Technischen Universität München eingereicht und durch die Fakultät für Elektrotechnik und Informationstechnik am 29.01.2007 angenommen.

Meiner Familie gewidmet

Acknowledgements

I would like to express my sincere gratitude to the supervisor of my doctoral thesis Prof. Wolfgang Utschick from the Technische Universität München. He pointed out the IBM Research Laboratory in Rüschlikon as a potential employer for me, where I started to work towards my doctoral thesis. From the initial stage until completion of this work he gave me valuable inspiration. Particular were his suggestions regarding partial channel information, multiple antenna systems and the presentation of the content.

In the same way, my thanks go to Prof. Franz Hlawatsch from the Vienna University of Technology. He taught me the basics of writing technical text and to love precise argumentation and clear representation. Also, I am thankful for his technical suggestions improving my work considerably and for his effort in helping me make the thesis more graspable.

I wish to sincerely thank Walter Hirt for having been my mentor at the Sensor Networks Group of the IBM Research Laboratory. With just the right portion of guidance, he tought me how to find a topic within a new research field. He encouraged me to try out new ideas and helped me to question them critically. His confidence in the significance of my work motivated me to bring it to the conclusion.

Besides Walter Hirt, my thanks go to Pierre Cheviallat, my senior at the IBM Research Laboratory. With his educated person he enriched my "lab-life" through colorful discussions about technology, God and the world. In particular, I am grateful that he made it possible for me to work in the same topic during my entire stay at IBM.

I heartly thank my parents for the freedom they gave me and for having steadily supported my goals.

A big thank you goes to Jaleh for her understanding during the many hours I was occupied with my work. Maybe she contributed less to technical issues, but much in enabling them.

Abstract

Ultra-wideband communication systems use radio signals whose bandwidth is in the range of some hundred MHz to several GHz. The first application of these signals was military radar. The reasons for using signals with such an extremely large bandwidth are manifold. The resulting high temoral signal-resolution is a prerequisit for precise radar systems. Radio channels with dense multipath propagation achieve high multipath diversity, which can be used to improve the robustness and capacity of the communication channel. Furthermore, the large bandwidth allows to transmit signals with a small power spectral density such that, the interference to other radio signals will be negligible, even if they lie within the same frequency band.

With the advances in integrated circuit technology made in the past years, the opportunity has come to use these signals also for civil communication, position location, and radar applications. However, the large signal bandwidth is still an obstacle when it comes to implementing low power devices that are simple and at the same time take full advantage of the capabilities of ultra-wideband radio. Therefore, practical systems cannot exploit all the benefits offered by UWB signals.

In this work the focus is on low-complexity receiver architectures for communication systems. These architectures are found by identifying the receiver tasks whose implementation is complex or which require a high signal-processing speed. Accordingly, a simple receiver should not perform channel estimation or equalization. As a consequence, the receiver must be noncoherent. This conclusion is confirmed by deriving the optimum (maximum-likelihood) receiver, under the assumption that the receiver has no information about the propagation channel. Many important properties of the noncohrerent receiver are discussed, such as sensitivity, vulnerability to narrowband interference, and robustness to synchronization inaccuracies. Furthermore, an approach for the robust design of a key system parameter, the integration duration, is derived for some simplifying assumptions on the propagation channel.

A meaningful extension of this simple noncoherent receiver is obtained by assuming that the receiver knows the power delay profile of the propagation channel. The resulting maximum-likelihood receiver is derived and its performance is compared with that of the simpler receiver which has no channel information. Another extension is to use more than one receiver antenna, each, leading to a separate noncoherent receiver. The reasonable distance between the receiver antennas is discussed, i.e., whether micro diversity or macro diversity can be exploited. The optimum scheme to combine the individual received signals is derived and the performance of this optimum scheme is compared with the suboptimum selection-combining scheme.

A totally different approach to simplify receivers consists in designing the transmit signal such that the signal acquisition gets simple. A novel multiple access scheme for uncoordinated users, called rate division multiple access, follows this idea.

Kurzfassung

Ultra breitbandige (UWB) Kommunikationssysteme verwenden Funksignale deren Bandbreite zwischen einigen hundert MHz bis zu einigen GHz liegt. Erstmals wurden derart breitbandige Funksignale für militärische Radaranlagen verwendet. Die Gründe für die Benützung grosser Signalbandbreiten sind vielfältig: Die resultierende hohe zeitliche Signalauflösung ist Voraussetzung für Radar mit hoher Genauigkeit. Bei Funkkanälen mit dichter Mehrpfad-Ausbreitung führt Sie zu einer entsprechend grossen Mehrpfad-Diversität, welche die Robustheit und Kapazität des Kommunikationskanals verbessern kann. Die grosse Bandbreite erlaubt es ausserdem, Signal mit einer geringen spektralen Leistungsdichte auszusenden, sodass die Interferenz auf Funksignale gering bleibt auch wenn diese im selben Frequenzband liegen.

In den letzten Jahren wurden auf dem Gebiet der Halbleitertechnik grosse Fortschritte in Richtung höher Schaltgeschwindigkeit bei gleichzeitig geringerer Leistungsaufnahme gemacht. Damit ist es möglich geworden, UWB Signale auch für Massenanwendungen einzusetzen. Dennoch ist die grosse Bandbreite von UWB Systemen nach wie vor ein Hindernis beim Bau von günstigen Geräten die gleichzeitig alle Vorteile von UWB Signalen auszunützen und wenig Energie verbrauchen. Deshalb können praktische Systeme nicht alle Vorteile gleichzeitig nützen, die durch die Verwendung von UWB Signal potenziell zur Verfügung stehen.

Diese Arbeit beschäftigt sich mit einfachen Empfängerarchitekturen für Kommunikationssysteme. Solch werden gefunden indem, an sich sinvolle aber aufwendige, Signalverarbeitungsschritte eines Empfängers identifiziert und vermieden werden. Einer der aufwendigsten Verarbeitungsschritte ist die Kanalschätzung und die Korrektur des Kanals durch einen Equalizer. Wird auf die Kanalschätzung verzichtet, so folgt, dass der Empfänger nichtkohärent sein muss. Diese Folgerung wird bestätigt durch eine mathematische Herleitung des optimalen bzw. Maximum-Likelihood-Empfängers der den Übertragungskanal nicht kennt.

Der nichkohärente Empfänger unterscheidet sich wesentlich vom kohärenten Empfänger in den Eigenschaften Sensitivität, Empfindlichkeit gegenüber schmalbandigen Störsignalen und der Empfindlichkeit gegenüber Ungenauigkeiten in der Synchronisation. Diese Eigenschaften werden theoretisch und/oder mittels Simulation untersucht. Beim nichtkohärenten Empfänger ist die sogenannte Integrationsdauer ein Schlüsselparameter. Dieser Parameter wird, für einige vereinfachende Annahmen über den Kanal, so gewählt, dass der Empfänger robust gegenüber Kanaländerungen ist.

Eine Erweiterung dieses einfachen nichtkohärenten Empfägners erhält man unter der Annahme, dass der Empfänger Kenntnis über das power-delay Profil der Kanalimpulsantwort besitzt und ausnützt. Der entsprechende Maximum-Likelihood-Empfänger wird hergeleitet. Eine andere Erweiterung des einfachen nichtkohärenten Empfängers besteht in der Verwendung von mehereren Empfangsantennen, von denen jede auf einen separaten nichkohärenten Empfänger führt. In diesem Zusammenhang wird die sinnvolle Distanz der Antennen untereinander diskutiert, bzw. ob Makro- oder Mikrodiversität genützt werden kann. Zudem wird das optimale Schema zur Kombination der Empfangssignale der einzelnen Empfänger hergeleitet und mit dem suboptimalen Selection-Combining-Schema verglichen.

Ein völlig anderer Ansatz zur Vereinfachung von Empfängern besteht in einer geziehlten Gestaltung des Sendesignal, sodass eine einfache Signalerfassung möglich ist. Ein entsprechendes neuartiges Zugriffsverfahren für unkoordinierte Nutzer wird vorgestellt.

Contents

1. Introduction

The development of ultra-wideband (UWB) radio technology started in the late 1960's, but for decades mainly focused on military RADAR (Radio Detection and Ranging) applications [4]. In the late 1990's the idea was born to use UWB radio signals for civil communications and position location applications. The extremely large bandwidth of UWB systems promises the following outstanding performance aspects: (i) The power spectral density (PSD) of UWB signals could be kept very low such that existing inband narrowband services would not be stronger affected by UWB signals than by any other unintentionally radiated radio signals, e.g., from a computer or other household appliances. (ii) Furthermore, the extremely large bandwidth would provide very high channel capacity, and thus enable multiuser communications at high data rates (iii) Also, this large bandwidth causes a large diversity which enables robust communication links. (iv) UWB signals can be generated as a sequence of ultra-short and modulated pulses. This method allows to circumvent up and down conversion, thus resulting in simple transmitter and receiver circuits. (v) Also the possibility was discussed that ultra short pulses, i.e., UWB pulses, are perfectly suited for high-precision position location.

Stimulated by these promised benefits, a first break-through for the success of commercial UWB applications occurred in 2002, when for the first time a radio spectrum administration allowed an appropriate frequency band to be used without a license [21]. As a result the research efforts in the field were increased and it soon became clear that the promised benefits cannot all be achieved at the same time. The reasons are that the large delay spread and high multipath resolution of the UWB radio channel not only cause the large diversity, but also make it hard to achieve data rates that approach the channel capacity. The large delay spread and temporal resolution of the channel require channel estimation, rake or equalizer architectures and accurate synchronization. Implementation of corresponding circuits for the ultrawide signal bandwidths is expensive, and the resulting circuits exhibit a high power consumption. Other effects of the channel, such as the occasional attenuation of the line-of-sight echo, turned out to be a problem for accurate position location. For these reasons it can be concluded that with state-of-the-art or even near-future technology, it will not be possible to achieve all the goals mentioned at the same time.

1.1 Concept of this Work

According to this insight the focus of this work is put on simple, low-power and robust receivers for low data-rate communication, i.e., this work does not consider methods that are particularly aimed to achieve high data rates. Simple receiver architectures can be found by getting aware of the receiver tasks that require complex and/or fast signal processing. These tasks are channel estimation, equalization, signal acquisition, precise synchronization, rake filtering, multiuser detection

and expensive demodulation of e.g. OFDM signals. A receiver type that works without these tasks is the noncoherent or energy collecting receiver for M-ary pulse position modulated (PPM) signals. The data rate that can be achieved with noncoherent receivers and M-ary PPM is investigated in [64], which mentions the noncoherent receiver concept for the first time in the UWB context. The simplicity and performance of the noncoherent receiver for 2PPM signals is discussed in [73, 71], in particular, an expression for the bit error probability (BEP) is derived, a simple acquisition and synchronization algorithm is proposed, and its high tolerance to synchronization inaccuracies of up to several nanoseconds is pointed out.

Complementary to the practical motivation of noncoherent receivers is a theoretical derivation which follows the approach of the generalized maximum likelihood (GML) receiver (GMLR). The fact that the noncoherent receiver is equivalent to the generalized ML receiver in the absence of channel information is pointed out in [9, 44]. Partial channel state information that can be obtained relatively easy is the power delay profile (PDP). A receiver architecture with an improved sensitivity over the GMLR can be achieved by deriving the ML receiver for the assumption that the PDP is known at the receiver. This receiver is called the maximum likelihood receiver with partial channel state information (MLRP).

Another tradeoff towards receivers with somewhat higher performance and complexity is to combine multiple noncoherent receivers to form an improved receiver. One of the main reasons why multiple antennas are proposed for narrowband systems is the increased diversity, which can be used to improve the link. However, UWB indoor channels offer already an inherently large frequency diversity such that further diversity improvement does not increase the link quality significantly [69]. These considerations are valid for so called small-scale diversity which is obtained by multiple antennas with an inter antenna spacing on the order of some centimeters to some tens of a centimeter. If however antennas are distributed over a larger range, e.g., over several rooms, then the shadow or large-scale fading effect causes an energy per received pulse that depends on the individual antenna position. This effect is called *large-scale diversity*. As the received energy is significant for the performance of a noncoherent receiver, it follows that noncoherent receivers can exploit large-scale diversity. A broad class of indoor applications allows the usage of multiple antennas with large distances between the elements only at either the receiver or the transmitter side, i.e., possible applications are of the multiple-input single-output (MISO) or single-input mulitple-output (SIMO) type. As this work considers the aspect of receivers, the attention is restricted to the application of noncoherent receivers in a SIMO configuration.

A receiver's complexity depends last but not least also on the modulation of the received signals. A modulation scheme that is much discussed in the context of UWB is called time-hopped pulse-position modulation (TH-PPM) and was proposed in [75]. This scheme is based on pseudo random time hopping sequences, which require a complex signal acquisition at the receiver. An alternative modulation scheme for uncoordinated multiuser access called rate division multiple access (RDMA) is proposed. In contrast to TH-PPM the RDMA scheme uses signals that have a deterministic and more regular structure and thus enable relatively easy signal acquisition at the receiver.

1.2 Outline and Notation

This work consists of two parts. Part I discusses Noncoherent UWB receivers in the Chapters 2 to 4. Chapter 2 gives an overview of the most important properties of the UWB indoor channel and is a basis to understand the subsequent chapters.

In Chapter 3 the noncoherent receiver architecture is motivated by practical arguments and by a detailed derivation of the GMLR based on a detection theoretic approach. Also the MLRP which forms an improvement over the GMLR is motivated from a practical and a theoretical point of view. For this purpose a simplified channel model is introduced that enables this derivation and that is close to realistic channel models at the same time. Furthermore, this chapter contains a derivation of various properties of the GMLR for binary PPM (2PPM) signals, e.g., the BEP and the sensitivity to narrowband interference (NBI). Also proposed is a method for a robust design of the integration duration, which is an essential parameter of the GMLR.

Chapter 4 is motivated by the potential of noncoherent receivers to exploit large-scale diversity, and discusses the application of noncoherent receivers in a SIMO system. The optimum scheme for combining noncoherent receivers in a SIMO scheme is derived and the corresponding performance is compared with that of a selection combining scheme.

Part II of this work considers the multiple-access scheme RDMA, which is an approach to reduce the receiver complexity. This subject is independent of the receivers discussed in Part I and is therefore treated separately.

A legend of the abbreviations, variables and mathematical symbols that are used in this work is provided in Appendix A.

Notation: Random variables are denoted by upper case roman letters, e.g., X. Variables and realizations of random variables are denoted by italic lower case letters, e.g., x. Accordingly, the realization of a random process $\mathrm{B}(t)$ is denoted as $b(t)$. Sets are denoted by calligraphic letters, e.g., $\mathcal{M}$. Vectors and realizations of vector-valued random variables are denoted by bold lowercase italic letters, e.g., $\boldsymbol{x}$, whereas random vectors are denoted by uppercase bold roman letters, e.g., $\mathbf{X}$. A list of mathematical symbols used in this work is given in Appendix B.

1.3 Contributions

The major contributions of this work are:

- Discussion on the appropriateness of representing UWB signals in complex baseband.
- Derivation of a convenient approximate expression for the BEP of the GMLR for 2PPM signals.
- A method for the robust design of the GMLR by proper choice of the integration duration.
- Computation of the sensitivity of the GMLR to narrowband interference and a comparison with the coherent ML receiver.
- Derivation of the ML receiver assuming knowledge of the channel's PDP and the definition of a channel model that enables this analytical derivation and is close to realistic models at the same time.
- Derivation of an approximation to the BEP of the aforementioned receiver.
- Derivation of the optimum combiner for SIMO systems with noncoherent receivers.
- Proposal of a novel multiple access scheme for uncoordinated users (RDMA).
- Derivation of optimum pulse rates for the users in a RDMA system.

Part I

Noncoherent Reception

2. The UWB Indoor Channel

In this chapter we consider the most important properties of the UWB indoor channel, which are necessary to understand the requirements to the transmitter and the receiver of an indoor communication system. When writing about channels, implicitly indoor channels are meant. Originally the bandwidth of UWB signals was thought to start at several 100 MHz and end at several GHz [76]. However, a first regulation for the use of UWB signals limits the signal bandwidth to the range between 3.1 and 10.6 GHz [21], in addition, this regulation limits the signal bandwidth to a minimum of 500 MHz. According to this, the bandwidth of UWB signals is considerably larger than for narrowband or even wideband signals. Therefore, channel models for narrowband and wideband channels are not suited to describe UWB channels, but provide some fruitful modelling approaches for the UWB channel. A thorough overview on narrowband and wideband channels is given in [26].

In the past few years considerable effort has been undertaken to study the UWB channel in home, office and industrial environments [11, 10, 38, 62, 23, 24, 60, 29, 8, 63]. All these contributions investigate exclusively time invariant channels. The speed at which a channel impulse response (CIR) varies over time for typical UWB indoor channels is investigated in [59]; it turns out that this speed is small enough to justify the assumption of the UWB channel to be quasi static.

The following sections give a summary of the most important UWB channel features and a basis to understand the contributions of this work. Section 2.1 explains propagation effects of UWB pulses in indoor environments. Section 2.2 presents measures that are used to quantitatively characterize deterministic and stochastic properties of channel impulse responses. In Section 2.3 the major differences between the UWB and the narrowband channels are pointed out. A discussion whether complex baseband or passband representation should be used is given in Section 2.4. Section 2.5 gives a conclusion.

2.1 Indoor Propagation of UWB Pulses

We assume that an isotropic, i.e., non-directed, transmitter and receiver antenna are placed within a room and the antennas are in line-of-sight (LOS) to each other. A short pulse $p(t)$ with a duration of $T = 1$ ns is fed to the transmitter antenna. The bandwidth B of this pulse is approximately the reciprocal value of the pulse duration, i.e., $B = 1/T$. The pulse results in an electromagnetic wave that propagates from the transmitter antenna with speed $c = 3 \cdot 10^8$ m/s and has the length $l = cT = 30$ cm. One can imagine the energy of the propagating wave to be concentrated between the surface areas of two concentric spheres, with the transmitter antenna located in their center. The radii of the spheres have the constant difference l and grow with speed c.

A portion of the energy of this spherical wave is captured by the receiver antenna and generates a pulse, called the *LOS echo*, at its feed point. Where the wave impinges on an obstacle, it is reflected or scattered. Portions of these reflected or scattered waves will be captured by the receiver antenna and cause so called *NLOS echoes* at its feed point. Clearly, multiple reflections can occur which cause futher echoes. The energy of an echo decays the more, the longer it takes to arrive at the receiver. The delay between the rising edge of the LOS echo and the falling edge of the latest considered echo is called *delay spread*. The *excess delay* is counted from the rising edge of the LOS echo, i.e., points on the time axis that are on the left or on the right of the rising edge correspond to a negative or positive excess delay, respectively. Typically the energy of an LOS echo is larger than that of an NLOS echo, in this case we speak about an LOS channel. If the LOS path is obstructed such that the LOS echo is weaker than any NLOS echo we speak about an NLOS channel.

The pulse shape of the echoes differs strongly from the shape of the transmitted pulse $p(t)$. There are two reasons for this effect:

(i) The antennas are considered as a part of the radio channel. Practical antennas have a non-ideal, i.e., non- flat frequency characteristic, therefore, signal dispersion is introduced. As a consequence, the received signal component from an LOS path appears like an oscillating signal which is spread over several nanoseconds.

(ii) The geometry and the building materials of the reflectors and scatterers influence the shape of the corresponding NLOS echoes.

These two effects can be modelled by considering the echoes as sequences of weighted and tightly spaced replicas of the pulse $p(t)$, also called *multipath components*. Therefore, the term *multipath cluster* is synonymously used for the term echo [38].

In practice, several echoes can interfere with each other such that they are hard to be distinguished. As an example we consider some real CIRs that were recorded during a measurement campaign in an office building [38]. The measurements were made in the frequency interval from 1 to 11 GHz. A network analyzer was used for the channel sounding. Fig. 2.1 shows the corresponding CIR in the time domain, i.e., the inverse Fourier transform of the frequency spectrum that was recorded by the network analyzer. To reduce the signal bandwidth, a Kaiser window [25] with a -3 dB bandwidth of 2 GHz and a center frequency of $f_0 = 6$ GHz was applied before computing the inverse Fourier transformation. The CIR shows a strong LOS echo and some weaker echoes that stem from signal reflections. A corresponding CIR for an NLOS channel that was recorded in an office is shown in Fig. 2.2. It can be observed that the LOS echo is strongly attenuated, such that it is even weaker than the reflected echoes. In particular for the CIR of the NLOS channel shown in Fig. 2.2 individual echoes overlap such that it is not possible to clearly distinguish them.

2.2 Properties of the UWB Indoor Channel

In general the CIR of an UWB channel depends on many unknown parameters, the detailed geometry, the materials of the building, the relative position of the transmitter and the receiver within the building. It is therefore a complex task to predict properties of realistic CIRs. A common method to cope with this large set of unknown parameters is statistical channel modeling. According to this approach, a given CIR is considered as a realization of a random process; the properties of this process are described by a statistical channel model. The basic measures for UWB channels that are typically described by statistical models are given in this section. As a basis for the statistical analysis, typically two sets of CIRs are used to quantify channel properties. A first set of CIRs that

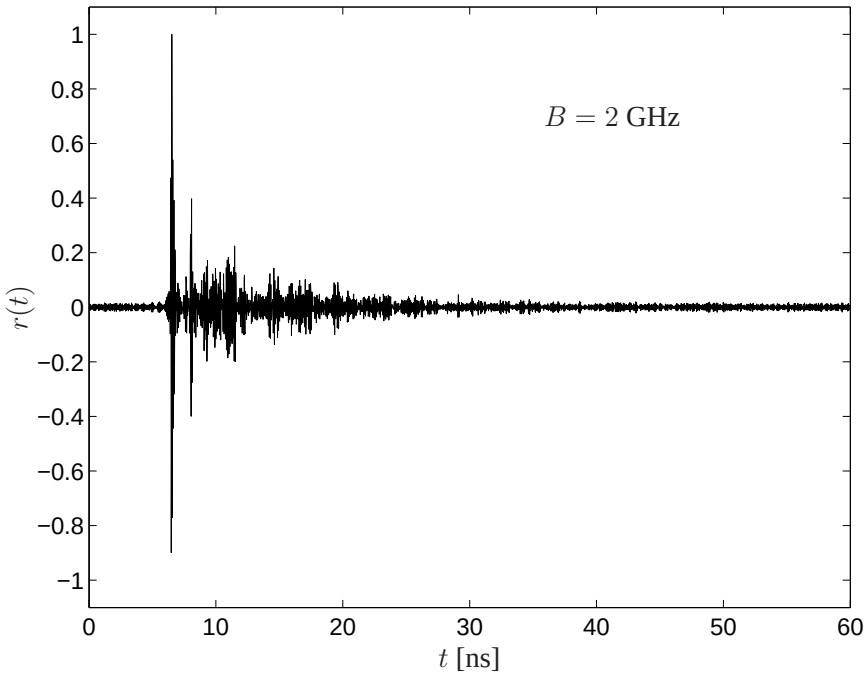

Fig. 2.1. Measured CIR of an LOS channel with bandwidth $B = 2$ GHz and center frequency $f_0 = 6$ GHz [*Measurement data obtained from IMST GmbH, Kamp-Lintfort, Germany*].

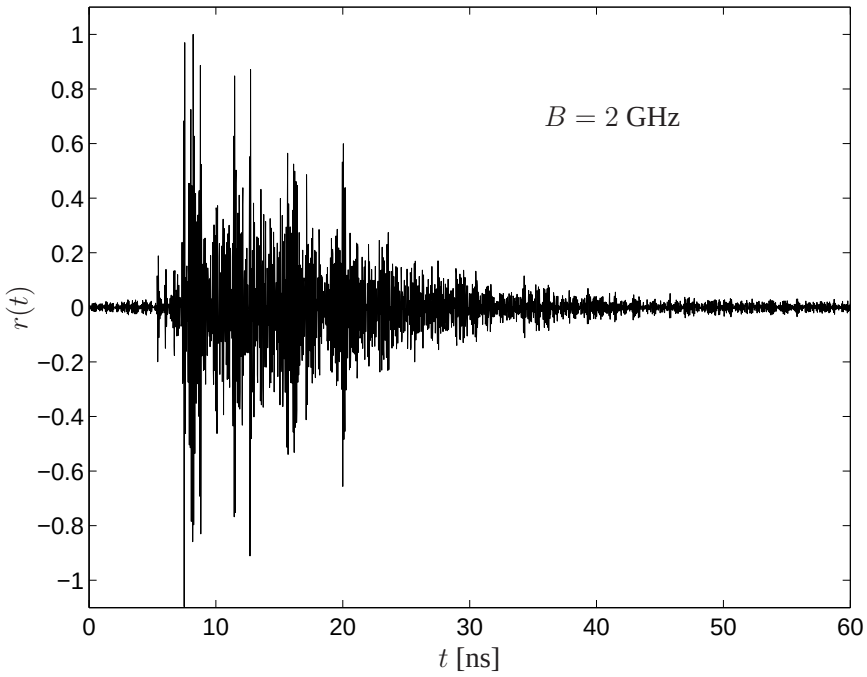

Fig. 2.2. Measured CIR of an NLOS channel with bandwidth $B = 2$ GHz and center frequency $f_0 = 6$ GHz [*Measurement data obtained from IMST GmbH, Kamp-Lintfort, Germany*].

vary only with large-scale movements (*large-scale effects*) and a second set of CIRs that vary even under small-scale movements (*small-scale effects*) of the antennas. These sets are: (i) a so called *large-scale set* $\mathcal{L}$ of CIRs that corresponds to a fixed transmitter position and various receiver positions that are several meters apart from each other; (ii) a so called *small-scale set* $\mathcal{S}$ of CIRs that

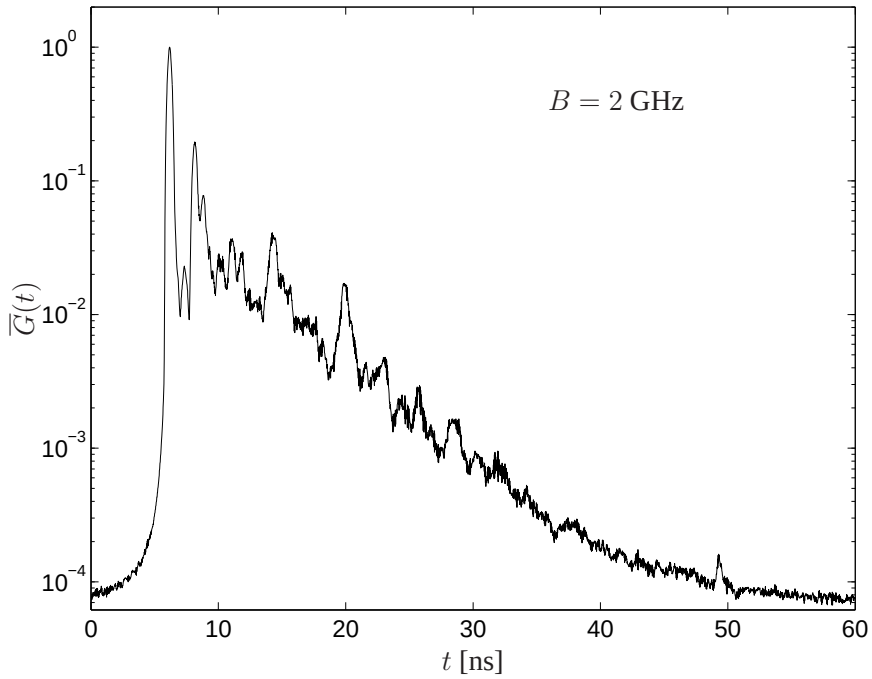

Fig. 2.3. APDP averaged over 900 LOS channels with bandwidth $B = 2$ GHz, and center frequency $f_0 = 6$ GHz, [*Measurement data obtained from IMST GmbH, Kamp-Lintfort, Germany*].

corresponds to a fixed position of the transmitter and various receiver positions, where the variable antenna positions lie within a small range, e.g., within half a square meter.

2.2.1 Average Power Delay Profile

The power delay profile (PDP) of a CIR $r_n(t)$ is defined as the square $r_n^2(t)$. The empirical average power delay profile (APDP) [38] is defined as the average over a set of PDPs,

$$\overline{G}(t) = \frac{1}{N} \sum_{n=1}^{N} r_n^2(t), \tag{2.1}$$

where $r_n(t)$ with $n \in \{1, \ldots, N\}$ are the elements of the small-scale set $\mathcal{S}$. This definition implies that the APDP is a large-scale property, i.e., it is approximately constant under small-scale movements.

A typical APDP for an LOS channel is shown in Fig. 2.3. The average is computed over a number of 900 CIRs that correspond to transmitter positions within a square of 30×30 cm. We observe some peaks at low excess delay and an approximately exponential decay at medium and large excess delay. The reason for the peaks is that individual echoes can be resolved; at larger excess delay the rate of echoes is increased such that individual echoes cannot be distinguished any more. The decay of the APDP can roughly be described by a linear regression line. As the APDP is represented in a semi logarithmic graph, the linear regression line corresponds to an exponential decay. Numerical values for the corresponding decay constant γ are specified in [37] and [23]. Fig. 2.4 shows the APDP for an NLOS channel. As explained above, we can observe that the first echo, i.e., the LOS echo has lower energy than the reflected echoes. The exponential decay of the APDP can be observed in this case as well. The APDP plays an important role in Section 3.2.3.

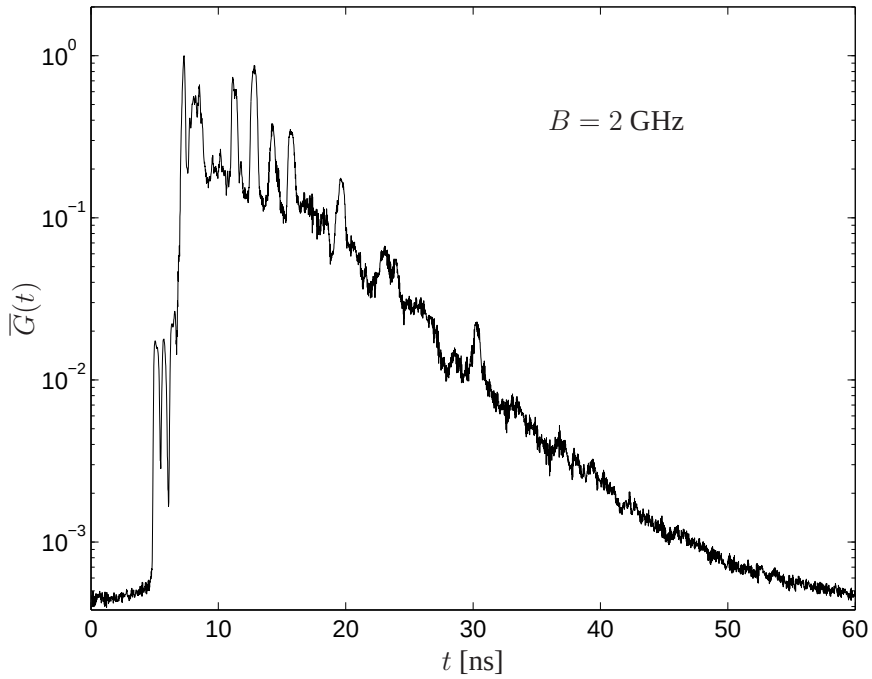

Fig. 2.4. APDP averaged over 900 NLOS channels with bandwidth $B = 2$ GHz and center frequency $f_0 = 6$ GHz, [*Measurement data obtained from IMST GmbH, Kamp-Lintfort, Germany*].

2.2.2 Path Gain

The path gain, α, is roughly spoken the ratio of the energy E_r of the received pulse over the energy E_t of the transmitted pulse and is an important measure for the link budget analysis. The path gain is aimed to reflect shadowing phenomena caused by obstacles. As shadowing is typically a large-scale effect, it is computed by averaging out the small-scale effects, hence, the empirical path gain is defined as the average ratio

$$\alpha = \frac{1}{N} \sum_{n=1}^{N} \frac{E_{r,n}}{E_t} \tag{2.2}$$

where $E_{r,n}$ is the energy of the CIR $r_n(t)$, and $r_n(t)$ for $n = 1, \ldots, N$ are the elements of the small-scale set $\mathcal{S}$. Note that the path gain is affected by the *large-scale fading*.

The reciprocal value of the path gain α is called path loss α^{-1}. A statistical model for the path loss as a function of the transmitter-to-receiver distance d is given in [24] by

$$\alpha^{-1}(d) = \alpha_0^{-1} \left(\frac{d}{1\text{m}} \right)^{\nu} s, \tag{2.3}$$

where α_0 is the free space path gain for a transmitter to receiver distance $d = 1$ m. The equivalent of the constant α_0 expressed in units of dB is denoted as $A_0 = 10 \log_{10}(\alpha_0)$. The factor s is denoted shadow fading term; it is a lognormal distributed random variable, i.e., its equivalent in units of dB, $S = 10 \log_{10}(s)$, is Gaussian distributed with variance σ_S^2 [24]. The variance σ_S^2 is again considered as a random variable. It is assumed that each building is characterized by a specific realization σ_S^2.

The constant ν is denoted *path loss exponent*. It equals 2 for free space propagation, is larger than 2 for most indoor scenarios and smaller than 2 e.g. for hallways in which a waveguide effect occurs. The same statistical path loss model was introduced in [55] for narrowband channels; it was shown to also be suited for UWB channels in [24].

2.2.3 Amplitude Distribution

In general, the amplitude of a CIR $r_n(t_0)$ at a given excess delay t_0 is the superposition of multiple received echoes. There is much discussion in the literature about the number of echoes that contribute to the CIR. Some authors report of a single echo only and justify this with the high temporal resolution of UWB signals, while others assume a large enough number of echoes such that with application of the central limit theorem it can be assumed that $r_n(t_0)$ is the realization of a Gaussian random variable. Similarly different are the reported amplitude distributions: Nakagami [10, 11], Ricean with low K value (i.e., almost Rayleigh) [38], lognormal distributed [23, 33]. [2] reports about a Weibull distribution of the PDP. A possible reason for these different findings is given in [61], where from a set of distributions the one is chosen with the minimum Kullback distance to the amplitude statistics of the observed CIRs. It turns out that depending on the excess delay, the amplitude statistics is either more Rayleigh, lognormal or Weibull distributed.

2.2.4 Average Energy Spectrum

Now we consider the energy spectral density of CIRs. These energy spectra show strong attenuation for some, and weaker attenuation for other signal frequencies. Computing the average energy spectral density over a sufficiently large set of CIRs, one would expect a constant energy spectral density for all signal frequencies under observation. However, according to [29, 38] this is not the case. In [38] the average energy spectrum was evaluated for a measured small-scale set of CIRs. Numerical fitting unveiled a f^{-m} dependency where the m-parameter varies between 1.6 and 2.8 for different environments. The reason for this effect lies in antenna properties, a detailed explanation is provided in [37] and [38]. Section 3.5 gives a short discussion on the impact of this effect on the performance of a noncoherent receiver. In the literature about receivers for UWB signals this aspect has been ignored so far.

2.2.5 Small-Scale Fading

The term *small-scale fading* denotes the effect of fluctuating received energy per pulse, when the receiver or the transmitter is moved within a *small* area. Hence, the small-scale fading statistics together with the large-scale fading statistics of the path gain provide the total statistics of the received signal energy.

The small-scale effect can be explained by assuming that echoes form different directions arrive at the same time at the receiver antenna; the superposition of these echoes results in the received signal. When the position of the receiver antenna is shifted, then the relative arrival times of the echoes change so that the superposition of the echoes results in a changed shape of the received pulse. As explained, an echo comprises multipath components. For signals with a large bandwidth and thus with a large multipath resolution, the number of resolvable multipath components and the number of resolvable echoes themselves is large. This effect is known as *multipath diversity*, in the frequency domain this effect is called *frequency diversity*. The multipath components of different echoes that impinge at the receiver at the same delay are superimposed in a constructive or destructive way. However, as the channel's temporal resolution is high it follows that the number of echoes and of their resolvable multipath components is large. Thus, the constructive and destructive interference effects at different time instances cancel each other out to a large degree so that the energy per received pulse, E_r, is almost independent of small scale variations of the antenna positions; hence, only minor small-scale fading is observed for UWB channels, [53, 38].

In a communication system deep fades reduce the performance (e.g. the bit error rate) below the average performance level. Depending on the fading statistics, the transmitted signal power must be increased to compensate for this performance reduction. This increase in signal power is called *fading margin*. For UWB signals propagating in indoor environments, fading margins have been reported with small values between 1 and 5 dB [38, 53, 77, 22].

In narrowband systems where multipath or frequency diversity is missing, destructive superposition of echoes can result in very deep fades. Narrowband communication systems require a fading margin of up to 35 dB [53].

2.3 Basic Difference Between Narrowband and UWB Channels

As mentioned above, signals with very large bandwidth offer the ability to highly resolve individual echoes and their multipath components of a CIR. This ability, called *multipath resolution*, has several effects that narrowband channels with their much lower temporal resolution do not show:

(i) Because the CIR of a channel is determined by the position of the transmitter and the receiver antennas and by the propagation environment, the high temporal resolution implies that the CIR is like a specific signature of a channel. Hence, for different channels, like the individual subchannels of a multiple-input multiple-output (MIMO) channel, the CIRs are only weakly correlated.

(ii) As mentioned in the preceding section, the small-scale fading of the received energy is a minor effect. In contrast the received energy of a narrowband signal can be completely canceled out due to destructive overlap of multiple echoes.

(iii) The CIR has a complex signature and therefore many parameters are required for its description. This makes the estimation of a CIR expensive.

Consequences of these features for SIMO communication over the UWB channel and with noncoherent receivers are discussed in Chapter 4.

2.4 Complex Baseband or Passband Representation

Narrowband and wideband channels are usually represented in the complex baseband (see Appendix D), for which there are three reasons:

(i) Communication systems are typically described in the complex baseband domain. This description is more compact than the passband representation because the procedure of up and down conversion in the transmitter and the receiver, respectively, can be dropped.

(ii) Particularly for simulation purposes there is an advantage from the reduced number of signal samples that can be taken for the complex baseband representation.

(iii) The up and down conversion in communication systems is equivalent to the passband-to-complex-baseband-transformation and vice versa. Communication systems with up and down conversion allow the symbol clock to be locked to the carrier phase, i.e., there is no drift between carrier phase and symbol clock. This drift is assumed to be zero in most of the literature about digital communications, e.g., in [49, 41]. When the drift is zero it can formally be ignored. This results in the simple representation of digitally modulated complex baseband signals given in [49] and [41].

In this work we consider simple UWB transmitters that unlike conventional transmitters directly generate the transmitted signal as a sequence of UWB pulses, see Chapter 3.1. This approach implies that a carrier frequency, which must be specified for the complex baseband transform, is

not uniquely defined. In order to describe the signals in complex baseband, one could introduce a virtual carrier signal with an arbitrary frequency. However, in a realistic model, the symbol clock would not be locked to this virtual carrier's phase; this would have to be taken into account by a phase term that changes randomly for each transmitted pulse. Note further that UWB signals have a bandwidth that is on the order of their center frequency. Thus, a UWB signal in complex baseband representation requires still a relatively high sampling rate for a discrete-time representation. Because of this and primarily because of the random phase term to be considered in the complex baseband representation of pulse UWB signals, in this work, we choose the passband representation of signals.

2.5 Conclusion

The statistical channel modelling approach discussed in this chapter is based on the time domain representation of signals. An approach that has gained less attention models statistical channel properties in the frequency domain [31, 67, 30].

The subsequent chapters of this work contain simulation results and numerical examples. The CIRs involved in the corresponding computations are taken from a set of channel realizations included in the electronic reference [23], which are generated by the statistical channel model described in [23]. This model is aimed to support the development of the physical layer standard IEEE802.15.3a and is thus widely used. In this model, the distribution of the amplitude of the discrete time CIRs is lognormal. The arrival time of pulses is modelled in accordance to the Saleh-Valenzuela model [58]. The path gain model used in this work is adopted from [24].

3. Noncoherent Receivers

In the literature, there exist different definitions for coherent or noncoherent receivers. In this work a coherent receiver is distinguished from a noncoherent receiver through its ability to detect the sign of a received pulse, or the phase of a received pulse in the case of complex baseband demodulation. For a classical coherent narrowband receiver this means that the synchronization with the carrier signal must have a timing error $\ll 1/(2f_0)$, where f_0 is the carrier frequency. The same holds for UWB receivers, where f_0 is the center frequency of the UWB signal; e.g., an admissible timing error of the symbol synchronization of 0.01 ns is specified in [42]. Note, that in this work UWB signals are represented as passband signals rather than as complex baseband signals which is usual in the digital communications literature, see 2.4. Therefore, a carrier signal is not involved, which means that carrier synchronization is neither required nor possible. A receiver for carrier-less pulsed UWB signals needs to synchronize only to the symbol clock.

A noncoherent receiver cannot detect the sign or the phase of a pulse, therefore its decision is solely based on the amount of energy that is captured per symbol. This must be taken into account when choosing a modulation scheme for noncoherent reception.

Noncoherent radio receivers have a long history. They were used since the beginning of radio communications because of their low complexity. Later, noncoherent receivers were employed for interception and RADAR applications [65, 68, 19, 45]. Noncoherent low complexity architectures were desirable as long as the technology was not advanced enough for an efficient implementation of more powerful coherent receiver architectures. Today we face a similar situation when using UWB signals for communication purposes, because the technology is not advanced enough to enable cheap low-power coherent receivers. A first paper that mentions noncoherent receivers for UWB communication is [64]. It points out that this receiver type operates without an estimate of the received pulse shape and investigates the capacity of a system that includes an M-ary PPM transmitter and the corresponding noncoherent receiver. The same authors considered noncoherent receivers for UWB peer-to-peer networks [34], and investigated upper and lower performance bounds for multiuser interference mitigation techniques. An analytical derivation of the BER of the noncoherent receiver for 2PPM signals is given in [71] and in [52], details are presented in Section 3.3. The optimum detection threshold for the reception of on-off keyed (OOK) signals and the corresponding BER is derived in [48]; this paper considers noncoherent receivers for parallel UWB channels to achieve higher data rates.

A receiver type that from its concept is between the correlation receiver which is coherent, and the noncoherent receiver is the transmitted reference receiver [27], [80]. The corresponding transmitter emits a reference pulse prior to each data bearing pulse. The receiver uses the reference pulse as an estimate of the channel impulse response and as a correlation template to coherently receive the subsequent data bearing pulse. The major disadvantage of the transmitted reference

receiver is that it requires a mechanism to delay the received reference pulse for some tens of a nanosecond. For this task delay lines are proposed, however, an elegant and easy to integrate way to implement this has not been suggested up to now. An exception is short range communication over a few meters only. In this case, the delay spread of the CIR is a few ns only such that a reference pulse delay of some ns is sufficient to avoid ISI. A delay of a few ns can, e.g., be realized with relatively short delay lines.

A hybrid of the noncoherent and the coherent receiver has been investigated in [62]. It is assumed that a part of the received pulse shape is perfectly known, while the rest is unknown. The energy of the known part is received coherently with a rake, while the remaining energy is captured noncoherently by energy collection. The considered modulation scheme is M-ary PPM. It is shown that a receiver with close to full-rake receiver performance typically needs to estimate a few channel taps only.

In this chapter only noncoherent receivers for 2PPM signals are considered; higher order modulation would require an even more intricate mathematical treatment and therefore go beyond the scope of this work. The signal model is presented in Section 3.1. Two types of noncoherent receivers are derived in Section 3.2 on the basis of classical results from detection theory:

(i) The generalized maximum likelihood receiver (GMLR) is derived, which assumes no side information on the channel. A similar but less in-depth derivation of this GMLR can be found in [9] and [44].

(ii) Channel parameters that can be estimated with relative ease are the instantaneous average power of the received impulse response. Optimum exploitation of this channel state information in the ML sense leads again to a noncoherent receiver type, which in contrast to the GMLR, performs a weighting of the received signal. This receiver is called the maximum likelihood receiver for partial channel state information (MLRP). A channel model that has the APDP as an explicit parameter is introduced and, based on this the MLRP is derived. It turns out that this receiver is a generalization of the GMLR.

The bit error probability (BEP) of the GMLR and the MLRP is derived in Subsection 3.3 and subsection 3.3.2, respectively. For the GMLR, an exact as well as an approximate expression for the BEP is given. The latter allows better insight into the principal mechanisms that determine the BEP. The BEP of the coherent ML receiver (MLR) is given for reference and is compared with the BEP of the GMLR and the MLRP. The basic difference and similarities between the different receiver architectures are discussed. To derive the BEP of the MLRP analytically we make a simplification, which results in an approximate expression for the BEP. This expression is the more accurate, the more the energy of the received pulses is spread over time, i.e., the longer the channel delay spread is. However, for channel delay spreads of typical indoor UWB channels, which is on the order of some tens of a nanosecond, this approximate expression is still to inaccurate to be useful. For a more precise determination of the BEP, numerical evaluations can be perform, e.g, by simulation.

A key parameter in the design of the GMLR is the length T_I of the time window during which the energy of the received signal is collected. Section 3.4 proposes a design approach that minimizes the maximum BEP for a given set of received pulse shapes. The impact of the signal bandwidth on the GMLR is discussed in Section 3.5. It is shown that an optimum bandwidth exists if the $1/f$ path loss characteristic explained in Chapter 2 is assumed. A measure for the sensitivity to narrowband interference (NBI) is derived in Section 3.7. Comparison of the GMLR with the MLR shows that the latter exhibits much better immunity to NBI. The effect of timing jitter on the BEP is documented in Section 3.8 for the GMLR and the MLR. In supplement to the theoretical

motivation of the noncoherent receivers, Section 3.9 gives some practical arguments for using the GMLR or the MLRP instead of the MLR.

In Section 3.2 and 3.3 extensive use is made of the complex baseband transform. We switch between two representations because the channel and the considered receivers are given in passband representation, however, to do a compact mathematical representation of the involved passband stochastic processes we transform them into complex baseband. To prepare this, Appendix D reviews in detail some rules for the baseband transform which are used to prove further rules that could not be found in the literature.

3.1 Received-Signal Model for 2PPM Signals

The transmitter modulates the symbol sequence $\langle a_k \rangle$ with $a_k \in \{0, 1\}$, such that each symbol determines the position of one UWB pulse. The shape of an individual pulse is defined by $g(t)$, which is the impulse response of an ideal bandpass filter with center frequency f_0 and bandwidth B. The pulse $g(t)$ has energy $2B$, i.e., $\|g\|^2 = \int_{-\infty}^{\infty} g^2(t)\,dt = 2B$. The choice of an ideal bandpass filter $g(t)$ is made, because in contrast to an implementable but more complex filter, the ideal bandpass filter results in simpler analytical expressions for the signals involved in the receiver. From [71] we observed that the receiver characteristics will change within a certain range when another, more realistic bandpass filter is assumed. The transmitted signal is of the form

$$u(t) = \sqrt{\frac{E_t}{2B}} \sum_{k=0}^{K-1} c_k\, g(t - kT - a_k \Delta_T) \tag{3.1}$$

and represents a data block which consists of K data symbols. The time interval available for the transmission of an individual symbol is T. The corresponding data symbol a_k determines whether the pulse is transmitted at the beginning of this interval or with a time offset Δ_T, with $\Delta_T \leq T/2$.

The energy per transmitted pulse is E_t. The sequence $\langle c_k \rangle,\ c_k \in \{-1, +1\}$, is an i.i.d. pseudo-random binary sequence that randomizes the polarity of the transmitted pulses to smoothen the power spectrum of the signal $u(t)$. Note that the power spectrum of a 2PPM signal shows spectral lines, if however the polarity of each pulse is randomly chosen with equally probable positive and negative signs, then the power spectrum is proportional to the energy spectrum of an individual transmitted pulse $\sqrt{E_t/(2B)}g(t)$. [74] discusses requirements to signals that have a power spectrum that is smooth in the sense of the FCC's emission rules [21]. According to this, 2PPM signals with a symbol rate higher than 1 MHz can exploit the power limit of -41.25 dBm/MHz only if polarity randomization is used. The sequence $\langle c_k \rangle$ has no impact on the receiver's design or performance, as we consider noncoherent receivers which ignore the pulse polarity.

To maintain the orthogonality of the received symbols and to prevent intersymbol interference it is required that Δ_T and $T - \Delta_T$ exceed both the maximum channel delay spread τ_c. Note that this condition limits the maximum data rate to $1/(2\tau_c)$ for 2PPM. The signal $b(t)$ is the received pulse shape and represents the combined response of transmitter filter $g(t)$, transmitter antenna, propagation channel, and receiver antenna [23], and can be described by any channel model mentioned in Chapter 2. Note that because of the wide bandwidth, the received pulse shape is not only influenced by the transmitter filter and the channel impulse response but also by the transmitter's and receiver's amplifiers and antennas. For this and various other reasons, channel models for the UWB channel include the characteristic of the transmitter and receiver antenna. We assume that the *channel impulse response* (CIR), $b(t)$, corresponds to this convention.

We assume the received pulse to have the same shape as $b(t)$, because we assume the signal at the transmitter antenna feedpoint and the impulse response of the receiver frontend to be ideal bandpass impulse responses with signal bandwidth B. Note that the support time of the CIR is infinite in theory, because of the strictly bandlimited transmitted pulse, $g(t)$. The bandwidth of $g(t)$ is $B \gg 1/\tau_c$ we can therefore assume by approximation that the support time of the CIR is equal to the channel delay spread τ_c. The signal that appears at the feed point of the receiver antenna and that corresponds to the symbol a_k is

$$r(a_k, t) = c_k b(t - kT - a_k \Delta_T), . \tag{3.2}$$

This notation shows that the received signal depends on the transmitted symbol a_k. Subsequently, the argument a_k is omitted where the context does allow this, i.e., we write $r(t)$ instead of $r(a_k, t)$. The energy of the received pulse within its support interval $[0, \tau_c]$ is

$$E_r = \int_0^{\tau_c} b^2(t)\, dt. \tag{3.3}$$

We define the path gain α as the ratio of the received to the transmitted energy by

$$\alpha = \frac{E_r}{E_t}. \tag{3.4}$$

This ratio incorporates both the small-scale and the large-scale fading effect.

3.2 Derivation of Noncoherent Receivers from Detection Theory

We consider the binary detection problem that corresponds to the type of modulation and channel described above from a detection theory perspective. The modulation parameters T and Δ_T are chosen such that ISI is avoided and that the received symbols are orthogonal; this allows us to derive the receiver by solely considering the reception of a single symbol, a_k. The symbol a_k is mapped by the 2PPM transmitter and the propagation channel to the received signal, $r(a_k, t)$, which depends on the transmitted symbol, on the modulation details and on the actual received pulse or channel realization, see (3.2). For simplicity and where an easy understanding is still possible, the symbol $r(t)$ is synonymously used for $r(a_k, t)$. $r(a_k, t)$ is a realization of the stochastic process $\mathrm{R}(a_k, t)$. The receiver adds a realization $n(t)$ of the noise process $\mathrm{N}(t)$ to the received signal $r(a_k, t)$ and bases its decision $\hat{a}_k \in \{0, 1\}$ on the sum signal $y(t) = r(a_k, t) + n(t)$, where the observation time interval is $[kT, kT+T]$. The power spectrum of the noise process $\mathrm{N}(t)$ is nonzero and constant only within the signal bandwidth and zero outside. The mappings from the transmitted symbol to the symbol decision at the receiver are formally indicated by

$$a_k \in \{0, 1\} \overset{\text{Modulator and channel}}{\longmapsto} r(a_k, t) \overset{\text{Additive noise}}{\longmapsto} r(a_k, t) + n(t) \overset{\text{Detector}}{\longmapsto} \hat{a}_k \in \{0, 1\}.$$

We define the space of received signals $\mathcal{R}$, which is the set of all possible received signals $r(a_k, t)$ for $a_k \in \{0, 1\}$ and all possible realizations $b(t)$ of the received pulse shapes. Furthermore, we define $\mathcal{Y}$ as the set of all observable signals $y(t)$. Not that the functions in $\mathcal{R}$ and $\mathcal{Y}$ are defined only within the interval $[kT, kT + T]$, i.e., for the time interval when the symbol a_k is being transmitted.

To describe this system in terms of detection theory we adopt the notation used in [66]. The hypothesis H_0 assumes that $a_k = 0$, while hypothesis H_1 assumes that $a_k = 1$. The details of

the modulator and the actual pulse shape $b(t)$ are formally contained in the mapping $\mathbf{\Theta}$ which maps the symbol a_k to the received signal space $\mathcal{R}$. We define two subspaces, $\mathcal{R}_0$ and $\mathcal{R}_1$, of the received signal space $\mathcal{R}$; these subspaces are spanned by all possible received signal realizations $r(a_k, t)$ if hypothesis H_0 or H_1 is true, respectively. Note that the 2PPM scheme presented in Section 3.1 guarantees that $\mathcal{R}_0 \cap \mathcal{R}_1 = \{\}$ because of the particular parameter choice that satisfies $T - \Delta_T,\ \Delta_T \geq \tau_m$ and thus, guarantees orthogonality of the received symbols. The observation $y(t)$ is the sum of any element of $\mathcal{R}$ added with any realization $n(t)$ of the receiver noise and lies within the received signal space $\mathcal{Y}$. Based on the observation $y(t)$ is the decision whether hypothesis H_0 or H_1 is true. These three mappings are expressed by the formulas

$$\begin{aligned} a_k \in \{0,1\};\ a_k &\xmapsto{\mathbf{\Theta}} r(a_k,t); & r(a_k,t) &\in \mathcal{R} \\ r(a_k,t) &\xmapsto{\text{Channel noise}} y(t); & y(t) &\in \mathcal{Y} \\ y(t) &\xmapsto{\text{Detector}} \hat{a}_k; & \hat{a}_k &\in \{H_0, H_1\}. \end{aligned}$$

The detector must separate the observation space into two regions that correspond to hypotheses H_0 and H_1. The decision is based on whether the observed variable is in the one or the other region. When the random noise process $\mathbf{N}(t)$ is turned off, the observation space $\mathcal{Y}$ and the parameter space $\mathcal{R}$ are identical. In this case, a correct decision is always possible because $\mathcal{R}_0$ and $\mathcal{R}_1$ are disjoint.

We distinguish three degrees to which the channel impulse response is known to the receiver:

(i) The receiver can measure $b(t)$ perfectly. It is well known that in this case the Maximum Likelihood (ML) receiver is feasible and corresponds to the correlation or matched-filter receiver, which belongs to the class of coherent receivers, see [39, 12, 15, 53].

(ii) The receiver cannot estimate the received pulse $b(t)$ and a statistical description of the corresponding process $\mathrm{B}(t)$ is not available either. In [66] two approaches are proposed for the corresponding type of detection problem. The uniformly most powerful (UMP) detector, which is for any received pulse $b(t)$ as least as good as the ML receiver with perfect channel knowledge. Unfortunately the UMP test does not exist for this problem. This is because the derivation of the corresponding ML receiver shows that to minimize the BEP perfect channel knowledge is required. The other proposal is to use a Generalized Maximum Likelihood (GML) approach. The basic idea behind this is to use the noisy received signal $y(t)$ as if it was a perfect estimate for the noiseless signal $r(t)$. A detailed description of this approach and the derivation of the corresponding receiver are given in Subsection 3.2.2. This approach results in a very simple noncoherent receiver, the so called energy collecting receiver.

(iii) The receiver knows some statistical properties of the CIR, which can be interpret as partial channel state information. An ML receiver is derived in 3.2.3 for the case where the receiver has knowledge about the channel's APDP.

The detection problem (i) arises due to the non-deterministic mapping of the received signal $r(t)$ to the observation $y(t)$, this mapping consists in the addition $y(t) = r(t) + n(t)$. The detection problems (ii) and (iii) belong to the class of composite hypothesis testing problems, the reason for classifying them as such is that there are two non-deterministic mappings involved, namely the convolution with the unknown channel $b(t)$ and the addition of the noise signal $n(t)$ [66].

To prepare an easy derivation of the GML receiver and the ML receiver for partial channel state information, an orthogonal expansion of the involved signals is introduced similar as in [66, 39, 49]. As no ISI occurs, we are allowed to derive the mentioned receivers by only considering the time interval $[kT, kT + T]$ during which the symbol a_k is conveyed.

3.2.1 Orthogonal Signal Expansion

An arbitrary set of orthonormal basis functions $\phi_n(t),\ n \in \{1,\ldots,N\}$ is assumed that spans the signal space $\mathcal{Y}$ of the involved signals $r(a_k,t)$, $n(t)$, and $y(t)$, which have a finite one-sided bandwidth B. Therefore, the signal space dimension N can be finite. The assumption of a finite signal bandwidth implies that the corresponding signals have an infinite support in the time domain. Despite of this, we assume that these signals are nonzero only within the time interval $[kT, kT+T]$. This assumption represents a good approximation because the bandwidth B is typically more than ten times larger than the reciprocal of the considered time interval T. The orthogonality of the basis functions is expressed by the formula

$$\int_{kT}^{kT+T} \phi_n(t)\phi_m(t)\,dt = \delta_{m,n},$$

with $\delta_{m,n} = 0$ for $m \neq n$ and $\delta_{m,n} = 1$ otherwise. A compact notation is obtained by collecting all basis functions $\phi_n(t)$ into a vector $\boldsymbol{\phi}(t) = [\phi_1(t),\ldots,\phi_N(t)]^T$; with this we can write

$$r(a_k,t) = \boldsymbol{\phi}^T(t)\,\boldsymbol{r}(a_k), \qquad \text{with} \qquad \boldsymbol{r}(a_k) = \int_{kT}^{kT+T} \boldsymbol{\phi}(t)\,r(a_k,t)\,dt, \tag{3.5}$$

$$y(t) = \boldsymbol{\phi}^T(t)\,\boldsymbol{y}, \qquad \text{with} \qquad \boldsymbol{y} = \int_{kT}^{kT+T} \boldsymbol{\phi}(t)\,y(t)\,dt, \tag{3.6}$$

$$n(t) = \boldsymbol{\phi}^T(t)\,\boldsymbol{n}, \qquad \text{with} \qquad \boldsymbol{n} = \int_{kT}^{kT+T} \boldsymbol{\phi}(t)\,n(t)\,dt. \tag{3.7}$$

The noise process The $\mathbf{N}(t)$ has one sided PSD N_0 and one sided bandwidth B. Hence, the components of the noise vector process $\mathbf{N}$ are statistically independent and identically distributed zero mean and real gaussian random variables with variance N_0B. With these properties, the PDF of $\mathbf{N}$ is given by

$$f_{\mathbf{N}}(\boldsymbol{n}) = \frac{1}{\sqrt{2\pi N_0 B}^N}\, e^{-\frac{\boldsymbol{n}^T\boldsymbol{n}}{2N_0B}}. \tag{3.8}$$

The introduced signal expansion is a linear operation which leads to the equivalence

$$y(t) = r(a_k,t) + n(t) \quad \Longleftrightarrow \quad \boldsymbol{y} = \boldsymbol{r}(a_k) + \boldsymbol{n}.$$

The vector $\boldsymbol{y}$ takes the role of the observation variable and the basis function vector $\boldsymbol{\phi}(t)$ spans the observation space $\mathcal{Y}$, while $\boldsymbol{r}(a_k)$ lies in the parameter space $\mathcal{R}$ and at the same time in the observation space $\mathcal{Y}$. Note that $\boldsymbol{r}(a_k)$ depends on the modulation parameters and on the received pulse shape $b(t)$.

3.2.2 Generalized Maximum Likelihood Detector

The classical ML detector decides for the variable $\hat{a}_k \in \{0,1\}$ that maximizes the likelihood function under the assumption of a known received pulse shape $b(t)$ and thus of a known vector $\boldsymbol{r}(a_k)$ for $a_k \in \{0,1\}$. For the given modulation scheme and channel, the likelihood function or conditional PDF of the signal vector $\mathbf{Y}$ is $P_{\mathbf{Y}|\mathbf{R},\mathrm{A}}(\boldsymbol{y}|\boldsymbol{r}(a_k),a_k)$. For our example, the classical ML

decision rule is expressed via the likelihood ratio

$$\Lambda(\boldsymbol{y}) = \frac{P_{\mathbf{Y}|\mathbf{R},\mathrm{A}}(\boldsymbol{y}|\boldsymbol{r}(a_k), a_k = 1)}{P_{\mathbf{Y}|\mathbf{R},\mathrm{A}}(\boldsymbol{y}|\boldsymbol{r}(a_k), a_k = 0)} \underset{\hat{a}_k=0}{\overset{\hat{a}_k=1}{\gtrless}} 1$$

$$= \frac{P_{\mathbf{Y}|\mathbf{R}}(\boldsymbol{y}|\boldsymbol{r}(a_k = 1))}{P_{\mathbf{Y}|\mathbf{R}}(\boldsymbol{y}|\boldsymbol{r}(a_k = 0))} \underset{\hat{a}_k=0}{\overset{\hat{a}_k=1}{\gtrless}} 1. \tag{3.9}$$

This reads as: 'if the PDF conditioned on $a_k = 1$ is larger than the PDF conditioned on $a_k = 0$, than chose $\hat{a}_k = 1$, and otherwise use $\hat{a}_k = 0$. From e.g. [39] we know that this decision rule results in the well known correlation or matched filter receiver that makes use of the knowledge of the received pulse $b(t)$. We are however interested in the case where no channel information is known to the receiver, except the information that $b(t)$ has a finite support or delay spread, τ_c, satisfying $\tau_c < \Delta_T$, and $\tau_c < T - \Delta_T$.

For this type of estimation problem, [66] suggests a method called *Generalized Maximum Likelihood* (GML) test. The notion of this test is to estimate the vector $\boldsymbol{r}(a_k)$ on the basis of the observation variable $\boldsymbol{y}$ and the (possibly wrong) assumption that $a_k = 0$, which means that $\boldsymbol{r}(a_k) \in \mathcal{R}_0$. This estimate for $\boldsymbol{r}(a_k = 0)$ is called $\hat{\boldsymbol{r}}_0$. The procedure is repeated for the assumption $a_k = 1$. The corresponding ML estimation procedures are

$$\hat{\boldsymbol{r}}_0 = \arg\max_{\boldsymbol{r}\in\mathcal{R}_0} \left\{ P_{\mathbf{Y}|\mathbf{R}}(\boldsymbol{y}|\boldsymbol{r}) \right\},$$

and

$$\hat{\boldsymbol{r}}_1 = \arg\max_{\boldsymbol{r}\in\mathcal{R}_1} \left\{ P_{\mathbf{Y}|\mathbf{R}}(\boldsymbol{y}|\boldsymbol{r}) \right\}.$$

These estimates are then used in the maximum likelihood ratio test as if they were exact. This is justified because better estimates are not available. Hence, using the estimates $\hat{\boldsymbol{r}}_0$ and $\hat{\boldsymbol{r}}_1$ instead of the true vectors $\boldsymbol{r}(a_k = 0)$ and $\boldsymbol{r}(a_k = 1)$ in the ML ratio test (3.9) results in the GML ratio test

$$\Lambda_g(\boldsymbol{y}) = \frac{P_{\mathbf{Y}|\mathbf{R}}(\boldsymbol{y}|\hat{\boldsymbol{r}}_1)}{P_{\mathbf{Y}|\mathbf{R}}(\boldsymbol{y}|\hat{\boldsymbol{r}}_0)} \underset{\hat{a}_k=0}{\overset{\hat{a}_k=1}{\gtrless}} 1. \tag{3.10}$$

Substituting the estimates $\hat{\boldsymbol{r}}_1$ and $\hat{\boldsymbol{r}}_0$ by the estimation procedures which are given above, the GML detection rule is expressed by

$$\Lambda_g(\boldsymbol{y}) = \frac{\max\limits_{\boldsymbol{r}\in\mathcal{R}_1} P_{\mathbf{Y}|\mathbf{R}}(\boldsymbol{y}|\boldsymbol{r})}{\max\limits_{\boldsymbol{r}\in\mathcal{R}_0} P_{\mathbf{Y}|\mathbf{R}}(\boldsymbol{y}|\boldsymbol{r})} \underset{\hat{a}_k=0}{\overset{\hat{a}_k=1}{\gtrless}} 1. \tag{3.11}$$

Now we derive a simplified and modified expression $\Lambda'_g(\boldsymbol{y})$ for the GML ratio $\Lambda_g(\boldsymbol{y})$, which results in the same decisions, i.e., $\lambda'_g(\boldsymbol{y}) > 1 \Leftrightarrow \lambda_g(\boldsymbol{y}) > 1$. We use the channel's additive noise structure, which results in the expression

$$\boldsymbol{n} = \boldsymbol{y} - \boldsymbol{r}(a_k).$$

As $\boldsymbol{r}(a_k)$ depends deterministically, even though in an unknown fashion, on the data symbol a_k, this implies that

$$P_{\mathbf{Y}|\mathbf{R},\mathrm{A}}(\boldsymbol{y}|\boldsymbol{r}(a_k), a_k) = P_{\mathbf{N}|\mathbf{R},\mathrm{A}}(\boldsymbol{y} - \boldsymbol{r}(a_k)|\boldsymbol{r}(a_k), a_k) = P_{\mathbf{N}}(\boldsymbol{y} - \boldsymbol{r}(a_k)). \tag{3.12}$$

An expression for the a-posteriori probability that reveals all the important details for our derivation is obtained by combining (3.12) and (3.8) which yields

$$P_{\mathbf{Y}|\mathbf{R},\mathrm{A}}(\boldsymbol{y}|\boldsymbol{r}(a_k),a_k) = \frac{1}{\sqrt{2\pi N_0 B}^N}\, e^{-\frac{\|\boldsymbol{y}-\boldsymbol{r}(a_k)\|^2}{2N_0 B}}.$$

We use this explicit representation of the a-posteriori probability to derive the mentioned simplified expression for $\Lambda'_g(\boldsymbol{y})$. First, some common factors of the nominator and the denominator are skipped and the logarithm is taken of both of them, i.e.,

$$\begin{aligned}
\Lambda_g(\boldsymbol{y}) > 1 &\Leftrightarrow \frac{\max\limits_{\boldsymbol{r}\in\mathcal{R}_1} P_{\mathbf{Y}|\mathbf{R}}(\boldsymbol{y}|\boldsymbol{r})}{\max\limits_{\boldsymbol{r}\in\mathcal{R}_0} P_{\mathbf{Y}|\mathbf{R}}(\boldsymbol{y}|\boldsymbol{r})} > 1 \\
&\Leftrightarrow \frac{\max\limits_{\boldsymbol{r}\in\mathcal{R}_1} \frac{1}{\sqrt{2\pi N_0 B}^N}\, e^{-\frac{\|\boldsymbol{y}-\boldsymbol{r}\|^2}{2N_0 B}}}{\max\limits_{\boldsymbol{r}\in\mathcal{R}_0} \frac{1}{\sqrt{2\pi N_0 B}^N}\, e^{-\frac{\|\boldsymbol{y}-\boldsymbol{r}\|^2}{2N_0 B}}} > 1 \\
&\Leftrightarrow \max_{\boldsymbol{r}\in\mathcal{R}_1} -\frac{\|\boldsymbol{y}-\boldsymbol{r}\|^2}{2N_0 B} > \max_{\boldsymbol{r}\in\mathcal{R}_0} -\frac{\|\boldsymbol{y}-\boldsymbol{r}\|^2}{2N_0 B} \\
&\Leftrightarrow \min_{\boldsymbol{r}\in\mathcal{R}_1} \frac{\|\boldsymbol{y}-\boldsymbol{r}\|^2}{2N_0 B} < \min_{\boldsymbol{r}\in\mathcal{R}_0} \frac{\|\boldsymbol{y}-\boldsymbol{r}\|^2}{2N_0 B} \\
&\Leftrightarrow \frac{\min\limits_{\boldsymbol{r}\in\mathcal{R}_0} \{\|\boldsymbol{y}-\boldsymbol{r}\|^2\}}{\min\limits_{\boldsymbol{r}\in\mathcal{R}_1} \{\|\boldsymbol{y}-\boldsymbol{r}\|^2\}} > 1;
\end{aligned} \tag{3.13}$$

these manipulations don't impact the inequality at the right hand side. The term $\|\boldsymbol{y}-\boldsymbol{r}\|^2$ can be expressed as a function of the continuous-time signals $y(t)$ and $r(t)$:

$$|\boldsymbol{y}-\boldsymbol{r}(a_k)\|^2 = \int_{kT}^{kT+T} [y(t)-r(a_k,t)]^2\, dt, \tag{3.14}$$

where $r(a_k,t) = \boldsymbol{\phi}^T(t)\boldsymbol{r}(a_k)$, see (3.5), which together with the substitution of $y(t)$ by $\boldsymbol{\phi}^T(t)\boldsymbol{y}$ results in (3.14). For convenience, we denote the signal space that is spanned by the signals $r(t) = \boldsymbol{\phi}^T(t)\boldsymbol{r}$ for $\boldsymbol{r}\in\mathcal{R}_1$ by $\mathcal{R}_1$ and correspondingly by $\mathcal{R}_0$ for $\boldsymbol{r}\in\mathcal{R}_0$. With this we can write the denominator in (3.13) as

$$\min_{\boldsymbol{r}\in\mathcal{R}_1} \left\{\|\boldsymbol{y}-\boldsymbol{r}\|^2\right\} = \min_{r(t)\in\mathcal{R}_1} \left\{ \int_{kT}^{kT+T} [y(t)-r(t)]^2\, dt \right\}. \tag{3.15}$$

At this point we use the fact that $r(t)\in\mathcal{R}_1$, or equivalently $r(a_k=1,t)$, is nonzero only for $t\in[kT+\Delta_T, kT+T]$. Note that $r(t)\in\mathcal{R}_0$, or equivalently $r(a_k=0,t)$, is nonzero only for $t\in[kT, kT+\Delta_T)$. Thus, for $r(t)\in\mathcal{R}_1$ we have

$$\int_{kT}^{kT+T} [y(t)-r(t)]^2\, dt = \int_{kT}^{kT+\Delta_T} y^2(t)\, dt + \int_{kT+\Delta_T}^{kT+T} [y(t)-r(t)]^2\, dt. \tag{3.16}$$

The two integrals at the right hand side are both greater or equal than zero because of the squared arguments. The second of them is zero if and only if $r(t)$ and $y(t)$ are equal for $t \in [kT+\Delta_T, kT+T]$. Based on this observation and with (3.15), the numerator in (3.13) is minimized for

$$r(t) = \hat{r}_1(t) := \begin{cases} y(t), & \text{for } kT + \Delta_T \leq t \leq kT + T, \\ 0, & \text{else.} \end{cases}$$

Note, that $\hat{r}_1(t) = \boldsymbol{\phi}^T(t)\,\hat{\boldsymbol{r}}_1$. With this, the numerator in (3.13) becomes

$$\min_{\boldsymbol{r}\in\mathcal{R}_1} \left\{ \|\boldsymbol{y} - \boldsymbol{r}\|^2 \right\} = \int_{kT}^{kT+\Delta_T} y^2(t)\,dt. \tag{3.17}$$

Note that this minimization is constraint on $\boldsymbol{r} \in \mathcal{R}_1$. The signal space $\mathcal{R}_1$ contains any possible signal $y(t)$ as we assume no knowledge about the channel. This assumption implies that $\mathcal{R}_1$ contains any signal that is in the same frequency band as the transmitted signal and whose support is restricted to the interval $[kT + \Delta_T, kT + T]$.

Making the corresponding derivation for the denominator of (3.13) results in the minimizing function

$$r(t) = \hat{r}_0(t) := \begin{cases} 0, & \text{else,} \\ y(t), & \text{for } kT \leq t \leq kT + \Delta_T, \end{cases}$$

and thus the denominator of (3.13) is

$$\min_{\boldsymbol{r}\in\mathcal{R}_0} \left\{ \|\boldsymbol{y} - \boldsymbol{r}\|^2 \right\} = \int_{kT+\Delta_T}^{kT+T} y^2(t)\,dt. \tag{3.18}$$

With this and (3.17) we can write (3.13) as

$$\Lambda_g(\boldsymbol{y}) > 1 \Leftrightarrow \frac{\int_{kT+\Delta_T}^{kT+T} y^2(t)\,dt}{\int_{kT}^{kT+\Delta_T} y^2(t)\,dt} > 1. \tag{3.19}$$

Hence, the simplified likelihood ratio test is given by

$$\Lambda'_g(\boldsymbol{y}) = \frac{\int_{kT+\Delta_T}^{kT+T} y^2(t)\,dt}{\int_{kT}^{kT+\Delta_T} y^2(t)\,dt} \underset{\hat{a}_k=0}{\overset{\hat{a}_k=1}{\gtrless}} 1. \tag{3.20}$$

This is the decision rule for the noncoherent receiver for 2PPM signals without ISI and for additive white Gaussian noise. An equivalent formulation for this decision rule is

$$\int_{kT+\Delta_T}^{kT+T} y^2(t)\,dt - \int_{kT}^{kT+\Delta_T} y^2(t)\,dt \underset{\hat{a}_k=0}{\overset{\hat{a}_k=1}{\gtrless}} 0. \tag{3.21}$$

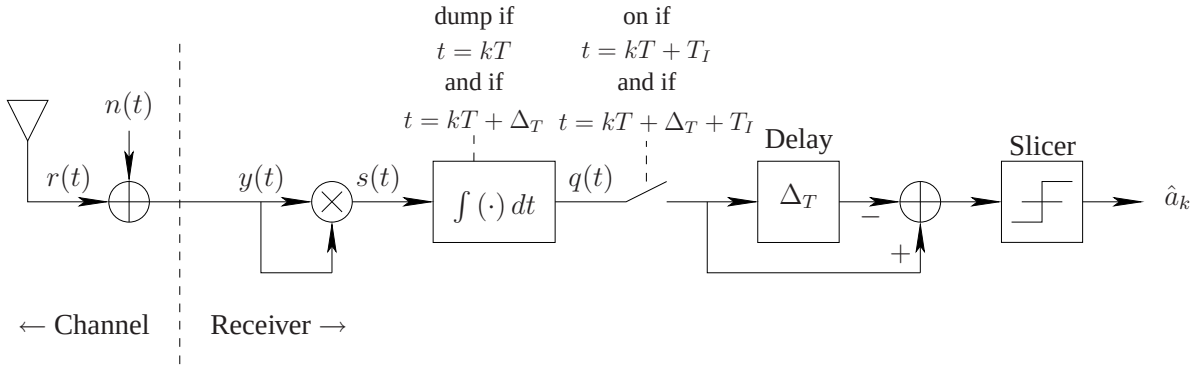

Fig. 3.1. An architecture of the generalized maximum likelihood receiver for 2PPM signals.

As the delay spread of the channel may vary from channel to channel, it can be smaller than the integration duration Δ_T. Thus, the integrator captures an unnecessarily large amount of noise energy. To allow an optimization of the integration duration independent of the modulation parameter Δ_T, we introduce the integration duration T_I wich is smaller than or equal to Δ_T. With this, the decision rule becomes:

$$\int_{kT+\Delta_T}^{kT+\Delta_T+T_I} y^2(t)\,dt - \int_{kT}^{kT+T_I} y^2(t)\,dt \underset{\hat{a}_k=0}{\overset{\hat{a}_k=1}{\gtrless}} 0. \tag{3.22}$$

A possible receiver architecture that implements this rule is shown in Fig. 3.1. This is the classical noncoherent receiver or energy collecting receiver for 2PPM signals, whose equivalence with the GMLR was already pointed out in [9]. The bit error probability of this receiver is investigated in Section 3.3.

3.2.3 Maximum Likelihood Receiver for Partial Channel State Information

The ML receiver is derived for a receiver having side information about the channel's APDP, we call this receiver the maximum likelihood receiver for partial channel state information (MLRP). For this purpose, a simplified channel model is introduced, that has the APDP as an explicit parameter and thus allows to analytically derive the corresponding ML receiver. This channel model is transformed into a discrete-time baseband representation. The purpose for this particular representation is to have statistically independent samples of the received pulse, which allows a compact and simple mathematical description.

3.2.3.1 Channel Model

Chapter 2 discusses channel models that are aimed to describe the properties of measured channels. However the models presented have a mathematical structure that prohibits analytical derivations of corresponding receivers. For this reason, here a simplified channel model is introduced that enables analytical derivations and at the same time shares the most important properties of practical channels.

We rely on [62] and assume that the distribution of channel taps is complex Gaussian for CIRs in complex baseband representation and thus Gaussian in passband representation. When looking at typical CIRs of the UWB indoor channel, we observe that the variance of the taps depends on

the excess delay. According to this observation, we model the CIR $b(t)$ as the product

$$\mathrm{B}(t) = \sigma(t)\mathrm{V}(t), \tag{3.23}$$

where $\mathrm{V(T)}$ is a bandlimited white Gaussian process, whose two-sided power spectral density (PSD) is $1/(2B)$ within the signal band and zero outside. Thus, the power of the process $\mathrm{V}(t)$, whose bandwidth equals B, is $\mathbb{E}\left\{\mathrm{V}^2(t)\right\} = 1$. Furthermore, the variance is $\sigma^2(t)$ at excess delay t, and can be interpreted as the APDP [37] because

$$\mathbb{E}\left\{\mathrm{B}^2(t)\right\} = \mathbb{E}\left\{\sigma^2(t)\mathrm{V}^2(t)\right\} = \sigma^2(t).$$

To bend the support of the CIR to the interval $[0, \tau_c]$ we set $\sigma(t) = 0$ for $t \notin [0, \tau_c]$. We assume further that $\sigma(t)$ is a lowpass signal with two-sided effective bandwidth B_σ which is much smaller than the bandwidth B of the noise realization $v(t)$. However, as $\sigma(t)$ is a time-limited function its spectrum has an infinite support. To avoid this contradiction, we define the term effective bandwidth B_σ as the width of the frequency band that contains most of the energy of $\sigma(t)$.

The equivalent baseband transform of the CIR according to (D.1) is given by

$$b_l(t) = [\sigma(t)v(t) + i \quad \{\sigma(t)v(t)\}]e^{-i2\pi f_0 t}.$$

Typically, the support of the signal spectrum is limited to the interval $[3.1,\ 10.6]$ GHz. With this and the assumption that $B_\sigma \ll B$ we can apply (D.12) which yields

$$b_l(t) = \sigma(t)v_l(t),$$

with

$$v_l(t) = [v(t) + i \quad \{v(t)\}]\, e^{-i2\pi f_0 t}.$$

The small bandwidth of the signal $\sigma(t)$ allows us to assume that the band of the signal $b_l(t)$ is limited to the same interval as the signal $v_l(t)$, i.e., to the interval $[-B/2, +B/2]$. Therefore the Nyquist sampling rate for the signal $b_l(t)$ is B, and the delay between consecutive samples is $T_s = 1/B$. The support constraint of $\sigma(t)$ together with its low signal bandwidth causes a smooth fade-in and fade-out of the CIR $b(t)$, see (3.23). We define the sampled signal

$$b_n = b_l(nT_s) = \sigma_n v_n, \tag{3.24}$$

with $\sigma_n = \sigma(nT_s)$ and $v_n = v_l(nT_s)$. The support time τ_c of $b(t)$ is smaller than or equal to the modulation parameter Δ_T; therefore, a number of $N_\Delta = \Delta_T/T_s$ samples of the signal $b_l(t)$ are sufficient for its description. We assume for simplicity that Δ_T is an integer multiple of T_s. As only a marginal portion of the energy of $b_l(t)$ spreads outside the frequency interval $[-B/2, B/2]$, the energy of the sampled signal b_n is given by the approximation

$$T_s \sum_{n=0}^{N_\Delta - 1} |b_n|^2 \approx \int_0^{\Delta_T} |b_l(t)|^2\, dt = 2\int_0^{\Delta_T} b^2(t)\, dt. \tag{3.25}$$

The right hand equation follows from (D.10).

Note that the samples v_n are obtained by sampling with Nyquist rate a white Gaussian random process with PSD $1/(2B)$ that is filtered by an ideal bandpass filter. Therefore, the samples v_n are statistically independent and identically distributed zero-mean complex Gaussian random

variables. Thus, the real and imaginary part of the samples v_n have unit variance, [49]. With this property and with (3.24) the pdf of the n-th sample b_n is

$$P_{\mathrm{B}_n}(b_n) = \frac{1}{2\pi\sigma_n^2} e^{-\frac{|b_n|^2}{2\sigma_n^2}}. \tag{3.26}$$

This description implies the statistical independence of random variables B_n with unequal indices.

Now we want to discuss the energy spectrum of this process. For this purpose we introduce the Fourier transform of the CIR process B_n as

$$\Theta_m = \sum_{n=0}^{N_\Delta - 1} \mathrm{B}_n e^{-\frac{2\pi n m}{N_\Delta T_s}}. \tag{3.27}$$

We call the expectation value of the squared absolute value $\mathbb{E}\{|\Theta_m|^2\}$ the energy spectrum of the CIR process B_n. The name "energy spectrum" is chosen because the sum of the N_Δ terms $\mathbb{E}\{|\Theta_m|^2\}$ equals the expectation value of the energy of the time limited process B_n. This energy spectrum is independent of the frequency index m, i.e., constant. This can be shown by inserting the definition (3.27) into the expression $\mathbb{E}\{|\Theta_m|^2\}$ and by using the property of uncorrelated samples described by (3.26). In contradiction to this result, in Subsection 2.2.4 the energy spectrum of the CIR process $B(t)$ is reported to be proportional to $1/f^2$. This implies that the assumption of uncorrelated samples of the process B_n is not valid. To assess how strong the correlation between the samples is, we compute the inverse Fourier transform of the energy spectrum $1/f^2$ in complex baseband representation, for a center frequency $f_0 = 3.85$ GHz and a bandwidth of 1.5 GHz. We compute the autocorrelation function (ACF) $\varphi_{BB,n,m} = \mathbb{E}\left\{B_m B_{m+n}^*\right\}$ of the discrete time process B_n that is obtained by Nyquist rate sampling the process $\mathrm{B}(t)$. Numerical evaluation for the specified parameters shows that the largest value of the normalized ACF $\max_m \varphi_{BB,n,m} / \max_m \varphi_{BB,0,m}$ is unity as expected and the second largest value $\max_m \varphi_{BB,1,m} / \max_m \varphi_{BB,0,m}$ is already smaller than 0.13. Furthermore we have observed, that the ACF decays fast with growing absolute index $|n|$. From this we conclude that the correlation between adjacent samples of the CIR process B_n is only marginal. Therefore, and to allow a clear analytical derivation of the MLRP, we make an approximation of the true model. This approximation consists in ignoring the correlation between the samples of the process B_n that is caused by the $1/f^2$ characteristics of the CIR's energy spectrum.

3.2.3.2 Received Signal

We assume that no intersymbol interference (ISI) occurs and that the binary transmitted symbols are orthogonal at both the transmitter and the receiver. These assumptions imply that both Δ_T and $T - \Delta_T$ exceed τ_c. Thus, without loss of generality, to derive the MLRP we are allowed to consider only the symbol with index $k = 0$. The received signal $r(t)$ has the complex baseband transform $r_l(t)$, it conveys the symbol a_k within the symbol interval $[kT, kT + T)$, see (3.2). Hence, for detecting the symbol a_0 only the samples $r_n = r_l(nT_s)$, for $n = 0$ to $N - 1$ where $N = T/T_s$, need to be considered. For simplicity we assume that T as well as Δ_T are integer multiples of T_s. Also, for the sake of simplicity, we assume that the factor c_k in (3.2) is set to the value $c_k = 1$. This has an effect only on the spectrum of the transmitted signal but not on the receiver architecture and its performance. With the definition $N_\Delta = \Delta_T/T_s$, the received 2PPM signal described by (3.2) can be expressed by the samples r_n as a function of the discrete time CIR samples b_n and the

transmitted symbol a_0. For $a_0 = 0$ we have

$$r_n(a_0 = 0) = \begin{cases} b_n, & \text{for } 0 \le n < N_\Delta \\ 0, & \text{for } N_\Delta \le n < N \end{cases}, \tag{3.28}$$

while $a_0 = 1$ yields

$$r_n(a_0 = 1) = \begin{cases} 0, & \text{for } 0 \le n < N_\Delta \\ b_{n-N_\Delta} e^{i\varphi}, & \text{for } N_\Delta \le n < N \end{cases}, \tag{3.29}$$

where the phase $\varphi = -2\pi f_0 \Delta_T$, which appears in the complex baseband transform when the corresponding passband pulse, $b(t)$ is shifted in time by Δ_T; this is the case for $a_0 = 1$, see (D.6). With these definitions and with the PDF of the CIR samples, given by (3.26), we can write the conditional PDF of the discrete-time received signal samples r_n as

$$P_{\mathrm{R}_n|\mathrm{A}}(r_n|a_0 = 0) = \frac{1}{2\pi s_{0,n}^2} e^{-\frac{|r_n|^2}{2s_{0,n}^2}}, \quad \text{for } 0 \le n < N, \tag{3.30}$$

and

$$P_{\mathrm{R}_n|\mathrm{A}}(r_n|a_0 = 1) = \frac{1}{2\pi s_{1,n}^2} e^{-\frac{|r_n|^2}{2s_{1,n}^2}}, \quad \text{for } 0 \le n < N, \tag{3.31}$$

for $0 \le n < N$, where

$$s_{0,n} = \begin{cases} \sigma_n, & \text{for } 0 \le n < N_\Delta \\ 0, & \text{for } N_\Delta \le n < N \end{cases} \tag{3.32}$$

and

$$s_{1,n} = \begin{cases} 0, & \text{for } 0 \le n < N_\Delta \\ \sigma_{n-N_\Delta}, & \text{for } N_\Delta \le n < N \end{cases}. \tag{3.33}$$

The corresponding continuous-time signals $s_0(t)$ and $s_1(t)$ are given by $s_0(t) = \sigma(t)$ and $s_1(t) = \sigma(t - \Delta_T)$. Note that the signals $s_0(t)$ and $s_1(t)$ are not directly related to the signal $s(t)$ used in Fig. 3.1, Fig. 3.2, and Fig. 3.3. As expressions (3.30) and (3.31) are discontinuous at $s_{0,n}^2 = 0$ and $s_{1,n}^2$, respectively, we define the Gaussian PDF of a circular symmetric complex random variable z with real part x, imaginary part y, and zero-variance σ^2 to be given by

$$\left. \frac{1}{2\pi\sigma^2} e^{-\frac{|z|^2}{2\sigma^2}} \right|_{\sigma=0} := \delta(x)\delta(y).$$

With this, the equations (3.30) and (3.31) provide the statistical description of the random channel response including the modulation, i.e., (3.30) and (3.31) describe the statistics of the received signal samples in complex baseband representation.

3.2.3.3 Additive Gaussian Noise

The additive noise signal $n(t)$ is a passband Gaussian noise realization with bandwidth B and center frequency f_0, the two-sided PSD is $N_0/2$. The equivalent baseband signal is denoted as $n_l(t)$, its samples are $n_n = n_l(nT_s)$ and are realizations of zero mean Gaussian i.i.d. random variables that are complex and circularly symmetric. Consequently, both the imaginary and the real

part have variance N_0B. Thus, the statistical characterization of the discrete-time random-process is

$$P_{\mathrm{N}}(n_n) = \frac{1}{2\pi N_0 B} e^{-\frac{|n_n|^2}{2N_0B}}. \tag{3.34}$$

The baseband transform of the received signal $r(t)$ is denoted by $r_l(t)$, its discrete-time representation is $r_n = r_l(nT_s)$. With this, the discrete-time representation of the observed signal is

$$y_n = r_n + n_n. \tag{3.35}$$

For a compact notation we collect the signal samples that blong to the time interval of interest, i.e., $[0, T)$, in the respective vectors $\boldsymbol{r} = (r_0, r_1, \ldots, r_{N-1})^T$, $\boldsymbol{n} = (n_0, n_1, \ldots, n_{N-1})^T$ and $\boldsymbol{y} = (y_0, y_1, \ldots, y_{N-1})^T$. The pdf of the observed signal vector, $\boldsymbol{y}$, is written as $P_{\mathbf{Y}|\mathbf{R},\mathrm{A}}(\boldsymbol{y}|\boldsymbol{r}, a_0)$, which emphasizes the dependency of $\boldsymbol{r}$ on a_0. For a given received signal sample, r_n, we can write the statistics of the observed signal samples in (3.35). Using the same argumentation as in Section 3.2.2 we have

$$P_{\mathrm{Y}_n|\mathrm{R}_n,\mathrm{A}}(y_n|r_n, a_0) = P_{\mathrm{N}|\mathrm{R}_n,\mathrm{A}}(y_n - r_n|r_n, a_0) = P_{\mathrm{N}}(y_n - r_n). \tag{3.36}$$

3.2.3.4 ML Decision Rule

The detection problem is a composite hypothesis testing problem because the signal samples y_n contain two random components, the channel and the noise. The partial channel knowledge consists of the APDP, $\sigma^2(t)$, and the noisie density N_0 is also assumed to be known. The corresponding ML decision rule is expressed by

$$\Lambda(\boldsymbol{y}) = \frac{P_{\mathbf{Y}|\mathrm{A}}(\boldsymbol{y}|a_0 = 1)}{P_{\mathbf{Y}|\mathrm{A}}(\boldsymbol{y}|a_0 = 0)} \underset{\hat{a}_0=0}{\overset{\hat{a}_0=1}{\gtrless}} 1. \tag{3.37}$$

In contrast to (3.9), here the received signal vector $\boldsymbol{r}(a_0)$ is unknown; only the instantaneous variances $s_{0,n}$ and $s_{1,n}$ are known but are not emphasized in (3.37) for simplicity. The conditional PDF $P_{\mathbf{Y}|\mathrm{A}}(\boldsymbol{y}|a_0)$ characterizes the transmission path consisting of the modulator, the channel, and the additive receiver noise. The modulator and the channel are characterized by (3.30) for $a_0 = 0$ and (3.31) for $a_0 = 1$, while the receiver noise is described by (3.36). Combining these expressions results in the desired conditional PDF

$$P_{\mathbf{Y}|\mathrm{A}}(\boldsymbol{y}|a_0) = \int_{\mathcal{R}} P_{\mathbf{Y}|\mathbf{R},\mathrm{A}}(\boldsymbol{y}|\boldsymbol{r}, a_0) P_{\mathbf{R}|\mathrm{A}}(\boldsymbol{r}|a_0)\, d\boldsymbol{r}. \tag{3.38}$$

The components of the random noise vector $\mathbf{N}$ are statistically independent, the same holds for the components of the received pulse.

Equation (3.38) can be expressed componentwise by exploiting the statistical independence of the components of $\mathbf{R}$ and $\mathbf{N}$, i.e.,

$$P_{\mathbf{Y}|\mathrm{A}}(\boldsymbol{y}|a_0) = \prod_{n=0}^{N-1} P_{\mathrm{Y}_n|\mathrm{A}}(y_n|a_0), \tag{3.39}$$

where

$$\begin{aligned} P_{\mathrm{Y}_n|\mathrm{A}}(y_n|a_0) &= \int_{-\infty}^{\infty} P_{\mathrm{Y}_n|\mathrm{R}_n,\mathrm{A}}(y_n|r_n, a_0) P_{\mathrm{R}_n|\mathrm{A}}(r_n|a_0)\, dr_n. \\ &= \int_{-\infty}^{\infty} P_{\mathrm{N}}(y_n - r_n|a_0) P_{\mathrm{R}_n|\mathrm{A}}(r_n|a_0)\, dr_n. \end{aligned}$$

To evaluate this integral for $a_0 = 0$ we insert (3.30), (3.34), and (3.36), yielding

$$P_{\mathrm{Y}_n|\mathrm{A}}(y_n|a_0 = 0) = \int_{-\infty}^{\infty} \frac{1}{2\pi N_0 B} e^{-\frac{|y_n - r_n|^2}{2N_0 B}} \frac{1}{2\pi s_{n,0}^2} e^{-\frac{|r_n|^2}{2s_{n,0}^2}} \, dr_n, \quad \text{for} \quad 0 \le n \le N. \tag{3.40}$$

This represents the convolution of two Gaussian PDFs, which yields again a Gaussian PDF whose variance is the sum of the variances of the two original PDFs. Hence, we can write

$$P_{\mathrm{Y}_n|\mathrm{A}}(y_n|a_0 = 0) = \frac{1}{2\pi(s_{0,n}^2 + N_0 B)} e^{-\frac{|y_n|^2}{2(s_{0,n}^2 + N_0 B)}}, \quad \text{for} \quad 0 \le n \le N. \tag{3.41}$$

Similarly, the evaluation for $a_0 = 1$ requires insertion of (3.31), (3.34), and (3.36) and results in

$$P_{\mathrm{Y}_n|\mathrm{A}}(y_n|a_0 = 1) = \frac{1}{2\pi(s_{1,n}^2 + N_0 B)} e^{-\frac{|y_n|^2}{2(s_{1,n}^2 + N_0 B)}}, \quad \text{for} \quad 0 \le n \le N. \tag{3.42}$$

Inserting the last two expressions into (3.39) yields the a-posteriori probabilities

$$P_{\mathbf{Y}|\mathrm{A}}(\boldsymbol{y}|a_0 = 0) = \prod_{n=0}^{N-1} \frac{1}{2\pi(s_{0,n}^2 + N_0 B)} e^{-\frac{|y_n|^2}{2(s_{0,n}^2 + N_0 B)}}, \tag{3.43}$$

for $a_0 = 0$, and for $a_0 = 1$

$$P_{\mathbf{Y}|\mathrm{A}}(\boldsymbol{y}|a_0 = 1) = \prod_{n=0}^{N-1} \frac{1}{2\pi(s_{1,n}^2 + N_0 B)} e^{-\frac{|y_n|^2}{2(s_{1,n}^2 + N_0 B)}}. \tag{3.44}$$

With these results we can express the ML decision rule (3.37) as

$$\begin{aligned} \Lambda(\boldsymbol{y}) &= \frac{\prod_{n=0}^{N-1} \frac{1}{2\pi(s_{1,n}^2 + N_0 B)} e^{-\frac{|y_n|^2}{2(s_{1,n}^2 + N_0 B)}}}{\prod_{n=0}^{N-1} \frac{1}{2\pi(s_{0,n}^2 + N_0 B)} e^{-\frac{|y_n|^2}{2(s_{0,n}^2 + N_0 B)}}} \quad \underset{\hat{a}_0=0}{\overset{\hat{a}_0=1}{\gtrless}} \quad 1 \\ &= \frac{\prod_{n=0}^{N-1} e^{-\frac{|y_n|^2}{2(s_{1,n}^2 + N_0 B)}}}{\prod_{n=0}^{N-1} e^{-\frac{|y_n|^2}{2(s_{0,n}^2 + N_0 B)}}} \quad \underset{\hat{a}_0=0}{\overset{\hat{a}_0=1}{\gtrless}} \quad 1. \end{aligned} \tag{3.45}$$

The last simplification is possible because

$$\prod_{n=0}^{N-1} \frac{1}{s_{0,n}^2 + N_0 B} = \prod_{n=0}^{N-1} \frac{1}{s_{1,n}^2 + N_0 B},$$

which follows from the sequence $\langle s_{0,n} \rangle$ being a permutation of the sequence $\langle s_{1,n} \rangle$, see (3.32) and (3.33). Now we derive a modified likelihood ratio $\Lambda'(\boldsymbol{y})$ that is easier to compute than (3.45). This modified likelihood ratio will result in the same decisions if both, $\Lambda(\boldsymbol{y}) > 1$ and $\Lambda'(\boldsymbol{y}) > 1$ are true

or false at the same time. The simplification consists in taking the logarithm of the denominator and the numerator and in changing the sign of both, i.e.,

$$\begin{aligned}
\Lambda(\boldsymbol{y}) > 1 &\Leftrightarrow \frac{\prod_{n=0}^{N-1} e^{-\frac{|y_n|^2}{2(s_{1,n}^2+N_0)B}}}{\prod_{n=0}^{N-1} e^{-\frac{|y_n|^2}{2(s_{0,n}^2+N_0B)}}} > 1 \\
&\Leftrightarrow \prod_{n=0}^{N-1} e^{-\frac{|y_n|^2}{2(s_{1,n}^2+N_0)B}} > \prod_{n=0}^{N-1} e^{-\frac{|y_n|^2}{2(s_{0,n}^2+N_0B)}} \\
&\Leftrightarrow -\sum_{n=0}^{N-1} \frac{|y_n|^2}{s_{0,n}^2+N_0B} > -\sum_{n=0}^{N-1} \frac{|y_n|^2}{s_{1,n}^2+N_0B} \\
&\Leftrightarrow \frac{\sum_{n=0}^{N-1} \frac{|y_n|^2}{s_{0,n}^2+N_0B}}{\sum_{n=0}^{N-1} \frac{|y_n|^2}{s_{1,n}^2+N_0B}} < 1.
\end{aligned} \tag{3.46}$$

With this, the modified decision rule is

$$\Lambda'(\boldsymbol{y}) = \frac{\sum_{n=0}^{N-1} \frac{|y_n|^2}{s_{0,n}^2+N_0B}}{\sum_{n=0}^{N-1} \frac{|y_n|^2}{s_{1,n}^2+N_0B}} \underset{\hat{a}_0=0}{\overset{\hat{a}_0=1}{\gtrless}} 1. \tag{3.47}$$

This formulation of the decision rule is appropriate for describing the implementation when discrete-time equivalent baseband signals are available within a receiver. However, we are seeking a simple continuous-time implementation, therefore, we must represent the numerator and denominator as a function of the continuous time signals $\sigma(t)$ and $y(t)$. The sequence $\langle\sigma_n\rangle$ has a much lower bandwidth than the sequence $\langle y_n\rangle$. As the sampling rate is the Nyquist sampling rate of the signal $y(t)$, this implies that $s_{0,n} \approx s_{0,n+1}$ and $s_{1,n} \approx s_{1,n+1}$. Therefore, we can approximate the sum in the numerator in (3.47) by an integral:

$$\sum_{n=0}^{N-1} \frac{|y_n|^2}{s_{0,n}^2+N_0B} \approx \frac{1}{T_s}\int_0^T \frac{|y_l(t)|^2}{s_0^2(t)+N_0B}\,dt = \frac{2}{T_s}\int_0^T \frac{y^2(t)}{s_0^2(t)+N_0B}\,dt. \tag{3.48}$$

Making the same approximation for the denominator, and generalizing the result for arbitrary symbol indices k, we can write an approximation for the decision rule (3.47):

$$\Lambda'(\boldsymbol{y}) = \frac{\int_{kT}^{kT+T} \frac{y^2(t)}{s_0^2(t-kT)+N_0B}\,dt}{\int_{kT}^{kT+T} \frac{y^2(t)}{s_1^2(t-kT)+N_0B}\,dt} \underset{\hat{a}_k=0}{\overset{\hat{a}_k=1}{\gtrless}} 1. \tag{3.49}$$

This rule is equivalent to

$$\int_{kT}^{kT+T} \frac{y^2(t)}{s_0^2(t-kT)+N_0B}\,dt - \int_{kT}^{kT+T} \frac{y^2(t)}{s_1^2(t-kT)+N_0B}\,dt \underset{\hat{a}_k=0}{\overset{\hat{a}_k=1}{\gtrless}} 0,$$

and thus equivalent to

$$\int_{kT}^{kT+T} y^2(t)\, w(t-kT)\, dt \underset{\hat{a}_k=0}{\overset{\hat{a}_k=1}{\gtrless}} 0, \tag{3.50}$$

where

$$w(t) = \frac{s_1^2(t) - s_0^2(t)}{(s_0^2(t) + N_0B)(s_1^2(t) + N_0B)} = \frac{1}{N_0B}\frac{s_1^2(t) - s_0^2(t)}{s_0^2(t) + s_1^2(t) + N_0B}. \tag{3.51}$$

The simplification in the last step is based on the property $s_1(t)s_2(t) = 0$, which follows from the definitions (3.32) and (3.33). The constant factor $1/N_0B$ does not influence the decision and can be skipped. Note that the factor $c_k \in \{-1, +1\}$ in (3.2) has no impact on the decision because the sign of the received signal is ignored owing to the squaring of the observed signal $y(t)$. An architecture for this maximum likelihood receiver with partial channel state information (MLRP) is given in Fig. 3.2. The signal $\sum_k w(t-kT)$ in this figure causes a repeated application of the weighting function in order to receive each symbols a_k.

This receiver description can be simplified under the assumption that $\sigma(t)$ is a constant c within the time interval $[0, \Delta_T]$ and zero outside, i.e., that the average power delay profile of the channel is completely uniform. With the definition of the signals $s_0(t)$ and $s_1(t)$, and skipping the factor $1/(N_0B)$ in (3.51) we have

$$w(t) = \begin{cases} -\frac{c^2}{c^2+N_0B}, & \text{for } kT \le t \le kT + \Delta_T, \\ \frac{c^2}{c^2+N_0B}, & \text{for } kT + \Delta_T < t \le kT + T. \end{cases} \tag{3.52}$$

This weighting function makes the decision rule (3.50) equivalent to the decision rule (3.20) of the GMLR in Section 3.2.2. To show this we insert (3.52) into the decision rule (3.50), which yields

$$\begin{aligned} & \frac{c^2}{c^2 + N_0B}\left(\int_{kT+\Delta_T}^{kT+T} y^2(t)\, dt \; - \int_{kT}^{kT+\Delta_T} y^2(t)\, dt\right) \underset{\hat{a}_k=0}{\overset{\hat{a}_k=1}{\gtrless}} 0, \\ \Leftrightarrow \quad & \int_{kT+\Delta_T}^{kT+T} y^2(t)\, dt \; - \int_{kT}^{kT+\Delta_T} y^2(t)\, dt \underset{\hat{a}_k=0}{\overset{\hat{a}_k=1}{\gtrless}} 0, \\ \Leftrightarrow \quad & \frac{\int_{kT+\Delta_T}^{kT+T} y^2(t)\, dt}{\int_{kT}^{kT+\Delta_T} y^2(t)\, dt} \underset{\hat{a}_k=0}{\overset{\hat{a}_k=1}{\gtrless}} 1. \end{aligned} \tag{3.53}$$

This is equivalent to the decision rule of the GMLR (3.20). Remember that the GMLR works without channel state information. Hence, we conclude that the GML decision rule makes the implicit assumption that the channel's APDP is a constant within the interval $[0, \Delta_T]$.

3.3 Performance of Receivers for 2PPM Signals

The BEP of the GMLR and MLRP receivers can be discussed on the basis of the decision rule (3.47) which is based on the discrete-time representation of the equivalent baseband signals. A unified derivation of the exact BEP for both receiver types is possible only for the special case

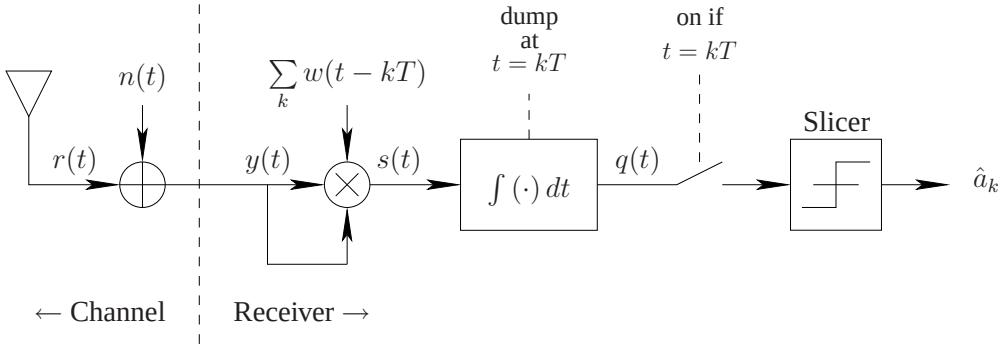

Fig. 3.2. An architecture of the maximum likelihood receiver with partial channel state information for 2PPM signals.

where $\sigma(t) \equiv c$ for $t \in [0, \Delta_T]$, i.e., where the MLRP is equivalent to the GMLR, see the paragraph below (3.51). A simpler, but approximate expression for the BEP of the GMLR can be found by (i) approximating the exact result for the BEP of the GMLR; and (ii) by deriving an approximate BEP expression for the MLRP and specializing this result for the GMLR.

In Subsection 3.3.1 we derive an exact and an approximate expression for the BEP of the GMLR. An approximation for the BEP of the MLRP is derived in Subsection 3.3.2, specialization for $\sigma(t) \equiv c$ results in the mentionedapproximation for the BEP of the GMLR. For comparison we discuss the BEP of the MLR (maximum likelihood receiver with perfect knowledge of the received pulse shape) in Subsection 3.3.3. The subsequent paragraphs contain a preparation for these derivations.

The decision rule for the symbol a_k in (3.47) can be translated into the form

$$
\begin{aligned}
&\frac{\sum_{n=0}^{N-1} \frac{|y_n|^2}{s_{0,n}^2 + N_0 B}}{\sum_{n=0}^{N-1} \frac{|y_n|^2}{s_{1,n}^2 + N_0 B}} \underset{\hat{a}_0=0}{\overset{\hat{a}_0=1}{\gtrless}} 1 \\
\Leftrightarrow &\sum_{n=0}^{N-1} \left[\frac{|y_n|^2}{s_{0,n}^2 + N_0 B} - \frac{|y_n|^2}{s_{1,n}^2 + N_0 B} \right] \underset{\hat{a}_0=0}{\overset{\hat{a}_0=1}{\gtrless}} 0 \\
\Leftrightarrow &\sum_{n=0}^{N-1} \frac{|y_n|^2 \left(s_{1,n}^2 - s_{0,n}^2 \right)}{s_{0,n}^2 + s_{1,n}^2 + N_0 B} \underset{\hat{a}_0=0}{\overset{\hat{a}_0=1}{\gtrless}} 0 \\
\Leftrightarrow &\sum_{n=0}^{N-1} \frac{|y_n|^2 s_{0,n}^2}{s_{0,n}^2 + s_{1,n}^2 + N_0 B} \underset{\hat{a}_0=1}{\overset{\hat{a}_0=0}{\gtrless}} \sum_{n=0}^{N-1} \frac{|y_n|^2 s_{1,n}^2}{s_{0,n}^2 + s_{1,n}^2 + N_0 B} \\
\Leftrightarrow &\sum_{n=0}^{N_\Delta - 1} \frac{|y_n|^2 \sigma_n^2}{\sigma_n^2 + N_0 B} \underset{\hat{a}_0=1}{\overset{\hat{a}_0=0}{\gtrless}} \sum_{n=N_\Delta}^{N-1} \frac{|y_n|^2 \sigma_{n-N_\Delta}^2}{\sigma_{n-N_\Delta}^2 + N_0 B}.
\end{aligned}
\tag{3.54}
$$

For this translation we used the definitions (3.32) and (3.33) and their property that $s_{0,n} s_{1,n} = 0$. The symmetry of the 2PPM scheme, and the assumption that no ISI occurs, allows us to consider only the case where the transmitted symbol $a_0 = 0$, i.e., to write the bit or symbol error probability

BEP as

$$\begin{aligned} P_e &= P(\hat{a}_0 = 1 | a_0 = 0) \\ &= P\left(\sum_{n=0}^{N_\Delta - 1} \frac{|y_n|^2 \sigma_n^2}{\sigma_n^2 + N_0 B} < \sum_{n=N_\Delta}^{N-1} \frac{|y_n|^2 \sigma_{n-N_\Delta}^2}{\sigma_{n-N_\Delta}^2 + N_0 B} \middle| a_0 = 0 \right), \end{aligned} \tag{3.55}$$

where the received signal samples, y_n, for $a_0 = 0$ are $y_n = \sigma_n v_n + n_n$ and $y_n = n_n$ for $0 \leq n \leq N_\Delta - 1$ and $N_\Delta \leq n \leq N$, respectively, see (3.24) and (3.35). With this we have

$$P_e = P\left(\sum_{n=0}^{N_\Delta - 1} \frac{\sigma_n^2}{\sigma_n^2 + N_0 B} |\sigma_n v_n + n_n|^2 \; < \; \sum_{n=0}^{N_\Delta - 1} \frac{\sigma_n^2}{\sigma_n^2 + N_0 B} |n_{n+N_\Delta}|^2 \right). \tag{3.56}$$

One way to compute this probability is to derive the PDFs $P_{\mathrm{F}}(f)$ and $P_{\mathrm{G}}(g)$ of the terms

$$f := \sum_{n=0}^{N_\Delta - 1} \frac{\sigma_n^2}{\sigma_n^2 + N_0 B} |\sigma_n v_n + n_n|^2, \tag{3.57}$$

and

$$g := \sum_{n=0}^{N_\Delta - 1} \frac{\sigma_n^2}{\sigma_n^2 + N_0 B} |n_{n+N_\Delta}|^2, \tag{3.58}$$

and to evaluate the integral

$$P_e = P(f < g) = \int_0^\infty \int_0^g P_{\mathrm{F,G}}(f, g)\, df\, dg.$$

The variables f and g are realizations of the statistically independent random variables F and G. Thus, $P_{\mathrm{F,G}}(f, g) = P_{\mathrm{F}}(f) P_{\mathrm{G}}(g)$ and hence,

$$P_e = \int_0^\infty \int_0^g P_{\mathrm{F}}(f) P_{\mathrm{G}}(g)\, df\, dg. \tag{3.59}$$

The expressions for the PDFs $P_{\mathrm{F}}(f)$ and $P_{\mathrm{G}}(g)$ are very complex; [54] gives a series expansion for them. To stay within the scope of this work, in 3.3.2 we derive only an approximate expression for P_e.

3.3.1 Bit Error Probability of the GMLR

We consider again the error probability $P_e = P(\hat{a}_0 = 1 | a_0 = 0)$. For the special case where $\sigma(t)$ is constant, i.e., $\sigma(t) = c$ for $t \in [0, \Delta_T]$, or equivalently $\sigma_n = c$ for $n \in [0, N_\Delta - 1]$, the above PDFs, $P_F(f)$ and $P_G(g)$ become non-central and central chi-square distributions with identical degree of freedom N_Δ, and are described by relatively simple analytical expressions given in Appendix E. Furthermore, we assume that the factor c_k in (3.2) is set to the value $c_k = 1$. This has an effect only on the spectrum of the transmitted signal but not on the receivers performance. We define the simplified expressions

$$f_s := f \frac{c^2 + N_0 B}{c^2} = \sum_{n=0}^{N_\Delta - 1} |c v_n + n_n|^2, \tag{3.60}$$

and

$$g_s := g\frac{c^2 + N_0B}{c^2} = \sum_{n=N_\Delta}^{N-1} |n_n|^2, \tag{3.61}$$

which are scaled versions of the variables f and g defined in (3.57) and (3.58). Thus, under the assumption that $a_k = 0$ and with (E.3), the distribution of f_s is

$$P_{\mathrm{F}_s}(f_s) = \frac{1}{2N_0B}\left(\frac{f_s}{s^2}\right)^{\frac{N_\Delta-1}{2}} e^{-\frac{s^2+f_s}{2N_0B}} \mathrm{I}_{N_\Delta-1}\left(\sqrt{f_s}\frac{s}{N_0B}\right),$$

where

$$s^2 = \sum_{n=0}^{N_\Delta-1} |b_n|^2, \tag{3.62}$$

and $b_n = cv_n$, see (3.24), $\mu_{f_s} = 2N_\Delta N_0B + s^2$, and $\sigma^2_{f_s} = 4N_\Delta(N_0B)^2 + 4N_0Bs^2$. The function $\mathrm{I}_\alpha(x)$ ist the α th-order modified Bessel function of the first kind. The distribution of g_s is for $a_k = 0$ and with (E.4)

$$P_{\mathrm{G}_s}(g_s) = \frac{1}{(2N_0B)^{N_\Delta}\,\Gamma\left(N_\Delta\right)}\, g_s^{N_\Delta-1} e^{-\frac{g_s}{2N_0B}},$$

where $\mu_{g_s} = 2N_\Delta N_0B$ and $\sigma^2_{g_s} = 4N_\Delta(N_0B)^2$. We compute the BEP from (3.59), i.e.,

$$\begin{aligned}
P_e &= \int_0^\infty \int_0^{g_s} P_{\mathrm{F}_s}(f_s) P_{\mathrm{G}_s}(g_s)\, df_s\, dg_s \\
&= \frac{e^{-\frac{s^2}{2N_0B}}}{(2N_0B)^{N_\Delta+1}\,\Gamma\left(N_\Delta\right)} \int_0^\infty \int_0^{g_s} \mathrm{I}_{N_\Delta-1}\left(\sqrt{f_s}\frac{s}{N_0B}\right) e^{-\frac{f_s+g_s}{2N_0B}} \left(\frac{f_s}{s^2}\right)^{\frac{N_\Delta-1}{2}} g_s^{N_\Delta-1}\, df_s\, dg_s \\
&= \frac{e^{-\frac{s^2}{2N_0B}}}{(2N_0B)^{N_\Delta+1}\,\Gamma\left(N_\Delta\right)} \int_0^\infty g_s^{N_\Delta-1} e^{-\frac{g_s}{2N_0B}} \int_0^{g_s} \mathrm{I}_{N_\Delta-1}\left(\sqrt{f_s}\frac{s}{N_0B}\right)\left(\frac{f_s}{s^2}\right)^{\frac{N_\Delta-1}{2}} e^{-\frac{f_s}{2N_0B}}\, df_s dg_s.
\end{aligned} \tag{3.63}$$

A closed-form expression for this integral has not been found by the author. A numerical evaluation is shown in Fig. 3.7 through 3.10.

3.3.1.1 Approximation

We derive an approximate expression for (3.63) that results in a closed-form expression and thus provides more insight into the qualitative behavior of the BEP. The approximation is based on the following observation: The expression $P_e = P(f_s < g_s)$ is equivalent to $P_e = P(z < 0)$ with the decision variable $z := f_s - g_s$. Both f_s and g_s are chi-square distributed; each of them is the sum of $2N_\Delta$ statistically independent and real random variables, see (3.60) and (3.61). One characteristic of the the chi-squared PDF is its asymmetry around the peak value. The variable z however, which is the difference of two chi-square distributed random variables, has a PDF that is approximately symmetric around its peak value which strongly resembles a Gaussian PDF. A

Gaussian approximation of the PDF of z is the more accurate the larger N_Δ is. Note that z is the sum of $4N_\Delta$ real random variables.

The decision variable z has the mean value

$$\begin{aligned}\mu_z &= \mu_{f_s} - \mu_{g_s} \\ &= 2N_\Delta N_0 B + s^2 - 2N_\Delta N_0 B \\ &= s^2,\end{aligned} \tag{3.64}$$

and the variance

$$\begin{aligned}\sigma_z^2 &= \sigma_{f_s}^2 + \sigma_{g_s}^2 \\ &= 4N_\Delta (N_0 B)^2 + 4N_0 B s^2 + 4N_\Delta (N_0 B)^2 \\ &= 8N_\Delta (N_0 B)^2 + 4N_0 B s^2.\end{aligned} \tag{3.65}$$

Assuming that z is a Gaussian random variable, the PDF of z is

$$P_{\mathrm{Z}}(z) = \frac{1}{\sqrt{2\pi\sigma_z^2}} e^{-\frac{(z-\mu_z)^2}{2\sigma_z^2}},$$

and we can write the BEP as

$$\begin{aligned}P_e &= P(z < 0) \\ &= \int_{-\infty}^{0} P_{\mathrm{Z}}(z)\, dz \\ &= \frac{1}{\sqrt{2\pi\sigma_z^2}} \int_{-\infty}^{0} e^{-\frac{(z-\mu_z)^2}{2\sigma_z^2}}\, dz \\ &= \frac{1}{\sqrt{2\pi\sigma_z^2}} \int_{-\infty}^{-\mu_z} e^{-\frac{u^2}{2\sigma_z^2}}\, du \\ &= \frac{1}{\sqrt{\pi}} \int_{-\infty}^{-\frac{\mu_z}{\sqrt{2}\sigma_z}} e^{-v^2}\, dv \\ &= \frac{1}{2}\mathrm{erfc}\left(\frac{\mu_z}{\sqrt{2}\sigma_z}\right),\end{aligned} \tag{3.66}$$

where $\mathrm{erfc}(x) = \frac{2}{\sqrt{\pi}} \int_x^\infty e^{-t^2} dt$. Inserting (3.64) and (3.65) yields

$$\begin{aligned}P_e &= \frac{1}{2}\mathrm{erfc}\left(\frac{s^2}{\sqrt{2(8N_\Delta N_0^2 B^2 + 4N_0 B s^2)}}\right) \\ &= \frac{1}{2}\mathrm{erfc}\left(\frac{s^2/(2N_0 B)}{2\sqrt{N_\Delta + s^2/(2N_0 B)}}\right).\end{aligned} \tag{3.67}$$

The variable s^2 is the energy of the discrete-time received pulse b_n, see (3.62), and is approximated as

$$s^2 = \sum_{n=0}^{N_\Delta - 1} |b_n|^2 \approx \frac{2}{T_s} \int_0^{\Delta_T} b^2(t)\, dt = 2BE_r,$$

where we made use of (3.25), (3.3), and $T_s = 1/B$. The number N_Δ is defined in Subsection 3.2.3 as $N_\Delta = \Delta_T/T_s = \Delta_T B$. Substituting the variables s^2 and N_Δ by these expressions we have

$$P_e = \frac{1}{2}\text{erfc}\left(\frac{E_r/N_0}{2\sqrt{\Delta_T B + E_r/N_0}}\right). \tag{3.68}$$

The term $\Delta_T B$ is caused by the receiver noise $n(t)$, i.e., the larger the time-bandwidth product $\Delta_T B$ is, the lower is the performance of the receiver. This term grows linearly with the integration duration Δ_T and the bandwidth B of the receiver filter, which equals the bandwidth of the receiver noise.

For practical power delay profiles it is possible to chose an integration duration $T_I < \Delta_T$ which allows to capture most of the energy E_r of the received pulse while reducing the noise contribution $\Delta_T B$. To consider this case we introduce the ratio $\eta(T_I)$ of the energy that is captured with an integration duration T_I to the total received energy E_r, i.e.,

$$\eta(T_I) = \frac{\int_0^{T_I} b^2(t)\,dt}{\int_0^{\Delta_T} b^2(t)\,dt}. \tag{3.69}$$

The reduced integration results in the modified variable

$$\tilde{s}^2 = 2\eta(T_I)BE_r \tag{3.70}$$

and the modified number

$$\tilde{N}_\Delta = T_I B.$$

Substituting these expressions into (3.67) yields

$$P_e = \frac{1}{2}\text{erfc}\left(\frac{\eta(T_I)E_r/N_0}{2\sqrt{T_I B + \eta(T_I)E_r/N_0}}\right). \tag{3.71}$$

The exact expression (3.63) can also be adapted to a reduced integration duration T_I, by substituting s^2 according to (3.70) and by substituting N_Δ by $\tilde{N}_\Delta = T_I B$. A comparison of this exact expression and the approximation (3.71) is given in Subsection 3.3.5 in terms of a numerical evaluation.

3.3.2 Bit Error Probability of the MLRP

In this subsection we derive an approximate expression for the integral (3.59). First we rewrite (3.57) and (3.58) as

$$f := \sum_{n=0}^{N_\Delta - 1} u_n |\sigma_n v_n + n_n|^2, \tag{3.72}$$

and

$$g := \sum_{n=0}^{N_\Delta - 1} u_n |n_{n+N_\Delta}|^2, \tag{3.73}$$

where $u_n = \sigma_n^2/(\sigma_n^2 + N_0 B)$. The sum f is a generalized non-central Chi-sqare distributed random variable, i.e., the variances of the individual summands in (3.72) depend on the index n. A closed

form expression for the PDF $P_{\mathrm{F}}(f)$ does not exist. As mentioned, this is the reason why we derive an approximation to the BER instead of an exact expression. For this purpose we introduce the difference $z = f - g$, as in Subsection 3.3.1, and write the BER as

$$P_e = P(z < 0).$$

The mentioned approximation consists in the assumption that z is a Gaussian distributed random variable. This assumption is the more justified the larger the number of summands is that contribute to z. This number of summands equals $2N_\Delta$, see (3.72) and (3.73). Note that $N_\Delta = B\Delta_T$, i.e., the longer the channel delay spread and thus Δ_T is, the closer is the distribution of z to a Gaussian distribution. The Gaussian approximation made in this derivation resembles to the Gaussian approximation made in Subsubsection 3.3.1.1 but is less accurate. The reason for this is that in contrast to Subsubsection 3.3.1.1 here the summands are weighted by the function u_n. Therefore, the variance of the summands depends on the index n. As a consequence, a larger number of summands is needed to result in Gaussian distributed sum. For a finite number $2N_\Delta$ of summands, the random variable z, deviates more or less from a Gaussian distribution. Thus, we have to write P_e as the approximation

$$P_e \approx \frac{1}{2}\mathrm{erfc}\left(\frac{\mu_z}{\sqrt{2\sigma_z^2}}\right), \tag{3.74}$$

which is a function of the mean μ_z and the variance σ_z^2 of z. To compute μ_z and σ_z^2 we consider the the summands of f and g and denote them as $f_n = u_n|b_n + n_n|^2$ and $g_n = u_n|n_{n+N_\Delta}|^2$, respectively. The samples f_n are statistically independent, which follows from the statistical independence of the samples $b_n = \sigma_n\nu_n$ and the samples n_n, see (3.35) and (3.24). The samples g_n are statistically independent for the same reasons. Based on this statistical independence we can write the mean value and the variance of z as

$$\mu_z = \sum_{n=0}^{N_\Delta - 1} \mu_{f_n} - \mu_{g_n}$$

and

$$\sigma_z^2 = \sum_{n=0}^{N_\Delta - 1} \sigma_{f_n}^2 + \sigma_{g_n}^2.$$

As mentioned, the samples f_n are noncentrally chi-square distributed. Their mean and variance can be shown to be $\mu_{f_n} = u_n(2N_0B + |b_n|^2)$ and $\sigma_{f_n}^2 = 4u_n^2(N_0^2B^2 + N_0B|b_n|^2)$, [49]. The samples g_n are centrally chi-square distributed with mean and variance $\mu_{g_n} = 2u_nN_0B$ and $\sigma_{g_n}^2 = 4u_n^2N_0^2B^2$, respectively. With this we have

$$\mu_z = \sum_{n=0}^{N_\Delta - 1} u_n|b_n|^2$$

and

$$\sigma_z^2 = \sum_{n=0}^{N_\Delta - 1} 4u_n^2(2N_0^2B^2 + N_0B|b_n|^2).$$

Inserting these results into (3.74) yields an approximation to the BER as a function of the received-pulse samples b_n and the weighting function samples u_n in complex baseband representation. Often, it is favorable to have the BER expressed as a function of signals given in continuous-time

passband representation. Therefore, in analogy to (3.48), we apply the approximations

$$\mu_z \approx \frac{2}{T_s}\int_0^{\Delta_T} u(t)b^2(t)\,dt$$

and

$$\begin{aligned}\sigma_z^2 &\approx \frac{4N_0B}{T_s}\int_0^{\Delta_T} u^2(t)[2N_0B + b_l^2(t)]\,dt \\ &= \frac{8N_0B}{T_s}\int_0^{\Delta_T} u^2(t)[N_0B + b^2(t)]\,dt,\end{aligned}$$

where $u(t) = \sigma^2(t)/[\sigma^2(t) + N_0B]$. With this, our approximation to the BER in (3.74) yields

$$P_e \approx \frac{1}{2}\mathrm{erfc}\left(\frac{\frac{1}{N_0}\int_0^{\Delta_T} u(t)b^2(t)\,dt}{2\sqrt{B\int_0^{\Delta_T} u^2(t)\,dt + \frac{1}{N_0}\int_0^{\Delta_T} u^2(t)b^2(t)\,dt}}\right). \tag{3.75}$$

For the special case when $u(t) = 1$, i.e., when $\sigma(t) \equiv c$ or eqivalently, when no time varying weighting of the integrator input is performed, (3.75) equals the approximation for the BER of the GMLR, see (3.68). A numerical evaluation of (3.75) and a comparison with simulation results is given in Subsection 3.3.5.

Note that the structure of (3.75) resembles the approximation to the BER of the mentioned transmitted-reference receiver with weighted correlation presented in [13]. This resemblance underlines the close relationship between noncoherent and transmitted-reference receivers.

3.3.3 Bit Error Probability of the MLR

For reference and to show how much performance is lost by using a noncoherent instead of a coherent receiver, we consider the BEP of the coherent maximum likelihood receiver (MLR) for 2PPM with perfect knowledge of the received pulse shape $b(t)$. We assume that the random polarity modulation in (3.1) is switched off, i.e., $c_k = 1$ for all k. Note that unlike noncoherent receivers, the coherent MLR would have an increased BEP when the pulse polarity is randomized and unknown to the receiver.

Note further that if a coherent MLR is used, the receiver's ability to recover the pulse polarity should be exploited through e.g. the usage of binary antipodal modulation instead of the orthogonal 2PPM. Using binary antipodal modulation instead of binary orthogonal modulation offers a 3 dB performance improvement [49]. Hence, in a practical competition between the noncoherent receivers considered in this work and the MLR, the MLR would have an additional performance advantage of 3 dB, which is not shown in this work.

The BEP of the MLR for 2PPM without polarity randomization is derived in Subsection 3.7.2 for the case of narrowband interference with power P_u. For $P_u = 0$ the BEP is given by (3.128) as

$$P_e = \frac{1}{2}\mathrm{erfc}\left(\sqrt{\frac{E_r}{2N_0}}\right). \tag{3.76}$$

3.3.4 Comparison of Receiver Structures

The three receiver types envisaged in this chapter are the MLR that uses perfect channel state information, the ML receiver with partial channel state information (MLRP), and the generalized ML receiver with no channel state information (GMLR). Even though they have different properties and pros and cons, their basic architectures share a common principle: The decision on the received symbol $\hat{a}_k$ is based on the correlation of the observed signal $y(t) = r(t) + n(t)$ with a template $x(t)$. This correlation can also be interpreted as a projection of $y(t) = r(t) + n(t)$ on the template $x(t)$.

To unveil this similarity we consider the 2PPM signaling scheme introduced in Subsection 3.1 and assume the symbol $a_0 = 0$ was transmitted and the polarity of the corresponding pulse is set to $c_0 = 1$. Hence, in the interval used to convey the symbol a_0 the received signal is

$$r(t) = \begin{cases} b(t), & \text{for } 0 \le t < \Delta_T, \\ 0, & \Delta_T \le t < T. \end{cases} \tag{3.77}$$

3.3.4.1 GMLR

The decision rule for the symbol a_0 of the GMLR in (3.21) with $T_I = \Delta_T$, can be reformulated as

$$z_0 \underset{\hat{a}_0=0}{\overset{\hat{a}_0=1}{\gtrless}} 0,$$

where

$$z_0 = \int_{\Delta_T}^{T} y^2(t)\, dt - \int_{0}^{\Delta_T} y^2(t)\, dt$$

or

$$z_0 = \int_{0}^{T} y^2(t) w(t)\, dt$$

with

$$w(t) = \begin{cases} -1, & \text{for } \; t < \Delta_T, \\ 1, & \text{for } \; \Delta_T < t. \end{cases} \tag{3.78}$$

We separate the expression for z_0 into its components by inserting $r(t) = c_k b(t - kT - a_k \Delta_T)$ (see Subsection 3.1), $y(t) = r(a_k, t) + n(t)$ (see Subsection 3.2), while assuming that $c_0 = 1$, and $a_0 = 0$. Taking into account that the channel delay spread τ_c, i.e., the support $b(t)$, is smaller than Δ_T, the decision variable is obtained as

$$\begin{aligned} z_0 &= \int_{\Delta_T}^{T} n^2(t)\, dt - \int_{0}^{\Delta_T} [b(t) + n(t)]^2\, dt \\ &= \int_{\Delta_T}^{T} n^2(t)\, dt - \int_{0}^{\Delta_T} \left[b^2(t) + 2b(t)n(t) \right]\, dt - \int_{0}^{\Delta_T} n^2(t)\, dt. \end{aligned} \tag{3.79}$$

3.3.4.2 MLR

The decision rule for the MLR is derived in [49] for the general case of orthogonal symbols. For 2PPM and the symbol a_0 it is given by

$$z_0 \underset{\hat{a}_0=0}{\overset{\hat{a}_0=1}{\gtrless}} 0,$$

where

$$z_0 = \int_{\Delta_T}^{T} b(t-\Delta_T)\, y(t)\, dt - \int_{0}^{\Delta_T} b(t)\, y(t)\, dt.$$

Inserting the expression for $y(t)$ from above, using the fact that $b(t)$ vanishes outside the interval $[0, \Delta_T)$ and assuming that $a_0 = 0$ this yields

$$\begin{aligned} z_0 &= \int_{\Delta_T}^{T} b(t-\Delta_T)\, n(t)\, dt - \int_{0}^{\Delta_T} b(t)\, [b(t)+n(t)]\, dt, \\ &= \int_{0}^{\Delta_T} [b(t)n(t+\Delta_T) - b(t)n(t) - b^2(t)]\, dt. \end{aligned} \tag{3.80}$$

The noise process $n(t)$ in the interval $[0, \Delta_T)$ and in the interval $[\Delta_T, T)$ can be assumed to be uncorrelated as the noise bandwidth is B and $B \gg 1/\Delta_T$. Therefore, we can replace the sum, $n(t) - n(t-\Delta_T)$, by the expression $\sqrt{2}n'(t)$ where $n'(t)$ has the same stochastic properties as $n(t)$. With this and for $a_0 = 0$ we get

$$z_0 = -\int_{0}^{T} \left[b^2(t) + \sqrt{2} b(t) n'(t) \right] dt. \tag{3.81}$$

Note that this variable is different from the decision variable z_0 in (3.79) but has the same statistics, which is sufficient for the BEP analysis.

We compare the performance of the GMLR with that of the MLR in the high SNR regime by letting the SNR go to infinity, hence the noise terms of the decision variables in (3.79) and (3.81) are expressed by $2b(t)n(t)$ and $\sqrt{2}b(t)n'(t)$, respectively, as the terms $n^2(t)$ and $n^2(t-\Delta_T)$ in (3.79) can be neglected. We conclude from this comparison that in the high SNR regime, the sensitivity to noise of the GMLR is stronger by 3 dB than for the MLR. The same observation can be made by computing the limit $E_r/N_0 \to \infty$ of (3.71), which yields

$$\lim_{E_r/N_0 \to \infty} \frac{1}{2}\mathrm{erfc}\left(\frac{E_r/N_0}{2\sqrt{T_I B + E_r/N_0}} \right) = \frac{1}{2}\mathrm{erfc}\left(\sqrt{\frac{E_r}{4N_0}} \right),$$

and by comparing this result with (3.76) (note that $\eta(T_I) = 1$ for $T_I = \Delta_T$).

Figure 3.3 shows a graphical representation of the signal path of these two receiver types. The primary difference is that the noncoherent receivers MLRP and GMLR use the received signal as their own correlation template, while the coherent ML receiver correlates with an exactly synchronized correlation template or received pulse shape $b(t)$.

3.3.5 Performance Evaluation

This section presents numerical evaluations of the BEP for the three receiver types GMLR, MLRP, and MLR. Both, analytical and simulation results are shown for the GMLR and the MLRP, whereas only analytical results are shown for the well known MLR. The evaluations are performed for two different received pulse shapes $b(t)$. They are the realization 1 of the channel model, CM1 and CM4 respectively, which are described in [23]. The bandwidth of the received pulse shapes is $B = 1$ GHz and the center frequency is $f_0 = 4$ GHz. Fig. 3.4 shows the plot of the corresponding CIRs.

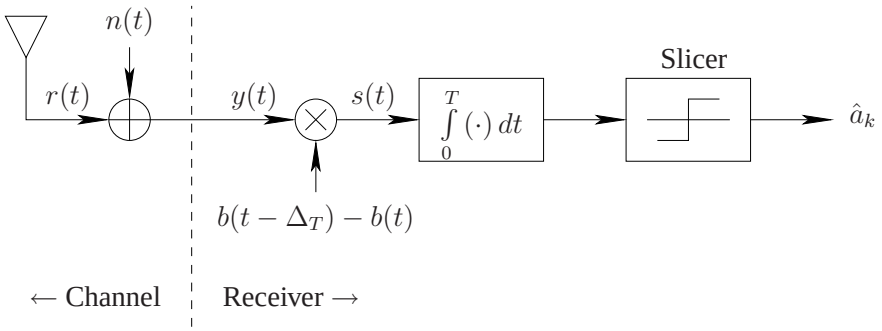

(a) Maximum likelihood receiver architecture (correlator receiver).

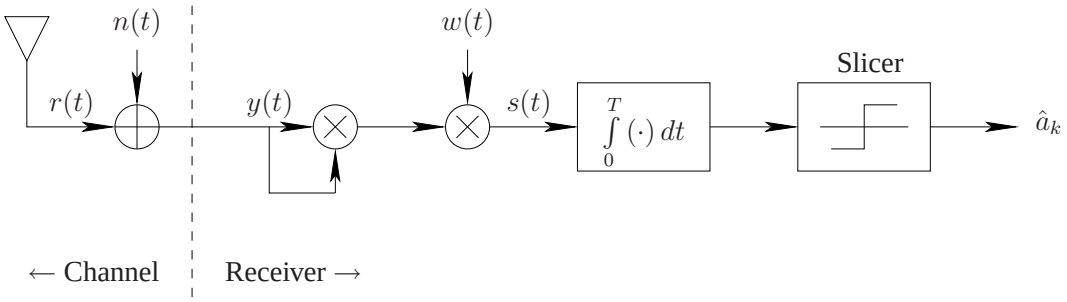

(b) GMLR and MLRP architecture.

Fig. 3.3. Architecture of the maximum likelihood receiver with perfect channel state information (MLR), the generalized maximum likelihood receiver (GMLR) and the maximum likelihood receiver with partial channel state information (MLRP). These simple architectures are suited to receive only the symbol a_k with index $k = 0$.

As an alternative to evaluate the BEP performance only for two channel realizations one could evaluate the BEP performance for a set of channel realizations and compute the average BEP. The decision to evaluate the performance for merely two channel realizations has the following reasons:

(i) One purpose of the numerical BEP evaluations is to verify the analytical expressions. This verification is more reliable when the BEP is evaluated for an individual channel realization. Considering the average BEP for a set of channel realizations could potentially hide relevant effects.

(ii) Another purpose of the numerical BEP evaluations is to compare the performance of the proposed noncoherent receivers with the performance of the coherent MLR. The basic effects can be observed by comparing BEP curves for two types of channels, one with a short and one with a large delay spread, respectively, i.e., for CM1 and CM4.

(iii) The large bandwidth of the UWB signals results in expensive simulation periods. Restricting the evaluation to the BEP for only two channel realizations reduces the required simulation time considerably.

The MLRP uses an estimate of $\sigma^2(t)$ which is the variance of the impulse response process $\mathrm{B}(t)$, i.e., $\sigma^2(t) = \mathbb{E}\{\mathrm{B}(t)\}$. In order to determine the estimate $\hat{\sigma}^2(t)$ of $\sigma^2(t)$, an ensemble of received pulse shapes is required; however, in a practical receiver only a single received pulse $b(t)$ may be available. The property that the bandwidth B_σ of the variance $\sigma^2(t)$ is much smaller than the bandwidth of the CIR, B, allows us to replace the ensemble average by a short-time average, i.e.,

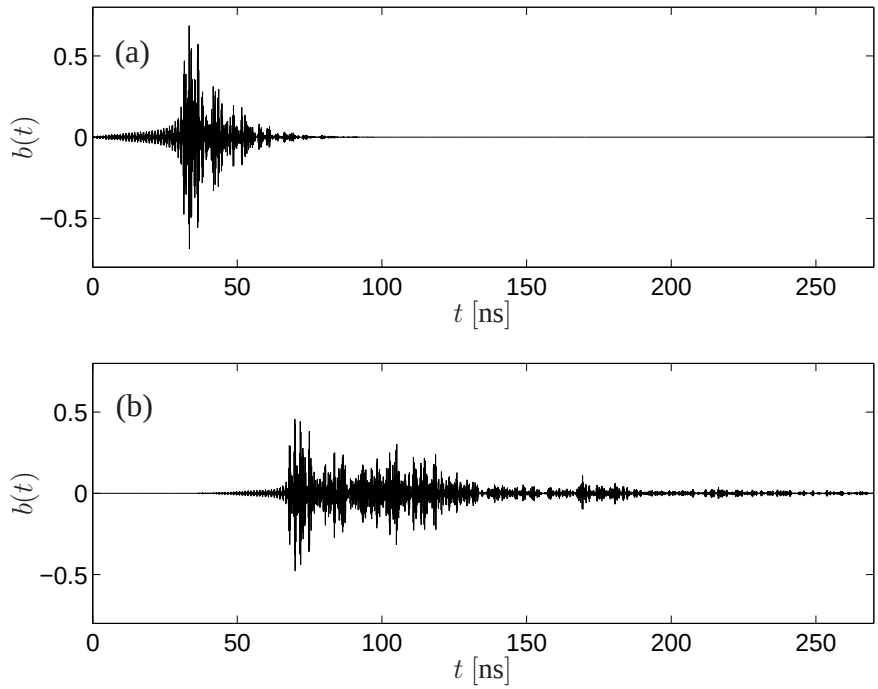

Fig. 3.4. Channel impulse responses of (a) CM1 realization 1 and (b) CM4 realization 1. The bandwidth is limited by an ideal bandpass filter with center frequency $f_0 = 4$ GHz and bandwidth $B = 1$ GHz.

to estimate $\sigma^2(t)$ by computing the short-time average of $b^2(t)$. We set

$$\hat{\sigma^2}(t) = \frac{1}{2LT_s} \int_{t-LT_s}^{t+LT_s} b^2(\tau) d\tau,$$

where $2LT_s$ is the duration over which the average is taken. $1/T_s$ is the Nyquist sampling rate of the received pulse shape in passband representation, i.e., $T_s = 1/(2f_0 + B)$. The estimate for $\sigma^2(t)$ is shown in Fig. 3.5 for the realization 1 of CM1 and for different averaging lengths LT_s. For $L = 0$ we observe, that the estimated standard deviation $\hat{\sigma}(t) = \sqrt{\hat{\sigma}^2(t)}$ follows the instantaneous power of the CIR; however, the larger L becomes, the less sensitive does the estimate $\hat{\sigma}(t)$ react to fast changes of the instantaneous power of the CIR. We conclude that the estimate is the more accurate and more peaky, the smaller L is. Note however, that an accurate estimator with small L is more challenging to implement than a less accurate one. The corresponding weight functions, $w(t)$, according to (3.51) are shown in Fig. 3.6 for different L values and for different values of received signal to noise ratio (SNR), which is defined as

$$\text{SNR} = \frac{E_r}{N_0}.$$

Now we compare Fig. 3.5 with Fig. 3.6, e.g., for the parameter $L = 0$. For large values of $\hat{\sigma}(t)$ we observe that the weighting function $w(t)$ has a value close to unity and thus passes the signal $y(t)$ with an unchanged amplitude to the integrator. In contrast, small values of $\hat{\sigma}(t)$ cause $w(t)$ to be small, too and thus to attenuate the integrators input signal. The amount of this attenuation is also influenced by the SNR. This is because the smaller the SNR is, the more relative noise power is contained in the signal $y(t)$ during periods of small instantaneous received power. Therefore, it is effective to attenuate the integrator's input signal in periods of small received power the more,

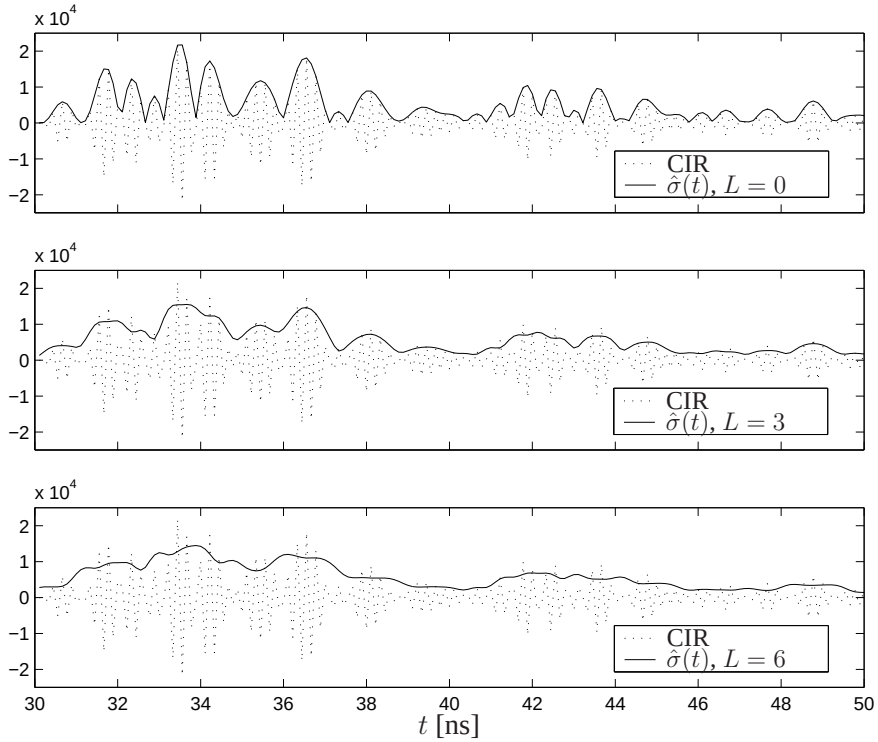

Fig. 3.5. Zoom into channel impulse responses realization 1 of channel model CM1 and corresponding estimate, $\hat{\sigma}(t)$.

the lower the SNR is. This property of the weighting function can be observed from Fig. 3.51 when comparing the graphs for SNR $= 5$ dB and SNR $= 15$ dB. Furthermore, we find that the weighting function controls the attenuation the more effective, the more accurate the estimate of the instantaneous received power is.

The BEP of the MLR is shown for reference in Fig. 3.7, 3.9, and 3.10 as a function of the SNR. Note that for this receiver the BEP does not depend on the shape of the received pulse $b(t)$ but only on its energy E_r and the noise power spectral density N_0, i.e, on the SNR. Figure 3.7 also shows the BEP of the GMLR which corresponds to the exact analytic expression (3.63) and the approximation (3.71). From both Fig. 3.7(a) and Fig. 3.7(b), we observe that for a BEP $P_e > 10^{-3}$ the expression (3.71) is a good approximation for (3.63). It is important to note that the parameter T_I has been chosen to minimize the BEP and that this minimization requires some a priori knowledge about the received pulse shape and the receiver SNR. Therefore, a GMLR that has no channel information cannot optimize the integration duration T_I. For the channel realizations 1 of CM1 and CM4 the optimum integration durations are $T_I = 15$ ns and $T_I = 50$ ns, respectively. Fig. 3.8 illustrates how the BEP of the GMLR depends on the choice of the integration duration T_I and on the SNR. The behavior of the BEP can be understood by inspecting expression (3.71) and the characteristics of the captured energy $\eta(T_I)E_r$, which is shown in Figs. 3.8(a.2) 3.8(b.2) for CM1 and CM4. There are two concurring effects impacting the BEP:

(i) Increasing T_I increases the ratio $\eta(T_I)E_r/N_0$ and thus reduces the BEP.

(ii) Increasing T_I increases the noise term $T_I B$ and therefore increases the BEP.

The particular shape of $\eta(T_I)$ causes a minimum in the BEP versus T_I function; this minimum shifts towards larger T_I the slower the captured energy increases with T_I. Note that the optimum value for T_I in general depends also on the SNR in addition to the function $\eta(T_I)$. Thus, in order

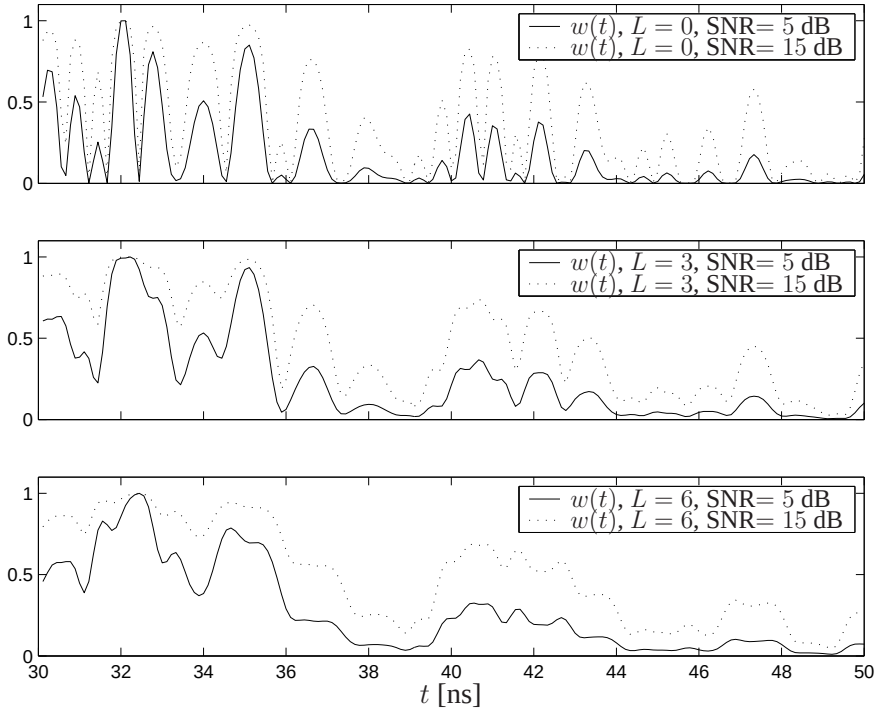

Fig. 3.6. Zoom into normalized weight functions for channel response realization 1 of channel model CM1 and different values of L and SNR.

to optimize the integration duration, knowledge of the function $\eta(T_I)$ and of the SNR is required. Section 3.4 presents a robust design approach for T_I that does not require this knowledge. Figure 3.9 shows the exact and simulated BEP as a function of the SNR for different values of T_I. We observe that the sensitivity loss of the GMLR when compared to the MLR is between 4.3 to 6.5 dB at $P_e = 10^{-3}$ for CM1 and CM4, respectively. The reason for this is the increased noise in the decision variable z_k, compare (3.79) and (3.80).

Unlike the GMLR, the MLRP has knowledge about the power delay profile of the received pulse shape $b(t)$, see Fig. 3.5. It uses this knowledge to weight the input signal of the integrator, see Fig. 3.3(b), and thus reduces the impact of the noise. For the case where the estimate of the power delay profile is most precise, i.e., for $L = 0$, the sensitivity can be enhanced by 1.3 to 2.2 dB for CM1 and CM4, respectively, see Fig. 3.7. In practice there are some reasons to use a larger L:

(i) Larger L can reduce the variance of the estimate in cases where a small number of received pulses is available or when the recovered symbol clock is disturbed by a timing jitter.

(ii) Furthermore, the signal $w(t)$ is the smoother the larger L is; this allows to use a less accurate synchronization, i.e., allows a larger timing jitter.

Figure 3.10 shows the BEP as a function of the SNR for different values of L. As well as for the GMLR, the BEP of the MLRP is the lower, the shorter the channel delay spread is. This is, because the amount of captured noise is lower for smaller delay spread, see Fig. 3.11(a) and 3.11(b).

The analytical approximation (3.75) to the BER was derived under the assumption that the APDP, $\sigma^2(t)$, is exactly known. However, in this Section the weighting function $w(t)$ is determined on basis of the estimated APDP $\hat{\sigma}^2(t)$. Therefore, to determine the corresponding BER, we substitute $u(t)$ by $\hat{u}(t) = \hat{\sigma}^2(t)/[\hat{\sigma}^2(t) + N_0 B]$ in (3.75). With this, the BER, P_e, becomes a function of L.

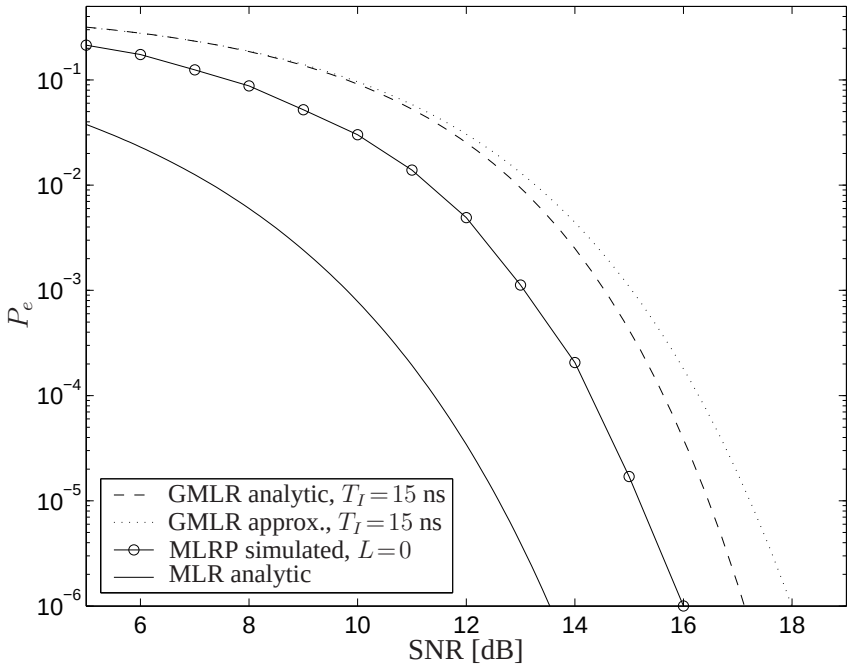

(a) For channel impulse response 1 of model CM1.

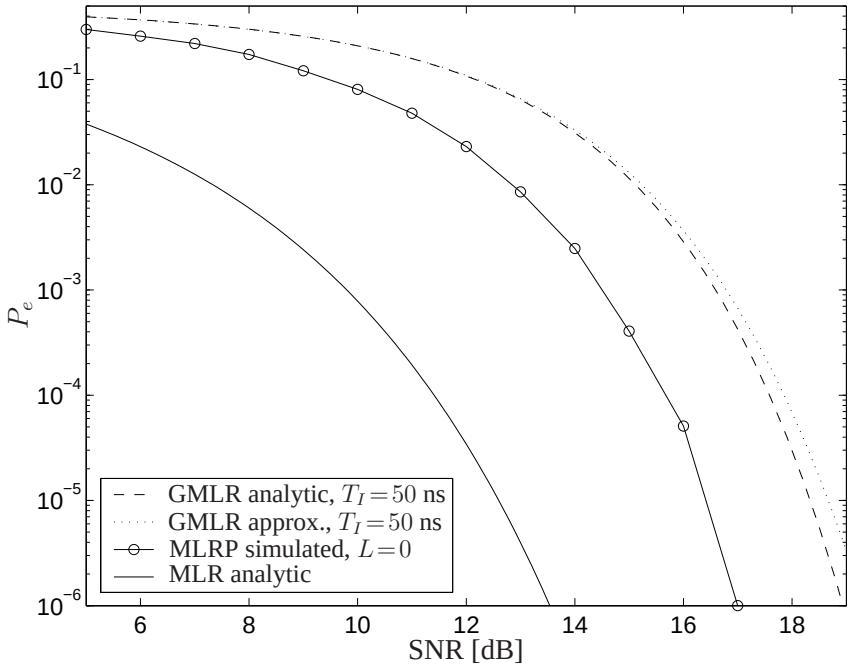

(b) For channel impulse response 1 of model CM4.

Fig. 3.7. BEP of the generalized maximum likelihood receiver (GMLR), the maximum likelihood receiver with partial channel state information (MLRP) and the maximum likelihood receiver with perfect channel state information (MLR).

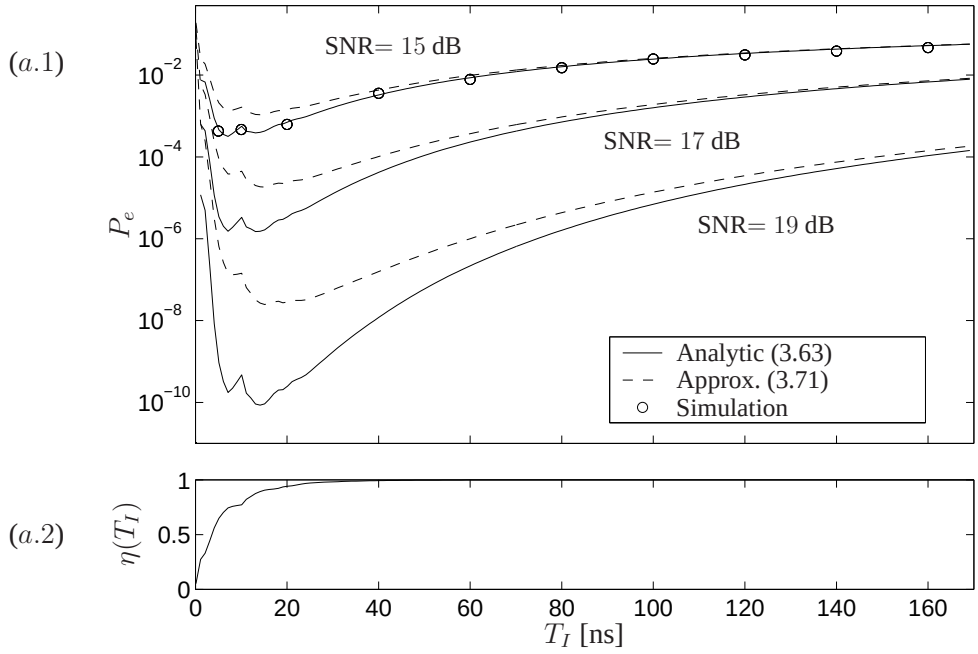

(a) For channel impulse response 1 of model CM1.

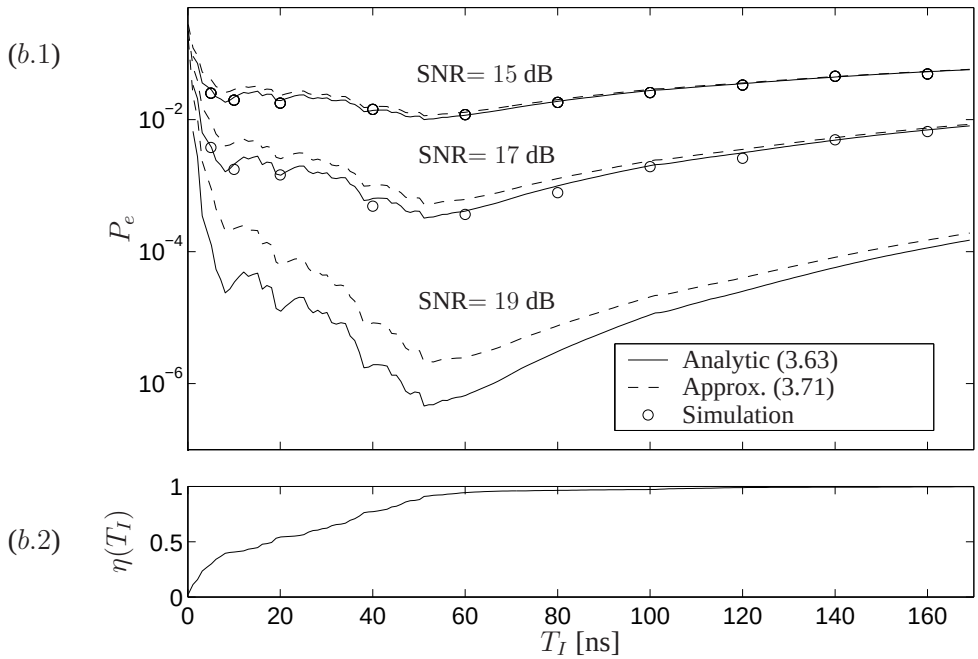

(b) For channel impulse response 1 of model CM4.

Fig. 3.8. The BEP of the GMLR as a function of the integration time T_I is given in $(a.1)$ and $(b.1)$; in $(a.2)$ and $(b.2)$ show the ratio of captured to received energy, $\eta(T_I)$.

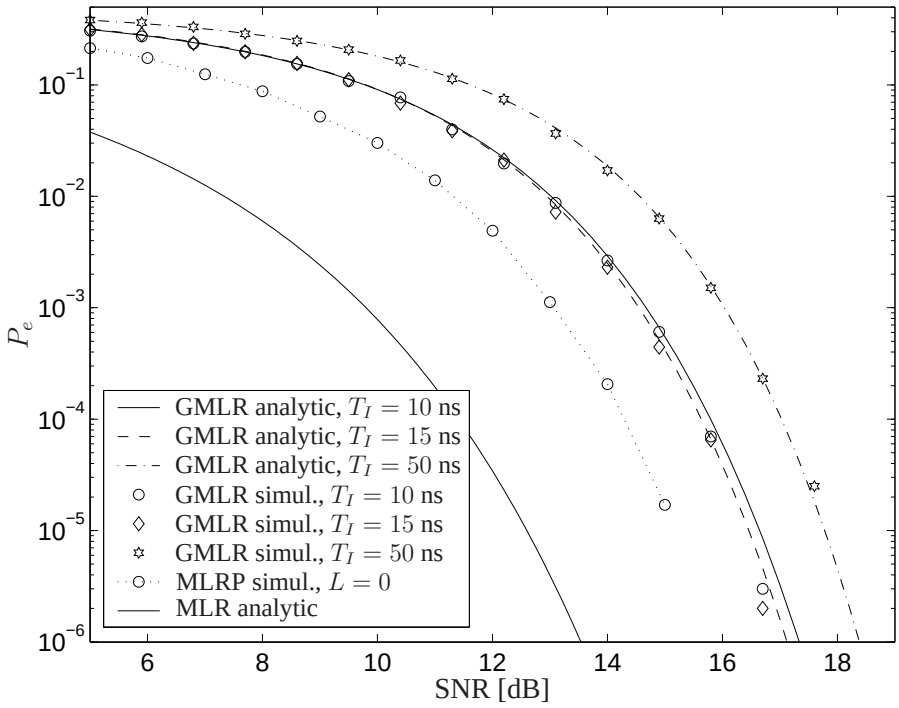

(a) For channel impulse response 1 of model CM1.

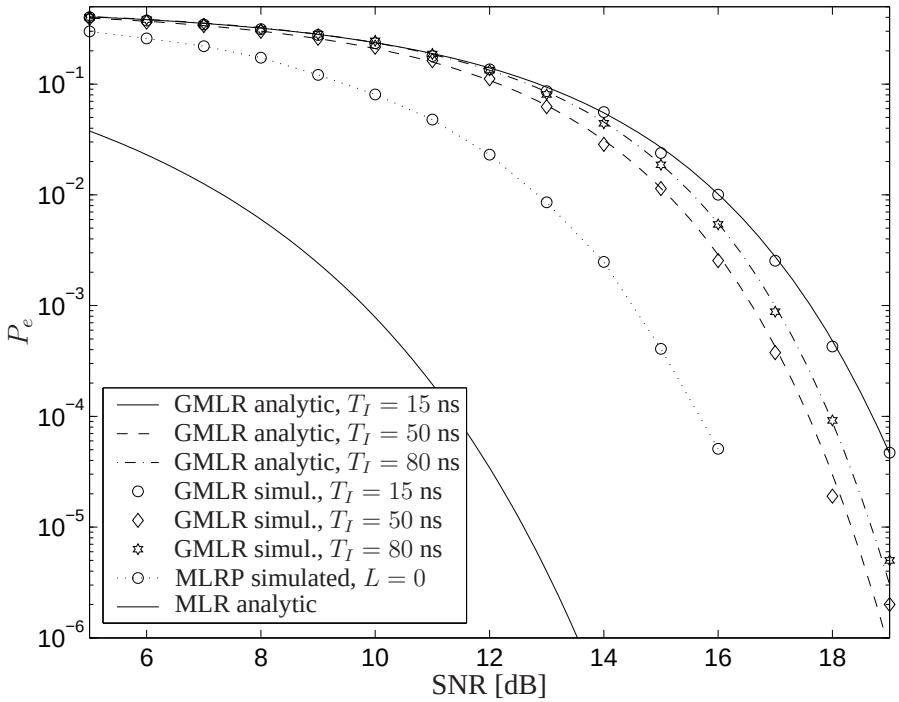

(b) For channel impulse response 1 of model CM4.

Fig. 3.9. BEP of GMLR for various integration durations T_I. The BEPs of the MLR and the MLRP with optimum parameter $L = 0$ are given for reference.

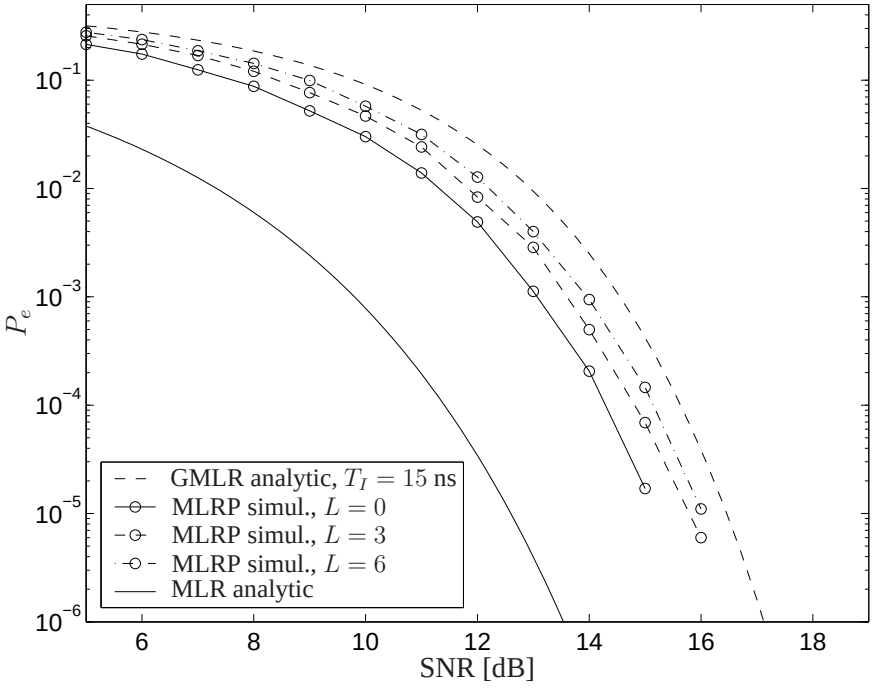

(a) For channel impulse response 1 of model CM1.

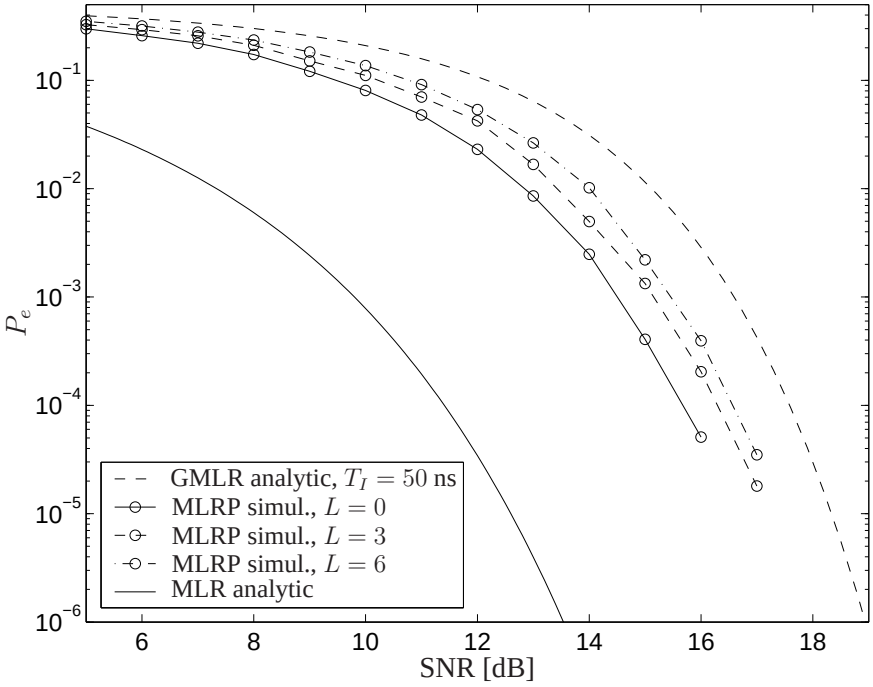

(b) For channel impulse response 1 of model CM4.

Fig. 3.10. BEP of MLRP for various estimators for $\sigma(t)$, i.e. filter lengths L. The BEPs of the MLR and the GMLR with optimum integration durations $T_I = 15$ and 50 ns are given for reference.

The resulting approximation to the BER is shown as a function of the SNR in Fig. 3.11 for $L = 0$ and $L = 6$, whereas Fig. 3.11(a) and Fig. 3.11(b) are valid for the first channel realization of the channel models CM1 and CM4, respectively. For comparison, these two figures also show the simulated BER and the BER of the GMLR with optimum integration duration. The latter represents an upper bound to the BER of the MLRP. This is because the GMLR implicitly assumes that the APDP is a constant within the integration duration, and therefore corresponds to an MLRP with an inappropriate weighting function $w(t)$.

The approximation to the BER of the MLRP given by (3.75) is shown in Fig. 3.11(a) for the channel model CM1. We observe that this approximation is quite inaccurate and overestimates the BER. Moreover, for SNRs larger than 14 dB, a closer approximation is represented by the BER curve of the GMLR. Our approximation provides such inaccurate results because the sum z of the terms f_n and g_n is not Gaussian distributed, i.e., the central limit theorem cannot be applied. There are two reasons for this: (i) Too few terms f_n and g_n are involved, and (ii) the weights u_n cause the variances of the summands f_n and g_n to be too different.

Channels with a larger delay spread result in a larger number of sums N_Δ, thus leading to a distribution of the decision variable that is closer to Gaussian. Hence, (3.75) is the more accurate, the longer the channel delay spread is. As an example, we consider the first realization of CM4. The corresponding approximative BER curve is shown in Fig. 3.11(b) and provides a reasonable good match for BERs beyond 10^{-2}. We conclude that the application of our approximation should be restricted to channels with a relatively long delay spread. Channels with a particularly long delay spread, reaching to several hundred nanoseconds, are encountered in large halls, e.g., industrial environments.

3.4 Robust Design of the GMLR

The optimum receiver performance is achieved if the integration duration T_I is adapted to the received pulse shape, see Fig. 3.8. In many practical communication systems, however, a guaranteed minimum performance is required, and the fact that the performance will be above this minimum in some or most cases is not relevant. The robust approach presented in this section is suited for this type of applications. It chooses T_I such that it minimizes the maximum BEP that can occur for a given set $\mathcal{B}$ of received pulses $b(t)$, i.e.,

$$T_{I,\text{opt}} = \min_{T_I} \max_{b(t)\in\mathcal{B}} \left\{ P_e\left(T_I, b(t)\right) \right\}. \tag{3.82}$$

In order to solve this minimax problem, the set of received pulses $\mathcal{B}$ must be known. To get a solution that does not depend on the CIRs realizations, that will be trialled during the operation of the considered communication system, we assume a simplified channel model. This model still reflects the most important properties of realistic channels discussed in Chapter 2. The simplification consists of the three assumptions:

(i) The captured energy ratio is modeled by the expression $\eta(T_I) = 1 - e^{-t/\gamma}$; this function is plotted in Fig. 3.12(b). The variable γ is the exponential decay constant of the PDP, see (2.1). The curves for the empirical function $\eta(T_I)$ are shown in Figs. 3.8(a.2) and 3.8(b.2); they show only approximately exponential characteristics.

(ii) The exponential decay constant, γ, strictly increases with the transmitter-to-receiver distance d.

(iii) The path gain α is a strictly decreasing function of the transmitter-to-receiver distance d.

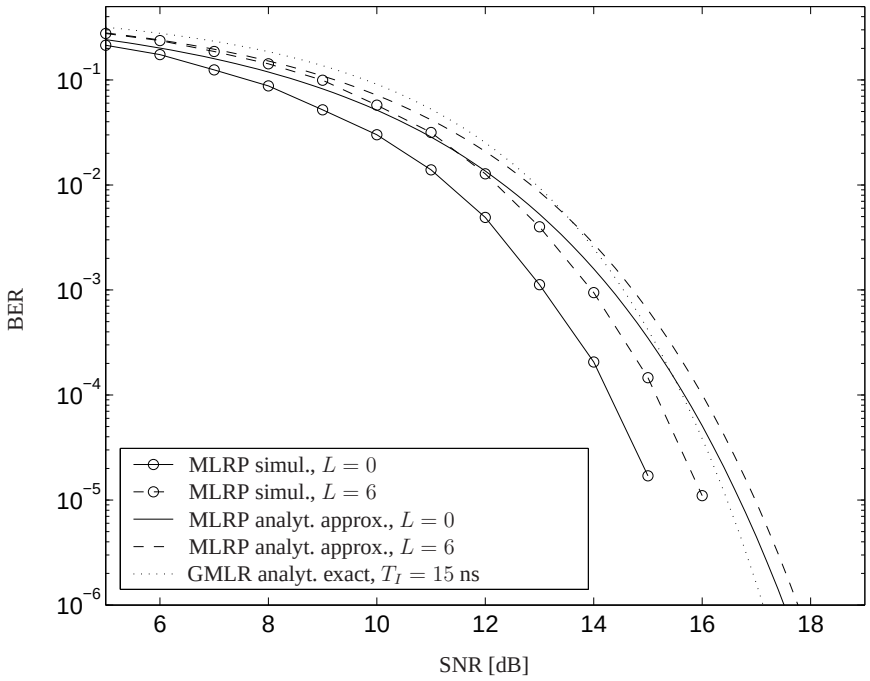

(a) BER for channel impulse response 1 of model CM1.

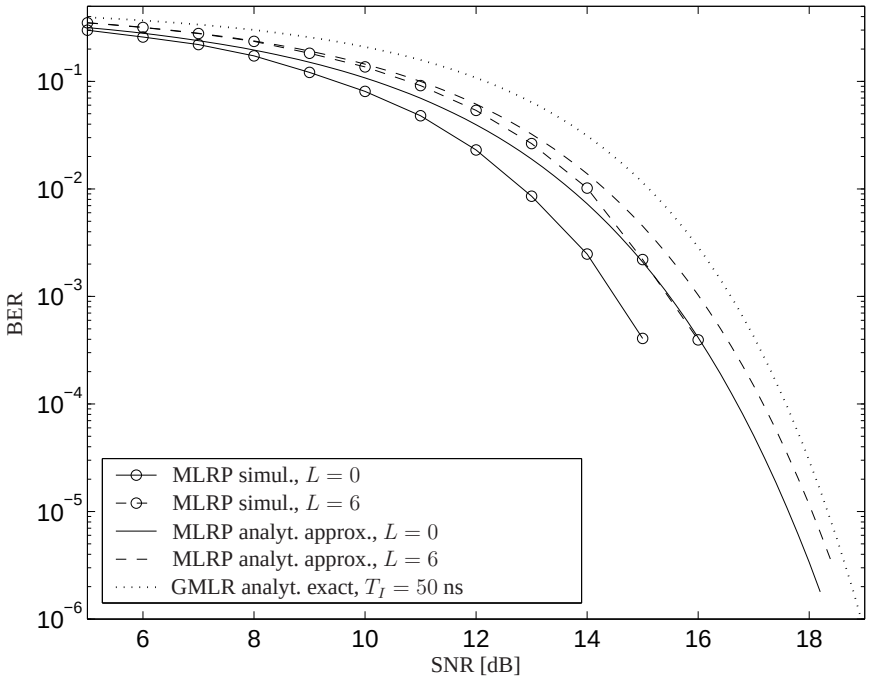

(b) BER for channel impulse response 1 of model CM4.

Fig. 3.11. Simulated BER and analytic approximation of the BER for the MLRP for various estimators of $\sigma(t)$, i.e., filter lengths L. For reference, also the exact BER [52] of the GMLR with optimum integration durations $T_I = 15$ and 50 ns is given [71].

Note that the path gain is defined in (3.4) as the ratio of the received energy per pulse to the transmitted energy per pulse, i.e., $\alpha = E_r/E_t$.

The two approximations γ and α being a strictly increasing function and a strictly decreasing function of d, respectively, are justified by the linear regression curves for γ and α presented in [63] and [24]. With the above definitions the product $E_r\eta(T_I)$ is expressed as

$$\begin{aligned} E_r\eta(T_I) &= E_t\alpha(d)\eta(T_I) \\ &= E_t\alpha(d)[1 - e^{-t/\gamma(d)}] \end{aligned} \tag{3.83}$$

and is a strictly decreasing function of d, i.e., $\partial E_r\eta(T_I)/\partial d < 0$. Based on this observation we conclude that (3.71) strictly increases with d, i.e., $\partial P_e/\partial d > 0$. With (3.83) we can express P_e as a function of d instead of $b(t)$. Thus, we can rewrite the problem (3.82) as

$$\begin{aligned} T_{I,\text{opt}} &= \min_{T_I} \max_{d\in\mathcal{D}} \{P_e\,(T_I, d))\} \\ &= \min_{T_I} \{P_e\,(T_I, d_{\text{max}})\} \\ &= \min_{T_I} \left\{ \frac{1}{2}\text{erfc}\left(\frac{\eta(T_I, d_{\text{max}})\,\alpha(d_{\text{max}})\,E_t/N_0}{2\sqrt{T_I B + \eta(T_I, d_{\text{max}})\,\alpha(d_{\text{max}})\,E_t/N_0}} \right) \right\}, \end{aligned} \tag{3.84}$$

where $\mathcal{D}$ is the set of transmitter-to-receiver distances associated with the channels of the set $\mathcal{B}$, and d_{max} is the largest element of $\mathcal{D}$, i.e., the largest transmitter-to-receiver distance of all received pulses in $\mathcal{B}$. Expression (3.84) can be solved numerically for T_I and yields the robust solution.

Example: We assume that the emitted signal is an ideal bandpass pulse with bandwidth $B = 1$ GHz, the maximal transmitter-to-receiver distance is $d_{\text{max}} = 40$ m, the corresponding path gain $\alpha(d_{\text{max}})$ is -79 dB. The exponential decay constant of the power delay profile is $\gamma(d_{\text{max}}) = 10$ ns. The noise power spectral density for an assumed noise temperature of 6 dB is $N_0 = 10^{F_N/10}\,K\,T = 1.65 \cdot 10^{-20}$ Ws, where k ist the Boltzmann konstant, $k = 1.38 \cdot 10^{-23}$ Ws/K, $T = 300$ K and the receiver noise-figure is $F_N = 6$ dB. The emitted energy per pulse is $E_t = 75$ pW which results in a power spectral density of -41.25 dBm/MHz for a symbol rate of 1 MHz.

Fig. 3.12 shows the function to be minimized in (3.84), as well as $\eta(T_I, d_{\text{max}}) = 1 - e^{-t/\gamma(d_{\text{max}})}$ as a function of T_I and for the given parameters. The optimum value for T_I obtained by evaluation of (3.84) is

$$T_{I,\text{opt}} = 23.9\,\text{ns},$$

which results in the minimum BEP as can be seen from Fig. 3.12. The resulting receiver is robust against channel variations in the sense that the BEP is minimized for the worst case channel; all other channels of the set $\mathcal{B}$ will result in a superior performance. In Fig. 3.12 the BEP of the GMLR is compared with that of a coherent selective rake receiver as a function of the integration duration T_I. Note that the selective rake receiver is a modification of the MLR which captures only a certain portion $\eta(T_I)E_r$ of the total received energy E_r, as is the case for the GMLR.

For the derivation of T_I we have assumed an exponentially decaying power delay profile, strictly increasing decay parameter $\gamma(d)$ and path gain $\alpha(d)$ with the transmitter-to-receiver distance d. These assumptions are only approximately satisfied by a set of practical channels $\mathcal{B}$ Hence, the presented solution for the integration duration T_I is only an approximation to the optimal duration. However, the advantage of this method is that the set of channels $\mathcal{B}$ does not need to be known a priori. In contrast, the optimal integration duration can only be determined when $\mathcal{B}$ is known.

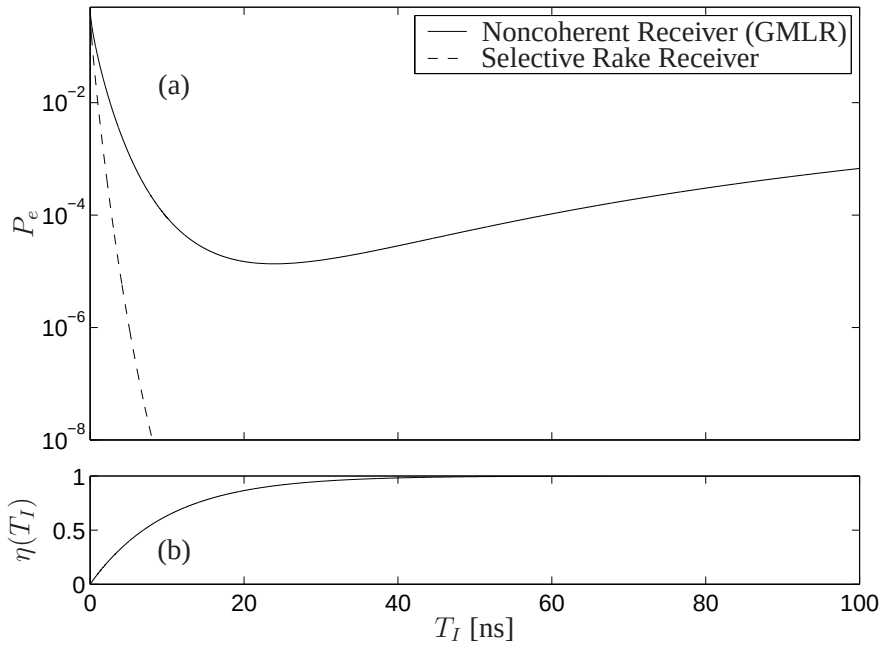

Fig. 3.12. The BEP of the GMLR as a function of the integration time T_I is given in (a); in (b) the ratio of captured to received energy, $\eta(T_I)$, is shown.

The MLRP makes the selection of the integration duration which is described in this Section unnecessary, because it determines by channel estimation in what time periods the received signal has to be considered or ignored.

3.5 Effects of the Signal Bandwidth

Three primary effects on the system performance can be observed that depend on the signal bandwidth:

(i) The emission regulation for UWB signals specifies an admissible power spectral density; hence, the total emitted power of a transmitter that fully exploits this limit will grow in proportion with the emitted signal bandwidth B.

(ii) The frequency diversity increases with the signal bandwidth, which implies that the energy that is captured by the receiver suffers less small-scale fading for a larger signal bandwidth. Fading effects are described by the statistics of the path gain α. Note that the received energy per pulse is given by $E_r = \alpha E_t$.

(iii) An effect that is ignored in the literature on UWB receiver design is that the path gain α is a function $\alpha(f) \sim 1/f^m$ (see Section 2.2.4). For the free space propagation channel this is $\alpha(f) = (c/4\pi df)^m$, with $m = 2$ see [36, 37]; here c is the speed of light and d is the separation between transmitter and receiver antenna. This effect is caused by the effective aperture of the receiver antenna, which scales with $1/f^2$; the received energy is proportional to this aperture.

We investigate the effect of (i) and (iii) on the BEP of the GMLR as a function of the SNR. We assume free space propagation; thus fading effects mentioned under (ii) have no impact. We assume that a transmitted UWB pulse has the energy spectral density D within the signal bandwidth B, and the lower and upper cut-off frequencies are f_l and f_u, i.e., $B = f_u - f_l$. Note, that in practice, a constant energy spectral density, D, cannot be realized. This is in particular the case at the slopes of the signal band. Hence, assuming a constant D introduces an error in the modelling of a practical

transmission system which, depends on the implementation of the transmission system. In this work we ignore this implementation aspect and assume a constant D, which greatly simplifies our derivations.

With the frequency dependent path gain given above and the theoretical free-space path gain $\alpha' = (c/4\pi d)^2$ and $E_t = DB$, the received energy per pulse is given by

$$\begin{aligned} E_r &= \int_{f_l}^{f_u} D\,\alpha(f)\,df = D\,\alpha' \int_{f_l}^{f_u} \frac{df}{f^2} = -\frac{D\,\alpha'}{f}\Big|_{f_l}^{f_u} \\ &= D\,\alpha'\left(\frac{1}{f_l} - \frac{1}{f_u}\right) = \frac{E_t\alpha'}{f_u f_l}. \end{aligned} \tag{3.85}$$

Inserting this expression into the approximate expression (3.71) for the BEP of the GMLR yields

$$\begin{aligned} P_e &= \frac{1}{2}\text{erfc}\left(\frac{E_t\alpha'\eta(T_I)/(N_0 f_l f_u)}{2\sqrt{T_I(f_u - f_l) + E_t\alpha'\eta(T_I)/(N_0 f_l f_u)}}\right) \\ &= \frac{1}{2}\text{erfc}\left(\frac{D(f_u - f_l)c^2\eta(T_I)/(16\pi^2 N_0 d^2 f_l f_u)}{2\sqrt{T_I(f_u - f_l) + D(f_u - f_l)c^2\eta(T_I)/(16\pi^2 N_0 d^2 f_l f_u)}}\right). \end{aligned} \tag{3.86}$$

Assuming that all parameters are fixed except the upper cut-off frequency f_u, this expression has a minimum for a certain f_u, which is given by

$$f_{u,\text{opt}} = \arg\min_{f_u}\{P_e(f_u, d)\} = f_l + \sqrt{f_l^2 + \frac{c^2 D\eta(T_I)}{16\pi^2 N_0 T_I d^2}}. \tag{3.87}$$

Fig. 3.13 shows the evaluation of the BEP in (3.86) as a function of the upper cut-off frequency f_u and for different transmitter-to-receiver distances, while all other parameters are fixed: The energy spectral density of a single pulse is $D = E_0 10^{-6}$ s such that for a symbol rate of 1 MHz the energy spectral density is $E_0 = -41.25$ dBm/MHz. The lower cut-off frequency is $f_l = 3.5$ GHz, the integration duation is $T_I = 40$ ns, the ratio of the captured to received energy per pulse is $\eta(T_I) = 0.8$, $c = 3 \cdot 10^8$ m/s is the speed of light, the noise PSD is $N_0 = kT10^{F_N/10}$, with the Boltzmann constant $k = 1.38 \cdot 10^{-23}$ Ws/K, the environmental temperature $T = 300$ K, and the receiver noise figure $F_N = 6$ dB. We observe that above a certain value of f_u the BEP increases when the bandwidth and thus the energy per received pulse is increased. An explanation for this behavior is the following. The captured energy grows with f_u; however, this growth is the slower the larger f_u is (this is because of the channel's $1/f^2$ characteristic). The captured noise energy, however, grows linearly with f_u; therefore, the BEP is minimized for a finite frequency f_u and thus for a finite bandwidth $B = f_u - f_l$. The reason for this is that the receiver filter is an optimum bandpass filter and is not adapted to the spectrum of the received pulse. To optimize the receiver performance, the receiver filter should be adapted to the $1/f$ frequency-characteristic of the channel.

3.6 Effect of Finite Integrator Bandwidth of the GMLR

Ideally, the integrator will compute the integral of the signal $s(t) = y^2(t)$ over the interval $[0, T_I]$, i.e, the integrator output is

$$q = \int_0^{T_I} y^2(t)\,dt.$$

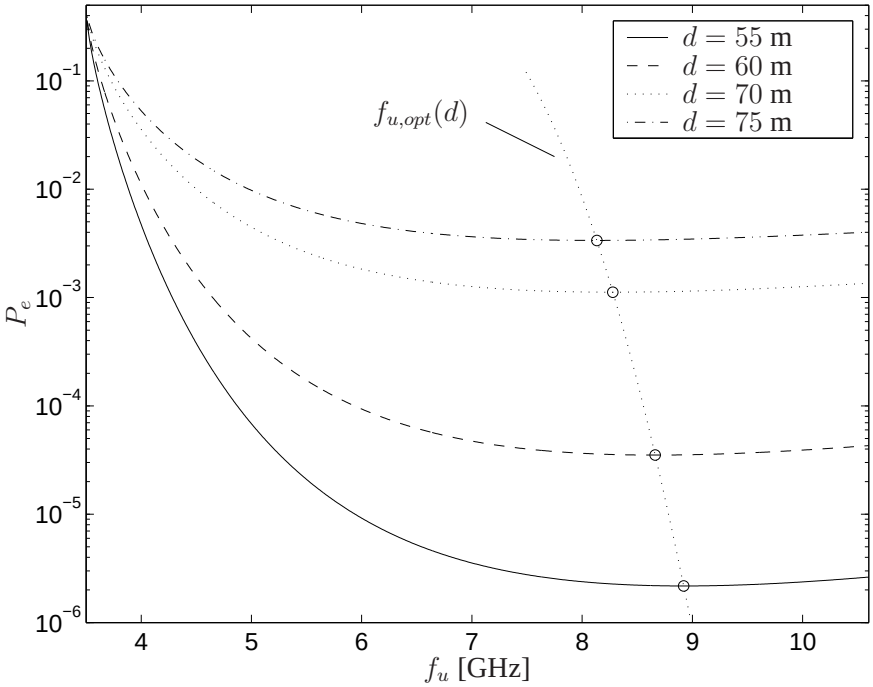

Fig. 3.13. BEP depending on the upper cut-off frequency f_u and on the transmitter to receiver distance d.

Practical implementations of the integrator reduce the bandwidth of the signal $y^2(t)$. This effect is modelled by the convolution with the response of an ideal lowpass filter response $x(t)$ with one-sided bandwidth B and no attenuation in the passband, hence,

$$x(t) = \frac{4B\sin(2\pi Bt)}{2\pi Bt} \overset{t,f}{\circ\!\!-\!\!\bullet} \begin{cases} 1, & \text{for } |f| < B, \\ 0, & \text{else.} \end{cases}$$

We compute the integrator output as

$$q' = \int_0^{T_I} [y^2(t) * x(t)]\, dt.$$

To see the impact of the bandwidth B on the integrator output q' we compare q' with the output q of the ideal integrator having an infinite bandwidth B. The impulse response of the lowpass filter, $x(t)$, decays to zero in proportion to $1/t$. Assuming for example $B = 2$ GHz, the impulse response $x(t)$ has decayed to a tenth of its maximum value, $x(0)$, at $t_{10} = 10/(2\pi B) = 0.8$ ns. The support of the convolution $y^2(t) * x(t)$ is infinite in principle. As the channels considered in this work have a delay spread in the order of some tens of a ns it follows that $T_I \gg t_{10}$. Therefore, when we consider only an individual received symbol, it is more than sufficient to consider a support of T_I for the signal $y(t)$. This allows us to write

$$q' = \int_0^{T_I} [y^2(t) * x(t)]\, dt \approx \int_{-\infty}^{\infty} [y^2(t) * x(t)]\, dt. \tag{3.88}$$

With

$$y^2(t) * x(t) \overset{t,f}{\circ\!\!-\!\!\bullet} [Y(f) * Y(f)]\,\text{rect}(f/B),$$

where $y(t) \circ\!\!-\!\!\bullet^{t,f} S(f)$ and rect(f) = 1 for $|f| < 1$ and zero outside, we can write

$$\begin{aligned} q' \approx \int_{-\infty}^{\infty} y^2(t) * g(t)\, e^{-2\pi f t}\, dt \Big|_{f=0} &= [Y(f) * Y(f)]\text{rect}(f/B)|_{f=0} \\ &= [Y(f) * Y(f)]|_{f=0} \\ &= \int_{-\infty}^{\infty} Y(f)Y(-f)\, df \\ &= \int_{-\infty}^{\infty} Y(f)Y^*(f)\, df \\ &= \int_{-\infty}^{\infty} |Y(f)|^2\, df. \end{aligned} \tag{3.89}$$

Note that

$$q = \int_0^{T_I} y^2(t)\, dt \approx \int_{-\infty}^{\infty} |Y(f)|^2\, dt,$$

i.e., we conclude from the above approximation that $q' \approx q$. This means that a lowpass filter with sufficiently large bandwidth B has only a negligible impact on the receiver performance. Here, sufficiently large means that the bandwidth B is large enough such that the approximation (3.88) is valid. This condition is equivalent to the property that the support of the lowpass filter's impulse response $x(t)$ is much smaller than T_I. As a practical example we assume an integration duration of $T_I = 40$ ns and a support time of $x(t)$ that is equivalent to $1/B$. In order to satisfy $q' \approx q$, it must be guaranteed that $B \gg 1/T_I = 2.5$ MHz, i.e., an integrator bandwidth of only 100 MHz would be sufficiently large to provide the same performance that would be achieved with an ideal integrator. An intuitive explanation for this result is that the short time integration over the interval $[0, T_I]$ is equivalent to a lowpass filtering; thus, the effect of an additional lowpass filter changes the result only marginally.

3.7 Effect of Narrowband Interference

Narrowband interference reduces the sensitivity of a receiver, i.e., for a given SNR the BEP is increased. In this section, we compare the impact of narrowband interference on the BEP for the GMLR and the MLR. The most direct way to do this is to compute the BEP as a function of the intensity of narrowband interference for both receiver types. However, computing the BEP as a function of the narrowband interference is difficult because for the GMLR, the random component of the decision variable is no longer Gaussian distributed as in the narrowband-interference-free case, but has a much more complex distribution.

Therefore we consider an indirect measure for the narrowband interference, namely the ratio of the mean value of the decision variable to its standard deviation. Without loss of generality, these computations are made under the assumption that the symbol $a_0 = 0$ was transmitted.

Note that the ratio of the decision variable's mean value to its standard deviation appears also as a factor in the argument of the erfc$(\cdot)$ function in (3.66) and in (3.76) that describe the BEP of the GMLR and the MLR, respectively.

3.7.1 Decision Variable Statistics for the GMLR

We start by deriving the statistics of the decision variable z under the assumption of noise plus narrowband interference

$$u(t) = \sqrt{2P_u}\cos(2\pi f_0 t + \varphi_0),$$

here P_u is the power of $u(t)$. Note that the transmitted signal is also denoted $u(t)$, see (3.1); as the transmitted signal does not appear explicitly in this derivation there is no risk of confusion.

In the same way as in Section 3.3.1 and under the assumption that the transmitted symbol is $a_0 = 0$ we represent the decision variable as the difference $z = f_s - g_s$, where f_s and g_s are given by (3.60) and (3.61). To simplify the derivation of the decision variable statistics we put these expressions into an integral form. Furthermore, to get rid of some constants, here we define f_s as well as g_s to have only half of the values specified in (3.60) and (3.61). For our derivation we need the equations $N = T/T_s$ and $N_\Delta = \Delta_T/T_s$ from Subsubsection 3.2.3.2, the equation $n_n = n_l(kT + nT_s)$ from Subsubsection 3.2.3.3, and (3.24). With these equations and by introducing the mentioned factor $1/2$ we write (3.60) in the form

$$f_s = \frac{1}{2}\sum_{n=0}^{N_\Delta - 1} |cv_n + n_n|^2 \approx \frac{1}{2}\int_0^{\Delta_T} [b_l(t) + n_l(t)]^2\, dt = \int_0^{\Delta_T} [b(t) + n(t)]^2\, dt. \tag{3.90}$$

Adding the narrowband interference signal $u(t)$ to the noise signal $n(t)$, and assuming the variable integration duration T_I instead of the constant integration duration Δ_T we get

$$f_s = \int_0^{T_I} [b(t) + u(t) + n(t)]^2\, dt. \tag{3.91}$$

Similarly, we obtain for (3.61),

$$g_s = \frac{1}{2}\sum_{n=N_\Delta}^{N-1} |n_n|^2 \approx \frac{1}{2}\int_{\Delta_T}^{T} [n_l(t)]^2\, dt = \int_{\Delta_T}^{T} [n(t)]^2\, dt. \tag{3.92}$$

As above, we add the interference signal $u(t)$ to the noise signal $n(t)$, and assume the variable integration duration T_I, yielding

$$g_s = \int_{\Delta_T}^{\Delta_T + T_I} [u(t) + n(t)]^2\, dt = \int_0^{T_I} [u(t + \Delta_T) + n(t + \Delta_T)]^2\, dt. \tag{3.93}$$

The interference signal $u(t)$ will typically be a modulated signal, therefore we assume that the phase of $u(t)$ is random and uniformly distributed within the interval $[0, 2\pi)$. Furthermore, we assume in accordance with the channel properties reported in Chapter 2 that the CIR $b(t)$ is a realization of the random process $\mathrm{B}(t)$. The ratio of the captured energy to the received energy $\eta(T_I)$, defined in (3.69), is assumed to be identical for all realizations of $\mathrm{B}(t)$.

To compute the PDF of the decision variable $z = f_s - g_s$ we proceed in two steps. In the first step we assume that $b(t)$ and $u(t)$ are deterministic and known. The variables f_s and g_s that are conditioned on this assumption are denoted as f_s' and g_s'. Then, the statistics of $z' = f_s' - g_s'$ is computed. In the second step, we again consider $b(t)$ and $u(t)$ as random signals and compute the statistics for z on the basis of the statistics of the conditional variable z'.

3.7.1.1 Step I: Conditional Statistics of the Decision Variable

The mean value and the standard deviation of the conditional decision variable z' are called the conditional mean μ'_z and standard deviation σ'_z, respectively. To derive expressions for these terms, we use the approximation

$$y = 2\int_0^{T_I} [x(t) + n(t)]^2\, dt \approx \sum_{n=0}^{N_I-1} |x_n + n_n|^2, \tag{3.94}$$

where x_n and n_n are the samples of the equivalent baseband signals of $x(t)$ and $n(t)$, respectively, with the samples taken at Nyquist rate (cf. (3.90)), and where $x(t)$ is deterministic and $n(t)$ is the realization of a white Gaussian noise process with limited bandwidth B. The number of considered samples is $N_I = T_I/T_s$, where $T_s = 1/B$ is the sampling period, i.e., the reciprocal of the Nyquist rate. This discrete time representation allows us to apply the result of Appendix E, which says that the sum in (3.94) is non-central chi-square distributed with pdf

$$f_{\mathrm{Y}}(y) = \frac{1}{2N_0}\left(\frac{y}{s^2}\right)\frac{N_I-1}{2}\, e^{-\frac{s^2+y}{2N_0}}\, \mathrm{I}_{N_I-1}\left(\sqrt{y}\frac{s}{N_0}\right),$$

where

$$s^2 \approx 2\int_0^{T_I} x^2(t)\, dt,$$

and the degree of freedom

$$2N_I = 2T_I B.$$

The mean value of y is

$$\mu_y = 2N_I N_0 + s^2 \approx 2N_0 T_I B + 2\int_0^{T_I} x^2(t)\, dt,$$

and the variance is

$$\sigma_y^2 = 4N_I N_0^2 + 4N_0 s^2 \approx 4N_0^2 T_I B + 8N_0 \int_0^{T_I} x^2(t)\, dt.$$

Setting $x(t) = b(t)+u(t)$ leads to the equality $y = 2f'_s$, alternatively, setting $x(t) = u(t)$ results in $y = 2g'_s$. From these equivalences we infer that f'_s and g'_s are non-central chi-square distributed random variables with the degree of freedom $2N_I$. Note that f'_s and g'_s are statistically independent because of the time shift Δ_T in the noise signal's argument. The shift Δ_T is not present in (3.91) but in (3.93). According to the distribution of y which is given above, the mean and variance of f'_s and g'_s are

$$\begin{aligned}
\mu_{f'_s} &= N_0 T_I B + \int_0^{T_I} [b(t) + u(t)]^2\, dt,\\
\sigma^2_{f'_s} &= N_0^2 T_I B + 2N_0 \int_0^{T_I} [b(t) + u(t)]^2\, dt,\\
\mu_{g'_s} &= N_0 T_I B + \int_0^{T_I} u^2(t + \Delta_T)\, dt,
\end{aligned} \tag{3.95}$$

and

$$\sigma^2_{g'_s} = N_0^2 T_I B + 2N_0 \int_0^{T_I} u^2(t + \Delta_T)\, dt. \tag{3.96}$$

With this, the conditional decision variable $z' = f'_s - g'_s$ has the mean value

$$\begin{aligned}\mu_{z'} &= \mu_{f'_s} - \mu_{g'_s} \\ &= \int_0^{T_I} b^2(t)\, dt + 2\int_0^{T_I} b(t)u(t)\, dt + \int_0^{T_I} u^2(t)\, dt - \int_0^{T_I} u^2(t + \Delta_T)\, dt,\end{aligned} \tag{3.97}$$

and the variance

$$\sigma^2_{z'} = \sigma^2_{f'_s} + \sigma^2_{g'_s}, \tag{3.98}$$

which is simply the sum of the variances of the statistically independent variables f'_s and g'_s.

3.7.1.2 Step II: Non Conditional Statistics of the Decision Variable

Note that the expressions for μ'_z and $\sigma_{z'}$ are valid under the condition that $n(t)$ is a deterministic signal and φ is constant. Now we make the second step in the computation of the statistics of z, i.e., we assume that the signal $u(t)$ has the random parameter φ, and that $b(t)$ is a realization of the random process $\mathrm{B}(t)$. Furthermore, we assume that all realizations of this process result in the same function $\eta(T_I)$ defined in (3.69). This implies, that the variables $\mu_{z'} = \mu_{f'_s} - \mu_{g'_s}$, $\sigma^2_{f'_s}$, and $\sigma^2_{g'_s}$ become random variables. In this subsubsection we show that the mean value $\mu_{z'}$ has a nonzero variance $\sigma^2_{\mu_{z'}}$ and that the random variables $\sigma^2_{f'_s}$, and $\sigma^2_{g'_s}$ can be approximated as constants.

Evaluation of the first term of (3.97), using (3.3) and (3.69), yields

$$\int_0^{T_I} b^2(t)dt = E_r \eta(T_I). \tag{3.99}$$

Because of the large multipath diversity offered by UWB indoor channels, we assumed that for a reasonably large integration duration $T_I > 10$ ns, the captured energy of the received pulse is independent of the realization $b(t)$. The characterization of the second term of (3.97) is described in Appendix F by (F.13), i.e.,

$$2\int_0^{T_I} b(t)u(t)\, dt = 2\rho_{u,b} \sim \mathcal{N}\left(0, \frac{2P_u E_r \eta(T_I)}{B}\right). \tag{3.100}$$

The third term of (3.97) can be written by inserting the definition of $u(t)$:

$$\begin{aligned}\int_0^{T_I} u^2(t)\, dt &= 2P_u \int_0^{T_I} \cos^2(2\pi f_0 t + \varphi_0)\, dt \\ &= P_u \int_0^{T_I} [1 + \cos(4\pi f_0 t + 2\varphi_0)]\, dt \\ &= P_u T_I + \frac{P_u}{4\pi f_0} \sin(4\pi f_0 t + 2\varphi_0)\Big|_0^{T_I} \\ &= P_u T_I + \frac{P_u}{4\pi f_0} [\sin(4\pi f_0 T_I + 2\varphi_0) - \sin(2\varphi_0)] \\ &= P_u T_I + \frac{P_u}{2\pi f_0} \sin(2\pi f_0 T_I) \cos(2\pi f_0 T_I + 2\varphi_0).\end{aligned} \tag{3.101}$$

Similarly, the fourth term of (3.97) yields

$$\begin{aligned}\int_0^{T_I} u^2(t+\Delta_T)\,dt &= 2P_u \int_0^{T_I} \cos^2(2\pi f_0(t+\Delta_T)+\varphi_0)\,dt \\ &= 2P_u \int_{\Delta_T}^{T_I+\Delta_T} \cos^2(2\pi f_0 t+\varphi_0)\,dt \\ &= P_u T_I + \frac{P_u}{4\pi f_0}\sin(4\pi f_0 t+2\varphi_0)\Big|_{\Delta_T}^{T_I+\Delta_T} \\ &= P_u T_I + \frac{P_u}{4\pi f_0}[\sin(4\pi f_0(T_I+\Delta_T)+2\varphi_0)-\sin(4\pi f_0\Delta_T+2\varphi_0)] \\ &= P_u T_I + \frac{P_u}{2\pi f_0}\sin(2\pi f_0 T_I)\cos(4\pi f_0\Delta_T+2\pi f_0 T_I+2\varphi_0). \end{aligned} \tag{3.102}$$

In (3.97) there appears the difference of (3.101) and (3.102), which equals

$$\begin{aligned}\int_0^{T_I} u^2(t)\,dt - \int_0^{T_I} u^2(t+\Delta_T)\,dt &= \frac{P_u}{4\pi f_0}\sin(2\pi f_0 T_I) \\ &\quad\cdot[\cos(2\pi f_0 T_I+2\varphi_0)-\cos(4\pi f_0\Delta_T+2\pi f_0 T_I+2\varphi_0)] \\ &= \frac{P_u}{2\pi f_0}\sin(2\pi f_0 T_I)\sin(2\pi f_0\Delta_T)\sin(2\pi f_0(\Delta_T+T_I)+2\varphi_0). \end{aligned} \tag{3.103}$$

As mentioned, the phase φ_0 is randomly distributed within the interval $[0, 2\pi)$, which means that the difference (3.103) oscillates between $\pm\frac{P_u}{2\pi f_0}$ in the worst case, i.e., when the product $|\sin(2\pi f_0 T_I)\sin(2\pi f_0\Delta_T)|$ equals one. In this case the difference (3.103) has zero mean and variance $\frac{1}{2}\left(P_u/(2\pi f_0)\right)^2$, where we used the property that $\mathbb{E}\left\{\sin^2(\varphi)\right\} = \frac{1}{2}$.

With this result and with (3.99) and (3.100) we can write the mean and variance of $\mu_{z'}$ as

$$\mu_z = \mathbb{E}\left\{\mu_{z'}\right\} = E_r\eta(T_I), \tag{3.104}$$

and

$$\sigma^2_{\mu_{z'}} = \mathbb{E}\left\{(\mu_{z'}-\mu_z)^2\right\} = \frac{2P_u E_r\eta(T_I)}{B} + \frac{P_u^2}{8\pi^2 f_0^2}, \tag{3.105}$$

where we assumed that $\rho_{u,b}$ is statistically independent of (3.101) and (3.102). This assumption is justified as $\rho_{u,b}$ is a function of the product of the statistically independent random signals $\mathrm{U}(t)$ and $\mathrm{B}(t)$, which in addition have zero mean.

The variance $\sigma^2_{f_s'}$ given in (3.95) can be expanded to

$$\sigma^2_{f_s'} = N_0^2 T_I B + 2N_0\int_0^{T_I} b^2(t)\,dt + 4N_0\int_0^{T_I} b(t)u(t)\,dt + 2N_0\int_0^{T_I} u^2(t)\,dt. \tag{3.106}$$

With (3.99), (3.100) and (3.101) this becomes

$$\sigma^2_{f_s'} = N_0^2 T_I B + 2N_0 E_r\eta(T_I) + 4N_0\rho_{u,b} + 2N_0 P_u T_I, \tag{3.107}$$

where we ignored the second term in (3.101) which is much smaller than the contribution $2N_0 P_u T_I$ for practical cases where $1/f_0 \ll T_I$. From Fig. 3.8 we observe that meaningful integration durations T_I lie within the interval $[10, 60]$ ns for the channel models under consideration.

The sum term $4N_0\rho_{u,b}$ in the expression for the variance of $\sigma^2_{f'_s}$, see (3.107), is a random variable and therefore complicates the computation of σ^2_z. However, the term $4N_0\rho_{u,b}$ is with high probability smaller than the term $\sigma^2_1 := 2P_uE_r\eta(T_I)/B$ in (3.105) and the term $\sigma^2_2 := 2N_0E_r\eta(T_I)$ in (3.107) for the practical range of parameters, $T_I > 10/B$, and $E_r > 10N_0$, respectively. Therefore, an approximation of $\sigma^2_{f'_s}$ can be found by neglecting the component $4N_0\rho_{u,b}$. We compute the probability with which this approximation is valid. This probability corresponds to the probability with which the standard deviation of the neglected Gaussian distributed term $4N_0\rho_{u,b}$ is smaller than at least one of the terms σ^2_1 and σ^2_2. We do this for the given practical range of parameters $T_I > 10/B$ and $E_r > 10N_0$. If $P_u/B \leq N_0$ the term $\sigma^2_2 := 2N_0E_r\eta(T_I)$ is larger than the standard deviation of the variance $4N_0\rho_{u,b}$, which is $\sigma_3 := \sqrt{8N_0^2E_rP_u\eta(T_I)/B}$, i.e.,

$$\frac{\sigma^2_2}{\sigma_3} = \frac{2N_0E_r\eta(T_I)}{\sqrt{8N_0^2E_rP_u\eta(T_I)/B}} = \frac{\sqrt{E_r\eta(T_I)}}{\sqrt{2P_u}/B} > \frac{\sqrt{10N_0}}{\sqrt{2N_0}} = \sqrt{5},$$

whereas for the case $P_u/B > N_0$ the term σ^2_1 is larger than the standard deviation σ_3 of the variance $4N_0\rho_{u,b}$:

$$\frac{\sigma^2_1}{\sigma_3} = \frac{2(P_u/B)E_r\eta(T_I)}{\sqrt{8N_0^2E_rP_u\eta(T_I)/B}} = \frac{\sqrt{P_u/B}\sqrt{E_r\eta(T_I)}}{\sqrt{2}N_0} > \frac{\sqrt{N_0}\sqrt{10N_0}}{\sqrt{2}N_0} = \sqrt{5}.$$

Given these ratios, the probability that σ^2_1 or σ^2_2 is larger than the Gaussian random variable $4N_0\rho_{ub}$ is expressed by

$$P(\sigma^2_1 > 4N_0\rho_{ub}) = P(\sigma^2_2 > 4N_0\rho_{ub}) = \frac{1}{\sqrt{2\pi}}\int_{-\infty}^{\sqrt{5}} e^{x^2/(2)}dx = 0.985,$$

i.e., the Gaussian random variable $4N_0\rho_{ub}$ in (3.107) is smaller than the term $2N_0E_r\eta(T_I)$ or $2P_uE_r\eta(T_I)/B$ with a probability of 98.5 %. From this argumentation it follows that for most channel realizations $b(t)$ and phases φ, we get an approximation for $\sigma^2_{f'_s}$ by ignoring the term $4N_0\rho_{ub}$ in (3.107), i.e., we can write

$$\sigma^2_{f'_s} \approx N_0^2T_IB + 2N_0E_r\eta(T_I) + 2N_0P_uT_I. \tag{3.108}$$

The variance $\sigma^2_{g'_s}$ given by (3.96) becomes with (3.102)

$$\begin{aligned}\sigma^2_{g'_s} &= N_0^2T_IB + 2N_0\int_0^{T_I} u^2(t+\Delta_T)\,dt \\ &= N_0^2T_IB + 2N_0P_uT_I,\end{aligned} \tag{3.109}$$

where we ignored the second term in (3.102) for the same reason as above. The last expression and (3.108) show that the variances of f'_s and g'_s do not significantly depend on the realizations of the random functions $u(t)$ and $b(t)$.

The terms $\sigma^2_{f'_s}$ and $\sigma^2_{g'_s}$ stem from the noise process $\mathrm{N}(t)$ within the disjoint intervals $[kT, kT + \Delta_T]$ and $[kT + \Delta_T, kT + T]$ and are therefore the variances of statistically independent random variables. The term $\sigma^2_{\mu_{z'}}$ describes the variance of a random variable that stems from the random

channel process $\mathrm{B}(t)$ and the random phase φ_0 of the interference $u(t)$. With this, the total variance of the decision variable z is the sum

$$\begin{aligned}\sigma_z^2 &= \sigma_{\mu_{z'}}^2 + \sigma_{f_s'}^2 + \sigma_{g_s'}^2 \\ &= \frac{2P_u E_r \eta(T_I)}{B} + \frac{P_u^2}{8\pi^2 f_0^2} + 4N_0 P_u T_I + 2N_0^2 T_I B + 2N_0 E_r \eta(T_I),\end{aligned} \tag{3.110}$$

where we used the approximation (3.108). The mean value of z is (cf. 3.104)

$$\mu_z = E_r \eta(T_I). \tag{3.111}$$

3.7.1.3 Bit Error Probability for the GMLR with Narrowband Interference

Hence, the ratio of the mean value of z to the standard deviation of z is for the GMLR

$$R_{\text{GMLR}} = \frac{E_r \eta(T_I)}{\sqrt{\frac{2P_u E_r \eta(T_I)}{B} + \frac{P_u^2}{8\pi^2 f_0^2} + 4N_0 P_u T_I + 2N_0^2 T_I B + 2N_0 E_r \eta(T_I)}}. \tag{3.112}$$

This analytical expression has been tested by simulation for $T_I = 40$ ns which showed good agreement. To bring (3.112) into a clearer form we introduce the short hand notations $\gamma = E_r/N_0$ for the SNR and $\beta = P_u/(BN_0)$ for the interference-to-noise ratio (INR). Furthermore we write η instead of $\eta(T_I)$. With this, (3.112) yields

$$\begin{aligned}R_{\text{GMLR}} &= \frac{\eta}{\sqrt{2\eta\frac{\beta}{\gamma} + \frac{B^2}{8\pi^2 f_0^2}\frac{\beta^2}{\gamma^2} + 4T_I B\frac{\beta}{\gamma^2} + 2T_I B\frac{1}{\gamma^2} + 2\eta\frac{1}{\gamma}}} \\ &= \frac{\eta}{\sqrt{\frac{2\eta}{\gamma} + \frac{2T_I B}{\gamma^2} + \beta\frac{2\eta}{\gamma} + \beta\frac{4T_I B}{\gamma^2} + \beta^2 8\pi^2 f_0^2 \frac{2B}{(4\pi f_0 \gamma)^2}}} \\ &= \frac{1}{\sqrt{2}}\sqrt{\frac{\eta\gamma}{1 + \frac{T_I B}{\eta\gamma} + \beta\left(1 + \frac{2T_I B}{\eta\gamma}\right) + \beta^2\frac{B^2}{\eta\gamma(4\pi f_0)^2}}}.\end{aligned} \tag{3.113}$$

Parameters that result in a more or less satisfactory receiver performance lie in the following following ranges: practically relevant SNR varies between 10 and 30 dB (the corresponding BEP performance can be assessed from Fig. 3.9), i.e., $10 \leq \gamma \leq 1000$. The integration duration T_I is adapted to the channel delay spread τ_c, i.e., 10 ns $< TI <$ 100 ns. As an example for typical signal bandwidths we use the FCC's rules: 0.5 GHz $< B <$ 7.5 GHz, also these rules allow a range of 3.35 GHz $< f_0 <$ 10.25 GHz for the center frequency.

For these range limitations the term $\beta^2\frac{B^2}{(4\pi f_0)^2}$ in (3.113) is so small that it can be neglected. Note that this term represents the variance of one of the signal components of the decision variable z, and that this component is the only non-Gaussian component of the decision variable. Therefore, we conclude for the given ranges of parameters that the decision variable is Gaussian distributed.

Hence, the BEP under the assumption of narrowband interference is determined as (cf. (3.66))

$$\begin{aligned} P_e &= P(z<0) \\ &= \int_{-\infty}^{0} P_{\mathrm{Z}}(z)\,dz = \frac{1}{2}\mathrm{erfc}\left(\frac{\mu_z}{\sqrt{2}\sigma_z}\right) \\ &= \frac{1}{2}\mathrm{erfc}\left(\frac{1}{\sqrt{2}}R_{\text{GMLR}}\right) \\ &= \frac{1}{2}\mathrm{erfc}\left(\frac{1}{2}\sqrt{\frac{\eta\gamma}{1+\frac{T_IB}{\eta\gamma}+\beta\left(1+\frac{2T_IB}{\eta\gamma}\right)}}\right). \end{aligned} \tag{3.114}$$

It must be noted that for the general case of $P_u \neq 0$ the decision variable z is Gaussian distributed only under the assumption of a randomized CIR. Hence, the above expression corresponds to the average BEP, where the average is taken over an ensemble of CIRs having identical $\eta(T_I)$. For the interference-free case, i.e for $P_u = 0$ or equivalently $\beta = 0$ we obtain

$$\begin{aligned} P_e &= \frac{1}{2}\mathrm{erfc}\left(\frac{1}{\sqrt{2}}R_{\text{GMLR}}\right) \\ &= \frac{1}{2}\mathrm{erfc}\left(\frac{1}{\sqrt{2}}\sqrt{\frac{\eta\gamma}{2\left(1+T_IB\frac{1}{\eta\gamma}\right)}}\right) \\ &= \frac{1}{2}\mathrm{erfc}\left(\frac{E_r\eta(T_I)/N_0}{2\sqrt{T_IB+\eta(T_I)E_r/N_0}}\right), \end{aligned} \tag{3.115}$$

which is equivalent to the expression for the BEP in (3.71).

3.7.2 Decision Variable Statistics for the MLR

The MLR for 2PPM signals bases the symbol decision $\hat{a}_0$ on the variable $z = f_s - g_s$ in the same way as the GMLR. For the MLR, which is a coherent receiver, we assume that the polarity c_k in (3.1) is always positive, i.e., $c_k = 1$ for all k. For this type of receiver a random polarity would result in a reduced sensitivity. Unlike the GMLR which computes the correlation of the received signals with themselves, the MLR correlates the received signals with the template $b(t)$, see also Fig. 3.3. Hence, under the assumption that $a_0 = 0$ the samples at the correlator output are

$$f_s = \int_0^{\Delta_T} b(t)[b(t)+n(t)+u(t)]\,dt \tag{3.116}$$

and

$$g_s = \int_0^{\Delta_T} b(t)[n(t+\Delta_T)+u(t+\Delta_T)]\,dt, \tag{3.117}$$

compare with Subsubsection 3.3.4.2, and with (3.91) and (3.93).

Here f_s corresponds to the first sample taken during the symbol interval and g_s corresponds to the second sample within the symbol interval. Note that the coherent receiver captures the energy of the received pulse within an interval of duration Δ_T, while the optimum integration interval for

the noncoherent receiver is of the reduced duration T_I, with $T_I < \Delta_T$. The only components of these samples whose statistics are not yet described above, are the terms

$$\psi_f := \int_0^{\Delta_T} b(t)n(t)\,dt,$$

and

$$\psi_g := \int_0^{\Delta_T} b(t)n(t+\Delta_T)\,dt,$$

Note that the noise process $\mathrm{N}(t)$ is stationary, i.e., the statistics of ψ_f and ψ_g are equivalent. Note further, that the components ψ_f and ψ_g are statistically independent due to the offset Δ_T in the argument of $n(t+\Delta_T)$, which is present in (3.117), but not in (3.116). The mean value of ψ_f and ψ_g is zero because $n(t)$ has zero mean. The variance is computed by the idealized assumption that $n(t)$ is white Gaussian noise, i.e., the process $\mathrm{N}(t)$ has the ACF $(N_0/2)\delta(\tau)$. This assumption does not hold in practice because the signal bandwidth is limited in a practical receiver. However, the idealized assumption of a white noise does not change the result because the output of the matched filter that is implicitly contained in the MLR does not depend on the bandwidth of $n(t)$ as long as its bandwidth exceeds the bandwidth of the matched filter impulse response $b(t)$. The reason for this is that ψ_f and ψ_g are the projections of the noise signals onto the impulse response $b(t)$; thus, any signal component of $n(t)$ that is outside the one-dimensional signal space, spanned by $b(t)$ is ignored. Hence, the variance of ψ_f and ψ_g equals

$$\begin{aligned}
\sigma_\psi^2 &= \mathbb{E}\left\{\left[\int_0^{\Delta_T} b(t)n(t)\,dt\right]^2\right\} \\
&= \int_0^{\Delta_T}\int_0^{\Delta_T} b(t)b(\tau)\mathbb{E}\left\{n(t)n(\tau)\right\}\,dtd\tau \\
&= \frac{N_0}{2}\int_0^{\Delta_T}\int_0^{\Delta_T} b(t)b(\tau)\delta(t-\tau)\,dt\,d\tau \\
&= \frac{N_0}{2}\int_0^{\Delta_T} b^2(t)\,dt \\
&= \frac{N_0 E_r}{2}. \qquad (3.118)
\end{aligned}$$

As in the previous section, we assume that the phase φ_0 of the interference signal $u(t)$ is unknown. Therefore, we model φ_0 as a random variable with uniform distribution within the range $\varphi_0 \in [0, 2\pi)$. Using (F.1) and the definition of ψ_f we can represent f_s in (3.116) as

$$\begin{aligned}
f_s &= \int_0^{\Delta_T} b^2(t)\,dt + \int_0^{\Delta_T} b(t)n(t)\,dt + \int_0^{\Delta_T} b(t)u(t)\,dt \qquad (3.119)\\
&= E_r + \psi_f + \rho_{u,b}. \qquad (3.120)
\end{aligned}$$

The term E_r is constant, ψ_f is Gaussian distributed with zero mean and variance $N_0E_r/2$ and $\rho_{u,b}$ is, according to (F.13), also Gaussian distributed with zero mean and variance $E_rP_u/2B$. With this the statistics of f_s is specified by

$$f_s \sim \mathcal{N}\left(E_r, \frac{N_0E_r}{2} + \frac{P_uE_r}{2B}\right), \qquad (3.121)$$

where we used the property that $\rho_{u,b}$ and ψ_f are statistically independent. This property can be seen from the integral representation (3.119). Similarly, g_s in (3.117) can be described as

$$g_s = \int_0^{\Delta_T} b(t)n(t+\Delta_T)\,dt + \int_0^{\Delta_T} b(t)u(t+\Delta_T)\,dt \tag{3.122}$$

$$= \psi_g + \rho_{u,b}. \tag{3.123}$$

The statistics of g_s is described by

$$g_s \sim \mathcal{N}\left(0, \frac{N_0 E_r}{2} + \frac{P_u E_r}{2B}\right). \tag{3.124}$$

Note that the terms $\rho_{u,b}$ in (3.120) and (3.123) can be assumed to be statistically independent, if the phase φ_0 is statistically independent in the time intervals $[0, \Delta_T)$ and $[\Delta_T, T)$, i.e., if the phase is varying over time. This assumption is valid when
(i) the narrowband interference signal $u(t)$ is modulated, or when
(ii) the integration duration starts at time instances that are subject to a large enough jitter,
(iii) or if both, (i) and (ii) are true.
Remember that the components ψ_f and ψ_g are statistically independent, too. Hence, as all the components of f_s are statistically independent of the components of g_s, the decision variable $z = f_s - g_s$ is characterized by

$$z = f_s - g_s \sim \mathcal{N}\left(E_r, N_0 E_r + \frac{P_u E_r}{B}\right). \tag{3.125}$$

In the considered case, where $a_0 = 0$, a decision error occurs if $z < 0$. As the 2PPM scheme is symmetric with respect to $a_k = 0$ and $a_k = 1$, the BEP is $P_e = P(z < 0)$ and is given by

$$P_e = \frac{1}{2}\text{erfc}\left(\frac{1}{\sqrt{2}} R_{\text{MLR}}\right), \tag{3.126}$$

with

$$R_{\text{MLR}} = \frac{E_r}{\sqrt{N_0 E_r + \frac{P_u E_r}{B}}} = \sqrt{\frac{\gamma}{1+\beta}}, \tag{3.127}$$

where $\gamma = E_r/N_0$ is the SNR and $\beta = P_u/(BN_0)$ is the INR (interference-to-noise ratio). In the absence of narrowband interference, i.e., when $P_u = 0$, the BEP is

$$P_e = \frac{1}{2}\text{erfc}\left(\sqrt{\frac{\gamma}{2}}\right) = \frac{1}{2}\text{erfc}\left(\sqrt{\frac{E_r}{2N_0}}\right). \tag{3.128}$$

3.7.3 Comparison of GMLR and MLR

We compute the allowed INR β given a desired BEP P_e, as a function of the SNR γ. For the GMLR, this is obtained by solving (3.114) for β:

$$\beta = \left[\frac{\eta\gamma}{\left(2\,\text{erfc}^{-1}(2P_e)\right)^2} - \left(1 + \frac{T_I B}{\eta\gamma}\right)\right] \frac{1}{\left(1 + \frac{2T_I B}{\eta\gamma}\right)}.$$

For the MLR, and with (3.126) and (3.127) we get:

$$\beta = \frac{\gamma}{2\left(\text{erfc}^{-1}(2P_e)\right)^2} - 1.$$

In Fig. 3.14 these two functions are shown for various BEPs. The assumed system paramters are: $B = 1$ GHz, $f_0 = 4.5$ GHz, $T_I = 40$ ns, $\eta(T_I) = 0.8$. It turns out clearly that the MLR is

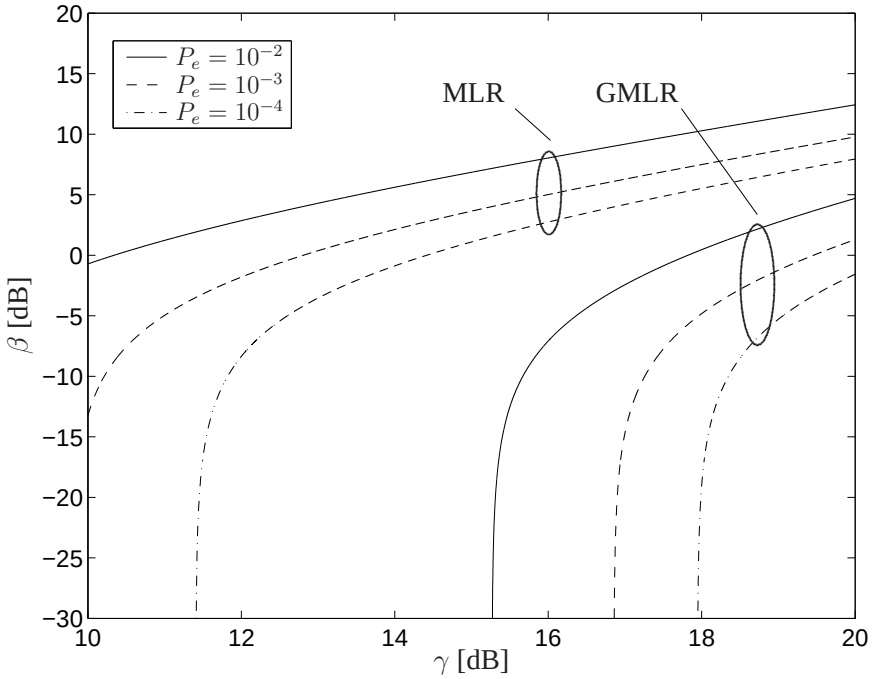

Fig. 3.14. Admissible INR $\beta = \frac{P_u}{BN_0}$ versus SNR $\gamma = \frac{E_r}{N_0}$ for a set of BEPs P_e for both the GMLR and the MLR.

more resistant to NBI than the GMLR. For example, for $P_e = 10^{-2}$ and an SNR of 18 dB the MLR tolerates an NBI interference level that is by 9 dB larger than that tolerated by the GMLR. This is plausible because the GMLR uses the received signal as a correlation template which contains any signal including NBI that passes the receiver filter. In contrast, the MLR has a fixed receiver template $b(t)$ that attenuates signal components which are not in the signal space spanned by the template, cf. Fig. 3.3. Hence, to get the same resistance to NBI as the MLR, the GMLR must be equipped with additional mechanisms to attenuate NBI.

For the MLRP, the sensitivity to NBI has not been investigated. It is obvious that the weighting function reduces the sensitivity to NBI when compared to that of the GMLR.

3.8 Sensitivity of the GMLR to Synchronization Errors

The output signal of the integrate, dump, and sampling unit at time t is described by the short-time integral

$$q(t) = \int_{t-T_I}^{t} s(\tau)\, d\tau,$$

where the integrator is dumped at $t - T_I$, and sampled at time t, see Fig. 3.15 for comparison. The sampling time instants, t, are determined by the synchronization or clock recovery algorithm.

Deviations from the optimum sampling instant will result in a degradation of the BEP that depends on the characteristics of the short-time integral $q(t)$. Figure 3.15 depicts $q(t)$ for realization 1 (see Subsection 3.3.5) of the channel models CM1 and CM4, and for an integration duration $T_I = 40$ ns. By inspecting the function $q(t)$ that corresponds to realization 1 of CM4 we observed that $q(t)$ shows its maximum value for a duration of approximately 1 ns. This implies that deviations Δ_t of the sampling instant from the optimal value do not deteriorate the BEP, as long as Δ_t is smaller than $\pm$ half the duration at which $q(t)$ is at its maximum. This is confirmed by Fig. 3.16 which shows the simulated BER of the GMLR for this channel as a function of the deviation Δ_t from the optimum sampling instant. This figure also shows the BER of a coherent ML receiver for 2PAM signals. We observe that for this receiver type, a deviation of only 0.05 ns can result in a drastically increased BER and in a receive failure; this confirms the statement in [42] which says that the sampling jitter must be below 100 to 10 ps for coherent UWB receivers. Note that coherent reception of 2PAM signals requires 3 dB less signal power than coherent reception of 2PPM signals to achieve the same BER. Hence, if a coherent receiver is implemented, 2PAM signals are preferred over 2PPM signals. Therefore, we chose to compare our noncoherent receiver for 2PPM signals with the coherent receiver for 2PAM signals.

For the realization of CM1, the short-time integral has an even wider peak with a duration of approximately 10 ns, i.e., for this channel a sampling time offset of ± 5 ns is allowed without the tradeoff of an increased BEP. We conclude that the synchronization accuracy requirements for noncoherent receivers are relaxed by up to two orders of magnitude when compared to coherent receivers.

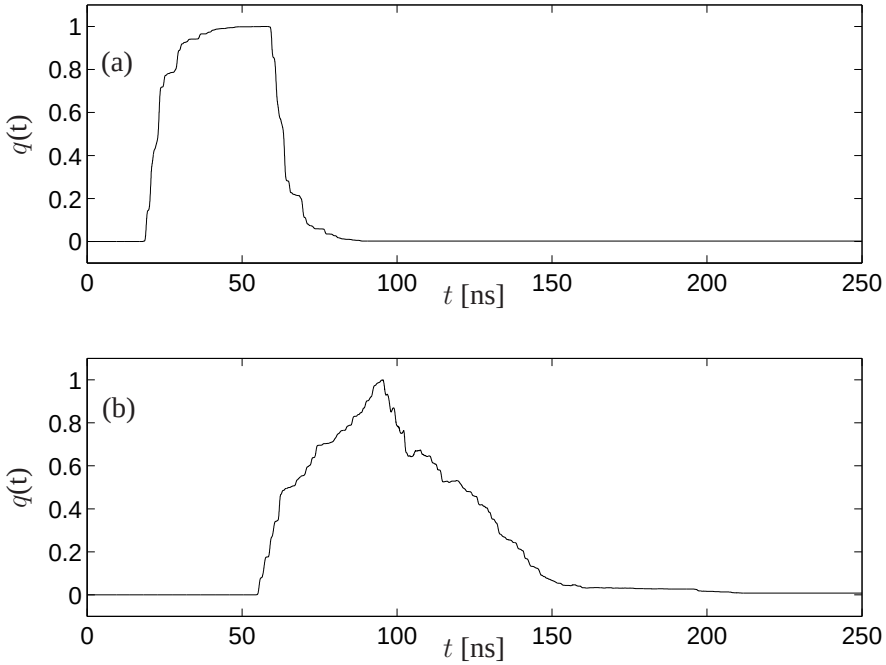

Fig. 3.15. Short-time integral $q(t)$ over the interval $[t-T_I, t]$ of the squared received pulse $b^2(t)$ for channel realization 1 of (a) CM1 and (b) CM4, for an integration duration of $T_I = 40$ ns.

3.9 Noncoherent Versus Coherent Receivers

A noncoherent GMLR has several advantages over a coherent receiver:

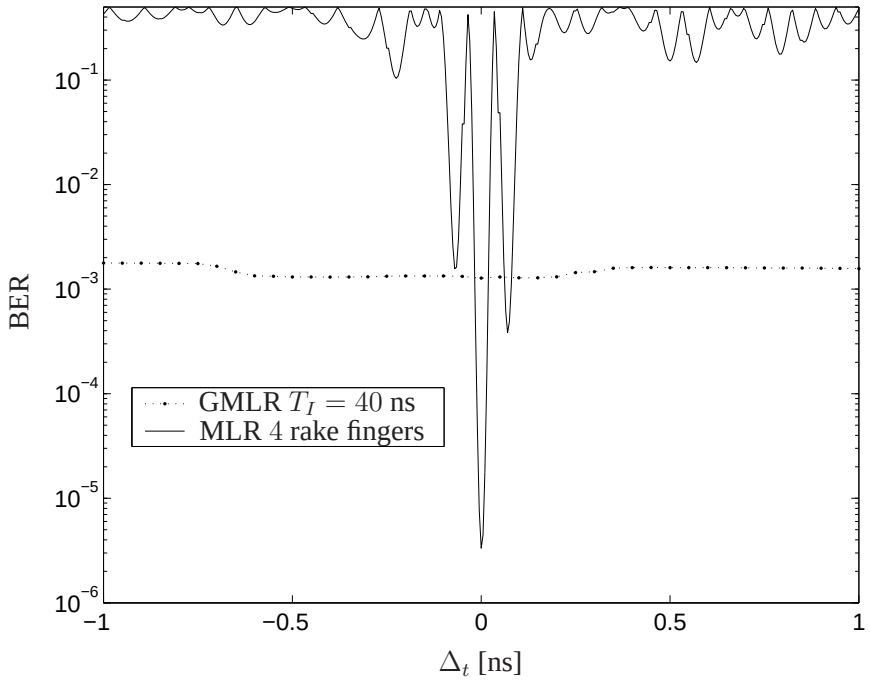

Fig. 3.16. BER performance for 2PAM modulation and coherent rake receiver and BER performance for 2PPM modulation and noncoherent receiver, for CM4, realization 1.

(a) In contrast to a coherent receiver, the GMLR architecture derived in Section 3.2 does not need a channel estimate.

(b) The required accuracy of symbol clock synchronization is much reduced. For noncoherent receivers the required synchronization accuracy is on the order of 1 to 10 ns depending on the power delay profile of the received pulse. For coherent receivers the required synchronization precision depends on the signal frequency and is for the frequency band from 3.1 to 10.6 GHz on the order of 10 to 100 ps [42]. Similar conclusions on the required synchronization accuracy can be deduced from Fig. 3.16.

(c) As no channel estimate is used, the receiver performance is somewhat poorer than, e.g., for the MLR. In return, however, it is robust against variations of the received pulse shape that are caused by fading effects.

(d) Components of a coherent receiver that require high signal processing power are the channel estimator, the correlator or matched filter, and the synchronization algorithm. For a noncoherent receiver the first two are not needed and the requirements regarding synchronization accuracy are much relaxed, so that the power consumption can be reduced.

(e) For the synchronization in coherent receivers several search methods are proposed that work with a single or several correlators [43, 28]. The preamble in a data packet that is used for synchronization must contain several pulses until the synchronization algorithm can lock. The number of required pulses is the higher the more accurate the synchronization must be. Note that the use of a matched filter is much more complex than use of correlators. This is because a correlator requires the generation of the template signal, a multiplier and an integrator, whereas a matched filter incorporates a convolution which is very complex for typical received waveforms $b(t)$. However, a matched filter implementation would in the optimum case allow the receiver to synchronize after the reception of only a single pulse. The proposed methods for synchronization in noncoherent receivers are similar to the correlator method [51]. However,

the number of pulses in the preamble can be reduced because of the relaxed requirement to synchronization accuracy. This property is particularly important for low data rate applications with short data packets. In this case the preamble length is constraint to be only a fraction of the packet length such that the resulting overhead is tolerable.

(f) In a noncoherent receiver, some sources of noise are not present that are inherent to the coherent receiver: A channel estimate inherently contains an estimation error. Additionally, the correlator or matched filter causes a quantization noise if the involved signals are represented by discrete numbers. In contrast, a noncoherent receiver will typically employ an analog circuit to compute the square of the observed signal $y(t)$.

The points (a) to (e) enable the implementation of GMLRs that have lower complexity and power consumption than a comparable coherent receiver or MLR. The GMLR has however some disadvantages compared to the MLR. Ignoring implementation losses, its sensitivity is reduced by about 4 to 7 dB for 2 PPM signals, see Section 3.3. A coherent receiver would, e.g., allow binary antipodal modulation (2PAM) which brings an additional 3 dB gain. Furthermore, the noncoherent receiver is more vulnerable to any kind of interference, e.g., from other UWB devices or narrowband interferers. This is because the noncoherent receiver captures all the energy of the observed signal that lies in the observed frequency band and integration time window; in addition to this there arise intermodulation products. In contrast, the matched filter or correlator of a coherent receiver captures only a projection of the observed signal onto the expected received pulse shape. Therefore, the sensitivity to narrowband interferers is by about 15 dB higher for the GMLR, see Section 3.7. If multiple receiver antennas are used, then the pulse shape that is received from a single transmitter will be different for each antenna. Coherent receivers can exploit this property of the UWB channel to push the link performance [69]. Noncoherent receivers capture only the energy of the observed signal and can therefore not benefit from this effect. It should also be pointed out that the input to the integrator in a noncoherent receiver has to process signal frequencies close to DC. This is because of the conversion down to DC that is implicitly performed by the square operation. In particular, CMOS transistors show an increased noise power spectral density in this frequency spectrum. This effect can seriously deteriorate the performance of energy-collecting receivers. The MLR receiver suffers the same problem when the direct implementation in Fig. 3.3 is used. However, in practice MLR receivers are often implemented as heterodyne receivers that allow to sample the I and Q components in an intermediate frequency band which does not contain DC components. This implementation allows to circumvent this disadvantage of CMOS technology.

The sensitivity of the GMLR can be improved if partial channel state information is included as discussed in Subsection 3.2.3 for the MLRP. This receiver architecture makes the selection of the integration duration (described in Section 3.4) unnecessary. Furthermore, the BEP is the lower the shorter the channel delay spread is because the amount of captured noise is lower for smaller delay spread (see Section 3.3.5). The gain of the MLRP over the GMLR is the larger the higher the estimation precision of the APDP is. However, to fully exploit the precision of the channel estimate also the synchronization accuracy must be increased. In the extreme case when the APDP is perfectly known, the same synchronization precision as for the coherent receiver is required to take the full performance advantage offered by the channel knowledge.

As a conclusion we can say that noncoherent receivers are well suited for low complexity, low data rate links when a moderate receiver performance is sufficient. A performance improvement can be achieved by implmenting an MLRP, which requests some more complexity.

4. Multiple Receiver Antennas and Noncoherent Reception

4.1 Introduction

The concept of multiple transmitter and receiver antennas has been investigated intensively in the past few years and has shown to be an excellent method for increasing the spectral efficiency of wireless links. The channel of an indoor narrowband wireless MIMO channel is described by a matrix whose coefficients are Rayleigh or Rician fading random variables. Among the gains that can be traded off for each other are

(i) the diversity gain that arises from a potential statistical independence of the channel coefficients,

(ii) a multiplexing gain that depends on the rank of the channel matrix,

(iii) the coherence gain which is proportional to the number of receiver antennas, and

(iv) the interference suppression gain.

To implement these gains with coherent receivers and for antenna arrays with element spacings on the order of half a wavelength, a variety of methods are available [3]. Typically, the performance of these methods depends on the reliability of channel estimates. A survey on channel estimation methods is given in [18]. The purpose of this chapter is to show the benefit of noncoherent SIMO architectures with antenna elements that are distributed over a larger region. In the conclusion of Chapter 3 we have summarized that the performance of noncoherent receivers is widely insensitive to small-scale fading effects. Therefore, the receiver performance is determined primarily by large-scale fading effects. These large scale effects are the fading of the path gains, and variations of the PDPs (cf. Section 2.2). For simplicity, in this work we ignore variations of the PDP and restrict our attention to the fading of the path gains. Thus, we implicitly assume that all considered channels have the same channel impulse response, which implies equivalent PDPs for all channels. This assumption is made throughout this entire Chapter.

The fading effect can be separated into small-scale fading and large-scale fading, see Chapter 2. This is a natural distinction, because small-scale fading is caused by the superposition of reflected signal components, while large-scale fading is caused by shadowing introduced by obstacles along propagation paths. For indoor channels and antenna arrays with dimensions of up to 1 m, the diversity of the channel coefficients is determined by the small-scale fading effect and is denoted as micro-diversity. When the antenna elements are distributed over a larger region, e.g., several meters, then the diversity of the channel coefficients is determined by large-scale fading, correspondingly we speak about macro-diversity.

The bandwidth of UWB signals is very large so that much frequency diversity is available. Therefore, the small-scale fading effect, i.e., the variation of the captured energy per received pulse, becomes marginal. The shape of the received pulses however still changes very sensitively with the

antenna positions or the environment geometry. The benefit of this effect has been investigated in [69] in the context of the UWB MIMO indoor channel. It has been shown that coherent receivers allow us to exploit the temporal signature of distinct channel impulse responses. It seems to be a property of the UWB channel that the channel impulse responses of spatially adjacent channels are only weakly correlated, see Chapter 2.

In this chapter we focus on noncoherent receivers, in particular on the GMLR which was discussed in detail in Chapter 3. This receiver type captures the energy of the received pulses, which shows only a marginal small-scale fading effect as explained. We conclude that for UWB systems, unlike for narrowband systems, it is not beneficial to aim at additional small-scale diversity. To improve the receiver performance macro-diversity can be exploited instead. This method is proposed in [16] where the benefit of macro-diversity for pure distance fading channels, i.e., LOS channels, is estimated. Similar to this proposal, we consider a communication system comprising one transmitter and a number N of distributed noncoherent receivers with indices $i = 1$ to N, creating N diversity branches. Each receiver is equipped with a separate antenna and a reduced GMLR. With a reduced GMLR we denote a GMLR that has no slicer, see Fig. 3.1. Hence, the output of the reduced GMLR is the decision variable $z_{k,i}$, cf. Fig. 4.2(a). Note that the soft decision output $z_{k,i}$ of receiver i is determined only by the captured energy per received pulse and by the receiver noise. The statistical path loss model from [24] is explained in Section 4.2, where in addition a proper definition of the average SNR is given.

Two different schemes for combining the soft decisions $z_{k,i}$ are investigated:

(i) The maximum ratio combiner (MRC) is determined in Section 4.3, and the BEP of this receiver type is derived for known path gains. Furthermore, it is shown that for noncoherent reception the MRC is an approximation to the optimum scheme for combining the soft decisions $z_{k,i}$, (note that the MRC is the optimum scheme when coherent receivers are used [41]). The BEP for a coherent multiple antenna receiver is derived for reference.

(ii) A less complex but suboptimal combiner, the so called generalized selection combiner (GSC) [35], is defined in Section 4.5. The BEP for this combiner is determined only by simulation.

Macro diversity has already been investigated for MRC and combining in conjunction with coherent SIMO receivers. [17] gives an upper and lower bound on the bit error outage probability (BEO) for BPSK, i.i.d. lognormal fading channels, and maximum ratio combining. An integral expression for the average BEP for a selection combining receiver in combination with an MRC for Rayleigh fading micro diversity is derived in [79] and [57]. Similarly, [1] gives integral expressions for the average and outage probability for statistically dependent lognormal fading channels. For noncoherent receivers the BEP expression is more complicated than for the coherent receiver, see (3.71) and (3.76). This prevents us from deriving meaningful analytical expressions for the average and the outage error probabilities for noncoherent SIMO receivers. In Section 4.4 we derive the average BEP and the coherence gain for a coherent SIMO receiver, which allows us to compare the performance of noncoherent and coherent SIMO receivers.

In Section 4.6 the BEP of the considered system is simulated for a fading and nonfading channel. Additionally, the BEP of coherent receivers is evaluated for reference. The conclusion reviews the most important properties of the noncoherent multiple antenna receivers.

4.2 SIMO Channel Model

In this section a SIMO channel model is developed on the basis of the UWB channel properties reported in Chapter 2 and some additional assumptions. The goal of this SIMO channel model is

to describe the statistics of the received energy per pulse, i.e., the level of the received signal at the individual receiver antennas. This signal level is determined, among other parameters, by the large-scale and the small-scale fading effect. For UWB signals the small-scale fading effect is only marginal when compared to the large-scale fading effect. This is because of the potential of UWB signals to highly resolve the temporal signature of the wireless channel and thus to provide large multipath diversity, see Chapter 2 and [53]. For this reason, we ignore the small-scale fading effect and model only the large-scale fading.

In practice, the path gains α_i for different channels i are determined by the environment geometry and the antenna setup. Thus, the path gains α_i are statistically dependent in general. A description of the statistical dependence of path gains for wireless channels does not seem to exist in the literature. A main difficulty to create such a model is that each of the considered receiver antennas can be placed at an arbitrary position. The statistical dependence of the corresponding path gains depends on the relative distances between the receiver antennas and on their distance to the transmitter antenna. To have a significant statistics of the path gains for various relative antenna distances, a very large number of channel measurements would be required. Because of the lack of such a model, we assume that the shadow fading terms S_i (see Subsection 2.2.2) are statistically independent.

To describe the path gains we use the statistical model for the path loss given in [24] and adapt it to the SIMO channel by simply assuming that the differently fading path losses are statistically independent. The path loss is the reciprocal value of the path gain and is defined as $\alpha_i^{-1} = E_t/E_{r,i}$, where E_t is the transmitted energy per pulse and $E_{r,i}$ is the random received energy per pulse at receiver i. According to (2.3), the path loss is expressed by

$$\alpha_i^{-1}(d) = \alpha_0^{-1} \left(\frac{d_i}{1\text{m}} \right)^{\nu} s_i, \tag{4.1}$$

where α_0^{-1} is the average path loss for a transmitter-to-receiver distance $d_i = 1$ m. The equivalent of the path gain α_0 in units of dB is denoted as $A_0 = 10\log_{10}(\alpha_0)$; according to [24] this is -47 dB for line-of-sight (LOS) and -51 dB for non-LOS (NLOS) propagation. The factor s_i is denoted shadow fading term; it is a lognormal distributed random variable, i.e., its equivalent in units of dB, $S_i = 10\log_{10}(s_i)$, is Gaussian distributed with zero mean and standard deviation $\sigma_S = 2.7$ dB for NLOS and $\sigma_S = 1.6$ dB for LOS indoor channels. The constant ν is denoted path loss exponent; it equals 2 for free space propagation. For indoor propagation, ν is Gaussian distributed with mean 1.7 and standard deviation 0.3 for LOS propagation and with mean 3.5 and standard deviation 0.97 for NLOS propagation. We assume that all the channels have the same parameters A_0, σ_S and ν. Furthermore, we assume throughout this chapter that the transmitter-to-receiver distance d_i is the same for all receivers.

4.2.1 Statistical Dependence of Path Gains

In practice, the path gains α_i for the different channels fade in a correlated fashion. Two extreme cases are (a) when all antennas are concentrated in a small region such that they have approximately the same path gains, (b) when the receiver antennas are uniformly distributed on a circle with the transmitter in its center. In case (b), any motion of the transmitter causes some path gains to increase and some others to decrease. A possible scenario where the channel behavior of case (b) is realizable is that of sensor networks, where deep fades of some links are compensated by other links with good connectivity and by the use of signal combining schemes like MRC. Case (a)

corresponds to the case to be discussed in Subsection 4.6.1 where no diversity is provided so that only the plain array gain is achieved. The remainder of this chapter is restricted to the discussion of case (b), i.e., it is assumed that $d_i = d, \forall i \in [1, \ldots, N]$.

4.2.2 SNR Definition

We define the instantaneous SNR at receiver i as

$$\gamma_i = \frac{E_{r,i}}{N_0}. \tag{4.2}$$

The channels from the transmitter to the receivers are all characterized by the same numerical parameters. However, the shadow fading realizations s_i are individual for each channel. As a representative parameter we define the average SNR

$$\overline{\gamma} = \mathbb{E}\left\{\frac{E_{r,i}}{N_0}\right\} = \frac{\mathbb{E}\left\{E_{r,i}\right\}}{N_0},$$

which depends on the average received power

$$\overline{E}_r = \mathbb{E}\left\{E_{r,i}\right\} = \mathbb{E}\left\{E_t \alpha_i\right\} = E_t\, \alpha_0 \left(\frac{d}{1\mathrm{m}}\right)^{-\nu} \mathbb{E}\left\{\frac{1}{s_i}\right\}.$$

The only unknown in this equation is $\mathbb{E}\left\{1/s_i\right\}$. To determine its value, we remember that s_i is lognormal distributed and that $S_i = 10\log_{10}(s_i)$ is normal distributed with zero mean and variance σ_S^2, i.e., $S_i \sim \mathcal{N}(0, \sigma_S^2)$. According to [7], a lognormal distributed random variable y, which satisfies $\ln(y) \sim \mathcal{N}(0, \sigma^2)$, has the expectation value $\mathbb{E}\left\{y\right\} = e^{\sigma^2/2}$. Note that y and its reciprocal, $\frac{1}{y}$, have both the same PDF. This is because the pdf $f_x(x)$ of $x = \ln(y)$ is Gaussian with zero mean, and therefore satisfies $f_x(x) = f_x(-x)$, and because $\ln(y) = -\ln(1/y)$. Hence, we can write $\ln(y) \sim \ln(1/y) \sim \mathcal{N}(0, \sigma^2)$. Setting $s_i = y$, we get $S_i = 10\log_{10}(y) = \frac{10}{\ln(10)}\ln(y)$. Furthermore, as $S_i \sim \mathcal{N}(0, \sigma_S^2)$ we get $\sigma = \frac{\ln(10)}{10}\sigma_S$. With these results, we can finally write for the expectation value of $1/s_i$,

$$\mathbb{E}\left\{1/s_i\right\} = \mathbb{E}\left\{y\right\} = e^{\frac{1}{2}\left(\frac{\ln(10)}{10}\sigma_S\right)^2}.$$

Note that even though the logarithmic shadow fading gain S_i has zero mean, the logarithm of the expectation value of the linear shadow fading gain, $\overline{S} := 10\log_{10}(\mathbb{E}\left\{1/s_i\right\}) = \sigma_S^2 \ln(10)/20$, is different from zero. Figure 4.1 depicts the cumulative distribution function (CDF) of S_i for a constant shadow fading variance, $\sigma_S = 2.7$ dB, i.e., the variance of σ_S^2 is set to zero. The corresponding average shadow fading gain $\overline{S} = 0.839$ is indicated in Fig. 4.1. With the above computations we can write the average SNR as

$$\overline{\gamma} := \mathbb{E}\left\{\frac{E_{r,i}}{N_0}\right\} = \frac{E_t}{N_0}\, \alpha_0 \left(\frac{d}{1\mathrm{m}}\right)^{-\nu} e^{\frac{1}{2}\left(\frac{\ln(10)}{10}\sigma_S\right)^2}.$$

In units of dB this can be written as

$$\overline{\Gamma} = 10\log_{10}\left(\overline{\gamma}\right) = A_0 + 10\log_{10}\left(\frac{E_t}{N_0}\right) - 10\,\nu\log_{10}(d/1\mathrm{m}) + \frac{\ln(10)}{20}\sigma_S^2.$$

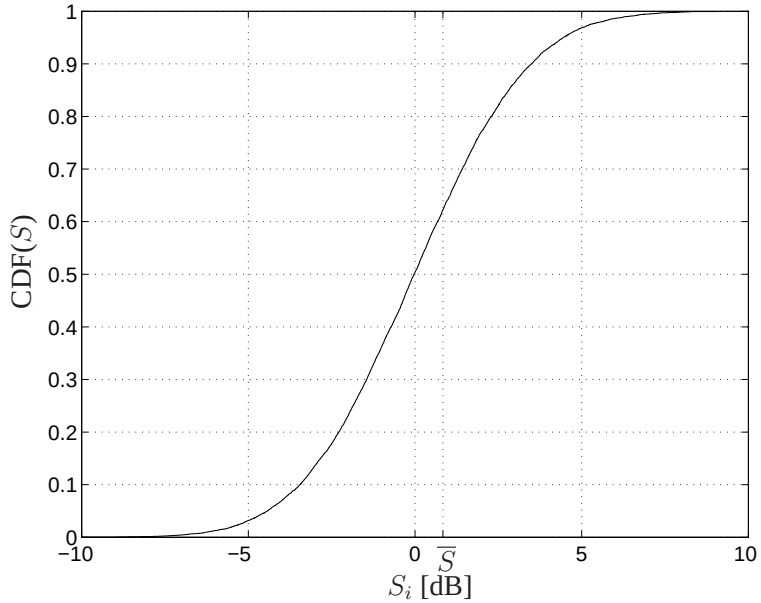

Fig. 4.1. CDF of shadow fading term for shadow fading standard deviation $\sigma_S = 2.7$ dB.

4.3 SIMO Receivers with Maximum Ratio Combining

In this section we discuss a method to combine the decision variables $z_{k,i}$ of multiple noncoherent receivers, that minimizes the BEP. The derivation of this method is derived subsequently. The average BEP for this combining method is derived in Subsections 4.3.2; the coherency and the diversity gain are discussed in 4.3.4 and 4.3.5, respectively. For a comparison of the performances of the introduced noncoherent SIMO receiver and a corresonding coherent receiver, the BEP and the coherency gain of the latter are derived in Subsection 4.4.1.

4.3.1 Noncoherent SIMO Receiver

The exact derivation of the optimum combining scheme and the corresponding BEP is intricate because of the distribution of the decision variables $z_{k,i}$ which is not perfectly Gaussian. A good approximation for the BEP can be based on the Gaussian characterization of the decision variables $z_{k,i}$ given by the equations (3.64), (3.65) and (3.70) of Subsection 3.3.1. This characterization is summarized by

$$z_{k,i} \sim \mathcal{N}\left(\mu_{z_{k,i}}, \sigma_{z_i}^2\right).$$

For $a_k = 0$ we have according to (3.64),

$$\begin{aligned}\mu_{z_{k,i}} &= \mu_{f_s} - \mu_{g_s} \\ &= (2N_\Delta N_0 + s^2) - 2N_\Delta N_0 \\ &= s^2,\end{aligned}$$

where s^2 is the captured energy of the received symbol and is contained in μ_{f_s}. For a variable integration duration T_I of the noncoherent receiver we have $s^2 = 2\eta(T_I)BE_r$, see (3.70). In turn, for $a_k = 1$ the energy of the transmitted symbol is contained in μ_{g_s}, i.e., we have

$$\begin{aligned}\mu_{z_{k,i}} &= \mu_{f_s} - \mu_{g_s} \\ &= (2N_\Delta N_0) - (2N_\Delta N_0 + s^2) \\ &= -s^2,\end{aligned}$$

Thus, $\mu_{z_{k,i}}$ is summarized by

$$\mu_{z_{k,i}} = \begin{cases} +2\eta_i(T_I)BE_{r,i}, & \text{for } a_k = 0 \\ -2\eta_i(T_I)BE_{r,i}, & \text{for } a_k = 1 \end{cases} . \tag{4.3}$$

The variance of $z_{k,i}$ is according to (3.65) given by $\sigma_{z_i}^2 = 8N_\Delta(BN_0)^2 + 4BN_0s^2$. With (3.70), $B = 1/T_s$, and by replacing the fixed integration duration $N_\Delta T_s = \Delta_T$ by the variable integration duration $T_I = N_I T_s$ we have

$$\sigma_{z_i}^2 = 8T_I B^3 N_0^2 + 8\eta_i(T_I)E_{r,i}B^2N_0. \tag{4.4}$$

Furthermore, we assume for simplicity that the ratio $\eta_i(T_I) = \eta(T_I)$ is the same for all receivers $i = 1 \ldots N$. This representation allows us to interpret the decision variable $z_{k,i}$ as the output of an AWGN channel with a binary phase shift keying (BPSK) transmitter at its input. Figure 4.2(b) depicts the signal model that corresponds to this interpretation. Note that the binary transmitted BPSK symbols are antipodal in contrast to the orthogonal 2PPM symbols of the original system. Consequently, the symbols a_k in the simplified transceiver model in 4.2(b) are either $+1$ or -1, i.e., $a_k \in \{-1, +1\}$ instead of $a_k \in \{0, 1\}$. The original system is shown in Fig. 4.2(a), it comprises a 2PPM transmitter and the GMLR from Chapter 3.

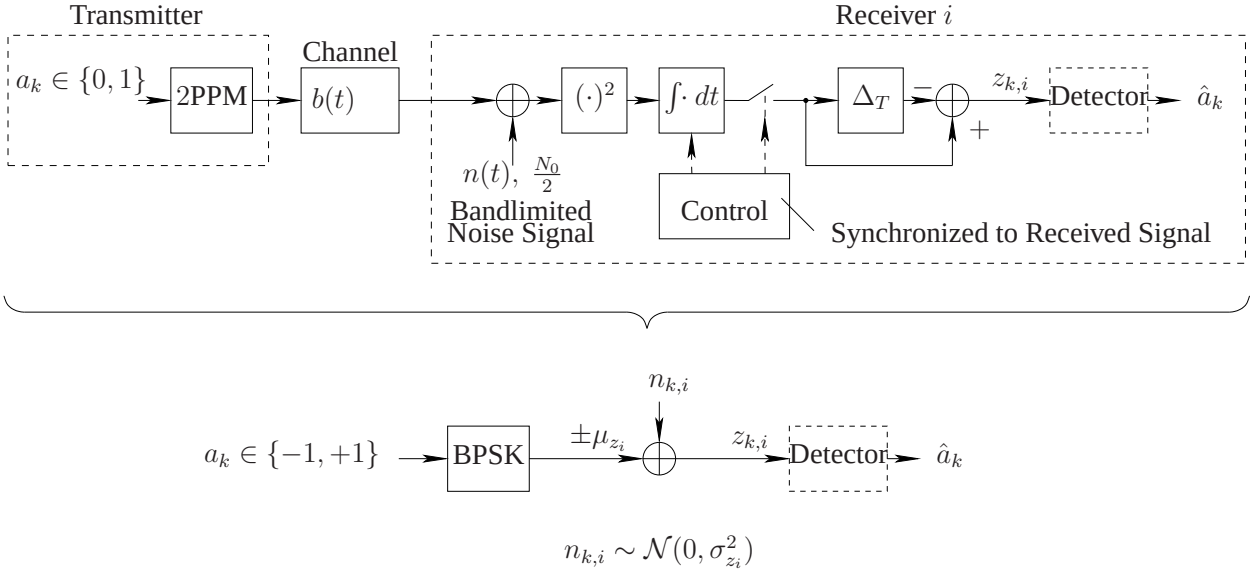

Fig. 4.2. Real and simplified transceiver model.

Assuming known path gains, the decision variables $z_{k,i}$ have still a random component which is exclusively caused by the receiver noise; therefore, the decision variables are statistically independent. Hence, the optimum way of combining them is maximum ratio combining (MRC) [41]. The MRC performs a weighted addition of the individual decision variables of the form

$$z_k = \sum_{i=1}^{N} w_i z_{k,i},$$

with weights w_i. For the special case of decision variables $z_{k,i}$ with identical variance $\sigma_{z_i}^2$, the optimum weights are $w_i = |\mu_{z_{k,i}}|$. The only property of $\mu_{z_{k,i}}$ that depends on the index k is its sign.

Therefore, the absolute value of the mean, w_i, is independent of k. In general, the variances $\sigma_{z_i}^2$ depend on the index i, see (4.4). Hence, to determine the optimum weights we divide the decision variables $z_{k,i}$ by the standard deviations σ_{z_i} to get the new decision variables $z'_{k,i} = z_{k,i}/\sigma_{z_i}$, which have unit variance. Then, the new mean values are $\mu'_{z_{k,i}} = \mu_{z_{k,i}}/\sigma_{z_i}$. As the variances of the transformed decision variables $z'_{k,i}$ are identical, the optimum weights are $w'_i = |\mu'_{z_{k,i}}|$. Based on these transformed variables, the final decision variable can be expressed as

$$\begin{aligned} z_k &= \sum_{i=1}^{N} w'_i z'_{k,i} = \sum_{i=1}^{N} |\mu'_{z_{k,i}}| z'_{k,i} = \sum_{i=1}^{N} \frac{|\mu_{z_{k,i}}|}{\sigma_{z_i}^2} z_{k,i} \\ &= \sum_{i=1}^{N} \frac{z_{k,i}\eta_i(T_I)E_{r,i}}{4T_I B^2 N_0^2 + 4\eta_i(T_I)E_{r,i}BN_0}. \end{aligned} \tag{4.5}$$

Thus, the final weights are

$$w_i = \frac{|\mu_{z_{k,i}}|}{\sigma_{z_i}^2} = \frac{\eta_i(T_I)E_{r,i}}{4T_I B^2 N_0^2 + 4E_{r,i}\eta_i(T_I)BN_0}.$$

In practice the determination of the weights w_i is simple, as the constants T_I, B, and N_0 are known and the captured energy $\eta_i(T_I)E_{r,i}$ can be estimated, e.g., by using the control variable of the automatic gain control.

Above we have mentioned that the variables $z_{k,i}$ are approximately Gaussian distributed. Therefore we are allowed to assume that z_k, which is their weighted sum, is a Gaussian random variable, too. The mean value of z_k is

$$\begin{aligned} \mu_{z_k} &= \mathbb{E}\{z_k\} = \sum_{i=1}^{N} \mathbb{E}\{w_i z_{k,i}\} = \sum_{i=1}^{N} \mathbb{E}\left\{\frac{|\mu_{z_{k,i}}|\mu_{z_{k,i}}}{\sigma_{z_i}^2}\right\} = \pm\sum_{i=1}^{N} \frac{\mu_{z_{k,i}}^2}{\sigma_{z_i}^2} \\ &= \pm\frac{1}{2}\sum_{i=1}^{N} \frac{\eta_i^2(T_I)E_{r,i}^2}{T_I BN_0^2 + \eta_i(T_I)E_{r,i}N_0}, \end{aligned} \tag{4.6}$$

where the sign is positive for $a_k = 0$ and negative for $a_k = 1$, cf. (4.3). The variance of the decision variable $z_k$is given by

$$\begin{aligned} \sigma_z^2 &= \sum_{i=1}^{N} {w_i}^2\sigma_{z_i}^2 = \sum_{i=1}^{N} \frac{\mu_{z_{k,i}}^2}{\sigma_{z_i}^4}\sigma_{z_i}^2 = \sum_{i=1}^{N} \frac{\mu_{z_{k,i}}^2}{\sigma_{z_i}^2} = |\mu_{z_k}| \\ &= \frac{1}{2}\sum_{i=1}^{N} \frac{\eta_i^2(T_I)E_{r,i}^2}{T_I BN_0^2 + \eta_i(T_I)E_{r,i}N_0}. \end{aligned} \tag{4.7}$$

The fact that $\sigma_{z_k}^2 = |\mu_{z_k}|$, which origins from the specific weights w_i, will greatly simplify the remaining computations. On the basis of this characterization of the decision variable statistics, and for the a-priori probabilities $P(a_k = 1) = P(a_k = 0) = \frac{1}{2}$, the ML decision rule minimizing the BEP is

$$\hat{a}_k = \begin{cases} 0, & \text{for } z_k > 0 \\ 1, & \text{else} \end{cases}.$$

The corresponding BEP is computed according to the same method as in (3.66):

$$\begin{aligned} P_e &= P(z_k < 0 | a_k = 0) \\ &= \frac{1}{2}\text{erfc}\left(\frac{\mu_z}{\sqrt{2}\sigma_z}\right) \\ &= \frac{1}{2}\text{erfc}\left(\frac{1}{2}\sqrt{\sum_{i=1}^{N}\frac{\eta_i^2(T_I)E_{r,i}^2}{T_I B N_0^2 + \eta_i(T_I)E_{r,i}N_0}}\right) \qquad (4.8) \\ &= \frac{1}{2}\text{erfc}\left(\frac{1}{2}\sqrt{\sum_{i=1}^{N}\frac{\alpha_i^2\eta_i^2(T_I)E_t^2}{T_I B N_0^2 + \alpha_i\eta_i(T_I)E_t N_0}}\right). \qquad (4.9) \end{aligned}$$

Note that the path gains α_i are random variables in general and thus also P_e is random. In this work only the physical layer of a communication system without coding is discussed.

Practical systems, would however use coding to implement a more reliable communication link. A particular problem of wireless channels, in particular for channels with a small bandwidth is, that the received energy may fade in a more or less fast fashion. For such fading channels it is convenient to use code words whose transmission period is much longer than the average time that passes between two deep fades. Thus, periods with a good link can be used to overcome periods of deep fades. To realize this, scramblers [49] are employed which have the effect of making the symbol error rate equivalent to the average symbol error rate of the physical layer, i.e., make the frequency of symbol errors time-invariant and therefore compensate the time-varying fading nature of the channel.

A meaningful and often used measure to assess the performance of communication systems for such fading channels which use this kind of coding is the average BEP. To allow an easy comparison of the performance of the herein presented noncoherent SIMO receiver with the performance of SIMO receivers for fast fading channels, we discuss this measure for our SIMO GMLR in Subsection 4.3.2. Not that in general, the path gains are slowly time-varying, such that an averaging over several channel realizations is not possible due to constraints of the data block length. Therefore, the average symbol error rate does not fully characterize the system performance. This emphasizes that we evaluate the average BEP of our noncoherent SIMO receiver only to compare its performance with that of well known communication systems for fast fading channels. An often used measure to characterize the performance of communication systems for slowly fading channels is the outage error probability or BEO which is discussed in Subsection 4.3.3.

4.3.2 Average BEP

The bit error probability in (4.9) is conditioned on the path gains α_i. The mean value $\overline{P}_e$ is computed by integrating over the product of this conditional error probability and the joint PDF, $\prod_{i-1}^{N} f_\alpha(\alpha_i)$, of the statistically independent path gains. Thus, the average BEP is

$$\overline{P}_e = \int \ldots \int \left(\prod_{i=1}^{N} f_\alpha(\alpha_i)\right) \frac{1}{2}\text{erfc}\left(\frac{1}{2}\sqrt{\sum_{i=1}^{N}\frac{\alpha_i^2\psi_i^2}{T_I B + \alpha_i\psi_i}}\right) d\alpha_1, \ldots, d\alpha_N, \qquad (4.10)$$

where $\psi_i = \eta_i(T_I)E_t/N_0$. This expression can be strongly simplified in the high SNR case which is given when $\alpha_i\psi_i \gg T_I B$. In this case, we have

$$P_e = \frac{1}{2}\text{erfc}\left(\frac{1}{2}\sqrt{\sum_{i=1}^{N}\alpha_i\psi_i}\right), \quad 0 < T_I < \Delta_T.$$

According to [5] the sum of the i.i.d. lognormal distributed random variables $\alpha_i\psi_i$ is an approximately lognormal distributed random variable, whereas the square root of a lognormal distributed random variable is exactly lognormal distributed. It follows that $s = \sqrt{\sum_{i=1}^{N}\alpha_i\psi_i}$ is approximatly lognormal distributed. Therefore, we can express (4.10) as

$$\overline{P}_e = \int f_s(s)\,\frac{1}{2}\text{erfc}\left(\frac{s}{2}\right)\,ds, \tag{4.11}$$

where $f_{\text{S}}(s)$ is the PDF of s. Unfortunately, the product $T_I B$ is on the order of ten for practical systems. In Chapter 3, for example, $T_I B = 40$; the condition $\alpha_i\psi_i \gg TI + I_B$ requires that the SNR, $\gamma_i = \alpha_i\eta(T_I)E_t/N_0 \gg 40$, i.e., the SNR must be much larger than 16 dB. This means that our approximation is only applicable if the SNR is much larger than 16 dB. Therefore, the simplified expression for the average BEP is of little practical importance. Furthermore, it is not a closed form expression that would allow conclusions about the system's diversity order to be made. Because of the mentioned problems we refrain from deriving an expression for the average error probability. Instead, we use a semi-analytic approach by computing the BEP for a sufficiently large set of path gains and by averaging over these BEP realizations. Corresponding results are presented in Section 4.6.

4.3.3 Bit Error Outage

The bit error probability P_e in (4.9) is a random variable because of the varying path gains. We define the bit error outage probability P_a, which is also called the bit error outage probability (BEO), as the bit error probability that is exceeded with a probability of a%. The analytical derivation of both measures, the average BEP and the BEO, requires a closed form expression for the CDF of the argument of the erfc function in (4.9) [17, 46]. Because the determination of this CDF is an open problem, we determine the outage error probability with a semi-analytic approach. This approach is similar to the one we use to determine the average BEP, i.e., we compute the BEP for a sufficiently large set of path gains and determine the BEO as the BEP value that is exceeded with a probability of a%. Section 4.6 presents numerical results for the BEO. Note that even for the coherent MLR which has a simpler BER expression, no closed form expression for the BEO can be found [79].

4.3.4 Coherence Gain

The coherence gain of a SIMO receiver results from the coherent addition of the mean value of the M decision variables and the noncoherent addition of their noise components. In this work we use the following definition of the coherence gain: We assume that a receiver with a single antenna requires an SNR, γ', to achieve a predefined BEP. Furthermore, we assume that the M antennas of the SIMO receiver are all at same position, so that (i) they capture the same signals with the same signal energies, i.e., $E_{r,i} = E_r$ and $\gamma_i = \gamma$, and that (ii) the ratios of the captured energy to the

received energy are equivalent, i.e., $\eta_i(T_I) = \eta(T_I)$. The SIMO receiver achieves the predefined BEP for an SNR, $\gamma < \gamma'$. Than, the coherence gain is defined as the the difference $\gamma' - \gamma$.

As mentioned, to identify the coherency gain, all M radio channels with indizes $i \in \{1, \ldots, M\}$ must receive the same signals. The channel model specified in Section 4.2 satisfies this condition when we set the shadow fading variance to zero, i.e. $\sigma_S^2 = 0$, this corresponds to the assumption of free space propagation made under case (a) in 4.2[1]. For this scenario, the BEP expression (4.9) simplifies to

$$\begin{aligned} P_e &= \frac{1}{2}\text{erfc}\left(\frac{1}{2}\sqrt{\frac{N\eta^2(T_I)E_r^2}{T_I B N_0^2 + \eta(T_I)E_r N_0}}\right) \\ &= \frac{1}{2}\text{erfc}\left(\frac{\sqrt{N}\eta(T_I)\gamma}{2\sqrt{T_I B + \eta(T_I)\gamma}}\right). \end{aligned} \tag{4.12}$$

Note that this expression equals (3.71) if we set $N = 1$. When doubling the number of receiver antennas N, the coherence gain is 3 dB in SNR wen $\eta(T_I)\gamma \gg T_I B$ or equivalently when $\eta(T_I)\gamma \approx T_I B$, i.e., in the high SNR regime. For lower SNR, the coherence gain is lower than 3 dB because doubling N in (4.12) has less effect on the argument of the erfc$(\cdot)$ function than doubling the SNR γ. This effect can also be observed from Fig. 4.4 which shows simulation results for the BEP as a function of the SNR.

4.3.5 Diversity Order

A measure for the degree to which diversity is exploited by a communication system is the diversity order. Its analytical determination requires several approximations for the case of Rayleigh fading channels and with coherent reception [41]. A way to derive the diversity order of the considered SIMO GMLR with MRC is not known to the author. Typically the diversity order is defined by the steepness of the BEP versus SNR curve in the high SNR regime. For the GMLR, the high SNR approximation is valid for the SNR $\gamma \gg T_I B$, i.e., for an SNR much larger than 16 dB. As discussed in Section 4.3.2, this SNR region is beyond the operating point of a practical system. Therefore, the definition of the diversity order for the GMLR in the high SNR regime would probably have no practical relevance. The diversity order in terms of SNR gain is discussed in Section 4.6 on the basis of simulation results.

4.4 Coherent SIMO Receiver

In this section we derive the SIMO receiver that combines the decision variables of M coherent receivers (according to Subsection 3.3.2) according to the MRC principle. Furthermore we derive the corresponding BEP and the coherence gain for this receiver.

4.4.1 BEP of Coherent SIMO Receiver

Similar, as for the noncoherent receiver, we use the statistical characterization of the individual receiver's decision variables $z_{k,i}$ to determine the weights of the MRC. With (3.125) (and P_u which

[1]To determine the coherence gain we assume that the path gains of the individual channels indexed by $i \in [1, N]$ are equivalent. I.e., to determine the coherence gain, the assumption of uncorrelated fading path gains is violated.

denotes the power of a narrowband interferer set to zero) the exact characterization of the decision variable is

$$z_{k,i} \sim \mathcal{N}\left(\mu_{z_i}, \sigma_{z_i}^2\right),$$

with

$$\mu_{z_i} = \begin{cases} +E_{r,i}, & \text{for } a_k = 0 \\ -E_{r,i} & \text{for } a_k = 1 \end{cases},$$

$$\sigma_{z_i}^2 = N_0 E_{r,i}, \tag{4.13}$$

and where $E_{r,i}$ is the energy per pulse that is received by antenna i. In the same way as for the noncoherent receiver, the random components of the decision variables are statistically independent because of the statistical independence of the receiver noise processes. Therefore, the optimum way of combining them is again MRC, which is described as

$$z_k = \sum_{i=1}^{N} w_i z_{k,i}.$$

However, the weights w_i are different from the weights for noncoherent receivers. In general, the variances $\sigma_{z_i}^2$ are not equal, see (4.13). Therefore, we first divide the decision variables $z_{k,i}$ by their standard deviations $\sigma_{i,z}$ to let the new decision variables $z'_{k,i} = z_{k,i}/\sigma_{z_i}$ have unit variance. Then, the corresponding weights are $w'_i = |\mu'_{z_i}|$, where $\mu'_{z_i} = \mu_{z_i}/\sigma_{z_i}$. With this, the MRC has to compute the final decision variable

$$z_k = \sum_{i=1}^{N} w'_i z'_{k,i} = \sum_{i=1}^{N} |\mu'_{z_i}| z'_{k,i} = \sum_{i=1}^{N} \frac{|\mu_{z_i}|}{\sigma_{z_i}^2} z_{k,i} = \sum_{i=1}^{N} \frac{z_{k,i}}{N_0}, \tag{4.14}$$

i.e., $w_i = 1/N_0$. The combined decision variable is approximately Gaussian distributed as well as the individual decision variables $z_{k,i}$. Hence the decision rule that minimizes the BEP is

$$\hat{a}_k = \begin{cases} 0, & \text{for } z_k > 0 \\ 1, & \text{else} \end{cases}.$$

Since N_0 is a constant we can set $w_i = 1$ without changing the symbol decision of the resulting decision rule. Assuming the final decision variable z_k to be Gaussian distributed the statistics of z_k is given by its mean,

$$\begin{aligned} \mu_z &= \sum_{i=1}^{N} \mu_{z_i} \\ &= \pm \sum_{i=1}^{N} E_{r,i}, \end{aligned} \tag{4.15}$$

and variance,

$$\begin{aligned} \sigma_z^2 &= \sum_{i=1}^{N} \sigma_{z_i}^2 \\ &= \sum_{i=1}^{N} N_0 E_{r,i}. \end{aligned} \tag{4.16}$$

On the basis of this characterization, and as the conditional probabilities $P(z_k > 0|a_k = 1)$ and $P(z_k < 0|a_k = 0)$ are equivalent, the BEP yields

$$\begin{aligned} P_e &= P(z_k > 0|a_k = 1) \\ &= \frac{1}{2}\text{erfc}\left(\frac{\mu_z}{\sqrt{2}\sigma_z}\right) \\ &= \frac{1}{2}\text{erfc}\left(\frac{\sum_{i=1}^{N} E_{r,i}}{\sqrt{2\sum_{i=1}^{N} N_0 E_{r,i}}}\right) \qquad (4.17) \\ &= \frac{1}{2}\text{erfc}\left(\frac{\sum_{i=1}^{N} \alpha_i E_t}{\sqrt{2\sum_{i=1}^{N} N_0 \alpha_i E_t}}\right). \qquad (4.18) \end{aligned}$$

4.4.2 Coherence Gain

If the receiver antennas are located close together, there is only the small-scale fading effect that makes a difference in the received energies $E_{r,i}$. As this effect is very small for sufficiently large bandwidth, we can assume by approximation that $E_{r,i} = E_r$ for all i and thus (4.17) simplifies to

$$P_e = \frac{1}{2}\text{erfc}\left(\frac{NE_r}{\sqrt{2NN_0E_r}}\right) = \frac{1}{2}\text{erfc}\left(\sqrt{\frac{NE_r}{2N_0}}\right). \qquad (4.19)$$

This expression also holds for a single antenna system, i.e., for $N = 1$, see (3.128), and describes the plain coherence gain if there is no diversity of the received energies $E_{r,i}$. The coherence gain, when doubling the number of receiver antennas N is 3 dB in SNR, see also Fig. 4.5(b) in Section 4.6.

4.5 SIMO Receivers with Generalized Selection Combining

The SIMO scheme with MRC consists of N distributed receivers that communicate their decision variables either wireless or over wires to a central processing unit which performs the MRC. The amount of decision variables that has to be communicated from the receivers to the processing unit is proportional to N. For some applications it is desirable to reduce this traffic. This can be achieved by letting the MRC select only the m out of N receivers with the largest SNR, where $m < N$. Only these selected m receivers transmit their decision variables to the central processing unit. The selection reduce the number of variables to be communicated from the individual receivers to the central processing unit. We denote the system comprising N receivers and an MRC which combines the m strongest signals or diversity branches as an (m, N) generalized selection combiner (GSC) [35]. The GSC corresponds for the special case $m = 1$ to conventional selection combining and for $m = N$ to MRC discussed in Section 4.3.

The application of GSC is proposed to exploit both, micro diversity as well as macro diversity [1]. This selection combining method can be improved by estimating the SINR (signal to interference plus noise ratio) rather than the just the SNR. Selecting the m out of N decision variables with the largest SINR reduces the impact of interferers. In this work we base the selection exclusively on the SNR.

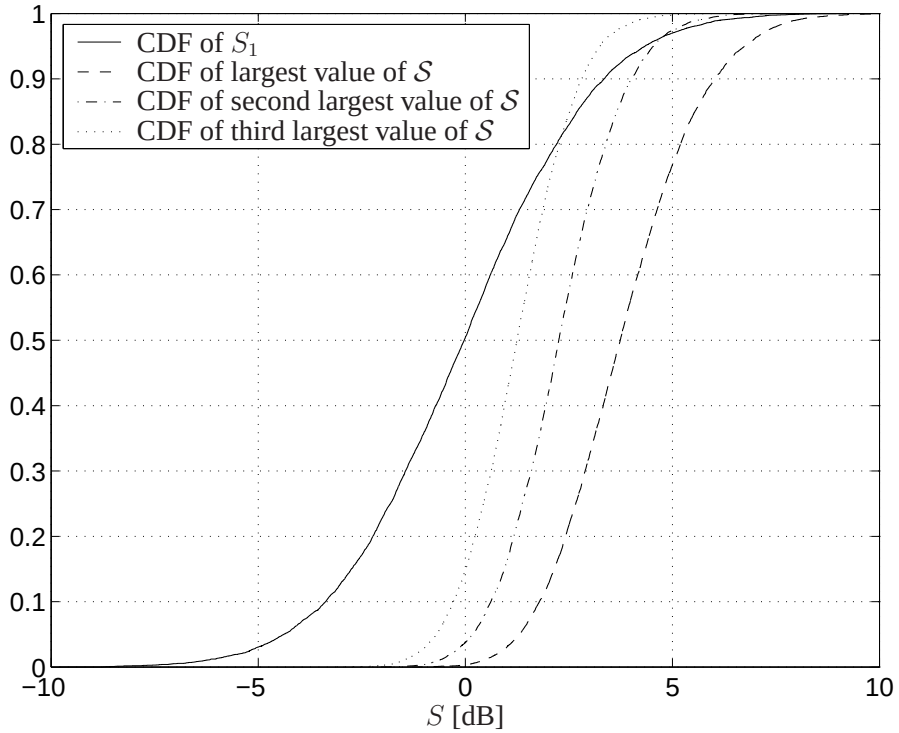

Fig. 4.3. CDF of lognormal distributed shadow fading variable S_1 and CDF of strongest, second strongest and third strongest fading variable of $\mathcal{S} := \{S_1, \ldots, S_8\}$. The variance of the fading variables S_i is $\sigma_S^2 = 2.7$ dB.

To explain the effect of choosing the m strongest out of N antenna signals we consider $N = 8$ corresponding lognormal shadow fading variables s_i, with $i \in \{1, \ldots, 8\}$, see Section 4.2. Their logarithm $S_i = 10\log(S_i)$ is normal distributed. The CDF of S_1 is depicted in Fig. 4.3; also shown are the CDF's of the strongest, the second-strongest and the third-strongest fading variables. The shown CDFs of these selected variables are steeper than the CDF of the original variables. This means, that the selected variables have a smaller variance than the original variables S_i. In addition, we observe that the selected variables have a larger mean value than the original variables S_i. To show the BEP for GSC, we use the semi-analytic approach from Subsection 4.3.2 and compute the BEP from (4.9) for a sufficiently large set of path gains. The resulting set of BEPs allows to determine any required statistics of the BEP. Results for the 10% outage probability P_{10} are presented in the subsequent section in Figs. 4.6, and 4.7.

4.6 Numerical Evaluation

In order to make visible different effects like the coherence gain and the diversity gain, we perform simulations for two different types of channels: for deterministic (or non-fading) channels and for fading channels.

4.6.1 Deterministic Channels

To verify the approximate expression (4.12) for the GMLR based SIMO receiver a simulation was run for equal path gains α_i for all $i \in \{1, \ldots, N\}$. In our channel model the assumption of constant path gains corresponds to the variance of the shadow fading variables $\sigma_S = 0$ dB. The resulting

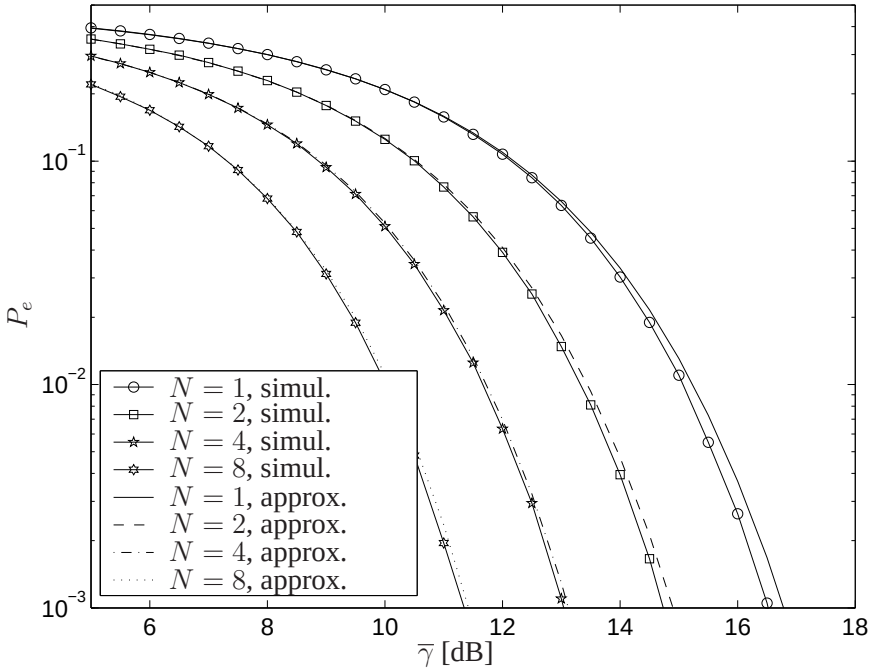

Fig. 4.4. BEP P_e versus SNR γ for multiple receiver antennas with equal and constant path gains. The simulated BEP is compared with the approximate analytic function (4.12).

BEP is depicted in Fig. 4.4 as a function of the average SNR, $\overline{\gamma}$ (for $\sigma_S = 0$ dB we have $\overline{\gamma} = \gamma$. In this figure, the simulation results are compared with the corresponding BEP curves obtained from the analytical expression (4.12). The deviations between the simulation and the approximate analytical formula become the smaller the larger the number of receiver antennas N is. This is because the Gaussian approximation that results in (4.12) is the more accurate the larger N is.

Given that all path gains are identical and constant, only the coherence gain can be observed. From Fig. 4.4 we observe that for a BEP lower than 10^{-1} the coherence gain is roughly 1.8 dB in SNR when the number of receiver antennas is doubled. The exact coherence gain however depends on N and on the SNR; this behavior was already discussed in Subsection 4.3.4 after equation (4.12). For coherent receivers, e.g., the MLR of Chapter 3, the coherence gain is exactly 3 dB. This can be seen from the $\overline{P}_e$ versus SNR curves in Fig. 4.5(b) for $\sigma_S = 0$ dB (identical channels), where the shift in SNR between the corresponding curves for $M = 1$ and $M = 2$ is exactly 3 dB, the same holds for $M = 2$ and $M = 4$. This unveils another performance disadvantage of the GMLR against the MLR, see the discussion in Section 3.9.

4.6.2 Fading Channels

The diversity gain comes from the effect that the total received energy of all antennas together has a variance that decreases with the number of antennas, N. Thus, the probability that the BEP is very high is decreased, and hence the average BEP decreases with N.

To quantitatively determine the effect of N on the BEP for fading channels, we evaluate the analytic expression (4.8) for a number of 10000 channel realizations. This semi-analytic approach is chosen because it speeds up the simulation dramatically over a pure simulation approach. The same assumptions about the channel are made as above, except that the standard deviation σ_S of the shadow fading term S is set to 2.7 dB; this variance corresponds to the NLOS indoor channel, see

Section 4.2. For simplicity the variance of the standard deviation σ_S is set to zero[2]. For each channel realization and receiver i, there results a different SNR. Therefore, we will show the average BEP, $\overline{P}_e$, as a function of the average SNR, $\overline{\gamma}$. The performance of the receivers with MRC and GSC are presented in the following subsections.

4.6.2.1 Maximum Ratio Combining.

Figure 4.5 shows the average BEP $\overline{P}_e$ as a function of the average SNR, $\overline{\gamma}$, for fading path gains with $\sigma_S = 2.7$ dB and for constant and identical path gains, i.e., $\sigma_S = 0$ dB. Note that for identical path gains it follows that the BEP and average BEP are equivalent, i.e., $\overline{P}_e = P_i$. As expected, we observe that the average BEP is increased when fading is introduced. This effect is weaker if the number of receivers is larger, i.e., if more diversity can be exploited. For example, to get the same BEP of 10^{-3} for nonfading and for fading channels, the SNR for fading channels must be increased by the fading margin, which is 4.1, 2.6, 1.8, and 1 dB for $N = 1$, 2, 4, and 8 receiver antennas. For comparison, Fig. 4.5(b) shows the performance of the same setup, but with the optimum coherent receiver or MLR instead of the noncoherent GMLR. For the same BEP of 10^{-3}, the fading margins are somewhat lower, i.e., 3.4, 2.1, 1.1, and 0.6 dB for $N = 1$, 2, 4, and 8 receiver antennas. This slight superiority in terms of fading margin can be interpreted as a better exploitation of the available diversity by the MLR. The total performance of the MLR is much better than that of the GMLR. As an example, the MLR achieves a BEP of 10^{-3} for an SNR of 13.4 dB with a single receiver antenna only, whereas the GMLR requires between $N = 4$ and 8 receiver antennas to achieve the same low BEP. It should be noted that practical implementations of the MLR show an implementation loss due to imperfect estimation of the CIR, synchronization errors and an incomplete number of rake fingers, whereas the implementation loss of a GMLR implementation is expected to be less dramatic because of the simple receiver architecture.

Figure 4.6 shows the average BEP $\overline{P}_e$ and the 10% BEO P_{10} for $N = 1,\ 2,\ 4$ and 8 receiver antennas. Comparing the BEO P_{10} with the average BEP shows that with growing number N the areas between the curves for the outage probabilities and the curves for the average BEP becomes smaller. This effect corresponds to an increasing quality of service. Furthermore, and in contrast to the case $N = 1$, the operating point $P_{10} = 10^{-3}$ improves by 3 dB for $N = 2$, by 5.8 dB for $N = 4$, and by 8.2 dB for $N = 8$. This corresponds to an almost 3 dB gain in sensitivity when the number of receiver antennas is doubled.

4.6.2.2 Generalized Selection Combining

The GSC scheme introduced in Section 4.5 is simulated for different total numbers of receivers N and selected number of receivers m. The 10% bit error outage is depicted in Fig. 4.7. Recall that the (N, N) GSC corresponds to the MRC with N receivers. One idea behind the GSC is to reduce the total data traffic from the receivers to the combiner. This goal can be achieved with relatively small performance losses; e.g., the $(1, 2)$ GSC looses less than 1 dB in performance compared to the $(2, 2)$ GSC, and still gains more than 2 dB over the single antenna receiver. Another interesting example is the $(4, 8)$ GSC, which shows almost the same performance as the $(8, 8)$ GSC while requiring only half of the data traffic.

[2]Note that the path gain model in [24] describes the logarithmic shadow fading term S as a Gaussian random variable with variance σ_S^2. This variance is again characterized as random variable with a nonzero variance.

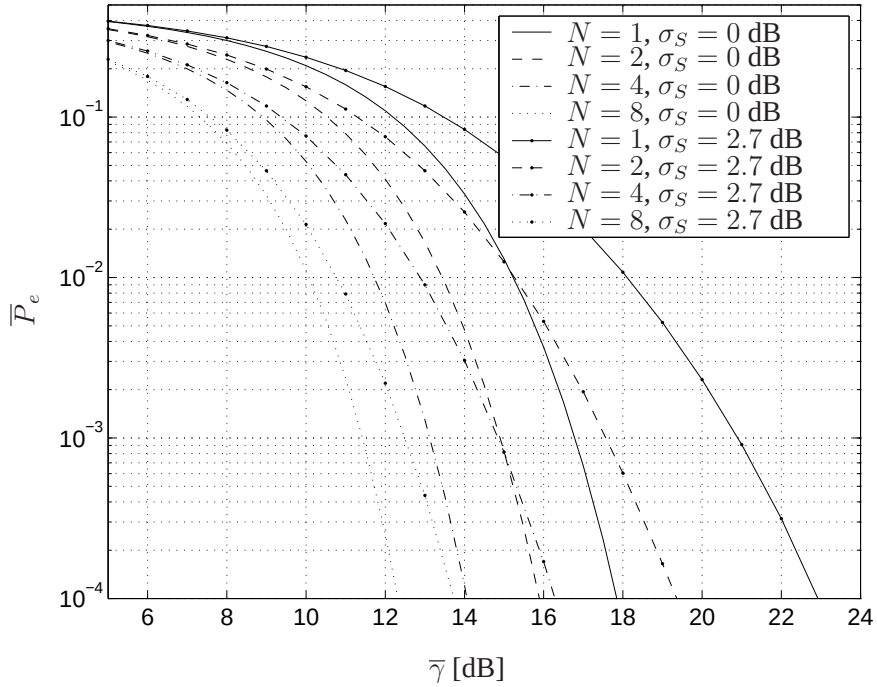

(a) GMLR performance

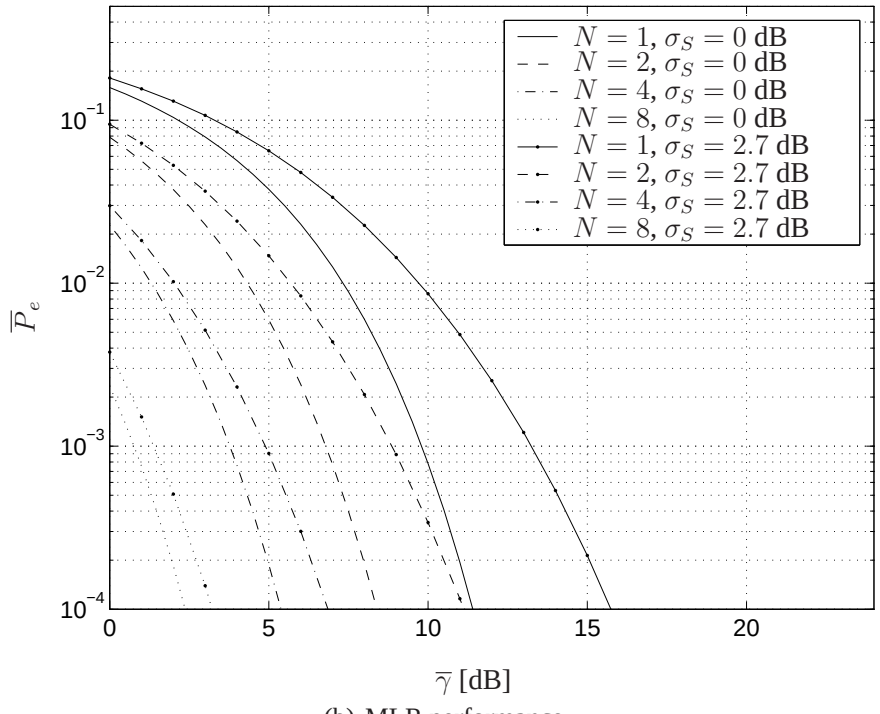

(b) MLR performance

Fig. 4.5. Average BEP $\overline{P}_e$ versus average SNR $\overline{\gamma}$ for N receiver antennas and for identical path gains, i.e., $\sigma_S = 0$ dB, and for fading channels with the same shadow fading, i.e., $\sigma_S = 2.7$ dB.

4.7 Conclusion

In this Chapter we have introduced two SIMO receivers that are suited to operate with antenna elements that are distributed over a large range. The two introduced SIMO receivers are both based on the noncoherent GMLR from Chapter 3, to each antenna element is associated one GMLR. The

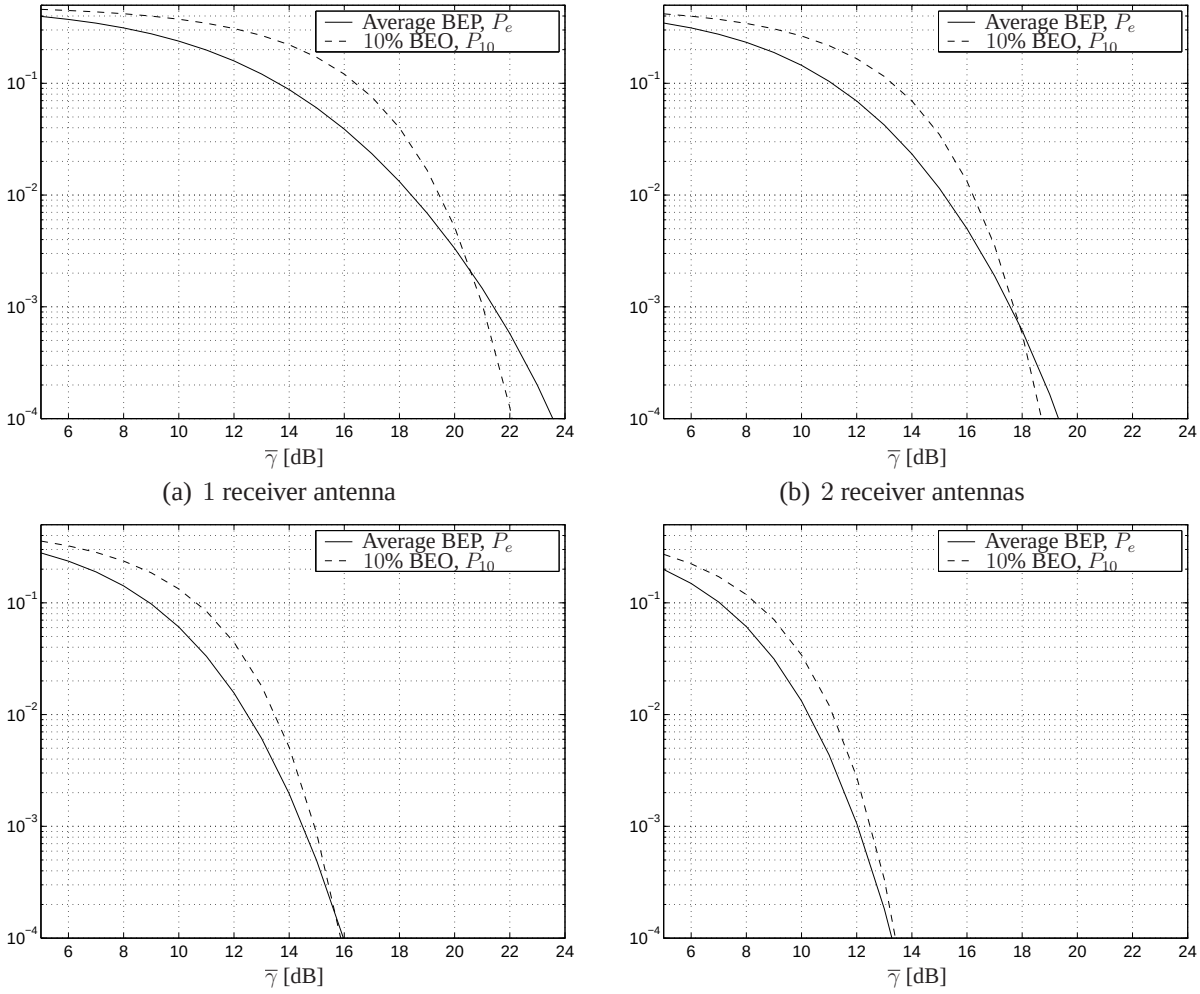

(a) 1 receiver antenna (b) 2 receiver antennas

(c) 4 receiver antennas (d) 8 receiver antennas

Fig. 4.6. Average BEP and 10% BEO versus average SNR $\overline{\gamma}$ for multiple receiver antennas with independently fading path gains and noncoherent receivers.

two receivers differ in the way that they combine the signals from individual GMLRs. According to these combining methods the SIMO receivers are give the attributes, maximum ratio combining (MRC) and generalized selection combining (GSC), respectively. For reference, the MRC and GSC receivers were also based on the coherent MLR, which was also discussed in Chapter 3. The performance of the noncoherent and coherent SIMO receivers was determined under the assumption that the received pulse shape and thus, the PDP is equivalent for all channels. The only channel parameter that was assumed to differ for various channels and the corresponding channel realizations was the lognormally fading path gain, the fading model for the path gains was adopted from a statistical path loss model for indoor UWB SISO channels. Hence, the benefit of using multiple receiver antennas is a coherence gain and a macro diversity gain.

It was shown that the MRC is an approximation to the optimum combiner for decision variables of several noncoherent receivers. The weighting coefficients of the MRC depend on the receiver noise figure and on the received signal strength; this is because the noise variance of the decision variables depends on both of these terms. A closed form expression of the BEP for deterministic path gains was given. This expression unveils that, unlike for the MLR, the array gain for the GMLR is less than 3 dB when the number of receiver antennas is doubled.

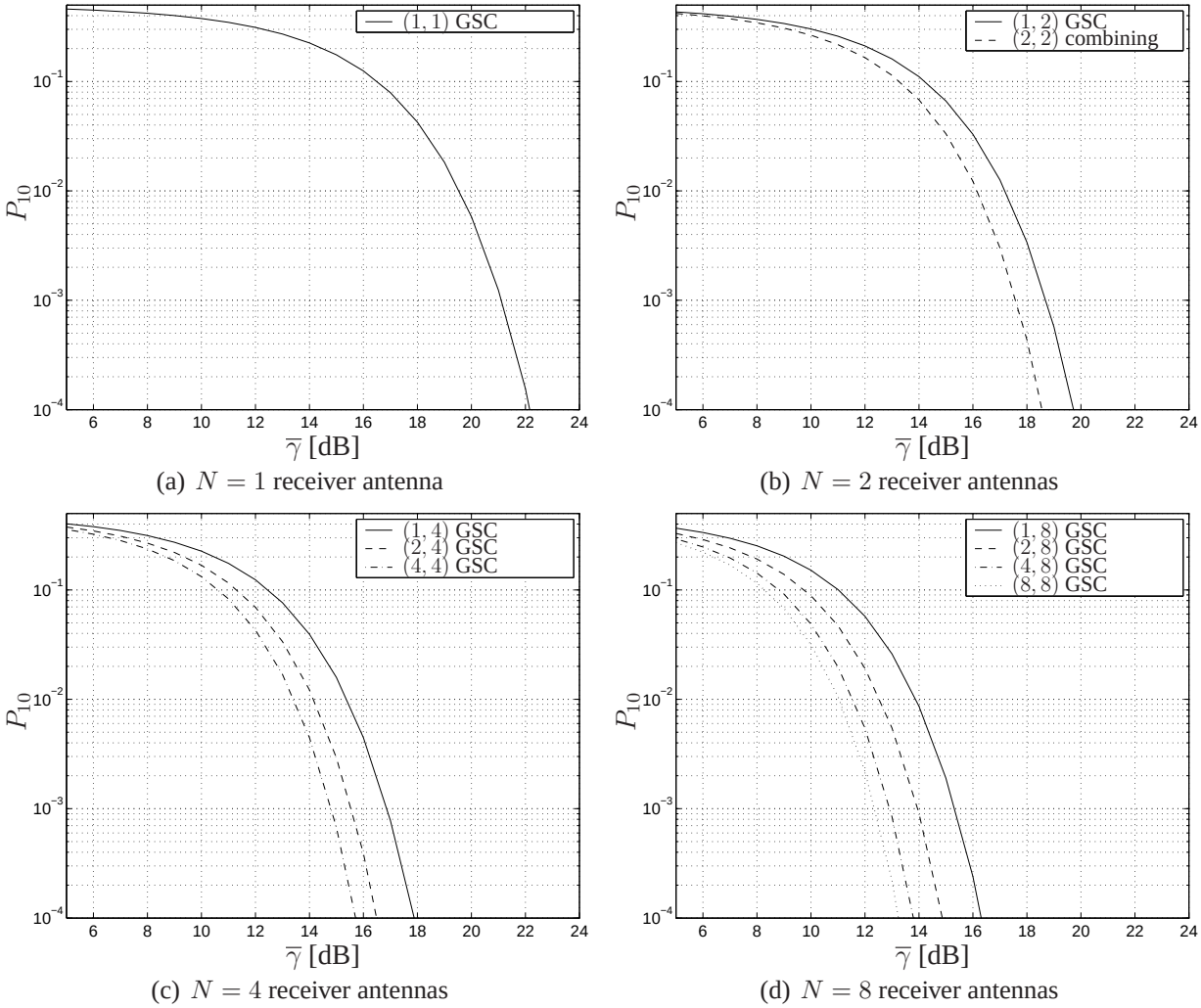

(a) $N = 1$ receiver antenna

(b) $N = 2$ receiver antennas

(c) $N = 4$ receiver antennas

(d) $N = 8$ receiver antennas

Fig. 4.7. 10% BEO P_{10} versus average SNR $\overline{\gamma}$ for GSC of m strongest out of N receiver signals, i.e., (m, N) GSC. The path gains of the N channels are fading independently.

An attempt to derive closed form expressions for the average BEP and the BEO for fading channels failed. One reason for this is that an approximate BEP expression which is sufficiently simple for the derivation of the average BEP and the BEO is available only in the high SNR regime, i.e., for SNRs larger than 16 dB. As practical receivers will be operated at lower SNR, the findings that would be based on this approach are not practically relevant. For Rayleigh fading channels and coherent receivers, the diversity order is typically defined only in the high SNR regime. Because for noncoherent receivers the high SNR regime begins with impractically high SNR, it is questionable if the diversity order as it is defined for coherent receivers is meaningful for the GMLR.

From numerical performance results it follows that a SIMO GMLR with MRC and $N = 4$ to 8 receiver antennas has approximately the same performance as an MLR with a single receiver antenna. This dramatic superiority of the MLR is in practice reduced by implementation losses which are expected to be larger for the MLR than for the GMLR. In addition to the MRC, the GSC has been proposed to reduce the total data traffic between the receivers and the combiner. Numerical evaluation of the BEP shows that the receiver sensitivity decreases only little for certain GSC configurations. The numerical results for the BEP and the BEO were obtained by a combination of

analytical expressions and simulation, because this method requires much less computation time to yield reliable results than plain simulation.

Part II

Rate-Division Multiple-Access

5. Rate-Division Multiple-Access Scheme

In a multiuser-communication scenario uncoordinated users compete for the use of a single channel. One class of multiple access methods suited for this type of operation accesses the channel at randomly chosen time instants. Because of the uncoordinated manner of access, collisions cannot be avoided. Therefore, the duty cycle of the user signals is kept low so that the resulting probability of collisions can be handled. The most popular methods based on this principle are ALOHA and time-hopping pulse position modulation (TH-PPM). The principle of the ALOHA scheme is that each user transmits data packets at a randomly chosen time instant. Thus, collisions occur with a certain probability and the corresponding data packets are destroyed. TH-PPM is a multiple access scheme for ultra-wideband (UWB) impulse radio (IR), where each modulated data symbol is represented by a sequence of up to a few hundred UWB pulses. These pulses have a low duty cycle and are placed at time instants that depend on the specific data symbols and on a pseudo-random or other TH sequence. A multiuser scenario often considered in this context comprises several transmitters, synonymously called users, and one or more receivers. In [78] each user is assigned an individual TH sequence; a receiver can capture the signal of the desired user if it knows its TH sequence.

The use of randomness introduces various difficulties. E.g., in an ALOHA system the arrival time of data packets is a random process, i.e., the delay between successive packets is sometimes larger and sometimes lower than the average. From a QoS (quality of service) perspective, however, the packet delay should be shortest possible for all packets. Another difficulty arises for TH-PPM signals where for signal acquisition the receiver must search for a relatively long pseudo random TH sequence. Proposed low complexity architectures perform the signal acquisition by the use of a sliding correlator, where the correlation is computed between the received signal and a reference signal whose length is determined by the TH sequence of the desired user. This approach requires long preambles even when sophisticated algorithms are used for signal acquisition [43, 28].

In this chapter, a novel and deterministic multiuser modulation scheme, *rate-division multiple-access* (RDMA), is introduced as an alternative to random channel-access based multiple access schemes. As RDMA is a simple deterministic scheme, it overcomes the mentioned problems of random multiple access schemes, while achieving similar bit-error-rates (BER) and throughput performance as random access schemes.

As mentioned, RDMA is a multiuser communication scheme for nonsynchronized or noncoordinated users. Each user transmits a pulse sequence with constant pulse rate. The transmitted signals are made distinguishable by using a different pulse-rate for each user, hence the name RDMA. If the pulse rates are chosen appropriately, the probability that user signals collide can be minimized and made nearly independent of the time asynchronism among the user signals.

The term *rate division multiple access* has already appeared in the context of a scheme that employs individual coding rates for the transmitters [56]; the symbol rates at the transmitter outputs, however, are identical, which is in contrast to the user-specific pulse rates (symbol rates) used for the RDMA scheme proposed in this chapter. A scheme with a similar name, *chip rate division multiple access* (CRDMA), has also been proposed for the use with code-division multiple-access (CDMA) [14], [50]. This scheme uses different chip rates that are power-of-two multiples of a basic chip rate to increase the number of chip sequences with good correlation properties; this scheme follows a CDMA approach and is therefore fundamentally different from RDMA.

The principle of the RDMA scheme is described for the application with binary-antipodal modulation. The notion of collisions is introduced, which is an indirect performance measure that is analytically much more tractable than the BER. The collision probability depends in general on the time asynchronism between the user signals; this results in varying system performance and is therefore undesirable. The key point in this chapter is to derive an analytical expression for the collision probability and its dependency on the time asynchronism, and finally to derive design rules for the system parameters that result in a collision probability that is independent of the time asynchronism.

This chapter is organized as follows. As an example of a physical layer, Section 5.1 introduces the signal model for binary antipodal modulation and coherent reception. In Section 5.2, the notion of collision probability is presented and an analytical expression for this probability is derived. Design rules for the user-specific rates that result in a robust collision probability are presented in Section 5.3. In practice, the transmitted data blocks will have finite length. A deleterious effect of this fact is discussed and a heuristic design rule to combat this effect is proposed. The efficiency of the design rules is confirmed by simulation results, which are presented in Section 5.4. Conclusions and an outlook are provided in Section 5.5.

5.1 RDMA Signal Model

A multiuser scenario with M nonsynchronized transmitters, synonymously called users, and a single receiver is considered. The users are indexed with numbers $m \in \mathcal{M} := \{1, 2, \ldots, M\}$; the user with index m is called user m for convenience. The user signals propagate over individual channels to the receiver antenna, where they are superimposed. The receiver's task is to detect the data sequence transmitted by the desired user, which in the following is indexed by i. The multiple-access communication system considered is shown in Fig. 5.1. User m modulates the (uncoded) data symbols $a_{m,k} \in \{-1, +1\}$, with time index $k \in \mathbb{Z}$ to produce a sequence of binary-antipodally modulated delta pulses,

$$u_m(t) = \sqrt{E_t} \sum_{k=-\infty}^{\infty} a_{m,k} \delta(t - kT_m - \tau_m). \tag{5.1}$$

By T_m we denote the symbol period, which is user-specific and allows the receiver to "tune" to the desired user. Therefore, we call the symbol period *user period*; its reciprocal corresponds to the symbol rate or *user rate* $1/T_m$. Without loss of generality, we define $T_1 < T_2 < \cdots < T_M$. The time shift τ_m represents the relative delay time between the instants at which user m and user i start their transmissions, hence $\tau_m \in \mathbb{R}$ and $\tau_i = 0$. The set of relative delays $\{\tau_m | \, m \in \mathcal{M}\}$ can be considered a realization of a random process determined by the start of transmission instants of the users; for simplicity we call such a realization as the *asynchronism* $\{\tau_m\}$, where we use the notation $\{\tau_m\} := \{\tau_m | \, m \in \mathcal{M}\}$.

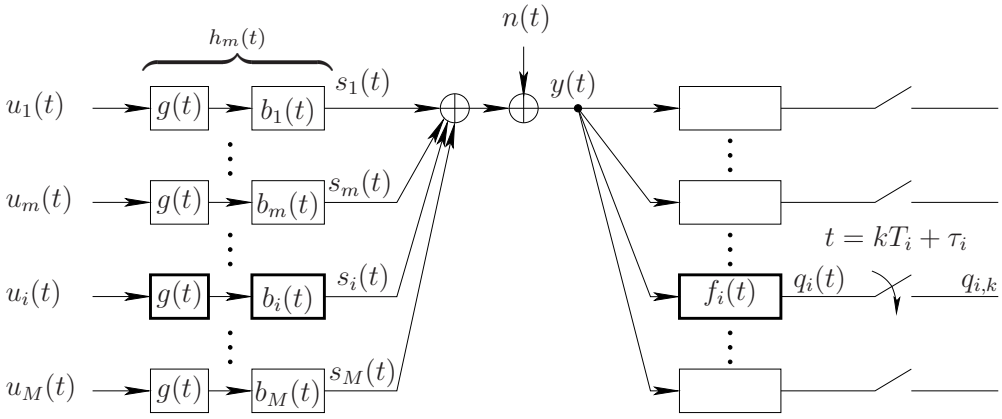

Fig. 5.1. Signal model for a rate-division multiple-access scheme.

The signals $u_m(t)$ are passed through the transmit filters with pulse shape $g(t)$ and fed to the corresponding transmitter antennas from where they propagate through the respective channels with the set of impulse responses $\{b_m(t)\}$. For simplicity, it is assumed that these channel impulse responses are causal and are nonzero at time $t = 0$, i.e., the channels' propagation delays are ignored. The pulse energy $\|g\|^2 = \int_{-\infty}^{\infty} g^2(t)dt$ is unity, so that E^t in (5.1) is the transmitted energy per pulse in the case of binary-antipodally modulated pulses.

At the receiver antenna's feed point, the signals

$$s_m(t) = h_m(t) * u_m(t), \;\; m \in \mathcal{M},$$

are superimposed and a white Gaussian noise signal $n(t)$ with two-sided power spectral density $N_0/2$ is added. Here, $h_m(t)$ is the received pulse shape $h_m(t) = b_m(t) * g(t)$ and '$*$' is the convolution operator. Thus, the noisy received signal is given by the expression

$$y(t) = \sum_{m \in \mathcal{M}} s_m(t) + n(t).$$

The energy per pulse that is received from user m is given by $E_m^r = E_p^t \|h_m\|^2$.

The receiver contains a filter with the impulse response $f_i(t)$ of unit energy, whose output signal

$$q_i(t) = f_i(t) * y(t)$$

is sampled with the symbol rate $1/T_i$ at the instants $t = kT_i, \; k \in \mathbb{Z}$, since $\tau_i = 0$ as explained above. The sampling instants are assumed to be perfectly synchronized with the corresponding user signal. For convenience, the shorthand notation

$$q_{i,k} = q_i(kT_i)$$

is defined. We can represent $q_{i,k}$ as the sum

$$q_{i,k} = w_{i,i,k} + \sum_{m \in \mathcal{M} \setminus \{i\}} w_{i,m,k} + z_{i,k}.$$

This sum consists of the sampled desired signal component

$$w_{i,i,k} = w_{i,i}(kT_i),$$

the multiuser interference (MUI) components

$$w_{i,m,k} = w_{i,m}(kT_i), \quad m \neq i, \tag{5.2}$$

where

$$w_{i,m}(t) = f_i(t) * s_m(t)$$

and the additive noise term

$$z_{i,k} = f_i(t) * n(t) \Big|_{t=kT_i}.$$

Figure 5.2 sketches possible signals $w_{i,m}(t)$ for $m = 1, i$, and j, under the assumption that the receiver filter $f_i(t)$ is matched to the desired received pulse shape $h_i(t)$, as indicated by the symmetry of the pulses $f_i(t) * h_i(t) = h_i(-t) * h_i(t)$ in the desired signal $w_{i,m}(t)$. The nonzero regions

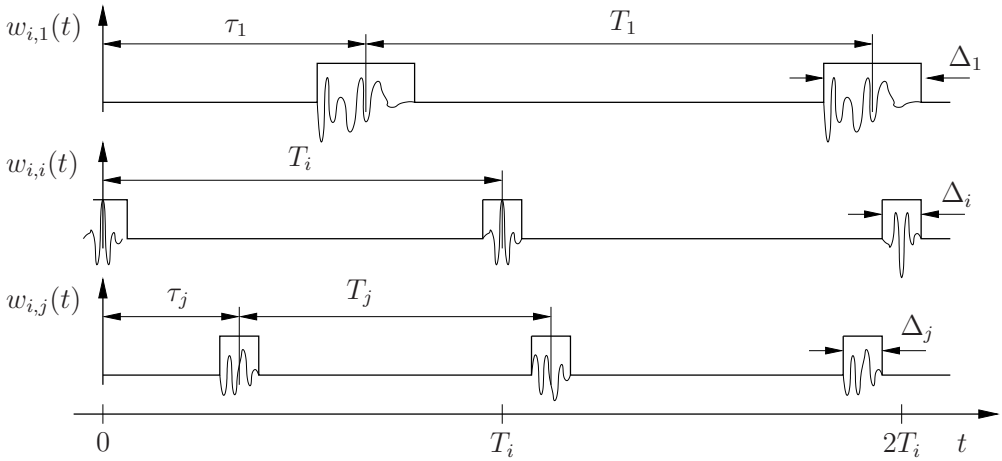

Fig. 5.2. Signals $w_{i,m}(t) = f_i(t) * s_m(t)$ caused by the users $m = 1, i$, and j. The support is indicated by the rectangular functions $\psi_{i,m}(t)$ of duration Δ_m. There occur two collisions because near by the instant $2T_i$ the signal $w_{i,1}(t)$ is nonzero when both the signal $w_{i,i}(t)$ and the signal $w_{i,j}(t)$ are sampled.

of the signals $w_{i,m}(t)$ are indicated by the value one of rectangular functions $\psi_{i,m}(t)$; the duration for which they are set to one, i.e. the support of the pulse $w_{i,m}(t)$ is Δ_m. [1] The functions $\psi_{i,m}(t)$ are used to define a signal-collision model in the next section. The noise samples $z_{i,k}$ have variance $N_0/2$ and are uncorrelated if the support of the receiver filter's impulse response $f_i(t)$ is smaller than T_i; this is satisfied for the simulation parameters chosen in Section 5.4.

The signal samples $q_{i,k}$ are fed to a threshold detector (slicer), generating the binary decisions $\hat{a}_{i,k} = \text{sgn}(q_{i,k})$. Note that the optimum receiver filter $f_i(t)$ is only equivalent to the matched filter $h_i(-t)$ if the multiuser interference terms $w_{i,m,k}$ are uncorrelated and Gaussian distributed; Section 5.4 will reveal that the latter condition (Gaussian distribution) is not the case in general, in particular when power control is missing, see also [20].

Since the users are not synchronized, there will be collisions among the signals $s_m(t)$ from different users, causing the multiuser interference terms $w_{i,m,k}$. The energy of the desired received signal, E_i^r, and the statistics of the terms $w_{i,m,k}$, together with the variance $N_0/2$ of the noise terms $z_{i,k}$, determine the probability of a detection error, $P(\hat{a}_{i,k} \neq a_{i,k})$. The multiuser interference terms depend on the pulse energy E^t, the received pulse shapes $\{h_m(t)\}$, the receiver filter $f_i(t)$, and the

[1] The duration Δ_m depends on the index i, however, as this has no impact on the subsequent derivation, the index i is skipped for simplicity.

set of user periods $\{T_m\}$. The aim of the following section is to formulate design rules for the set of user periods $\{T_m\}$ that make the BER independent of the asynchronism $\{\tau_m\}$ and minimum.

5.2 Collision Probability

It was pointed out that several effects impact the statistics of the multiuser interference terms $w_{i,k}$. This makes it difficult to find user periods that make the BER independent of the asynchronism $\{\tau_m\}$ and minimum. Instead of this difficult problem, we first solve the simpler one of finding design rules for the set of user periods $\{T_m\}$ that make the collision probability, instead of the BER, independent of the asynchronism and minimum at the same time. In this work only the collision probability is considered, which is just an indirect measure of the BER. However, in [70] it is shown by numerical simulation that application of the resulting user periods also leads to a BER statistics that is only weakly dependent on the asynchronism.

A collision with the desired signal, $q_{i,i}(t)$, at sampling instant $t = kT_i$ is defined as the event that one or more signals $q_{i,j}(t)$ with $j \neq i$, $j \in \mathcal{M}$, are nonzero at $t = kT_i$. To illustrate the notion of collisions, the time intervals where the signals $q_{i,j}(t)$ are nonzero are indicated by the value one of the rectangular functions $\psi_{i,j}(t)$ in Fig. 5.2. The only collision observable in this figure is caused by user 1, affecting the sampled signal $q_{i,k}$ at the sampling instant $t = 2T_i$.

5.2.1 Probability of Collision with a Single Interferer

The set $\mathcal{K}_{i,j}$ of sampling indices k_i for which the samples q_{i,k_i} are affected by a collision with user j is described as

$$\mathcal{K}_{i,j} = \left\{ k_i \in \mathbb{Z} \,\middle|\, \psi_{i,j}(k_i T_i) \neq 0 \right\}, \quad i \neq j. \tag{5.3}$$

Hence, for a given asynchronism $\{\tau_m\}$, there is nothing random with collisions. The relevant measure which describes the collision behavior is the relative frequency of collisions, i.e., the ratio of the number of collisions over the number of received pulses. To get from the relative frequency description of collisions to a probabilistic description of collisions, we introduce an artificial source of randomness. This step proves to be very useful as it allows us to apply probabilistic number theory [32]. Randomness is introduced by considering the probability $P_c(i)$ that any user collides with user i at a randomly chosen sampling instant kT_i, where the number $k \in \mathbb{Z}$ is uniformly distributed and represents the *artificially introduced source of randomness*. With this notion we can define the probability of collision between the ith and the jth user as

$$P_c(i,j) := P(k \in \mathcal{K}_{i,j}), \quad i \neq j. \tag{5.4}$$

To ensure that $P_c(i,j) < 1$, the functions $\psi_{i,j}(t)$, $i,j \in \mathcal{M}$ must have a duty cycle which is smaller than 1; this restriction is expressed by $\underset{j\in\mathcal{M}}{\forall} \Delta_j < T_j$. Note that Δ_j is the duration of the support of the pulse shape $w_{i,j}(t)$. Considering (5.3) and by inspection of Fig. 5.2, we can write

$$\mathcal{K}_{i,j} = \left\{ k_i \in \mathbb{Z} \,\middle|\, \underset{k_j\in\mathbb{Z}}{\exists} \left[k_j T_j + \tau_j - \frac{\Delta_j}{2} \;\leq\; k_i T_i \;<\; k_j T_j + \tau_j + \frac{\Delta_j}{2} \right] \right\}, \quad i \neq j. \tag{5.5}$$

Expressed in words, this means that $\mathcal{K}_{i,j}$ is the set of integer numbers k_i for which there exists at least one number $k_j \in \mathbb{Z}$ such that the inequality

$$k_j T_j + \tau_j - \frac{\Delta_j}{2} \leq\; k_i T_i \;<\; k_j T_j + \tau_j + \frac{\Delta_j}{2} \tag{5.6}$$

is satisfied. The notation used in expression (5.5) is defined in Appendix B.4. To determine the set $\mathcal{K}_{i,j}$ we transform this real-valued inequality into an integer-valued inequality. In a first step we assume that the user periods $T_i,\ i \in \mathcal{M}$ are integer multiples of a small time interval $T \in \mathbb{R}$, with $T \ll T_i$, $i \in \mathcal{M}$. Thus we can write

$$T_i := N_i T, \quad T_j := N_j T, \tag{5.7}$$

with $N_i, N_j \in \mathbb{N}$. We denote the numbers N_i, for $i \in \mathcal{M}$ as *user numbers* in dependence on the term user periods used to denote T_i, for $i \in \mathcal{M}$. Furthermore we define

$$r_j := \left(\tau_j - \frac{\Delta_j}{2}\right)\frac{1}{T}, \quad \text{and} \quad D_j := \frac{\Delta_j}{T}. \tag{5.8}$$

Equation (5.6) can be divided by T without an effect on its solutions. With the newly defined variables the division by T yields

$$k_j N_j + r_j \ \leq \ k_i N_i \ < \ k_j N_j + r_j + D_j. \tag{5.9}$$

Note that Δ_j and T_j are real-valued and thus $T, r_j, D_j \in \mathbb{R}$. Let F_{ij} denote the greatest common divisor of the integer numbers N_j and N_i. This implies the numbers

$$Q_j := N_j/F_{ij} \ \text{ and } \ Q_i := N_i/F_{ij} \tag{5.10}$$

to be relative prime.[2] Transforming the remaining terms, r_j and D_j, in (5.9) into integer-valued terms is done in the following steps:

$$\begin{aligned}
k_j N_j + r_j \ &\leq \ k_i N_i \ &< \ k_j N_j + r_j + D_j,\\
k_j Q_j F_{ij} + r_j \ &\leq \ k_i Q_i F_{ij} \ &< \ k_j Q_j F_{ij} + r_j + D_j,\\
k_j Q_j + \frac{r_j}{F_{ij}} \ &\leq \ k_i Q_i \ &< \ k_j Q_j + \frac{r_j + D_j}{F_{ij}},\\
k_j Q_j + \left\lceil \frac{r_j}{F_{ij}} \right\rceil \ &\leq \ k_i Q_i \ &< \ k_j Q_j + \left\lceil \frac{r_j + D_j}{F_{ij}} \right\rceil,
\end{aligned}$$

where $\lceil \cdot \rceil$ is the ceiling function, which rounds noninteger real-valued arguments to the next larger integer and leaves integer valued arguments unchanged. The equivalence of the last two lines is because $x \leq y$ implies that $\lceil x \rceil \leq y$ if y is an integer and because $y < z$ implies that $y < \lceil z \rceil$. As $k_i Q_i$ is integer-valued we we can apply these two rules. The last inequality only contains integer terms. Thus, (5.5) can be written as

$$\mathcal{K}_{i,j} = \left\{ k_i \in \mathbb{Z} \,\middle|\, \underset{k_j \in \mathbb{Z}}{\exists} \ \overset{L_{2,j}}{\underset{l=L_{1,j}}{\exists}} \ k_i Q_i = k_j Q_j + l \right\}, \ \ i \neq j \tag{5.11}$$

where

$$L_{1,j} := \left\lceil \frac{r_j}{F_{ij}} \right\rceil \ \text{ and } \ L_{2,j} := \left\lceil \frac{r_j + D_j}{F_{ij}} \right\rceil - 1. \tag{5.12}$$

The set (5.11) can be represented as the union

$$\mathcal{K}_{i,j} = \bigcup_{l=L_{1,j}}^{L_{2,j}} \mathcal{K}_{i,j}(l), \ \ i \neq j, \tag{5.13}$$

[2] Two integer numbers are *relative prime* if their greatest common divisor is unity.

with the sets

$$\mathcal{K}_{i,j}(l) := \left\{ k_i \in \mathbb{Z} \,\middle|\, \underset{k_j \in \mathbb{Z}}{\exists} k_i Q_i = k_j Q_j + l \right\}, \quad i \neq j. \tag{5.14}$$

According to Theorem 14 in Appendix G, these sets are disjoint[3] with respect to l. A necessary condition for the applicability of this theorem is that $L_{2,j} - L_{1,j} < Q_j$, which is satisfied for our assumption that $\Delta_j < T_j$. [4] The disjointness of the sets $\mathcal{K}_{i,j}(l)$ means that a collision at any sampling instant $k_i T_i$ stems only from one pulse of the interfering user j but not from overlapping pulses of the interfering user. Overlapping of interfering pulses from a single user is excluded if the duration of the interfering pulses Δ_j is shorter than the user period T_j (cf. Fig. 5.2).

With (5.4) and (5.13), the probability $P_c(i,j)$ is given by

$$P_c(i,j) = P(k \in \mathcal{K}_{i,j}) = P\left(k \in \bigcup_{l=L_{1,j}}^{L_{2,j}} \mathcal{K}_{i,j}(l) \right). \tag{5.15}$$

Note that the probability $P_c(i,j)$ is defined only for $i \neq j$. As the sets $\mathcal{K}_{i,j}(l)$ are disjoint with respect to l, we have

$$P_c(i,j) = \sum_{l=L_{1,j}}^{L_{2,j}} P(k \in \mathcal{K}_{i,j}(l)). \tag{5.16}$$

To determine the probability $P(k \in \mathcal{K}_{i,j}(l))$ we use Theorem 13 in Appendix G, which states that the elements in $\mathcal{K}_{i,j}(l)$ are numbers of an arithmetic series with the difference Q_j between consecutive elements. From this we conclude that on average every Q_jth realization of the random integer variable k is an element of $\mathcal{K}_{i,j}(l)$. Thus, we have

$$P(k \in \mathcal{K}_{i,j}(l)) = \frac{1}{Q_j}. \tag{5.17}$$

Inserting this into (5.16) yields

$$\begin{aligned} P_c(i,j) &= \sum_{l=L_{1,j}}^{L_{2,j}} \frac{1}{Q_j} \\ &= (L_{2,j} - L_{1,j} + 1)\frac{1}{Q_j} && (5.18) \\ &= \left(\left\lceil \frac{r_j + D_j}{F_{ij}} \right\rceil - \left\lceil \frac{r_j}{F_{ij}} \right\rceil \right) \frac{1}{Q_j} && (5.19) \\ &= \left(\lceil \gamma + \beta \rceil - \lceil \gamma \rceil \right) \frac{1}{Q_j}, && (5.20) \end{aligned}$$

where we used the definitions (5.12), as well as

$$\beta := D_j / F_{ij}, \text{ and } \gamma := r_j / F_{ij} \mod 1,$$

[3] An intuitive understanding of Theorem 14 can be obtained by graphically illustrating the involved number-sets on the number line.

[4] Combining $T > \Delta_j$ with (5.7), (5.8), and (5.10) implies that $\lceil D_j/F_{ij} \rceil - 1 < Q_j$; with $L_{2,j} - L_{1,j} = \lceil r_j/F_{ij} + D_j/F_{ij} \rceil - \lceil r_j/F_{ij} \rceil - 1 \leq \lceil D_j/F_{ij} \rceil - 1$ it follows that $L_{2,j} - L_{1,j} < Q_j$.

where the modulo operation $x \mod y$ yields the remainder of the division x/y. Replacing r_j/F_{ij} by $\gamma := r_j/F_{ij} \mod 1$ does not influence the result of (5.19), as in an expression $\lceil x+y \rceil - \lceil x \rceil$, the integer component of x cancels out. Assuming a sufficiently smooth pdf of $r_j \in \mathbb{R}$, the assumption is justified that γ is uniformly distributed in $[0,1)$. From (5.19) and (5.8) we observe that the collision probability in general is a function of the asynchronism τ_j. Note that the collision probability $P_c(i,j)$ depends on the random variable γ, i.e., on the asynchronism τ_j. Therefore, $P_c(i,j)$ is a random variable, too. To determine the average of the collision probability $P_c(i,j)$, where the average is taken over γ, i.e., over the asynchronism τ_j, we compute first the collision probability given that the parameter $\beta \notin \mathbb{N}$ and $\gamma \neq 0$:

$$P_c(i,j)\,\Big|_{\beta\notin\mathbb{N},\gamma\neq 0} = (L_{2,j} - L_{1,j} + 1)\frac{1}{Q_j}\Big|_{\beta\neq\mathbb{N},\gamma\neq 0} = \left(\lceil \gamma+\beta \rceil - \lceil \gamma \rceil\right)\frac{1}{Q_j}\Big|_{\beta\neq\mathbb{N},\gamma\neq 0} \tag{5.21}$$

To evaluate the term $(\lceil \gamma+\beta \rceil - \lceil \gamma \rceil)$ we represent β as the sum of its integer component $\beta' := \lfloor \beta \rfloor$ and its noninteger part $\beta'' := \beta - \lfloor \beta \rfloor$. Thus, $\beta = \beta' + \beta''$. This implies that $\lceil \beta \rceil = \beta' + \lceil \beta'' \rceil$ and $\lceil \beta' \rceil = 1$. Analogously, we represent γ as $\gamma = \gamma' + \gamma''$. As we consider only the case where $\gamma \neq 0$, γ is restricted to the interval $\in (0,1)$. Hence, $\gamma' := \lfloor \gamma \rfloor = 0$ and that $\lceil \gamma'' \rceil = 1$. From the definition of the variables γ'' and β'' it follows that they lie within the interval $(0,1)$. Therefore, we can write the two rules

$$\gamma+\beta > \lceil \gamma \rceil \Leftrightarrow \gamma''+\beta'' > \lceil \gamma'' \rceil \Leftrightarrow \lceil \gamma''+\beta'' \rceil > \lceil \gamma'' \rceil \Leftrightarrow \lceil \gamma''+\beta'' \rceil = 2,$$

and

$$\gamma+\beta \leq \lceil \gamma \rceil \Leftrightarrow \gamma''+\beta'' \leq \lceil \gamma'' \rceil \Leftrightarrow \lceil \gamma''+\beta'' \rceil = \lceil \gamma'' \rceil \Leftrightarrow \lceil \gamma''+\beta'' \rceil = 1.$$

With these rules and the above representations of β and γ we can write

$$\begin{aligned}
\lceil \gamma+\beta \rceil - \lceil \gamma \rceil &= \lceil \gamma'+\gamma''+\beta'+\beta'' \rceil - \lceil \gamma'+\gamma'' \rceil \\
&= \gamma'+\beta'+\lceil \gamma''+\beta'' \rceil - \gamma' - \lceil \gamma'' \rceil \\
&= \beta' - 1 + \lceil \gamma''+\beta'' \rceil \\
&= \beta' + 1 - 2 + \lceil \gamma''+\beta'' \rceil \\
&= \beta' + \lceil \beta'' \rceil - 2 + \lceil \gamma''+\beta'' \rceil \\
&= \lceil \beta \rceil - 2 + \lceil \gamma''+\beta'' \rceil \\
&= \begin{cases} \lceil \beta \rceil, & \text{for } \gamma+\beta > \lceil \gamma \rceil, \\ \lceil \beta \rceil - 1, & \text{for } \gamma+\beta \leq \lceil \gamma \rceil. \end{cases}
\end{aligned} \tag{5.22}$$

Applying this result to evaluate (5.21) we get

$$P_c(i,j)\,\Big|_{\beta\notin\mathbb{N}} = \begin{cases} \frac{\lceil \beta \rceil}{Q_j}, & \text{for } (\gamma \neq 0) \wedge (\gamma+\beta > \lceil \beta \rceil), \\ \frac{\lceil \beta \rceil - 1}{Q_j}, & \text{for } (\gamma \neq 0) \wedge (\gamma+\beta \leq \lceil \beta \rceil). \end{cases} \tag{5.23}$$

The event $\gamma = 0$ occurs with probability zero and can therefore be ignored. The first case in (5.23) occurs with probability

$$\begin{aligned} P_1 &= P\left[(\gamma \neq 0) \wedge (\gamma + \beta > \lceil \beta \rceil)\right] \Big|_{\beta \notin \mathbb{N}} \\ &= P\left(\gamma + \beta > \lceil \beta \rceil\right) \Big|_{\beta \notin \mathbb{N}} \\ &= P\left(\gamma > (1 - \beta) \mod 1\right) \Big|_{\beta \notin \mathbb{N}} \\ &= \beta \mod 1 \\ &= \beta - \lfloor \beta \rfloor, \end{aligned} \tag{5.24}$$

where the last but one step follows from γ being uniformally distributed. The second case in (5.23) occurs with probability $1 - P_1$. With this, (5.19), (5.23), (5.24), and the definition of β, we have the average probability

$$\begin{aligned} \overline{P_c}(i,j) \Big|_{\beta \notin \mathbb{N}} &= \mathbb{E}_{\tau_j} \left\{ P_c(i,j) \Big|_{\beta \notin \mathbb{N}} \right\} \\ &= \left[P_1 \lceil \beta \rceil + (1 - P_1)\left(\lceil \beta \rceil - 1\right)\right] \frac{1}{Q_j} \Big|_{\beta \notin \mathbb{N}} \\ &= \left(\lceil \beta \rceil - 1 + \beta - \lceil \beta \rceil\right) \frac{1}{Q_j} \Big|_{\beta \notin \mathbb{N}} \\ &= \frac{\beta}{Q_j} \\ &= \frac{D_j}{F_{ij} Q_j}. \end{aligned} \tag{5.25}$$

Next we compute the collision probability $P_c(i,j)$ for the complementary parameter assumption, $\beta \in \mathbb{N}$:

$$\begin{aligned} P_c(i,j) \Big|_{\beta \in \mathbb{N}} &= \left(\lceil \gamma + \beta \rceil - \lceil \gamma \rceil\right) \frac{1}{Q_j} \Big|_{\beta \in \mathbb{N}} \\ &= \frac{\beta}{Q_j} \end{aligned} \tag{5.26}$$

As this does not depend on γ, or implicitly on τ_j, the probability $P_c(i,j)$ for $\beta \in \mathbb{N}$ is not random but constant and yields

$$\overline{P_c}(i,j) \Big|_{\beta \in \mathbb{N}} = \mathbb{E}_{\tau_j} \left\{ P_c(i,j) \Big|_{\beta \in \mathbb{N}} \right\} = P_c(i,j) \Big|_{\beta \in \mathbb{N}} = \frac{\beta}{Q_j} \frac{D_j}{F_{ij} Q_j}, \tag{5.27}$$

where we used (5.26) and inserted the definition of β. As the probability $P_c(i,j)$ is the same for non-natural and for natural β – compare (5.25) (5.27) – we get

$$\overline{P_c}(i,j) = \frac{D_j}{F_{ij} Q_j}. \tag{5.28}$$

Substituting (5.8) and (5.10) we have

$$\overline{P_c}(i,j) = \frac{D_j}{N_j} = \frac{\Delta_j N_i}{T_i N_j} = \frac{\Delta_j}{T_j}. \tag{5.29}$$

This result is intuitively clear as it equals the duty cycle of the signal $\psi_{i,j}(t)$, i.e., the average collision probability $\overline{P_c}(i,j)$ is equivalent to the probability that the signal $\psi_{i,j}(t)$ is nonzero at a randomly chosen instant $t \in \mathbb{R}$. We conclude that the collision probability given in (5.20), which depends implicitly on the random variable τ_j, has the average $\overline{P_c}(i,j) = \Delta_j / T_j$. In contrast, the maximum collision probability can be determined using (5.20):

$$\hat{P}_c(i,j) = \max_{\tau_j} \{P_c(i,j)\} = \max_{\tau_j} \left\{ (\lceil \gamma + \beta \rceil - \lceil \gamma \rceil) \frac{1}{Q_j} \right\}.$$

In this expression, the only variable that depends on τ_j is γ. For any value $\gamma \in [0,1)$ a $\tau_j \in \mathbb{R}$ and for can be found; hence, the maximization can be performed over γ. Under the assumption that $\gamma \in [0,1)$ we get

$$\lceil \gamma + \beta \rceil - \lceil \gamma \rceil = \begin{cases} \lceil \beta \rceil - \lceil \gamma \rceil = \lceil \beta \rceil - 1, & \text{for } (\gamma > 0) \wedge (\lceil \gamma + \beta \rceil = \lceil \beta \rceil), \\ \lceil \beta \rceil + 1 - \lceil \gamma \rceil = \lceil \beta \rceil, & \text{for } (\gamma > 0) \wedge (\lceil \gamma + \beta \rceil > \lceil \beta \rceil), \\ \lceil \beta \rceil, & \text{for } (\gamma = 0). \end{cases}$$

Hence, we get

$$\begin{aligned} \hat{P}_c(i,j) &= \max_{\tau_j} \left\{ (\lceil \gamma + \beta \rceil - \lceil \gamma \rceil) \frac{1}{Q_j} \right\} \\ &= \lceil \beta \rceil \frac{1}{Q_j} \\ &= \left\lceil \frac{\Delta_j}{TF_{ij}} \right\rceil \frac{1}{Q_j}. \end{aligned} \tag{5.30}$$

Using the inequality $\lceil x \rceil < 1 + x$ and with $TF_{ij}Q_j = TN_j = T_j$ (see (5.7) and (5.10)), we get the upper bound

$$\hat{P}_c(i,j) < \left(1 + \frac{\Delta_j}{TF_{ij}}\right) \frac{1}{Q_j} = \frac{\Delta_j + TF_{ij}}{T_j}. \tag{5.31}$$

The difference between $\hat{P}_c(i,j)$ and the upper bound is smaller than $1/Q_j$.

5.2.2 Probability of Collision with Multiple Interferers

For the case of only one interfering user j, the probability of collision $P_c(i,j)$ is given by (5.20). In what follows we determine the probability

$$P_c(i) = P\left(k \in \bigcup_{j \in \mathcal{M} \setminus \{i\}} \mathcal{K}_{i,j} \right), \tag{5.32}$$

i.e., the probability that at least one user $j \in \mathcal{M} \setminus \{i\}$ collides with user i. The derivation greatly simplifies if the events of user j and user j' colliding with user i, with $j \neq j'$ and $j, j' \in \mathcal{M} \setminus \{i\}$, are statistically independent; this statistical independence is ensured if

$$P[(k \in \mathcal{K}_{i,j}) \ \wedge \ (k \in \mathcal{K}_{i,j'})] = P(k \in \mathcal{K}_{i,j}) P(k \in \mathcal{K}_{i,j'}). \tag{5.33}$$

That this is always true is proved in Appendix H. We can thus evaluate (5.32) as

$$\begin{aligned}
P_c(i) &= P\left(k \in \bigcup_{j\in\mathcal{M}\setminus\{i\}} \mathcal{K}_{i,j}\right) \\
&= 1 - P\left(k \notin \bigcup_{j\in\mathcal{M}\setminus\{i\}} \mathcal{K}_{i,j}\right) \\
&= 1 - P\left(k \in \bigcap_{j\in\mathcal{M}\setminus\{i\}} \mathbb{Z}\setminus\mathcal{K}_{i,j}\right) \\
&= 1 - \prod_{j\in\mathcal{M}\setminus\{i\}} P\left(k \in \mathbb{Z}\setminus\mathcal{K}_{i,j}\right) \\
&= 1 - \prod_{j\in\mathcal{M}\setminus\{i\}} \left[1 - P\left(k \in \mathcal{K}_{i,j}\right)\right] \\
&= 1 - \prod_{j\in\mathcal{M}\setminus\{i\}} \left[1 - P_c(i,j)\right] \qquad (5.34) \\
&= 1 - \prod_{j\in\mathcal{M}\setminus\{i\}} \left(1 - \frac{L_{2,j} - L_{1,j} + 1}{Q_j}\right), \qquad (5.35)
\end{aligned}$$

where we used (5.18). Expanding the expressions for $L_{2,j}$ and $L_{1,j}$ in (5.35) yields

$$\begin{aligned}
P_c(i) &= 1 - \prod_{j\in\mathcal{M}\setminus\{i\}} \left(1 - \frac{\left\lceil \frac{r_j+D}{F_{ij}} \right\rceil - \left\lceil \frac{r_j}{F_{ij}} \right\rceil}{Q_j}\right). \qquad (5.36) \\
&= 1 - \prod_{j\in\mathcal{M}\setminus\{i\}} \left(1 - \frac{\left\lceil \frac{\tau_j+\Delta_j/2}{F_{ij}\,T} \right\rceil - \left\lceil \frac{\tau_j-\Delta_j/2}{F_{ij}\,T} \right\rceil}{Q_j}\right). \qquad (5.37)
\end{aligned}$$

In the last line the variables r_j and D_j are expressed by the natural variables τ_j and Δ_j, see (5.8). The average collision probability is computed as the expectation value over the individual asynchronisms τ_j. Using (5.34) and (5.29) yields[5]

$$\begin{aligned}
\overline{P}_c(i) &= \mathbb{E}_{\tau_1}\mathbb{E}_{\tau_2}\cdots\mathbb{E}_{\tau_{j-1}}\mathbb{E}_{\tau_j}\cdots\mathbb{E}_{\tau_M}\left\{1 - \prod_{j\in\mathcal{M}\setminus\{i\}} \left[1 - P_c(i,j)\right]\right\} \\
&= 1 - \prod_{j\in\mathcal{M}\setminus\{i\}} \left[1 - \mathbb{E}_{\tau_j}\left\{P_c(i,j)\right\}\right] \\
&= 1 - \prod_{j\in\mathcal{M}\setminus\{i\}} \left[1 - \overline{P}_c(i,j)\right] \\
&= 1 - \prod_{j\in\mathcal{M}\setminus\{i\}} \left(1 - \frac{\Delta_j}{T_j}\right). \qquad (5.38)
\end{aligned}$$

[5]The expectation over individual asynchronisms is computed as
$\overline{P}_c(i) = \mathbb{E}_{\tau_1}\mathbb{E}_{\tau_2}\cdots\mathbb{E}_{\tau_{i-1}}\mathbb{E}_{\tau_{i+1}}\cdots\mathbb{E}_{\tau_M}\left\{P_c(i)\right\}$.

The same result is valid for multiple-access schemes where the time instants for pulse transmissions are chosen randomly, the average distance between the pulses of user j equals Δ_j, and the transmission times of the users are statistically independent. Note that TH-PPM falls into this class of access schemes; however, for this scheme, the average distance between pulses is the same for each user, i.e., $\Delta_j = \Delta$. For this type of access schemes the collision probability can be derived very easily. The probability that user j collides with user i is Δ_j/T_j. Hence, the probability that user j does not collide with user i is $1 - \Delta_j/T_j$. With the assumed statistical independence it follows that the probability that none of the users $j \in \mathcal{M} \setminus \{i\}$ collides with user i is the product of the probabilities $1 - \Delta_j/T_j$ over all interfering users $i \in \mathcal{M} \setminus \{i\}$. The complementary probability, i.e., the probability that at least one user j collides with user i is finally given by (5.38).

With the statistical independence expressed by (5.33), the worst-case or maximum collision probability is given by

$$\begin{aligned}\hat{P}_c(i) &= \max_{\{\tau_m\}} \{P_c(i)\} \\ &= 1 - \prod_{j \in \mathcal{M}\setminus\{i\}} \left(1 - \max_{\tau_j} \{P_c(i,j)\}\right) \\ &= 1 - \prod_{j \in \mathcal{M}\setminus\{i\}} \left(1 - \hat{P}_c(i,j)\right) \\ &= 1 - \prod_{j \in \mathcal{M}\setminus\{i\}} \left(1 - \left\lceil \frac{\Delta_j}{TF_{ij}} \right\rceil \frac{1}{Q_j}\right), \end{aligned} \tag{5.39}$$

where (5.30) was used. If (5.31) is used instead, an upper bound on $\hat{P}_c(i)$ is obtained:

$$\hat{P}_c(i) < 1 - \prod_{j \in \mathcal{M}\setminus\{i\}} \left(1 - \frac{\Delta_j + TF_{ij}}{T_j}\right). \tag{5.40}$$

The results (5.37) and (5.39) were confirmed by simulation.

5.3 User Period Design

5.3.1 User Period Design for Packets with Infinite Duration

In the previous section it turned out that the collision probability $P_c(i)$ is a random variable, where the source of the randomness is the random asynchronism $\{\tau_m\}$. Furthermore, the collision probability $P_c(i)$, the average collision probability $\overline{P}_c(i)$, and an upper bound on the collision probability, $\hat{P}_c(i)$, have been derived, see (5.37), (5.38) and (5.40). Now we want to choose the user periods T_j, $j \in \mathcal{M}$ such that $\hat{P}_c(i)$ is minimized; this is equivalent to requesting that $\hat{P}_c(i)$ is closest possible to $\overline{P}_c(i)$. From the upper bound (5.40), however, we conclude that choosing T_j is not the proper approach to minimize $\hat{P}_c(i)$. This because larger T_j not only reduces $\hat{P}_c(i)$, but also reduces the symbol rate $1/T_j$. Instead, we observe that the smaller TF_{ij} is compared to Δ_j, i.e., the smaller the ratio TF_{ij}/Δ_j is, the closer is the maximal collision probability to the average collision probability. Hence, for $TF_{ij}/\Delta_j \ll 1$ the maximum collision probability is approximately the average collision probability; roughly speaking this means that the collision probability is minimized and at the same time does not depend on the asynchronism. Note that the average collision probability is determined by the sum of the data rates $1/N_jT$ of the interfering users and by the channel delay

spreads, i.e., by Δ_j. Hence, a reduction of the average collision probability can only be achieved by reducing the sum data rate of all interfering users when we assume that the channel properties cannot be changed. The average collision probability influences the total throughput of a communication system. Note that the average collision probability that results in the maximum throughput depends on potential error correction capabilities of the higher layers in the communication system. As in this work only the physical layer is considered, the proper choice of the average collision probability goes beyond the scope of this work.

Both T and F_{ij} can be chosen to satisfy $TF_{ij} \ll \Delta_j, \forall\ i \neq j,\ i,j \in \mathcal{M}$. Remember that F_{ij} is the greatest common divisor of the user numbers N_i and N_j. Therefore, F_{ij} is minimized to the value $F_{ij} = 1, \forall\ i, \neq j,\ i,j \in \mathcal{M}$ if the user numbers $N_j,\ j \in \mathcal{M}$ do not share common divisors, i.e., if the user number N_j are relative prime. The user periods T_j are given by the product $T_j = TN_j$, see (5.7). Hence, the time base T can be interpreted as the granularity of the user periods T_j. As the minimum value of F_{ij} is one, T must be much smaller than the minimal pulse duration $\min\limits_{j\in\mathcal{M}} \Delta_j$ in order to satisfy $TF_{ij} \ll \Delta_j,\ \forall j \in \mathcal{M}$. With this we can formulate the two design rules:

- The time base T must be much smaller than the minimal pulse duration $\min\limits_{j\in\mathcal{M}}\Delta_j$.
- The user numbers $N_j,\ \forall j \in \mathcal{M}$ must be relative prime.

5.3.2 User Period Design for Packets with Finite Duration

Our derivation of the collision probability is valid for data packets with infinite duration, i.e., for symbol indices k reaching from $-\infty$ to ∞. In a practical system, however, the data packets have a finite duration. In this subsection we discuss the collision probability for finite packet durations. It turns out that packets with finite durations can result in a collision probability that depends strongly on the asynchronism even if the above design rules are applied. To mitigate this effect, an additional but heuristic design rule is presented.

To understand this rule we consider the effects that occur with data packets of finite length. Therefore, we introduce the notion of the *pulse pattern period* (PPP). We consider the two signals $u_i(t)$ and $u_j(t)$, $i \neq j$, see (5.1). It is first assumed that the corresponding data packets are still of infinite duration. If we ignore the modulation, i.e., for $a_{m,k} = 1,\ \forall k, m \in \mathcal{M}$, see (5.1), then the signals $u_i(t)$ and $u_j(t)$ have the periods T_i and T_j, respectively. An example for these signals with $T_i = 4T$ and $T_j = 5T$ is shown if Fig. 5.3.

To compute the duration of the PPP let us consider the pulse of the signal $u_i(t)$ that begins at the time instant k_iT_i also, we consider the pulse of the signal $u_j(t)$ that begins at the time instant $k_jT_j + \tau_j$. The difference between these two pulse positions is $k_iT_i - (k_jT_j + \tau_j)$. When the pulse pattern is periodic with the period duration T_{PPP}, as we have assumed, then there exists a pulse of the signal $u_i(t)$ and a pulse of the signal $u_j(t)$ that begins at the time instant $k_iT_i + T_{\text{PPP}}$ and $k_jT_j + \tau_j + T_{\text{PPP}}$, respectively. As the distance between pulses is T_i and T_j for the signals $u_i(t)$ and $u_j(t)$, respectively, we conclude, that T_{PPP} is an integer multiple of both T_i and T_j, i.e.,

$$T_{\text{PPP}} = K_iT_i = K_jT_j,$$

where K_i and K_j are the smallest integers that satisfy this equation. Applying Theorem 13 of Appendix G yields the solution $K_i = Q_j,\ K_j = Q_i$, and thus

$$T_{\text{ppp}}(i,j) = Q_jT_i = Q_iT_j = Q_jQ_iF_{ij}T. \tag{5.41}$$

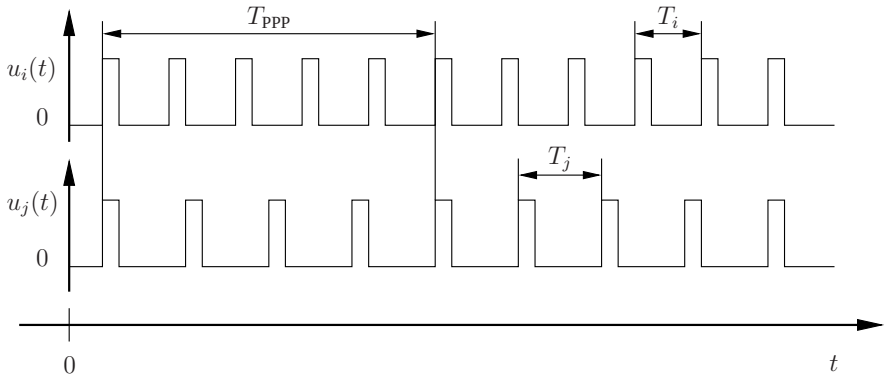

Fig. 5.3. Pulse pattern of the signals $u_i(t)$ and $u_j(t)$ with $T_i = 4T$ and $T_j = 5T$, The duration of the PPP is $T_{\text{PPP}} = 20T$.

As an example, the PPP for the signals in Fig. 5.3 has the period $T_{\text{PPP}} = Q_j Q_i F_{ij} T = 4 \cdot 5T = 20T$. In this example, the time intervals between collisions of user i and user j are equidistant. However, this is not the case in general; collisions can even occur in clusters. In the most extreme case all the collisions within a PPP occur as a single cluster of collisions, within which no pulse is free of collisions. Of course, in this case there is an interval within the PPP that is free of collisions such that the collision probability $\overline{P}_c(i)$ is maintained on average. As long as the data packets of user i have a duration which is a multiple of the PPP, the presence of collision clusters does not influence the average collision probability. If, however, the packet duration is not a multiple of the PPP but much shorter than the PPP, then a number of collisions below or above the average can hit the pulses of a data packet so that the collision probability deviates from the average value. The result is that the peak collision probability becomes significantly larger than the average collision probability.

To avoid this undesirable effect, the user periods should be chosen such that collision clusters are avoided, i.e., that collisions are uniformly distributed along the entire PPP. A general rule to achieve this could not be found. Instead we develop two heuristic rules:

(i) To break up collision clusters, we introduce a constraint that guarantees that after each collision there is at least one pulse that does not experience a collision. This is achieved by choosing the product of the time base T with the minimum difference between two user periods

$$D_{\min} = \min_{i,j \in \mathcal{M}, i \neq j} \{|N_i - N_j|\}$$

to be larger than the width of the widest pulse, i.e.,

$$T D_{\min} \geq \max_{j \in \mathcal{M}} \{\Delta_j\}.$$

(ii) If for packets with infinite duration the maximum collision probability $\hat{P}_c(i)$ is larger than the average collision probability $\overline{P}_c(i)$, then this is even more the case for packets with finite duration. The reason for this is that the achieved averaging effect is the stronger, the longer the duration of the data packets is. Therefore, at least for packets with infinite duration the maximum collision probability $\hat{P}_c(i)$ should be approximately equal to the average collision probability $\overline{P}_c(i)$; this requires that the design rules in the previous section are applied.

With this, the design rules for packets with finite duration are summarized as:

- The time base T must be much smaller than the minimal pulse duration $\min_{j\in\mathcal{M}}\Delta_j$.
- The user numbers $N_j,\ \forall j \in \mathcal{M}$ must be relative prime
- $TD_{\min} \geq \max_{j\in\mathcal{M}}\{\Delta_j\}$, where $D_{\min} = \min_{i,j\in\mathcal{M},i\neq j}\{|N_i - N_j|\}$.

An algorithm that generates user numbers according to these design rules is given in Fig. 5.4. This algorithm accepts the smallest user number N_1 as a parameter and iteratively generates the user numbers N_2 to N_M. In each iteration step, which is indexed by i, the potential next user number N'_{i+1} is computed as the sum $N'_{i+1} = N_i + D_{\min}$. The number N'_{i+1} is factorized and the resulting prime factors are compared with the set of prime factors that is contained in at least one of the previously determined user numbers $N_1, \cdots, N_i$. If there is one matching prime factor, this implies that N'_{i+1} is not relatively prime to each element of $\{N_1, \cdots, N_i\}$. Therefore, the next larger value $N'_{i+1} + 1$ is considered as the next potential user number N_{i+1}. Otherwise, if there is no matching prime factor, then N'_{i+1} is accepted as the user number N_{i+1} and its prime factors are added to the list of prime factors that are present in at least one of the numbers $N_1, \cdots, N_i$. The algorithm terminates when the largest user number N_M is computed. The user numbers that are generated by this algorithm are used for simulations of the corresponding collision probability. The corresponding simulation results are discussed in the following section.

Algorithm:

Start PrimeFactorList = **Factorize**(N_1)
for $i := 2$ to $i = M$
$N_i := N_{i-1} + D_{\min}$
Label PrimeFactors = **Factorize**(N_i)
if **CommonEntries**(PrimeFactorList,PrimeFactors) = true
$N_i := N_i + 1$
goto **Label**
end
PrimeFactorList := **Unify**(PrimeFactorList,PrimeFactors)
Stop end

Subfunctions:

(set of integers) = **Factorize**(integer)
% Returns the set of prime factors of the argument.

(boolean) = **CommonEntries**(set of integers, set of integers)
% Returns true if the two arguments contain at least one common element and false otherwise.

(set of integers) = **Unify**(set of integers, set of integers)
% The result is the union of the two arguments.

Fig. 5.4. An algorithm to generating relative prime numbers N_m according to the design rules for finite packet durations.

5.4 Simulation

In this section we illustrate the effect of the design rule given in Subsection 5.3.2 for both the case of data packets with infinite duration and for the case of data packets with finite duration. The additional rule from Subsection 5.3.2 that is not needed for packets with infinite duration has no effect for packets with infinite duration. This allows us to use the same design rule for packets with infinite and finite duration.

5.4.1 Infinite Packet Duration

To see the benefit of choosing the user periods according to the proposed design rules we compute the CDF of the collision probability for three different sets of user numbers for a total number of $M = 10$ users, $\Delta_j = 50T$, with the normalized time base $T = 1$, and the desired user index $i = 5$.

Relative Prime User Numbers: The user numbers are generated by the algorithm given in Fig. 5.4 which is called with the parameters $N_1 = 6001$, $M = 10$, $D_{\min} = 60$. The generated user numbers are: $(N_1, N_2, \ldots, N_{10}) = (6001, 6061, 6121, 6181, 6241, 6301, 6361, 6421, 6481, 6541)$. The resulting average collision probability (5.38) is $\overline{P}_c(i) = 0.0695$, the peak collision probability given by (5.40) yields $\hat{P}_c(i) = 0.0709$.

Equidistant User Numbers: The user numbers are defined as an increasing series defined by $N_{i+1} = N_i + D$, with $N_1 = 6000$ and $D = 60$. With this, the user numbers are $N_1 = 6000, N_2 = 6060, \ldots, N_{10} = 6540$. The resulting average collision probability is $\overline{P}_c(i) = 0.0695$ and the peak collision probability yields $\hat{P}_c(i) = 0.2124$. Note that these user numbers share the common divisor $F_{ij} = 60$; this is the reason why $\hat{P}_c(i)$ is significantly larger than $\overline{P}_c(i)$.

Identical User Numbers: All user numbers are identical and chosen such that the average collision probability is the same as for the equidistant and relative prime user numbers given above: $N_i = N_j = 6265$. As desired, the average collision probability is $\overline{P}_c(i) = 0.0696$. The peak collision probability is $\hat{P}_c(i) = 1$. This is an obvious result because identical user numbers correspond to TDMA (time division multiple access) without a controlled schedule; hence, with a certain probability all the transmitted pulses of the desired user i are subject to collision, which implies that $\hat{P}_c(i) = 1$.

The actual collision probability $P_c(i)$ expressed by (5.37) depends on the realization of the asynchronism $\{\tau_m\}$. Its CDF is shown in Fig. 5.5 for the three given sets of user numbers. For identical user numbers the collision probability $P_c(i)$ is either 0 or 1 depending on the asynchronism which determines if all pulses or no pulse of user i is subject to collision. For the set of equidistant user numbers, with the common factor 60, the collision probability $P_c(i)$ depends also on the asynchronism but to a much lesser extent than for the identical user numbers. An almost constant $P_c(i)$ with $P_c(i) \approx \overline{P}_c(i)$ is achieved for the set of relative prime user numbers. This confirms that the proposed design rules are appropriate. It must however be noted that the variance of the collision probability is not dramatically larger for user numbers that share some common factors. Hence, a practical system would not lose much in terms of QoS (quality of service) if some factors are common to several user numbers.

5.4.2 Finite Packet Duration

The additional design rule presented in Subsection 5.3.2 specifies a minimum difference between user numbers and is aimed to keep the collision probability as much as possible independent of the asynchronism even for packets with finite duration. The principle of this rule is to break up collision

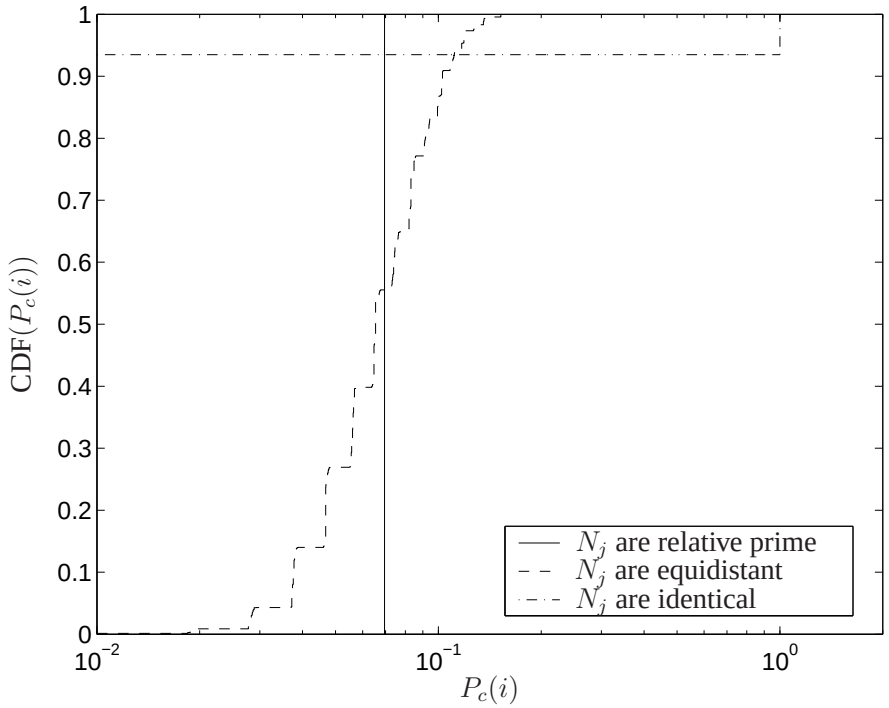

Fig. 5.5. CDF of the collision probability $P_c(i)$. The CDF depends on the asynchronism, $\{\tau_m\}$, for which 10000 realizations are considered. There are $M = 10$ users.

clusters by introducing a minimum distance between user numbers. To show the efficiency of this rule we compare two sets of parameters, one where the rule is violated and one where it is satisfied.

Minimum Distance Rule Violated: The pulse duration is $\Delta_j = 15$ ns, $\forall j \in \mathcal{M}$, the number of users is $M = 10$. The time base is set to $T = 1/8$ ns. The minimum distance rule would require that $D_{\min} \geq \frac{1}{T}\max_{j\in\mathcal{M}}\{\Delta_j\}$, i.e., $D_{\min} \geq 120$. To violate this constraint we set $D_{\min} = 1$. Furthermore, the user number N_1 is set to $N_1 = 8001$. With these parameters, the algorithm in Fig. 5.4 generates the user numbers $(N_1, N_2, \ldots, N_{10}) = (8001, 8002, 8003, 8005, 8009, 8011, 8017, 8021, 8023, 8027)$. For the desired user index $i = 1$, the minimum distance between N_i and any other user number N_j yields $D_{\min} = \min_{i,j\in\mathcal{M},i\neq j}\{|N_i - N_j|\} = 1$. Hence, the longest collision cluster consists of $\Delta_j/(TD_{\min}) = 120$ subsequent collisions.

Minimum Distance Rule Satisfied: The parameters $\Delta_j = 15$ ns $, \forall j \in \mathcal{M}$, $M = 10$, and $T = 1/8$ ns are the same as above. Implementing the minimum distance rule corresponds to setting $D_{\min} = 120$. With the user number N_1 set to $N_1 = 7501$, the algorithm in Fig. 5.4 generates the user numbers $(N_1, N_2, \ldots, N_{10}) = (7501, 7621, 7741, 7861, 7981, 8101, 8221, 8341, 8461, 8581)$.

The collision probability $P_c(i)$ is simulated for 500 realizations of the asynchronism $\{\tau_m\}$ and for different numbers of pulses per packet, namely $K = 50, 200, 1000, 10000$. If the minimum distance rule is violated, i.e., if $D_{\min} = 1$, the CDF is flat in particular for small values of K, see Fig. 5.6(a). This is because collision clusters including at most 120 colliding pulses can occur if the realization of the asynchronism $\{\tau_m\}$ is unfavorable. For a packet with length $K = 50$ this results in a peak collision probability $\hat{P}_c(i) = 1$.

Fig. 5.6(b) shows the CDF of the collision probability for the implemented minimum distance rule. Collision clusters are broken up which reduces the worst-case collision probability consid-

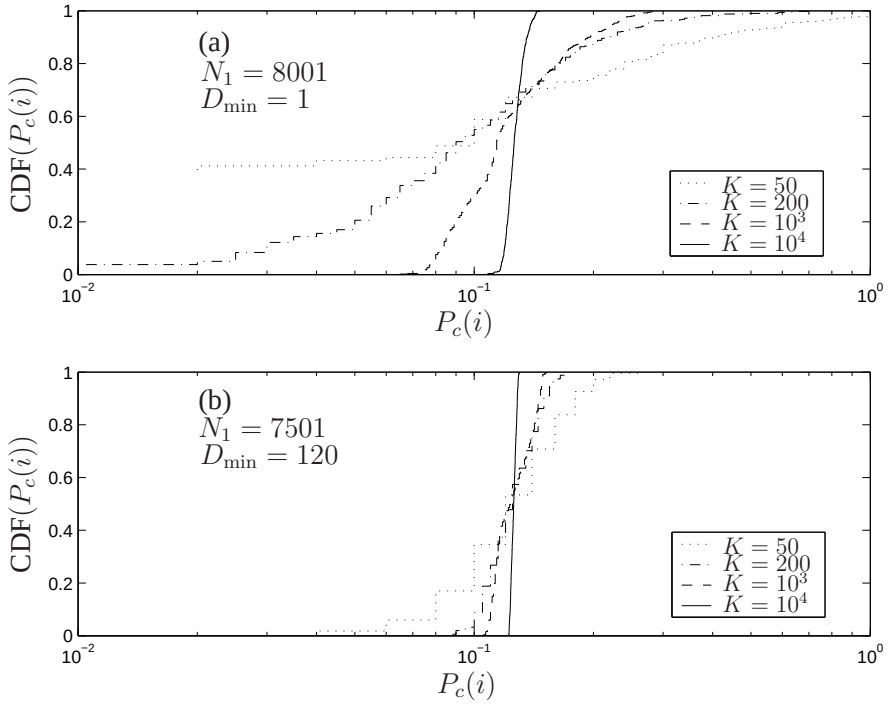

Fig. 5.6. CDF of the collision probability $P_c(i)$. The CDF depends on the asynchronism, $\{\tau_m\}$, for which 500 realizations are considered. The parameters are for (a) $N_1 = 8001$, $D_{\min} = 1$, $M = 10$, $T = 1/8$ ns and $\Delta_j = 15$ ns and for (b) $N_1 = 7501$, $D_{\min} = 120$, $M = 10$, $T = 1/8$ ns and $\Delta_j = 15$ ns. The user numbers are generated by the algorithm given in Fig. 5.4.

erably. We observe that a nearly constant collision probability is obtained only for longer data packets.

5.5 Conclusion and Outlook

In this Chapter RDMA was introduced as a scheme for uncoordinated multiuser access. The basic idea was explained and design parameters for quasi-optimal performance were proposed. As a measure of performance, for simplicity, the collision probability was used instead of the BER. The average and the peak collision probability was derived. It turned out that the peak collision probability depends on the time asynchronism between the users. It was pointed out that the average collision probability is equivalent to that of a corresponding random based access scheme. From a QoS or outage probability perspective it is desirable that the peak collision probability is close to the average collision probability. This can be achieved by choosing the user periods according to specific design rules, which are derived in this work.

As mentioned, for simplicity, the collision probability was considered instead of the BER that is a more direct performance measure. In [70] it was shown by simulation that a collision probability that is insensitive to the time asynchronism between users also results in a BER that is robust to variations of the asynchronism.

We conclude that from a performance point of view, RDMA is an alternative to existing random based multiple-access methods. Furthermore, as the pulse positions are equidistant for a given user, RDMA allows simpler signal acquisition than random based access schemes.

A particular property of the discussed RDMA scheme is the user dependent throughput, which is determined by the pulse rate $1/T_j = 1/(N_m T)$. One approach to achieve about the same average throughput for each user is to switch the pulse rate between two different rates. This can be done by dividing the data packets into blocks and to transmit every block with odd and even index with a pulse rate that is lower and higher than the average pulse rate, respectively. A detailed description of this method can be found in [72].

Appendices

A. Acronyms

APDP	Average Power Delay Profile
AWGN	Additive White Gaussian Noise
BEO	Bit Error Outage Probability
BEP	Bit Error Probability
BER	Bit Error Rate (empirical BEP)
BPSK	Binary Phase Shift Keying
BRDMA	Burst RDMA
CDF	Cumulative Distribution Function
CDMA	Code Division Mulitple-Access
CIR	Channel Impulse Response
CRDMA	Chip-Rate Division Multiple-Access
ECP	Empirical Collision Probability
GML	Generalized Maximum Likelihood
GMLR	Generalized Maximum Likelihood Receiver
GSC	Generalized Selection Combining
IR	Impulse Radio
ISI	Intersymbol Interference
LOS	Line-Of-Sight
MA	Multiple Access
MIMO	Multiple Input Multiple Output
ML	Maximum Likelihood
MLR	Maximum Likelihood Receiver
MLRP	Maximum Likelihood Receiver with Partial channel state information
MRC	Maximum Ratio Combiner
MUI	Multiuser Interference
NBI	Narrowband Interference
NLOS	Non Line-Of-Sight
OOK	On-Off Keying
PPM	Pulse Position Modulation
PPP	Pulse Pattern Period
PDF	Probability Density Function
PDP	Power Delay Profile
PSD	Power Spectral Density
QoS	Quality of Service
RDMA	Rate Division Multiple-Access

SIMO	Single Input Multiple Output
SNR	Signal-to-Noise Ratio
TH	Time Hopping
TR	Transmitter Receiver
UMP	Uniformly Most Powerful
UWB	Ultra Wideband
2PPM	Binary Pulse Position Modulation

B. Mathematical Symbols

B.1 Functions, Operators and Sets

$(\cdot)^*$	complex conjugate
$\Re\{\cdot\}$	real part
$\Im\{\cdot\}$	imaginary part
$(\cdot) * (\cdot)$	convolution
$(\cdot)^T$	tronspose
$\lvert \cdot \rvert$	absolute value
$\lfloor \cdot \rfloor$	integer part
$\lceil \cdot \rceil$	if not integer rounds to next larger integer
$\max(\cdot)$	maximum
$\min(\cdot)$	minimum
$a \mod b$	a modulo b operation
$\lim(\cdot)$	limes
$\mathrm{sgn}(\cdot)$	signum
$\gcd(\cdot, \cdot)$	greatest common divisor
$\wedge$	logical and
$\vee$	logical or
$\neg$	logical negation
$\forall$	for all
$\exists$	exists
$a \Rightarrow b$	a implies b
$a \mapsto b$	a is mapped to b
$\mathcal{A} \setminus \mathcal{B}$	set $\mathcal{A}$ without $\mathcal{B}$
$\in$	is element of
$\notin$	is not element of
$\cap$	intersection
$\cup$	unification
$\mathbb{E}\{\cdot\}$	expectation value of a random variable
$\mathcal{N}(\mu, \sigma^2)$	Gaussian distribution with mean μ and variance σ^2
$\mathcal{F}\{\cdot\}$	Fourier transform
$s(t) \circ\!\!-\!\!\bullet S(f)$	$S(f)$ is the Fourier transform of $s(t)$
$\mathcal{H}\{\cdot\}$	Hilbert transform
$s_l(t) \overset{\text{B,P}}{\longleftrightarrow} s(t)$	$s_l(t)$ is the complex baseband representation of $s(t)$.

$\mathrm{erfc}(\cdot)$	complementary error function
$\mathbb{Q}$	the set of rational numbers
$\mathbb{N}$	the set of natural numbers
$\mathbb{N}_0$	the set of natural numbers including $\{0\}$
$\mathbb{Z}$	the set of integer numbers
$\mathbb{R}$	the set of real numbers
$\mathbb{C}$	the set of complex numbers

B.2 Variables in Part I

A_0	path gain in units of dB
a_k	transmitted symbol
$\hat{a}_k$	decision for symbol a_k
α_0	path gain
α_0	path gain associated with receiver antenna i
$b(t)$	channel impulse response realization
$B(t)$	channel impulse response process
B	signal bandwidth
β	interference to noise ratio (INR)
c_k	random sequence of plus and minus one
γ	signal to noise ration (SNR)
γ_i	signal to noise ration (SNR) at antenna i
d_i	distance between transmitter and receiver antenna i
d	distance between transmitter and receiver antenna
D	energy spectral density of transmitted pulse
Δ_T	duration of the $2PPM$ time slots
E_r	energy per received pulse
$E_{i,r}$	energy per pulse received at antenna i
E_t	transmitted energy per pulse
f_0	center frequency
f_s	integral during first 2PPM time slot
g_s	integral during second 2PPM time slot
$g(t)$	shape of transmitted pulse
$\eta(T_I)$	ratio of captured energy to received energy
$\eta_i(T_I)$	ratio of captured energy to received energy for receiver i
i	index of receiver antenna
k	symbol index
L	averaging duration to estimate the PDP
$n(t)$	noise signal
$\mathrm{N}(t)$	noise process
N	number of receiver antennas
N_0	noise power spectral density
P_a	bit error outage probability
P_e	bit error probability

P_u	power of narrowband interference
$r(t)$	received signal including noise
s	shadow fading variable
S	shadow fading variable in units of dB
σ_S	variance of shadow fading variable S
$\sigma(t)$	Power delay profile of received pulse
T	symbol duration
T_I	integration duration
$u(t)$	transmitted signal or narrowband interference signal
$w(t)$	weighting function in noncoherent receiver
w_i	weighting factors for MRC
$y(t)$	noise free received signal
z_k	decision variable for symbol a_k

B.3 Variables in Part II

$\{x_m\}$	notation for the set $\{x_1, \ldots, x_M\}$
$b_j(t)$	channel impulse response from user j
Δ_j	duration of pulse from user j
F_{ij}	greatest common divisor of user numbers N_i and N_j
$h_j(t)$	received pulse shape from user j
i	index of desired user
j	index of any user
K	number of pulses within a data packet
m	index of any user
M	number of users
$\mathcal{M}$	set of user indices
N_j	user number of user j
$P_c(i)$	probability that any user collides with user i
$P_c(i,j)$	probability that user j collides with user i
$\overline{P}_c(i)$	expectation of $P_c(i)$
$\hat{P}_c(i)$	maximum of $P_c(i)$
Q_{ij}	N_j/F_{ij}
$s_j(t)$	received signal of user j
T	time base
T_j	user period of user j
$\{\tau_m\}$	set of asynchronisms
τ_j	asynchronism between user i and user j
$u_j(t)$	transmit signal of user j

B.4 Logical Expressions in Part II

$\underset{x\in\mathcal{X}}{\forall} P(x)$	for all $x \in \mathcal{X}$ the expression $P(x)$ is true
$\underset{x\in\mathcal{X}}{\forall} P(x,\cdots,y)$ $\vdots$ $\underset{y\in\mathcal{Y}}{}$	for all $x \in \mathcal{X}, \cdots$ and for all $y \in \mathcal{Y}$, $P(x,\cdots,y)$ is true
$\underset{x\in\mathcal{X}}{\exists} P(x)$	there exists at least one $x \in \mathcal{X}$ such that the expression $P(x)$ is true
$\underset{x\in\mathcal{X}}{\exists} P(x,\cdots,y)$ $\vdots$ $\underset{y\in\mathcal{Y}}{}$	there exists at least one $x \in \mathcal{X}, \cdots$, and at least one $y \in \mathcal{Y}$ such that $P(x,\cdots,y)$ is true
$\neg \underset{x\in\mathcal{X}}{\forall} P(x,\cdots,y)$ $\vdots$ $\underset{y\in\mathcal{Y}}{}$	it is not true that for all $x \in \mathcal{X}, \cdots$ and for all $y \in \mathcal{Y}$, $P(x,\cdots,y)$ is true (this is equivalent to the subsequent expression)
$\underset{x\in\mathcal{X}}{\exists} \neg P(x,\cdots,y)$ $\vdots$ $\underset{y\in\mathcal{Y}}{}$	there exists at least one $x \in \mathcal{X}, \cdots$ and at least one $y \in \mathcal{Y}$ such that $P(x,\cdots,y)$ is false
$\neg \underset{x\in\mathcal{X}}{\exists} P(x,\cdots,y)$ $\vdots$ $\underset{y\in\mathcal{Y}}{}$	it is not true that there exists at least one $x \in \mathcal{X}, \cdots$, and at least one $y \in \mathcal{Y}$ such that $P(x,\cdots,y)$ is true (this is equivalent to the subsequent expression)
$\underset{x\in\mathcal{X}}{\forall} \neg P(x,\cdots,y)$ $\vdots$ $\underset{y\in\mathcal{Y}}{}$	for all $x \in \mathcal{X}, \cdots$ and for all $y \in \mathcal{Y}$, $P(x,\cdots,y)$ is false

C. Hilbert Transform

In this appendix are discussed some theorems on the Hilbert transform, which are needed for proofs in Appendix D. The Hilbert transform of the signal $s(t)$ is denoted by $\hat{s}(t) = \{s(t)\}$, and is defined as

$$\{s(t)\} := \frac{1}{\pi t} * s(t) = \int_{-\infty}^{\infty} \frac{1}{\pi(t-\tau)} s(\tau)\, d\tau.$$

In the frequency domain this corresponds to

$$\hat{S}(f) = -i\,\mathrm{sgn}(f)\, S(f).$$

Theorem 1 (Product of Signals – Bedrosian's Theorem [6]) *For signals $u(t)$ and $s(t)$ with Fourier transforms $U(f)$ and $S(f)$ respectively, for which there exists a frequency $f_l \in \mathbb{R}^+$ such that $U(f) = 0$ for $|f| > f_l$ and $S(f) = 0$ for $|f| < f_l$, the Hilbert transform of the product $u(t)s(t)$ is given by*

$$\{u(t)\, s(t)\} = u(t) \quad \{s(t)\}\,. \tag{C.1}$$

Proof: The Fourier transform of $\{u(t)\, s(t)\}$ is $-i\,\mathrm{sgn}(f)[U(f) * S(f)]$. Under the specified conditions we have $\mathrm{sgn}(f)\,[U(f) * S(f)] = U(f) * [\mathrm{sgn}(f)\, S(f)]$. Inverse Fourier transform yields $\{u(t)s(t)\} = u(t) \quad \{s(t)\}$. □

Example C.1 A special case of this rule is

$$\begin{aligned} \{u(t)\cos(2\pi f_0 t + \varphi)\} &= u(t) \quad \{\cos(2\pi f_0 t + \varphi)\} \\ &= u(t)\sin(2\pi f_0 t + \varphi), \end{aligned} \tag{C.2}$$

where we used the rule $\{\cos(2\pi f_0 t + \varphi)\} = \sin(2\pi f_0 t + \varphi)$. This latter rule can be shown by using trigonometric addition theorems and the rules $\{\cos(\omega t)\} = \sin(\omega t)$ and $\{\sin(\omega t)\} = -\cos(\omega t)$.

Theorem 2 (Mirror) *The mirrored signal $s(-t)$ has the Hilbert transform*

$$\{s(-t)\} = -\hat{s}(-t). \tag{C.3}$$

Proof:

$$\begin{aligned}\{s(-t)\} &= \int_{-\infty}^{\infty} \frac{1}{\pi(t-\tau)} s(-\tau)\, d\tau \\ &= \int_{-\infty}^{\infty} \frac{1}{\pi(t+\tau)} s(\tau)\, d\tau \\ &= -\int_{-\infty}^{\infty} \frac{1}{\pi((-t)-\tau)} s(\tau)\, d\tau \\ &= - \quad \{s(v)\}|_{v=-t} \\ &= -\hat{s}(-t).\end{aligned}$$

□

Theorem 3 (Shift) *The Hilbert transform of the shifted signal* $s(t+u)$ *is*

$$\{s(t+u)\} = \hat{s}(t+u). \tag{C.4}$$

Proof: We use the definition of the Hilbert transform and get

$$\begin{aligned}\{s(t+u)\} &= \int_{-\infty}^{\infty} \frac{1}{\pi(t+u-\tau)} s(\tau)\, d\tau \\ &= \hat{s}(t+u).\end{aligned} \tag{C.5}$$

□

D. Equivalent Baseband Transform

The purpose of this appendix is to derive a theorem for the product of a lowpass signal with a passband signal. Tools for this derivation are the known correspondences of the complex baseband transform. An important aspect of the complex baseband transform is that it is unique only if the imaginary and real part of the considered baseband signal are a Hilbert transform pair. In the relevant literature this fact is often not explicitly mentioned [49, 40]. Ignoring this fact can result in erroneous conclusions. In this chapter the most important rules of the complex baseband transform are derived under consideration of this fact and provide a basis for the derivation of the product theorem for the multiplication of a lowpass signal with a passband signal.

We denote the baseband signal that corresponds to a passband signal by putting the subscript l. The transform from an arbitrary real valued signal $s(t)$ to the equivalent baseband signal $s_l(t)$ is generally given by

$$s_l(t) = \quad \{s(t)\} = \frac{1}{a}\left[s(t) + i \quad \{s(t)\}\right] e^{-i2\pi f_0 t}, \tag{D.1}$$

and the inverse transform is

$$s(t) = \quad ^{-1}\left\{s_l(t)\right\} = a\Re\left\{s_l(t)e^{i2\pi f_0 t}\right\}, \tag{D.2}$$

The properties that are required from $s_l(t)$ are discussed in the sequel. The variable f_0 is denoted the center frequency of the baseband transform and can assume any real value. However, for practical applications f_0 is often chosen as the center frequency of the passband signal that is to be transformed into the complex baseband domain. The factor a equals one in [49] and $\sqrt{2}$ in [39]. We will choose its value to obtain the simplest possible rules to convert operations on passband signals into operations on the corresponding baseband signals. To highlight that $s(t)$ and $s_l(t)$ are baseband transform pairs we write $s(t) \overset{\text{P,B}}{\longleftrightarrow} s_l(t)$.

Alternatively, we denote the transform from passband into baseband by $\quad : s(t) \mapsto s_l(t)$. The mapping $\quad$ is one-to-one, if and only if $s(t) \in \mathcal{R}_t$ and $s_l(t) \in \mathcal{C}_t^+$, where $\mathcal{R}_t$ is the set of all possible real-valued functions, and $\mathcal{C}_t^+$ is the set of complex-valued functions whose imaginary part is the Hilbert transform of the real part (we denote this type of signals as *baseband signals*). However, for each signal $s_l(t) \in \mathcal{C}_t^+$ there exist an infinite number of complex-valued signals $g(t) \notin \mathcal{C}_t^+$ (non baseband signals) such that $\quad ^{-1}\{g(t)\} = \quad ^{-1}\{s_l(t)\}$ and $\quad \{\quad ^{-1}\{g(t)\}\} \neq g(t)$. As an example, consider the signals $g(t) = \frac{1}{a}s(t)e^{-i2\pi f_0 t}$ and $s_l(t) = \frac{1}{a}[s(t) + i \quad \{s(t)\}]\, e^{-i2\pi f_0 t}$, yielding $\quad ^{-1}\{g(t)\} = \quad ^{-1}\{s_l(t)\} = s(t)$ and $\quad \{\quad ^{-1}\{g(t)\}\} = s_l(t)$. As a consequence of this, it is allowed to conclude from $s(t) = a\,\Re\left\{f(t)e^{i2\pi f_0 t}\right\}$ that $s(t) \overset{\text{P,B}}{\longleftrightarrow} f(t)$ only under the premise that $f(t) \in \mathcal{C}_t^+$.

In the frequency domain the baseband transform is expressed by

$$\begin{aligned} S_l(f) &= \frac{1}{a}[S(f) + \text{sgn}(f)S(f)] * \delta(f + f_0) \\ &= \frac{1}{a}[1 + \text{sgn}(f + f_0)]S(f + f_0) \end{aligned} \tag{D.3}$$

and the inversive transform is

$$S(f) = \frac{a}{2}[S_l(f - f_0) + S_l^*(-(f + f_0))]. \tag{D.4}$$

In the same way as for time-domain signals, we express baseband transform pairs in the frequency domain by writing $S(f) \overset{\text{P,B}}{\longleftrightarrow} S_l(f)$.

Subsequently we give some rules that help to determine the equivalent baseband signal of a given signal, or vice versa. The proofs of these statements are conducted by only using (D.1) or (D.3). We refrain from making use of the inverse transform expressed by (D.2) or (D.4), as it provides a valid passband signal even when the signal to be transformed is not a baseband signal. To show that a pair of signals forms a complex baseband transform pair, the Hilbert transform of the real part of the baseband signal must be performed, which implicitly corresponds to relying on (D.1) or (D.3).

We assume the arbitrary real valued signals $g(t)$ and $s(t)$, the highpass signal $p(t)$ with Fourier transform $P(f)$ and $P(f) = 0$ for $|f| < f_l$, and the lowpass signal $u(t)$ with Fourier transform $U(f)$ and $U(f) = 0$ for $|f| > f_l$. Furthermore we assume that $g(t) \overset{\text{P,B}}{\longleftrightarrow} g_l(t)$, $s(t) \overset{\text{P,B}}{\longleftrightarrow} s_l(t)$, $p(t) \overset{\text{P,B}}{\longleftrightarrow} p_l(t)$, and that $u(t) \overset{\text{P,B}}{\longleftrightarrow} u_l(t)$. With these signals we can express the following rules for equivalent baseband transform pairs.

Theorem 4 (Mirror)

$$s(-t) \overset{P,B}{\longleftrightarrow} s_l^*(-t) \tag{D.5}$$

Proof: Formally introducing $s_l'(t)$ as the equivalent lowpass signal of $s(-t)$ and replacing $s(t)$ by $s(-t)$ in the definition (D.1) yields $s_l'(t) = [s(-t) + i \quad \{s(-t)\}]e^{-i2\pi f_0 t}$. Defining $\hat{s}(t) := \quad \{s(t)\}$ and using (C.3) this is expressed as $s_l'(t) = [s(-t) - i\hat{s}(-t)]e^{-i2\pi f_0 t}$; substitution with $-t = \tau$ yields $s_l'(-\tau) = [s(\tau) - i\hat{s}(\tau)]e^{i2\pi f_0 \tau}$. This is the complex conjugate of $s_l(\tau)$, which is by definition $s_l(\tau) = \quad \{s(\tau)\} = [s(\tau) + i\hat{s}(\tau)]e^{-i2\pi f_0 \tau}$, i.e., $s_l'(-\tau) = s_l^*(\tau)$. Back substitution with $\tau = -t$ yields $s_l'(t) = s_l^*(-t)$; hence, we can write $s_l^*(-t) = \quad \{s(-t)\}$, which completes the proof. □

Theorem 5 (Shift)

$$s(t + \tau) \overset{P,B}{\longleftrightarrow} s_l(t + \tau)\, e^{i2\pi f_0 \tau} \tag{D.6}$$

Proof: Formally introducing $s_l'(t)$ as the equivalent lowpass signal of $s(t + \tau)$ and replacing $s(t)$ by $s(t + \tau)$ in the definition (D.1) yields $s_l'(t) = [s(t + \tau) + i \quad \{s(t + \tau)\}]e^{-i2\pi f_0 t}$. Defining $\hat{s}(t) := \quad \{s(t)\}$ and using (C.4) this is expressed as $s_l'(t) = [s(t + \tau) - i\hat{s}(t + \tau)]\, e^{-i2\pi f_0 t}$, i.e, by $s_l'(t) = [s(t + \tau) - i\hat{s}(t + \tau)]\, e^{i2\pi f_0 \tau}\, e^{-i2\pi f_0 (t+\tau)}$. This is equivalent to $s_l'(t) = s_l(t + \tau)\, e^{i2\pi f_0 \tau}$. □

Theorem 6 (Convolution)

$$g(t) * s(t) \overset{\text{P,B}}{\longleftrightarrow} \frac{a}{2} g_l(t) * s_l(t) \tag{D.7}$$

Proof: In the frequency domain the convolution $g(t) * s(t)$ writes as $G(f)S(f)$. With the definition of the equivalent baseband transform in the frequency domain (D.3) we can express the equivalent baseband signal $Z_l(f) \overset{\text{B,P}}{\longleftrightarrow} G(f)S(f)$ as $Z_l(f) = \frac{1}{a}[1 + \text{sgn}(f + f_0)]G(f + f_0)S(f + f_0)$. Hence, $Z_l(f)$ can be expressed as a function of the product $G_l(f)S_l(f)$; we express this product by the passband signals $G(f)$ and $S(f)$ as $G_l(f)S_l(f) = \frac{1}{a^2}[1+\text{sgn}(f+f_0)]^2 G(f+f_0)S(f+f_0)$, where we have applied (D.3) two times. As $[1 + \text{sgn}(f)]^2 = 2\,[1 + \text{sgn}(f)]$ we get $\frac{a}{2}G_l(f)S_l(f) = \frac{1}{a}[1 + \text{sgn}(f + f_0)]G(f + f_0)S(f + f_0)$. Once again applying (D.3) yields $\frac{a}{2}G_l(f)S_l(f) \overset{\text{B,P}}{\longleftrightarrow} G(f)S(f)$. Inversive Fourier transform of this equation completes the proof. □

Theorem 7 *(Deterministic Correlation)*

$$g(t) * s(-t) \overset{\text{P,B}}{\longleftrightarrow} \frac{a}{2} g_l(t) * s_l^*(-t) \tag{D.8}$$

Proof: Inserting (D.5) into (D.7) confirms the statement. □

Theorem 8 *(Deterministic Autocorrelation)*

$$g(t) * g(-t) \overset{\text{P,B}}{\longleftrightarrow} \frac{a}{2} g_l(t) * g_l^*(-t) \tag{D.9}$$

Proof: Setting $s(t) = g(t)$ in (D.8) confirms the statement. □

Theorem 9 (Energy)

$$\int g^2(t)\,dt = \frac{a^2}{2} \int |g_l(t)|^2 dt \tag{D.10}$$

Proof: We write (D.9) in the form $g(t) * g(t) = a\Re\{(a/2)[g_l(t) * g_l^*(t)]e^{-i2\pi f_0 t}\}$. Setting $t = 0$ and with $g(t) * g^*(-t) = \int_{-\infty}^{\infty} g(\tau)g^*(\tau - t)\,d\tau = \int_{-\infty}^{\infty} |g(\tau)|^2\,d\tau$ we get $\int_{-\infty}^{\infty} g^2(\tau)\,d\tau = \frac{a^2}{2}\Re\{g_l(t) * g_l^*(t)|_{t=0}\} = \frac{a^2}{2}\int_{-\infty}^{\infty} |g(\tau)|^2\,d\tau$, which completes the proof. □

Theorem 10 (Product of Lowpass Signal with Cosine Function) *For any signal $u(t)$ with Fourier transform $U(f)$ satisfying $U(f) = 0$ for $f > f_c$ and for an arbitrary signal frequency $f_c \in \mathbb{R}^+$ we have the equivalent baseband transform pair*

$$u(t)\,\cos(2\pi f_0 t + \varphi) \overset{\text{P,B}}{\longleftrightarrow} u(t)\,e^{i\varphi} \tag{D.11}$$

Proof: Inserting $s(t) = u(t)\,\cos(2\pi f_0 t + \varphi)$ into the right hand side of (D.1), and applying (C.2) yields $s_l(t) = u(t)[\cos(2\pi f_0 t + \varphi) + i\,\sin(2\pi f_0 t + \varphi)]\,e^{-i2\pi f_0 t} = u(t)\,e^{i(2\pi f_0 t + \varphi)}\,e^{-i2\pi f_0 t}$, which simplifies to the statement. □

Theorem 11 (Product of Lowpass Signal with Passband Signal) *For signals $u(t)$ and $p(t)$ with Fourier transforms $U(f)$ and $P(f)$ respectively, for which a frequency $f_l \in \mathbb{R}^+$ exists such that $U(f) = 0$ for $|f| > f_l$, and $P(f) = 0$ for $|f| < f_l$, we have the equivalent lowpass transform pair*

$$u(t)\,p(t) \;\overset{P,B}{\longleftrightarrow}\; u(t)\,p_l(t) \tag{D.12}$$

Proof: Inserting $s(t) = u(t)\,p(t)$ into the right hand side of (D.1), and applying (C.1) yields $s_l(t) = u(t)[p(t) + i \quad \{p(t)\}]\,e^{-i2\pi f_0 t} = u(t)\,p_l(t)$, which is equivalent to the statement.

□

General Product A simplification as provided by the above theorems could not be found for the product of general signals, hence for generic signals $s(t)$ and $g(t)$ we must write

$$g(t)s(t) \;\overset{\text{P,B}}{\longleftrightarrow}\; \frac{1}{a}\,[g(t)s(t) + i \quad \{g(t)s(t)\}]e^{-i2\pi f_0 t}. \tag{D.13}$$

Stochastic Correlation Functions The connection between the correlation functions $\mathbb{E}\{g(t)s(t+\tau)\}$ and $\mathbb{E}\{g_l^*(t)s_l(t+\tau)\}$ is intricate in general and cannot be expressed in such a simple way as e.g. the deterministic correlation, see (D.8).

Constant Factor Inspecting the expressions (D.7), (D.8), (D.9), and (D.10), we observe that no value for a can eliminate the prefixed factors. However, if we chose $a = 1$, the only appearing factor is $1/2$, and moreover the smallest number of prefixed factors is obtained. Thus we prefer the equivalent baseband transform introduced in [49] over that in [39]. To conserve the signal energy under complex baseband transformation, $a = \sqrt{2}$ would be the proper choice.

E. Chi-Square Distribution of Complex Random Variables

The sum of the squared magnitude of independent Gaussian random variables X_n, with identical variance σ^2 and possibly different means m_n,

$$\mathrm{Y} = \sum_{n=1}^{N} |\mathrm{X}_n|^2,$$

is chi-square distributed. The corresponding PDF for real-valued random variables, $\mathrm{X}_n \in \mathbb{R}$, is given in [49] by

$$P_{\mathrm{Y}}(y) = \frac{1}{2\sigma^2}\left(\frac{y}{s^2}\right)^{\frac{N-2}{4}} e^{-\frac{s^2+y}{2\sigma^2}}\, \mathrm{I}_{N/2-1}\left(\sqrt{y}\frac{s}{\sigma^2}\right), \tag{E.1}$$

where $s^2 = \sum_{n=1}^{N} m_n^2$ and $\mathrm{I}_\alpha(x)$ is the α th-order modified Bessel function of the first kind. This distribution is valid for $s \neq 0$ and is denoted the non-central chi-square distribution. The mean value of Y is $\mathbb{E}\{\mathrm{Y}\} = N\sigma^2 + s^2$, the variance is $\sigma_y^2 = 2N\sigma^4 + 4\sigma^2 s^2$.

For zero-mean random variables, i.e., for $m_n = 0$, the variable y is characterized by a central chi-square distribution [49] with the PDF

$$P_{\mathrm{Y}}(y) = \frac{1}{\sigma^N 2^{\frac{N}{2}}\Gamma\left(\frac{N}{2}\right)} y^{\frac{N}{2}-1} e^{-\frac{y}{2\sigma^2}}, \tag{E.2}$$

and has the mean value $\mathbb{E}\{\mathrm{Y}\} = N\sigma^2$ and variance $\sigma_y^2 = 2N\sigma^4$.

The generalization to circular distributed complex random variables $\mathrm{X}_i \in \mathbb{C}$, with statistically independent real and imaginary part $\Re\{\mathrm{X}_n\}$ and $\Im\{\mathrm{X}_n\}$ with variance σ^2 each and complex means $m_n \in \mathbb{C}$, is straightforward and based on the observation that

$$\mathrm{Y} = \sum_{n=1}^{N} |\mathrm{X}_n|^2 = \sum_{n=1}^{N} (\Re\{\mathrm{X}_n\})^2 + \sum_{n=1}^{N} (\Im\{\mathrm{X}_n\})^2$$

is composed of $2N$ instead of N sums. Hence the PDF of a sum of complex random variables, Y, is given by the non-central chi-square distribution

$$P_{\mathrm{Y}}(y) = \frac{1}{2\sigma^2}\left(\frac{y}{s^2}\right)^{\frac{N-1}{2}} e^{-\frac{s^2+y}{2\sigma^2}}\, \mathrm{I}_{N-1}\left(\sqrt{y}\frac{s}{\sigma^2}\right), \tag{E.3}$$

with $s^2 = \sum_{n=1}^{N} |m_n|^2$. The mean value of Y is $\mathbb{E}\{\mathrm{Y}\} = 2N\sigma^2 + s^2$, and the variance is $\sigma_y^2 = 4N\sigma^4 + 4\sigma^2 s^2$.

The generalization of the central chi-square distribution (E.2) to complex random variables is obtained in the same way through substituting N by $2N$ such that

$$P_{\mathrm{Y}}(y) = \frac{1}{\sigma^{2N}\, 2^N\, \Gamma\left(N\right)}\, y^{N-1} e^{-\frac{y}{2\sigma^2}}. \tag{E.4}$$

The mean value is $\mathbb{E}\left\{\mathrm{Y}\right\} = 2N\sigma^2$ and the variance is $\sigma_y^2 = 4N\sigma^4$.

F. Response of a Correlator to a Cosine Signal

We assume a correlation template $b(t)$ which is multiplied by the received narrowband signal $u(t) = \sqrt{2P_u}\cos(2\pi f_I t + \varphi_0)$. This product is integrated over the interval $[0, T_I]$ and denoted as $\rho_{u,b}$, i.e.,

$$\rho_{u,b} = \int_0^{T_I} u(t)b(t)\,dt. \tag{F.1}$$

The template signal $b(t)$ is a real valued passband signal with energy E_r. The spectrum of $b(t)$ is limited to the frequency interval $[f_0 - B/2, f_0 + B/2]$, with the center frequency f_0. The frequency, f_I, of the narrowband signal $u(t)$ lies within the spectrum of $b(t)$, i.e., $u(t)$ represents an inband interference.

In the sequel, we derive a statistical characterization of $\rho_{u,b}$ on the basis of the statistical properties of the template $b(t)$ and the phase φ_0. For the sake of simplicity we define the normalized template signal $\bar{b(t)} := b(t)/\sqrt{E_r/(2B)}$, having the energy $\|\bar{b}(t)\|^2 = 2B$. Thus, the two-sided energy spectral density of $\bar{b}(t)$ is unity. The Fourier transform of $\bar{b}(t)$ which considers only the integration interval $[0, T_I]$ is

$$\bar{B}(f) := \int_0^{T_I} \bar{b}(t)e^{-i2\pi ft}\,dt.$$

This integral over the random received pulse shape weighted with an exponential function can be approximated by the sum of many statistically independent random variables. From this consideration and the central limit theorem it follows that $\bar{B}(f)$ is for any f a complex Gaussian distributed random variable. As the real and imaginary parts of the complex function $\cos(2\pi f_0 t) - i\sin(2\pi f_0 t) = e^{-i2\pi f_0 t}$ are orthogonal, it follows that the imaginary and the real part of $\bar{B}(f)$ are statistically independent. Remember that $\bar{b}(t)$ is assumed to be bandlimited to the frequency interval $[f_0 - B/2, f_0 + B/2]$. The spectrum $\bar{B}(f)$, however, is not bandlimited because the considered interval $[0, T_I]$ represents a limitation on the time axis. For practical bandwidths B on the order of 1 GHz and integration durations T_I on the order of several tens of a ns, the time bandwidth product $T_I B \gg 1$. Hence, we can assume by approximation that the spectrum $\bar{B}(f)$ is nonzero only for $f \in [f_0 - B/2, f_0 + B/2]$.

The energy of $\bar{B}(f)$ is identical to the fraction of the energy of $\bar{b}(t)$ that falls into the interval $[0, T_I]$, i.e.,

$$\int_{-\infty}^{\infty} |\bar{B}(f)|^2\,df = \int_0^{T_I} |\bar{b}(t)|^2\,dt = 2B\,\eta(T_I). \tag{F.2}$$

The definition of $\eta(T_I)$ is given in (3.69). Note that the period Δ_T is the duration of the support of $\bar{b}(t)$. We assume further that for an integration interval shorter than the absolute channel delay

spread τ_c, the number of echoes that fall into the integration interval is large enough so that $\bar{B}(f)$ can still be assumed to be Gaussian distributed for any $f \in [f_0 - B/2, f_0 + B/2]$.

For simplicity, we assume that within this frequency interval, the variance of $\bar{B}(f)$, i.e., $\mathbb{E}\left\{|\bar{B}(f)|^2\right\}$ does not depend on f. We thus obtain

$$\begin{aligned}\int_{f_0-B/2}^{f_0+B/2} |\bar{B}(f)|^2\, df &= \mathbb{E}\left\{\int_{f_0-B/2}^{f_0+B/2} |\bar{B}(f)|^2\, df\right\} \\ &= \int_{f_0-B/2}^{f_0+B/2} \mathbb{E}\left\{|\bar{B}(f)|^2\right\}\, df \\ &= 2B\mathbb{E}\left\{|\bar{B}(f)|^2\right\}.\end{aligned} \tag{F.3}$$

On the other hand, with (F.2), we have

$$\int_{f_0-B/2}^{f_0+B/2} |\bar{B}(f)|^2\, df = 2B\eta(T_I). \tag{F.4}$$

This implies that $\mathbb{E}\left\{|\bar{B}(f)|^2\right\} = \eta(T_I)$. Thus, it follows that

$$\Re\left\{\bar{B}(f)\right\}, \Im\left\{\bar{B}(f)\right\} \sim \mathcal{N}(0, \eta(T_I)/2). \tag{F.5}$$

We denote the complex baseband transform of $\bar{B}(f)$ as $\bar{B}_l(f)$, with real and imaginary part $\bar{B}_{r,l}(f)$ and $\bar{B}_{i,l}(f)$, respectively. From the definition of the equivalent baseband transform in (D.3) with $a = 1$ it follows that $\bar{B}_{r,l}(f) = \frac{1}{2}[1 + \text{sgn}(f + f_0)]\Re\left\{\bar{B}(f + f_0)\right\}$ and that $\bar{B}_{i,l}(f) = \frac{1}{2}[1 + \text{sgn}(f + f_0)]\Im\left\{\bar{B}(f + f_0)\right\}$. Both components, $\bar{B}_{r,l}(f)$ and $\bar{B}_{i,l}(f)$, are i.i.d. for any f and Gaussian distributed [49]. With (F.5) and because the energy of the signal is half the energy of the equivalent signal in baseband representation, we conclude that the variance of these terms is $2\eta(TI)$, hence

$$\bar{B}_{i,l}(f),\ \bar{B}_{r,l}(f) \sim \mathcal{N}(0, 2\eta(T_I)). \tag{F.6}$$

To derive the distribution of $\rho_{u,b}$, we express (F.1) as a function of $\bar{B}(f)$:

$$\begin{aligned}\rho_{u,b} &= \sqrt{\frac{E_r}{2B}} \int_0^{T_I} u(t)\bar{b}(t)\, dt \\ &= \sqrt{\frac{E_r}{2B}} \int_0^{T_I} u(t)\bar{b}(t)e^{-i2\pi ft}\, dt\Big|_{f=0} \\ &= \sqrt{\frac{E_r}{2B}}\, U(f) * \bar{B}(f)\big|_{f=0},\end{aligned} \tag{F.7}$$

with $U(f)$ and $\bar{B}(f)$ being the Fourier transforms of $u(t)$ and $\bar{b}(t)$, respectively. To compute $U(f)$ we write $u(t)$ in the form

$$u(t) = \sqrt{2P_u}\,[\cos(\varphi_0)\cos(2\pi f_I t) - \sin(\varphi_0)\sin(2\pi f_I t)];$$

its Fourier transform is

$$U(f) = \sqrt{2P_u}\,\left\{\frac{1}{2}[\delta(f + f_I) + \delta(f - f_I)]\cos(\varphi_0) - \frac{i}{2}[\delta(f + f_I) - \delta(f - f_I)]\sin(\varphi_0)\right\}. \tag{F.8}$$

To simplify the derivation we substitute $\bar{B}(f)$ by its equivalent lowpass transform:

$$\bar{B}(f) = \frac{1}{2}[\bar{B}_l(f - f_I) + \bar{B}_l^*(-(f + f_I))], \tag{F.9}$$

see (D.4). Note that for convenience, the frequency shift in the equivalent baseband transform is set equal to the frequency f_I of the narrowband interference signal $u(t)$. With (F.8) and (F.9) we can express (F.7) as

$$\begin{aligned}\rho_{u,b} &= \sqrt{\frac{E_r}{2B}}\, U(f) * \bar{B}(f)\big|_{f=0} \\ &= \sqrt{\frac{P_u E_r}{4B}} \left\{ \frac{1}{2}[\bar{B}_l(f - 2f_I) + \bar{B}_l^*(-f) + \bar{B}_l(f) + \bar{B}_l^*(f - 2f_I)] \cos(\varphi_0) \right. \\ &\quad \left. -\frac{i}{2}[\bar{B}_l(f) + \bar{B}_l^*(-f - 2f_I) - \bar{B}_l(f - 2f_I) - \bar{B}_l^*(-f)] \sin(\varphi_0) \right\}_{f=0}. \end{aligned} \tag{F.10}$$

The above choice of the frequency shift in the equivalent baseband transform guaranties that the terms $\bar{B}_l(f - 2f_I)$ and $\bar{B}_l(-f - 2f_I)$ are zero for $f = 0$ and for any choice of f_I from the signal frequency band $[f_0 - B/2, f_0 + B/2]$. Thus,

$$\rho_{u,b} = \sqrt{\frac{P_u E_r}{4B}} \left[\Re\left\{\bar{B}_l(0)\right\} \cos(\varphi_0) + \Im\left\{\bar{B}_l(0)\right\} \sin(\varphi_0) \right]. \tag{F.11}$$

From this we conclude that $\rho_{u,b}$ is a weighted sum of two statistically independent Gaussian random variables and, thus, Gaussian distributed with variance

$$\begin{aligned}\sigma_\rho^2 &= \mathbb{E}\left\{\rho_{u,b}^2\right\} \\ &= \frac{P_u E_r}{4B} \mathbb{E}\left\{\bar{B}_{r,l}^2(0)\cos^2(\varphi_0) + 2\bar{B}_{r,l}(0)\bar{B}_{i,l}(0)\cos(\varphi_0)\sin(\varphi_0) + \bar{B}_{i,l}^2(0)\sin^2(\varphi_0)\right\} \\ &= \frac{P_u E_r}{4B} \left[\mathbb{E}\left\{\bar{B}_{r,l}^2(0)\right\}\cos^2(\varphi_0) + \mathbb{E}\left\{\bar{B}_{i,l}^2(0)\right\}\sin^2(\varphi_0)\right] \\ &= \frac{P_u E_r}{4B} \left[2\eta(T_I)\cos^2(\varphi_0) + 2\eta(T_I)\sin^2(\varphi_0)\right] \\ &= \frac{P_u\, E_r \eta(T_I)}{2B}. \end{aligned} \tag{F.12}$$

In this derivation we used the statistical independence of the random variables $\bar{B}_{r,l}$ and $\bar{B}_{i,l}$ as well as (F.6). With (F.12) and since $\rho_{u,b}$ is Gaussian distributed, $\rho_{u,b}$ is characterized by

$$\rho_{u,b} \sim \mathcal{N}\left(0, \frac{P_u\, E_r\, \eta(T_I)}{2B}\right). \tag{F.13}$$

This result is confirmed by simulation. Note that the realization of $\rho_{u,b}$ is a deterministic function of the current channel realization $b(t)$ and the phase φ_0 of the interference signal $u(t)$. The variance of $\rho_{u,b}$ is the product of the one-sided energy spectral density E_r/B of the template $b(t)$, the captured energy ratio $\eta(T_I)$, and $\frac{1}{2}$ of the interference power P_u. The factor $\frac{1}{2}$ appears because the interference signal $u(t)$ in (F.1) which is a sine function, is orthogonal to half of the signal components of $b(t)$ that lie on the spectral line with frequency f_I.

G. Theorems from Number Theory

The following theorems are derived by the author; they should be available in possible, another form in the group theory literature, e.g., [47].

Theorem 12 *For any pair of relative prime numbers $p, q \in \mathbb{N}$ there is exactly one element δ in the set*

$$\mathcal{A} := \left\{ a \in \mathbb{N}_0 \,\middle|\, \underset{b\in\mathbb{Z}}{\exists}\, ap = bq + 1 \right\}$$

that satisfies

$$0 < \delta < q. \tag{G.1}$$

Furthermore δ and q are relatively prime.

Proof: With the set $\mathcal{Q} := \{x < q | x \in \mathbb{N}_0\}$, the expression

$$\underset{\delta\in\mathcal{Q}}{\forall}\ \underset{\substack{b\in\mathbb{Z}\\ d\in\mathcal{Q}}}{\exists}\ \delta p = bq + d \tag{G.2}$$

is always true as $\delta p \in \mathbb{N}_0$, and since $bq + d$ can assume any natural number. Now we assume, by hypothesis, that there exist two different numbers $\delta, \delta' \in \mathcal{Q}$ satisfying

$$\delta p = bq + d \tag{G.3}$$

and $\delta' p = b' q + d$, respectively, for a fixed $d \in \mathcal{Q}$ and arbitrary $b, b' \in \mathbb{Z}$. If this hypothesis was true, it would follow that $(\delta - \delta')p = (b - b')q$. However, as p and q are relative prime, the equation $(\delta - \delta')p = (b - b')q$ is satisfied only if $(\delta - \delta')$ is a multiple of q, which is in contradiction with the assumption that $\delta, \delta' \in \mathcal{Q}$. Hence, the above hypothesis is wrong and we conclude that for any $d \in \mathcal{Q}$, (G.3) is satisfied for at most one element $\delta \in \mathcal{Q}$. From (G.2), we infer that for any $\delta \in \mathcal{Q}$ there exists exactly one $d \in \mathcal{Q}$; this implies that exactly one $\delta \in \mathcal{Q}$ must exist for which $d = 1$; this is equivalent to the first statement of Theorem 12.

Furthermore it must be shown that q and the δ which satisfies (G.3) for $d = 1$ are relative prime. We show this by assuming the opposite, namely that δ and q are not relative prime, i.e., that $\gcd(\delta, q) = g > 1$, i.e., that $\delta = g\delta''$ and $q = gq''$. Inserting these products for δ and q into the equation $\delta p = bq + 1$ yields, $\delta'' gp = bq'' g + 1$, this is equivalent to $\delta'' p = bq'' + 1/g$. This equation has no solution because the term $1/g \notin \mathbb{Z}$. Hence the assumption made that q and δ are not relative prime, results in a contradiction, which proves that q and δ are in fact relative prime. □

Theorem 13 *For any pair of relative prime numbers $p, q \in \mathbb{N}$ and $s \in \mathbb{Z}$, the set*

$$\mathcal{A}(s) := \left\{ a \in \mathbb{Z} \,\middle|\, \underset{b\in\mathbb{Z}}{\exists} ap = bq + s \right\} \tag{G.4}$$

is equivalent to

$$\mathcal{A}(s) = \{kq + s\delta \,|k \in \mathbb{Z}\},$$

with $\delta \in \mathbb{N}_0$, $0 \leq \delta < q$ and $\gcd(\delta, q) = 1$. An equivalent representation of this is

$$\mathcal{A}(s) = \left\{ aq + d(s) \,\middle|\, a \in \mathbb{Z}, 0 \leq d(s) < q, d(s) \in \mathbb{N}_0 \right\}. \tag{G.5}$$

A specification of the function $d(s)$ is not needed and is therefore skipped.

Proof: With $bq + s = (b + \lfloor s/q \rfloor)q + (s \mod q)$, setting $c := b + \lfloor s/q \rfloor$ and $d := s \mod q$, (G.4) can be reformulated as

$$\mathcal{A}(s) := \left\{ a \in \mathbb{Z} \,\middle|\, \underset{c\in\mathbb{Z}}{\exists} ap = cq + d \right\}, \tag{G.6}$$

with $d \in \mathbb{N}$ and $0 < d < q$. The numbers $a \in \mathbb{Z}$ that satisfy $\underset{c\in\mathbb{N}_0}{\exists} ap = cq + d$ can be expressed as a linear combination of the numbers $\dot{a} \in \mathbb{Z}$ satisfying the homogenous expression $\underset{\dot{c}\in\mathbb{Z}}{\exists} \dot{a}p = \dot{c}q$ and the numbers $\ddot{a} \in \mathbb{N}_0$ satisfying the inhomogeneous expression $\underset{\ddot{c}\in\mathbb{N}_0}{\exists} \ddot{a}p = \ddot{c}q + 1$, i.e., $a = n\dot{a} + d\ddot{a}$, with $n \in \mathbb{Z}$. Hence, for any $n \in \mathbb{Z}$,

$$\mathcal{A}(s) = \{k\dot{a} + d\ddot{a} \,|k \in \mathbb{Z}\}. \tag{G.7}$$

The solution $\dot{a}$ of the homogeneous equation $\underset{\dot{c}\in\mathbb{N}_0}{\exists} \dot{a}p = \dot{c}q$ is periodic with period q. This follows because if $\dot{a}$ satisfies the expression $\underset{\dot{c}\in\mathbb{N}_0}{\exists} \dot{a}p = \dot{c}q$ then $\dot{a} + q$ is also a solution of this expression. The solution $\ddot{a}$ of the inhomogeneous expression is also periodic with period q. This is because the sum of the solutions $\ddot{a}$ and $\dot{a}$ is again a solution of the inhomogeneous expression and because the solution $\dot{a}$ is periodic with period q. From this property we get the general solution by putting the lowest nonzero solution,

$$\dot{a} = \inf \left\{ a \in \mathbb{N} \,\middle|\, \underset{c\in\mathbb{N}_0}{\exists} ap = cq \right\} = q,$$

for the homogeneous equation and the lowest nonzero solution,

$$\ddot{a} = \inf \left\{ a \in \mathbb{N} \,\middle|\, \underset{c\in\mathbb{N}_0}{\exists} ap = cq + 1 \right\} =: \delta,$$

for the inhomogeneous equation into (G.7). With Theorem 12, stating that $0 < \ddot{a} < q$ and $\gcd(\ddot{a}, q) = 1$, the theorem is proved. □

Theorem 14 *Given the numbers $l \neq r$, with $l, r \in \mathbb{Z}$ and $|l - r| < q$, a pair of relative prime numbers $p, q \in \mathbb{N}$, then the sets*

$$\mathcal{A}(d) := \left\{ a \in \mathbb{Z} \,\middle|\, \underset{b\in\mathbb{Z}}{\exists} ap = bq + d \right\},\ d \in \mathbb{Z}, \tag{G.8}$$

satisfy

$$\mathcal{A}(l) \cap \mathcal{A}(r) = \{\}. \tag{G.9}$$

Proof: According to Theorem 13,

$$\mathcal{A}(d) = \{kq + d\delta | k \in \mathbb{Z}\},$$

with $0 < \delta < q$ and $\gcd(\delta, q) = 1$. Thus, (G.9) is satisfied iff

$$\neg \underset{\substack{l \neq r \\ |l-r|<q \\ m,n \in \mathbb{Z}}}{\exists} nq + l\delta = mq + r\delta. \tag{G.10}$$

Without loss of generality it can be assumed that $r < l$. Defining $v := l - r$ and $n' := m - n$, (G.10) is equivalent to

$$\neg \underset{\substack{n' \in \mathbb{Z} \\ v \in \mathbb{N} \\ v<q}}{\exists} n'q = v\delta,$$

this is always satisfied, given the assumption that $\delta < q$ and $\gcd(\delta, q) = 1$, because the product $v\delta$ does not contain the factor q. □

H. Statistical Independence of Multiple User Collisions

As in (5.13) and (5.14), let

$$\mathcal{K}_{i,j} = \bigcup_{l=L_{1,j}}^{L_{2,j}} \mathcal{K}_{i,j}(l), \;\; i \neq j.$$

and

$$\mathcal{K}_{i,j}(l) = \left\{ k_i \in \mathbb{Z} \,\middle|\, \underset{k_j \in \mathbb{Z}}{\exists} k_i Q_i = k_j Q_j + l \right\}, \;\; i \neq j,$$

with $Q_i, Q_j \in \mathbb{N}$ relative prime and with $0 \leq l < Q_j$. Then the following expressions can be shown to be equivalent:

$$(k_i \in \mathcal{K}_{i,j}) \;\wedge\; (k_i \in \mathcal{K}_{i,j'})$$

$$k_i \in \bigcup_{l=L_{1,j}}^{L_{2,j}} \mathcal{K}_{i,j}(l) \cap \bigcup_{l'=L_{1,j'}}^{L_{2,j'}} \mathcal{K}_{i,j'}(l')$$

$$k_i \in \bigcup_{l=L_{1,j}}^{L_{2,j}} \bigcup_{l'=L_{1,j'}}^{L_{2,j'}} \mathcal{K}_{i,j}(l) \cap \mathcal{K}_{i,j'}(l'). \tag{H.1}$$

Using Theorem 14 in Appendix G, which states that $\mathcal{K}_{i,j}(l) \cap \mathcal{K}_{i,j}(r) = \{\}$ for $i, j \in \mathcal{M}$, $0 \leq l, r < Q_j$, and $l \neq r$, it can be shown that the intersection terms $\mathcal{K}_{i,j}(l) \cap \mathcal{K}_{i,j'}(l')$ in (H.1) are disjoint, i.e., that $[\mathcal{K}_{i,j}(l) \cap \mathcal{K}_{i,j'}(l')] \cap [\mathcal{K}_{i,j}(l) \cap \mathcal{K}_{i,j'}(l'')] = \{\}$ for $l' \neq l''$. This property allows us to express (5.33) as

$$\begin{aligned} P[(k_i \in \mathcal{K}_{i,j}) \;\wedge\; (k_i \in \mathcal{K}_{i,j'})] &= P\left[k_i \in \bigcup_{l=L_{1,j}}^{L_{2,j}} \bigcup_{l'=L_{1,j'}}^{L_{2,j'}} \mathcal{K}_{i,j}(l) \cap \mathcal{K}_{i,j'}(l') \right] \\ &= \sum_{l=L_{1,j}}^{L_{2,j}} \sum_{l'=L_{1,j'}}^{L_{2,j'}} P(k_i \in \mathcal{K}_{i,j}(l) \cap \mathcal{K}_{i,j'}(l')). \end{aligned} \tag{H.2}$$

According to (G.5) in Theorem 13, $\mathcal{K}_{i,j}(l)$ can be expressed as

$$\mathcal{K}_{i,j}(l) = \{ nQ_j + \delta_{i,j}(l) \,|\, n \in \mathbb{Z}, \delta_{i,j}(l) \in \mathbb{N}_0, 0 \leq \delta_{i,j}(l) < Q_j \}, \;\; i \neq j, \tag{H.3}$$

where $\delta_{i,j}(l)$ depends on Q_i, Q_j, and l. This expression is applied two times in the following derivation:

$$\begin{aligned}
\mathcal{K}_{i,j}(l) \cap \mathcal{K}_{i,j'}(l') &= \left\{ k_i \in \mathbb{Z} \,\middle|\, \underset{k_j,k_{j'}\in\mathbb{Z}}{\exists} k_iQ_i = k_jQ_j + l = k_{j'}Q_{j'} + l' \right\} \\
&= \left\{ k_i \in \mathbb{Z} \,\middle|\, \underset{k_j,k_{j'}\in\mathbb{Z}}{\exists} (k_iQ_i = k_jQ_j + l) \right. \\
&\qquad\qquad \left. \wedge\, (k_jQ_j = K_{j'}Q_{j'} + l' - l) \right\} \\
&= \left\{ k_i \in \mathbb{Z} \,\middle|\, \underset{k_j,n\in\mathbb{Z}}{\exists} (k_iQ_i = k_jQ_j + l) \right. \\
&\qquad\qquad \left. \wedge\, (k_j = nQ_{j'} + \delta_{j,j'}(l' - l) \right\} \\
&= \left\{ k_i \in \mathbb{Z} \,\middle|\, \underset{n\in\mathbb{Z}}{\exists} k_iQ_i = nQ_jQ_{j'} + Q_j\delta_{j,j'}(l' - l) + l \right\} \\
&= \{ aQ_jQ_{j'} + d \,|\, a \in \mathbb{Z}, d \in \mathbb{N}_0, 0 \le d < Q_jQ_{j'} \}\,. \qquad \text{(H.4)}
\end{aligned}$$

Note that d is a function of l, l', Q_j, and $Q_{j'}$. We observe that every Q_iQ_j-th integer number is contained in the set $\mathcal{K}_{i,j}(l) \cap \mathcal{K}_{i,j'}(l')$, hence, under the assumption that $k \in \mathbb{Z}$ is uniformly distributed we get

$$P(k_i \in \mathcal{K}_{i,j}(l) \cap \mathcal{K}_{i,j'}(l')) = \frac{1}{Q_jQ_{j'}}. \qquad \text{(H.5)}$$

Inserting (H.5) into (H.2) yields

$$P[(k_i \in \mathcal{K}_{i,j}) \wedge (k_i \in \mathcal{K}_{i,j'})] = \sum_{l=L_{1,j}}^{L_{2,j}} \sum_{l'=L_{1,j'}}^{L_{2,j'}} \frac{1}{Q_jQ_{j'}} = \frac{(L_{2,j} - L_{1,j} + 1)(L_{2,j'} - L_{1,j'} + 1)}{Q_jQ_{j'}}. \qquad \text{(H.6)}$$

comparing this result with (5.18) shows that

$$P[(k_i \in \mathcal{K}_{i,j}) \wedge (k_i \in \mathcal{K}_{i,j'})] = P(k_i \in \mathcal{K}_{i,j})P(k_i \in \mathcal{K}_{i,j'})$$

and therefore proves the statistical independence of the events $k_i \in \mathcal{K}_{i,j}$ and $k_i \in \mathcal{K}_{i,j'}$.

Bibliography

[1] A. Adinoyi, H. Yanikomeroglu, and S. Loyka, "Hybrid macro- and generalized selection combining microdiversity in lognormal shadowed rayleigh fading channels," in *Proc. IEEE ICC-04*, vol. 27, no. 1, June 2004, pp. 244–248.

[2] A. Alvarez, G. Valera, M. Lobeira, R. Torres, and J. L. Garcia, "New channel impulse response model for UWB indoor system simulations," in *Proc. IEEE VTC*, vol. 1, April 2003, pp. 1–5.

[3] J. Bach-Andersen, H. Boche, A. Bourdoux, J. Fonollosa, T. Kaiser, and W. Utschick, *Smart Antennas - State-of-the-Art*. EURASIP, Hindawi Publishing Corporation, 2005.

[4] T. W. Barrett, "History of ultra wideband (uwb) radar & communications: Pioneers and innovators," in *Progress In Electromagnetics Symposium 2000*, Cambridge, MA, July 2000.

[5] N. C. Beaulieu, A. Abu-Dayya, and P. J. McLane, "Estimating the distribution of a sum of independent lognormal random variables," *IEEE Transactions on Communications*, vol. 43, no. 12, pp. 2869–2873, 1995.

[6] E. Bedrosian, "A product theorem for hilbert transform," *Proc IEEE*, vol. 51, pp. 868–869, 1963.

[7] I. N. Bronstein, K. A. Semendjajew, G. Musiol, and H. Mühlig, *Taschenbuch der Mathematik*, 4th ed. Verlag Harri Deutsch, 1999.

[8] L. R. C. Prettie, D. Cheung, "Spatial correlation of UWB signals in a home environment," in *Proc. IEEE UWBST-2002*, May 2002.

[9] C. Carbonelli and U. Mengali, "Low complexity synchronization for noncoherent UWB receivers," in *Proc. Joint Workshop on Communications and Coding*, Florence, Italy, Oct. 2004.

[10] D. Cassioli, M. Z. Win, and A. F. Molisch, "A statistical model for the UWB indoor channel," in *Proc. IEEE VTC-Spring*, vol. 2, 2001, pp. 1159–1163.

[11] D. Cassioli and A. Durantini, "A time-domain propagation model of the UWB indoor channel in the FCC-compliant band 3.6 - 6 GHz based on PN-sequence channel measurements," in *Proc. IEEE VTC-Spring*, vol. 1, May 2004, pp. 213–217.

[12] D. Cassioli, M. Z. Win, F. Vatalaro, and A. F. Molisch, "Performance of low-complexity rake reception in a realistic UWB channel," in *Proc. IEEE ICC-02*, May 2002, pp. 763–767.

[13] Y.-L. Chao and R. A. Scholtz, "Weighted correlation receivers for ultra-wideband transmitted reference systems," in *Proc. IEEE GLOBECOM-04*, vol. 1, 2004, pp. 66–70.

[14] X. Chen and T. Lang, "Performance analysis of chip rate division multiple access (CRDMA) technique," in *Proc. IEEE International Conference on Communication Technology 1996, (ICCT'1996)*, vol. 2, May 1996, pp. 957–960.

[15] J. D. Choi and W. E. Stark, "Performance analysis of rake receivers for ultra-wideband communications with PPM and OOK in multipath channels," in *Proc. IEEE ICC-02*, vol. 3, 2002, pp. 1969–1973.

[16] P. Chow, A. Karim, V. Fung, and C. Dietrich, "Performance advantages of distributed antennas in indoor wireless communication systems," in *Proc. 44th IEEE Vehicular Technology Conference*, vol. 3, 1994, pp. 1522–1526.

[17] A. Conti, M. Z. Win, M. Chiani, and J. H. Winters, "Bit error outage for diversity reception in shadowing environment," *IEEE Commun. Letters*, vol. 7, no. 1, pp. 15–17, Jan. 2003.

[18] F. A. Dietrich and W. Utschick, "Pilot assisted channel estimation based on second order statistics," *IEEE Transactions on Signal Processing*, vol. 53, no. 3, pp. 1178–1193, Mar. 2005.

[19] F. F. Digham, M.-S. Alouini, and M. K. Simon, "On the energy detection of unknown signals over fading channels," in *Proc. IEEE ICC-03*, vol. 5, May 2003, pp. 3575–3579.

[20] G. Durisi and G. Romano, "On the validity of Gaussian approximation to characterize the multiuser capacity of UWB TH PPM," in *Proc. 2002 IEEE Conf. on Ultra Wideband Systems and Technologies*, May 2002, pp. 157–161.

[21] Federal Communications Commission (FCC). Revision of Part 15 of the Commission's rules regarding ultra-wideband transmission systems. *First Report and Order*, ET Docket 98-153, FCC 02-48, adopted on Feb. 14, 2002, released on Apr. 22, 2002. [Online]. Available: http://www.fcc.gov.

[22] J. R. Foerster, "The effects of multipath interference on the performance of UWB systems in an indoor wireless channel," *Proc. IEEE VTC-Spring*, vol. 2, pp. 1176–1180, May 2001.

[23] J. Foerster. Channel Modeling Sub-committee Report Final. 02490r1P802-15. [Online]. Available: http://grouper.ieee. org/groups/802/15/pub/2003/Mar03/

[24] S. S. Ghassemzadeh, R. Jana, C. W. Rice, W. Turin, and V. Tarok, "A statistical path loss model for in-home UWB channels," in *Proc. 2002 IEEE Conference on Ultra Wideband Systems and Technologies*, May 2002.

[25] F. J. Harris, "On the use of windows for harmonic analysis with the discrete fourier transform," *Proceedings of the IEEE*, vol. 66, no. 1, pp. 51–83, Jan. 1978.

[26] H. Hashemi, "Impulse response modeling of indoor radio propagation channels," *IEEE Journal on Selected Areas in Communications*, vol. 11, pp. 967–978, Sept. 1993.

[27] R. Hoctor and H. Tomlinson, "Delay-hopped transmitted-reference RF communications," in *Proc. 2002 IEEE Conf. on Ultra Wideband Systems and Technologies*, May 2002, pp. 265–269.

[28] E. A. Homier and R. A. Scholtz, "Rapid acquisition of ultra-wideband signals in the dense multipath channel," in *Proc. 2002 IEEE Conf. on Ultra Wideband Systems and Technologies*, May 2002, pp. 105–109.

[29] V. Hovinen, M. Hämäläinen, and T. Pätsi, "Ultra wideband indoor radio channel models: Preliminary results," in *Proc. IEEE UWBST-2002*, May 2002.

[30] S. J. Howard and K. Pahlavan, "Statistical autoregressive models for the indoor radio channel," in *Proc. IEEE ISCAS-90*, San Diego, CA, Dec. 1990, pp. 2–5.

[31] ——, "Autoregressive modeling of wide-band indoor radio propagation," *IEEE Transactions on Communications*, vol. COM-40, pp. 1540–1552, Sept. 1992.

[32] M. Kac, *Statistical Independence in Probability, Analysis and Number Theory*. Mathematical Association of America, 1959.

[33] J. Keignart and N. Daniele, "Channel sounding and modelling for indoor UWB communications," in *Proc. Int. Workshop on Ultra Wideband Systems*, Oulu, Finnland, June 2003.

[34] R. Knopp and Y. Souilmi, "Achievable rates for UWB peer-to-peer networks," in *Proc. 2004 Intl. Zurich Seminar on Communications*, Zurich, Switzerland, Feb. 2004, pp. 82–85.

[35] N. Kong and L. B. Milstein, "Average SNR of a generalized diversity selection combining scheme," *IEEE Communications Letters*, vol. 3, no. 3, pp. 57–59, Mar. 1999.

[36] J. D. Kraus and K. R. Carver, *Electromagnetics*, 2nd ed. New York: McGraw-Hill, 1973.

[37] J. Kunisch and J. Pamp. Radio channel model for indoor UWB WPAN environments. 02281r0P802-15. [Online]. Available: http://grouper.ieee.org/groups/802/15/pub/2002/Jul02/

[38] ——, "Measurement results and modeling aspects for the UWB radio channel," in *Proc. 2002 IEEE Conf. on Ultra Wideband Systems and Technologies*, Baltimore, May 2002, pp. 19–23.

[39] E. A. Lee and D. G. Messerschmitt, *Digital Communication*, 2nd ed. Boston (MA): Kluwer, 1994.

[40] ——, *Digital Communication*, 3rd ed. Boston (MA): Kluwer, 2003.

[41] ——, *Digital Communication*, 4th ed. Boston (MA): Kluwer, 2004.

[42] W. M. Lovelace and J. K. Townsend, "The effects of timing jitter and tracking on the performance of impulse radio," *IEEE Journal on Selected Areas in Communications*, vol. 20, no. 9, pp. 1646–1651, Dec. 2002.

[43] Y. Ma, F. Chin, B. Kannan, and S. Pasupathy, "Acquisition performance of an ultra wide-band communications system over a multiple-access fading channel," in *Proc. 2002 IEEE Conf. on Ultra Wideband Systems and Technologies*, May 2002, pp. 99–103.

[44] M. L. McCloud and M. K. Varanasi, "Modulation and coding for noncoherent communications," *J. VLSI Signal Processing Systems*, vol. 30, no. 1, pp. 35–54, Jan. 2002.

[45] R. F. Mills and G. E. Prescott, "A comparison of various radiometer detection models," *IEE Transactions on Aerospace and Electronic Systems*, vol. 32, no. 1, pp. 467–473, Jan. 1996.

[46] R. U. Nabar, H. Bölcskei, and A. J. Paulraj, "Outage properties of space-time block codes in correlated Rayleigh or Ricean fading environments," in *Proc. IEEE ICASSP 2002*, Orlando, May 2002, pp. 2381–2384.

[47] F. Nevanlinna, *Einführung in die Algebra und die Theorie der algebraischen Gleichungen*. Basel und Stuttgart: Birkhäuser Verlag, 1965.

[48] S. Paquelet, L.-M. Aubert, and B. Uguen, "An impulse radio asynchronous transceiver for high data rates," in *Proc. IEEE Joint UWBST & IWUWBS 2004*, Kyoto, Japan, May 2004, pp. 1–4.

[49] J. G. Proakis, *Digital Communications*, 3rd ed. New York: McGraw-Hill, 1995.

[50] R. C. Qiu, H. Liu, and X. S. Shen, "Ultra-wideband for multiple access communications," *IEEE Commun. Magazine*, pp. 80–87, Feb. 2005.

[51] A. Rabbachin and I. Oppermann, "Synchronization analysis for UWB systems with a low-complexity energy collection receiver," in *Proc. IEEE Joint UWBST & IWUWBS 2004*, Kyoto, May 2004, pp. 1–4.

[52] A. Rabbachin, R. Tesi, and I. Oppermann, "Bit error rate analysis for UWB systems with a low complexity, non-coherent energy collection receiver," in *Proc. IST Mobile & Wireless Telecommunications Summit*, Lyon, France, June 2004, pp. 1–4.

[53] F. Ramirez-Mireles, "On the performance of ultra-wide-band signals in Gaussian noise and dense multipath," *IEEE Transactions on Vehicular Technology*, vol. 50, no. 1, pp. 244–249, Jan. 2001.

[54] D. Raphaeli, "Distribution of noncentral indefinite quadratic forms in complex normal variables," *IEEE Transactions on Information Theory*, vol. 42, no. 3, pp. 1002–1007, May 1996.

[55] T. S. Rappaport, *Wireless Communications*. New Jersey: Prentice Hall, 1996.

[56] B. Rimoldi, "RDMA for multipath multiple access channels: An optimum asynchronous low complexity technique," in *Proc. Seventh Joint Swedish-Russian Intl. Workshop on Information Theory*, St.-Petersburg, Russia, June 1995, pp. 196–199.

[57] W. Roh and A. Paulraj, "Outage performance of the distributed antenna systems in a composite fading channel," in *IEEE VTC*, vol. 3, Sept. 2002, pp. 1520–1524.

[58] A. A. M. Saleh and R. A. Valenzuela, "A statistical model for indoor multipath propagation," *IEEE Journal on Selected Areas in Communications*, vol. SAC-5, no. 2, pp. 128–137, Feb. 1987.

[59] S. Schell. (2002, Nov.) Analysis of time variance of a UWB propagation channel. IEEE 802.15-02/452r0-SG3a. Proposal for IEEE P8002.15.3a channel model. [Online]. Available: http://grouper.ieee.org/groups/802/15/pub/2002/Nov02

[60] R. A. Scholtz, R. J. Cramer, and M. Z. Win, "Evaluation of the propagation characteristics of ultra-wideband communication channels," in *Proc. IEEE Antennas and Propagation Society International Symposium*, vol. 2, 1998, pp. 626–630.

[61] U. Schuster, H. Bölcskei, and G. Durisi, "Ultra-wideband channel modeling based on information-theoretic criteria," in *IEEE Journal on Selected Areas in Communications*, Mar. 2005, to appear.

[62] U. G. Schuster, M. Borgmann, and H. Bölcskei, "Semicoherent PPM for wideband communications," in *Proc. IEEE International Symposium on Information Theory (ISIT)*, Chicago, USA, June 2004, pp. 72–75.

[63] K. Siwiak and A. Petroff, "A path link model for ultra wide band pulse transmissions," in *Proceedings of the IEEE VTC Spring 2001*, Rhodes, 2001.

[64] Y. Souilmi and R. Knopp, "On the achievable rates of ultra-wideband PPM with non-coherent detection in multipath environments," in *IEEE ICC-03*, vol. 5, May 2003, pp. 3530– 3534.

[65] D. J. Torrieri, *Principles of Secure Communication Systems*. Artech House, 1985.

[66] H. L. V. Trees, *Detection, Estimation, and Modulation Theory*. Wiley, 1968.

[67] W. Turin, J. Rittwik, S. Ghassemzadeh, and C. W. Rice, "Autoregressive modeling of an indoor UWB channel," in *Proc. IEEE UWBST-2002*, May 2002.

[68] H. Urkowitz, "Energy detection of unknown deterministic signals," *Proc. the IEEE*, vol. 55, no. 4, pp. 523–531, Apr. 1967.

[69] M. Weisenhorn and W. Hirt, "Performance of binary antipodal signaling over the indoor UWB MIMO channel," in *Proc. IEEE ICC-03*, vol. 4, May 2003, pp. 2872– 2878.

[70] ——, "Novel rate-division multiple-access scheme for UWB-radio-based sensor networks," in *Proc. IEEE International Zurich Seminar on Communications*, Feb. 2004, pp. 76–81.

[71] ——, "Robust noncoherent receiver exploiting UWB channel properties," in *Proc. IEEE Joint UWBST & IWUWBS 2004*, Kyoto, Japan, May 2004, pp. 156–160.

[72] ——, "Uncoordinated rate-division multiple-access scheme for pulsed UWB signals," *IEEE Transactions on Vehicular Technology*, vol. 54, no. 5, pp. 1646–1662, Sept. 2005.

[73] ——, "UWB transceiver system architecture," Research Report RZ3516, IBM Zurich Res. Lab., Nov. 2003.

[74] ——, "Impact of the FCC average- and peak power constraints on the power of UWB radio signals," Research Report RZ3544, IBM Zurich Res. Lab., Sept. 2004.

[75] M. Z. Win and R. A. Scholtz, "Ultra-wide bandwidth signal propagation for indoor wireless communications," in *Proc. IEEE ICC-97*, Montreal, Canada, June 1997, pp. 56–60.

[76] ——, "Impulse radio: How it works," *IEEE Communication Letters*, vol. 2, no. 2, pp. 36–38, Feb. 1998.

[77] ——, "On the robustness of ultra-wide bandwidth signals in dense multipath environments," *IEEE Communication Letters*, vol. 2, no. 2, pp. 51–53, Feb. 1998.

[78] ——, "Ultra-wide bandwidth time-hopping spread-spectrum impulse radio for wireless multiple-access communications," *IEEE Transactions on Communications*, vol. 48, no. 4, pp. 679–691, Apr. 2000.

[79] W.-P. Yung, "Probability of bit error for MPSK modulation with diversity reception in rayleigh fading and log-normal shadowing channel," *IEEE Transactions on Communication*, vol. 38, no. 7, pp. 933–937, July 1990.

[80] T. Zasowski, F. Althaus, and A. Wittneben, "An energy efficient transmitted-reference scheme for ultra wideband communications," in *Proc. IEEE Joint UWBST & IWUWBS 2004*, Kyoto, Japan, May 2004, pp. 146–150.